The Thesis Committee for Jeremy Oran Wheeless
Certifies that this is the approved version of the following thesis:

Improving the Sulfate Resistance of Class C Fly Ash: A Scientific Approach to Making Bad Ash Concrete

APPROVED BY
SUPERVISING COMMITTEE:

Supervisor:

Kevin J. Folliard

Thanos Drimalas

Improving the Sulfate Resistance of Class C Fly Ash: A Scientific Approach to Making Bad Ash Concrete

by

Jeremy Oran Wheeless

Thesis

Presented to the Faculty of the Graduate School of

The University of Texas at Austin

in Partial Fulfillment

of the Requirements

for the Degree of

Master of Science in Engineering

The University of Texas at Austin

May, 2018

Dedication

A wise man once said “I am a great believer in luck, and I find the harder I work, the more I have of it.” While this sentiment is most certainly true for me, the work wouldn’t have happened if I were not supported. My wife and best friend, Erin Boardman, gives me purpose to strive and succeed and if not for her patience and calm confidence in me, these words, and those that follow surely would not be. Erin, thank you for your love and support while I whittled away on this project. You are not only a gift to me, but to everyone you come in contact with. I am lucky and love you so much.

I see a bright future in the making for a couple of important people in my life. Emma and Chloe, you are both so intelligent, beautiful, and capable. You both have inspired me to do my best and make you proud. I look forward to admiring what you two do next.

Opportunities come and go in life. My parents taught me to grab an opportunity, hold on tight, and run with it wherever it may take me. They showed me that in order to succeed you have to try. My father helped me understand what real work is and gave me the humility to respect the ways of construction. My mother’s undying persistence and beauty have taught me that life is what we make it, and that every day is a blessing. I love you both and am very grateful to have you as parents.

Acknowledgements

This research is the result of the collective efforts of many people. First and foremost, the inspiration and enthusiasm of my advisor and pal Kevin J. Folliard (your love for concrete and the materials therein is un-matched). Countless hours were spent standing over a mortar mixer in good company with my research partner Bruno Fong-Martinez (your organizational skills and work ethic helped make this thesis something I am proud of – thank you). Thanos Drimalas fielded countless head-scratching questions from me, and always answered with a smile (thanks for all your help in making the research fun and interesting). This work could not have been done without the financial support of the Texas Department of Transportation (thank you TxDOT for keeping our infrastructure the best in the nation). And lastly, thank you to all the teachers who taught me how to learn.

What started at the University of Texas at Austin changed my world.

Abstract

Improving the Sulfate Resistance of Class C Fly Ash: A Scientific Approach to Making Bad Ash Concrete

Jeremy Oran Wheeless, M.S.E.

The University of Texas at Austin, 2018

Supervisor: Kevin J. Folliard

Decades of research have shown that high calcium fly ash, when used as a partial replacement for portland cement, produces a binder that is susceptible to external sulfate attack. Previous research studies have shown that the external sulfate attack mechanism affecting these blends can be suppressed by using gypsum as an additive. In this research study, short-term expansion tests, calorimetry, and x-ray diffraction analysis have been used to show how gypsum affects the volumetric stability, hydration kinetics, and early age hydration products that form in these types of binders. Quantifying the hydration products that contribute to the external sulfate attack mechanism and correlating them to the amount of heat produced by the binder is a crucial step to determining the adequate amount of gypsum required to produce sulfate resistant cements containing high calcium fly ash. The use of these investigative techniques may allow for more widespread use of high calcium fly ashes as a replacement of portland cement.

Table of Contents

List of Tables

List of Figures

1.0 Introduction and Background

Historically, fly ash has proven to be a suitable partial replacement in a cement binder. In general, the type of fly ash used (Class F or Class C per ASTM C618) will produce different effects on the cement binder. Significant research has been done which shows that low-calcium (Class F) fly ash, produces a pozzolanic reaction which is beneficial to concrete in many ways. On the other hand, past research has shown that high-calcium (Class C) fly ash can produce a cement binder that is beneficial to concrete but is susceptible to a form of concrete degradation known as external sulfate attack. Recent changes in the raw material stream at coal burning power plants have led to an increase in the availability of Class C fly ash, presenting a common scenario where engineers, contractors, and ready-mix concrete producers only have access to Class C ashes to be used in concrete. This scenario has left many in the industry questioning how this material can be used safely in various applications. This research investigates how gypsum, when used as an additive, effects the hydration kinetics, hydration product formation, volumetric stability, and long-term sulfate exposure resistance of blends of Class C fly ash in neat cement paste and mortar. The findings of this study show a correlation between the formation of hydration products, volumetric stability, and heat of hydration, and also confirm theories posed in previous research.

External sulfate attack (“classical" sulfate attack) is a complex process that involves the formation of cement hydration products that depend on many factors which include: raw materials in the concrete mixture, time of exposure, and environment. In general, the onset of sulfate attack may occur when a concrete specimen is in direct contact with one of multiple forms of sulfate that exist naturally in the earth’s crust or in ground water [1]. Presently, there is agreement in literature [1, 2], material testing societies [3], and a

considerable amount of research that show the primary way to produce a sulfate attack resistant (sulfate resistant) cement binder is to limit the amount of tri-calcium aluminate (C_3A) within a given mixture.

A relatively recent compilation of research [4] outlines the typical hydration process of C_3A in portland cement. The compilation indicates that C_3A reacts with sulfates, mainly $CaSO_4 \cdot 2H_2O$ (gypsum), to rapidly form $C_6A\bar{S}_3H_{32}$ (AFt or ettringite). This reaction continues until the C_3A has depleted the sulfates, at which point the C_3A begins to react with the newly formed AFt, thereafter producing $3C_4A\bar{S}H_{12}$ (AFm or monosulfoaluminate). Once hydrated, most portland cements will have some amount of AFm or AFt within the cement paste matrix. If the AFm within the matrix comes in contact with external sulfates (from ground water or soil), the AFm may revert back to AFt. When this occurs, it is an expansive reaction that may lead to cracking and degradation of the concrete and general loss of cohesion between constituent materials within the cement paste matrix.

Several researchers have shown that using high-calcium fly ash at normal replacement levels (nominally less than 40% by weight) will produce cement binders with inferior sulfate resistance [5, 6, 7, 8, 9, 10, 11, 12]. The decrease in sulfate resistance has been attributed to mineralogical aspects of fly ash, namely calcium aluminate glass and C_3A content within the fly ash [5, 13, 14, 15]. The presence and form of C_3A in fly ash is the result of the type of coal burned and the coal burning process respectively. Researchers [10, 15] have shown that high calcium fly ashes containing a combination of calcium aluminate glass and crystalline forms of C_3A will typically lead to reduced sulfate resistance.

Research conducted on a wide variety of United States fly ash [16] showed that common crystalline phases in fly ash are: lime, hematite, magnetite, C_3A, periclase, mellite, quartz, mullite, and anhydrite. Researchers [7] have determined that the crystalline phases most responsible for initiating the sulfate attack mechanism in cementitious blends of fly ash and cement are C_3A, ghelenite, periclase, and anhydrite.

The location of the amorphous fraction of a fly ash when plotted on a ternary phase diagram of CaO, SiO_2 and Al_2O_3 has been used in previous research to indicate a fly ashes tendency to initiate sulfate attack when used in a cement binder. A researcher [5] plotted the amorphous composition of fly ashes (known to produce inferior sulfate resistance) on a ternary phase diagram that indicated the amorphous content will generally fall into one of three regions on the ternary phase diagram: mullite (A_3S_2), anorthoite (CAS_2), or gehlenite (C_2AS), each of which contain alumina (**Figure 1.1)**. When the composition of an ash exists in the gehlenite region of the diagram it was concluded [5] and has been shown [9, 17] to reduce the sulfate resistance. Research on this topic indicates that ashes that exist within the lower anorthoite, and gehlenite regions are believed to contain highly reactive calcium aluminate glass which will reduce the sulfate resistance when used in a cement binder. In general, when a given fly ash is known to produce inferior sulfate resistance, and its mineralogical composition is plotted on a ternary phase diagram (CaO - SiO_2 - Al_2O_3), there will typically be a cluster of points around the gehlenite region.

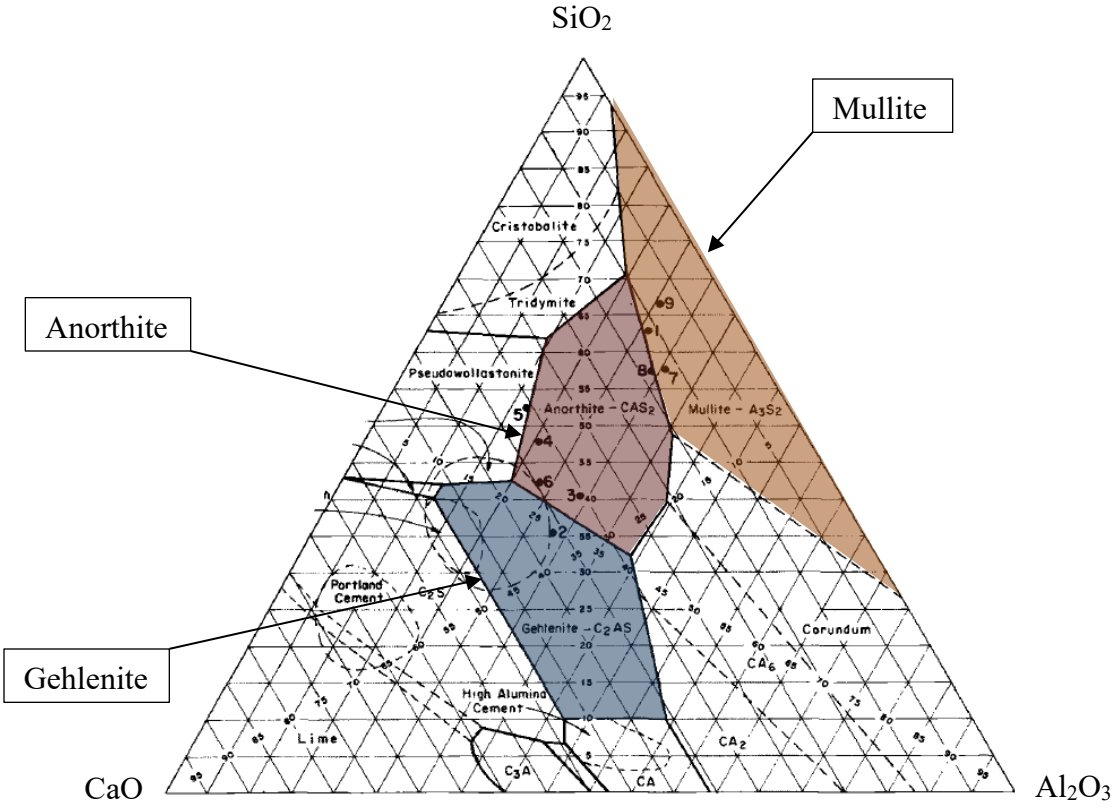

Figure 1.1 $CaO – SiO_2 – Al_2O_3$ ternary phase diagram [5] with mullite, anorthite, and ghelenite regions annotated by author.

Multiple methods for increasing the sulfate resistance of cement binders exist. A common method for producing a sulfate resistant cement binder is through the use of supplementary cementitious materials (SCM's). Utilizing pozzolanic SCM's such as silica fume or low calcium fly ash have shown to be effective at inhibiting or decreasing sulfate attack [5, 6, 18, 14, 17, 9]. Using ultra-fine fly ash (UFFA) as a replacement of cement has produced promising results in promoting sulfate resistance [9, 11]. Research studies [9, 17, 19] have indicated that using high volumes (greater than 60% replacement of cement) of high calcium fly ash have also proven effective. Another strategy for increasing sulfate resistance was lowering the water to cement ratio in an attempt to make the cement paste

matrix denser (i.e., less permeable) [9] thereby disallowing the ingress of sulfates into the paste matrix.

Researchers have developed approaches to mitigate sulfate attack in blends of high calcium fly ash and portland cement by using gypsum and other sulfates as additives [7, 20]. This approach is referred to as "super-sulfating" the mix. The underlying theory in this approach is that the addition of sulfates as an additive would react with the additional C_3A resulting from the inclusion of high calcium fly ash to produce and/or stabilize AFt during early ages of the cement or concretes lifespan. It is believed that if AFt is stabilized early, and AFm is inhibited from forming, then if the concrete/cement binder comes in contact with external sulfates there will be nothing for the external sulfates to react with and the sulfate attack mechanism will be controlled. This theory has been tested by researchers [8, 9, 20] at the University of Texas at Austin and is the primary focus of this research study.

2.0 Naming Convention

A naming convention and mixture identification number (Mix ID) system was established to clearly indicate which materials were used to conduct the research presented in this thesis. The naming and mixture identification convention consists of the following abbreviations:

C# : cement number

F#(%): fly ash number (% of cement replacement)

G(%): gypsum (% additive)

Example construction of a Mix ID

Assume the following materials were used:

- Cement: C1
- Fly Ash: F1 with a 35% replacement of cement
- 4% gypsum additive

Solution for the construction of a mixture identification number

Mix ID: C1-F1(35)-G(4)

3.0 Materials

All cements and fly ashes used in this research are commercially available products. Each material was analyzed with x-ray fluorescence (XRF) to determine the bulk oxide contents, as well as quantitative x-ray diffraction (QXRD) to determine the mineralogical composition of the given material. The XRF testing was performed by the Texas Department of Transportation Materials Lab in Cedar Park, Texas. The x-ray diffraction (XRD) was performed on a Siemens D500 Diffractometer with scanning parameters of 5 - 70 2θ degrees, with a step of 0.02, and 6 second dwell time. Rietveld refinement was performed on the XRD scans using TOPAS academic V4.1 software. Sample preparation for XRD included passing the cement or fly ash powders through a number 140 sieve, adding rutile as an internal standard at a constant value of 10.0 ± 0.01%, thoroughly mixing the rutile and the given powder into a slurry using 99.5% pure isopropanol, allowing the slurry to completely dry in a desiccator, followed by placing the powder into the sample holder with a razor blade and leveling the sample with a glass plate.

3.1 FLY ASH

Three commercially available Texas fly ash sources were utilized in this research study. The bulk oxide content and mineralogical composition for each of the fly ashes is presented in **Table 3.1.** Fly ash identification numbers shown in **Table 3.1** were organized to correlate with low to high CaO contents.

Table 3.1. XRF and QXRD analysis results for fly ashes.

	Fly Ashes				Fly Ashes		
XRF	F1	F2	F3	**QXRD**	F1	F2	F3
Oxides	wt. %	wt. %	wt. %	**Phase**	wt. %	wt. %	wt. %
CaO	21.7	24.5	26.6	Quartz	6.6	3.9	5.9
SiO_2	39.1	35.7	35.4	Anhydrite	1.1	2.0	1.5
Al_2O_3	20.6	19.4	17.7	Gehlenite	0.1	0.6	0.6
Fe_2O_3	6.0	6.1	5.3	Periclase	1.7	1.6	3.2
SO_3	1.0	2.4	1.5	$C_3A_{\ cubic}$	3.0	3.4	6.4
MgO	4.4	4.5	6.2	$C_3A_{\ orthorhombic}$	2.3	1.9	4.6
K_2O	0.7	0.5	0.4	Merwinite	4.1	2.4	4.5
Na_2O	1.3	1.5	1.9	$C_2S\ \beta$	3.8	4.3	6.0
Na_2O_e	1.8	1.9	2.1	Amorphous	77.3	80.0	67.4
$SiO_2+Al_2O_3+Fe_2O_3$	65.6	61.1	58.5	Total C_3A	5.3	5.3	11.0

3.2 CEMENTS

Two commercially available Texas cements were used in this research. The chemical and mineralogical composition for each of the cements is presented in **Table 3.2**. Additionally, the Bogue values are shown, and were calculated per ASTM C150-16.

Table 3.2. XRF, QXRD, and Bogue calculations for cements used in this study.

	Cements			Cements			Cements	
XRF	C1	C2	**QXRD**	C1	C2	**Bogue**	C1	C2
Oxide	wt. %	wt. %	**Phase**	wt. %	wt. %	**Phase**	wt. %	wt. %
CaO	64.8	64.5	Alite (C_3S)	49.1	46.5	Alite (C_3S)	63.2	59.3
SiO_2	19.8	20.7	Belite (C_2S)	19.1	24.2	Belite (C_2S)	9.1	14.5
Al_2O_3	5.5	4.9	$C_3A_{\ cubic}$	6.6	2.4	C_3A	10.8	7.1
Fe_2O_3	2.3	3.5	$C_3A_{\ orthorhombic}$	2.3	2.3	C_4AF	6.9	10.8
Na_2O	0.2	0.1	C_4AF	4.7	8.2			
MgO	1.2	1.2	Periclase	0.0	0.0			
K_2O	1.0	0.7	Arcanite	2.7	2.3			
P_2O_5	0.3	0.2	Anhydrite	0.0	0.0			
SO_3	3.4	2.8	Bassanite	7.3	4.2			
Cl	0.0	0.0	Gypsum	0.1	1.9			
TiO_2	0.2	0.2	Amorphous	8.2	8.1			
SrO	0.1	0.1	Total C_3A	8.9	4.6			
Mn_2O_3	0.0	0.0						
ZnO	0.0	0.0						
Cr_2O_3	0.0	0.0						

3.3 PARTICLE CHARACTERIZATION

Extensive work was performed by researchers [9, 10, 15] to characterize physical and chemical characteristics of fly ash. The work cited above was done on fly ashes from the same source as those which are part of this research study, and have nominally the same bulk oxide content, and mineralogical composition. A portion of the research cited above [9, 15] used scanning electron microscopy (SEM) in conjunction with energy dispersive X-ray analysis (EDXA), and XRF to quantify and delineate the glass, and crystalline composition of the fly ashes. That research allowed for the production of the differing fly ashes to be plotted on CaO-SiO_2-Al_2O_3 phase diagrams, which are presented in **Figure 3.1** below. Additionally, the SEM analysis allowed the researchers of the study to determine an average particle size of the glass. The average particle size of the glass as reported in [15] is presented in **Table 3.3**.

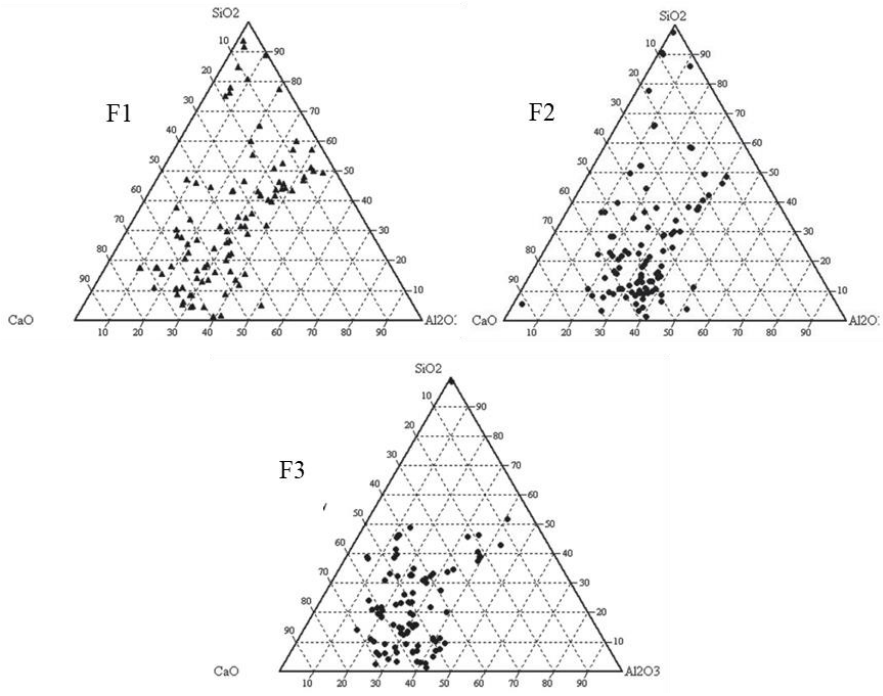

Figure 3.1. Fly ash glass distribution on CaO-SiO_2-Al_2O_3 ternary phase diagram [15].

The second portion of the research cited [10] in this section performed particle distribution analysis on a wide array of commercially available fly ashes. In general, particle size distribution analysis provides insight into the proportion of the volume of a given fly ash that is of a specific size range. Particle size distribution data from the aforementioned study is presented in **Table 3.3** below. One of the notable findings from the referenced study [10] (as it relates to this research) indicated that high calcium fly ashes containing relatively finer particles (not UFFA) tend to be more susceptible to sulfate attack when used in cement binders.

Table 3.3. Average particle size, and particle size distribution for ash used herein.

Fly Ash ID	*Average particle size	** Approximate percentage of volume of ash less than or equal to average particle size
	[μm]	[%]
F1	7.1	35
F2	3.7	20
F3	3.1	25

* Research performed by [15]

** Research performed by [10]

3.4 Material Characterization

3.4.1 Cement

Values shown in **Table 3.2** indicate that C1 and C2 meet the standard composition requirements outlined in ASTM C150-16 for a Type I and Type I/II cement respectively [3]. Note the discrepancy between the phase compositions determined by Bogue and those which were measured using QXRD analysis. The total C_3A content measured by QXRD of C1 and C2 was 8.9% and 4.7% respectively, whereas the Bogue composition showed C1 and C2 having 10.8% and 7.1% C_3A respectively. If the cements were classified using the QXRD analysis, cement C1 would be classified as a Type I and cement C2 a Type V by ASTM C 150-16.

3.4.2 Fly ash

Information presented in **Table 3.1** indicates the fly ashes used in this study meet the chemical requirements in ASTM C618 of a Class C fly ash [21]. Additionally, **Table 3.1** shows that the C_3A content increases with increasing CaO content.

As indicated in **Figure 3.1** the glass (amorphous) content of the fly ashes used in this study form a locust of points in the gehlenite region of the ternary phase diagram (highlighted in **Figure 1**), which indicates that the fly ashes used in this study should produce inferior sulfate resistance when used as a partial replacement for cement.

The research studies cited [9, 15] in section **3.3** of this thesis provided a delineation between amorphous and crystalline fractions of SiO_2, Al_2O_3, CaO, and SO_3 of fly ashes (of nominally equal chemical and mineralogical composition) as those used in this study. **Figure 3.1** indicates the relative percentages of crystalline and amorphous content of the minerals listed above.

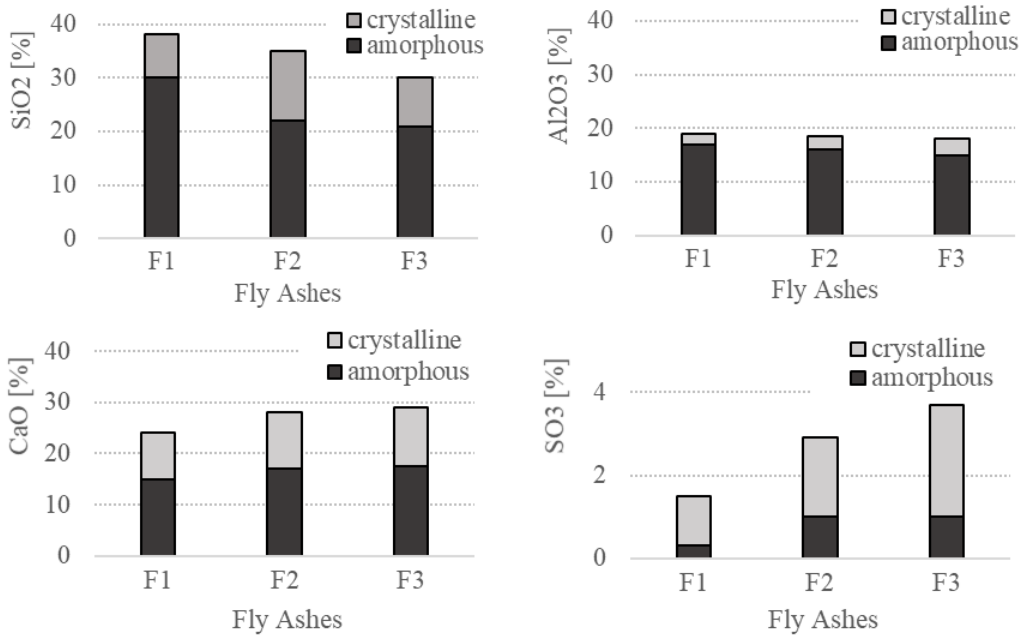

Figure 3.2. Crystalline and amorphous oxide contents of fly ashes [15].

3.4.3 Gypsum

A commercially available source of calcium sulfate dihydrate ($CaSO_4 \cdot 2H_2O$) meeting the requirements of ASTM C452-15 was procured from the U.S. Gypsum Company. The calcium sulfate dihydrate (gypsum) was Terra Alba, Food & Pharmaceuticals grade 100% gypsum by weight [22].

4.0 Testing Methods

4.1 ASTM C 1012 TESTING

Guidelines and provisions outlined in ASTM C 1012 [23] were followed with the exception that all mixtures were prepared with a constant water to cement ratio of 0.485. The mixture proportions for the specimens tested in ASTM C 1012 are presented in **Tables 4.1** and **4.2**. Two phases of ASTM C 1012 testing were performed, the reason for which will be discussed in section **5.5.2** of this thesis**.** To provide a clear distinction between phase one and two of ASTM C 1012 testing, Mix ID's corresponding to testing performed as part of phase 2 have been highlighted green in **Tables 4.1** and **4.2**. In total, 40 mixtures were prepared for phase 1, and 16 mixtures were prepared for phase 2.

Table 4.1. Mortar mixture proportions for ASTM C1012 testing of cement C1.

		Fly Ash			
MIX ID	Cement Type	F1(%)	F2(%)	F3(%)	Gypsum (%)
C1-F1(20)-G(0)	C1	20			0
C1-F1(20)-G(6)		20			6
C1-F1(20)-G(8.7)		20			8.7
C1-F1(20)-G(11.6)		20			11.6
C1-F1(20)-G(12.2)		20			12.2
C1-F1(20)-G(15.2)		20			15.2
C1-F1(35)-G(0)	C1	35			0
C1-F1(35)-G(8)		35			8
C1-F1(35)-G(10.5)		35			10.5
C1-F1(35)-G(11.8)		35			11.8
C1-F1(35)-G(14)		35			14
C1-F1(35)-G(15)		35			15
C1-F2(20)-G(0)	C1		20		0
C1-F2(20)-G(6)			20		6
C1-F2(20)-G(7.6)			20		7.6
C1-F2(20)-G(10.2)			20		10.2
C1-F2(20)-G(10.7)			20		10.7
C1-F2(20)-G(13.4)			20		13.4
C1-F2(35)-G(0)	C1		35		0
C1-F2(35)-G(8)			35		8
C1-F2(35)-G(8.5)			35		8.5
C1-F2(35)-G(11.4)			35		11.4
C1-F2(35)-G(11.9)			35		11.9
C1-F2(35)-G(14.8)			35		14.8
C1-F3(20)-G(0)	C1			20	0
C1-F3(20)-G(6)				20	6
C1-F3(35)-G(0)	C1			35	0
C1-F3(35)-G(8)				35	8

Table 4.2. Mortar mixture proportions for ASTM C1012 testing of cement C2.

		Fly Ash			
MIX ID	Cement Type	F1(%)	F2(%)	F3(%)	Gypsum (%)
C2-F1(20)-G(0)	C2	20			0
C2-F1(20)-G(3.2)		20			3.2
C2-F1(20)-G(4.3)		20			4.3
C2-F1(20)-G(6)		20			6
C2-F1(20)-G(9)		20			9
C2-F1(20)-G(11.2)		20			11.2
C2-F1(35)-G(0)	C2	35			0
C2-F1(35)-G(6)		35			6
C2-F1(35)-G(8)		35			8
C2-F1(35)-G(8)		35			8
C2-F1(35)-G(11.8)		35			11.8
C2-F1(35)-G(14.7)		35			14.7
C2-F2(20)-G(0)	C2		20		0
C2-F2(20)-G(2.1)			20		2.1
C2-F2(20)-G(2.8)			20		2.8
C2-F2(20)-G(6)			20		6
C2-F2(20)-G(7.5)			20		7.5
C2-F2(20)-G(9.4)			20		9.4
C2-F2(35)-G(0)	C2		35		0
C2-F2(35)-G(4.1)			35		4.1
C2-F2(35)-G(5.4)			35		5.4
C2-F2(35)-G(8)			35		8
C2-F2(35)-G(9.23)			35		9.23
C2-F2(35)-G(11.5)			35		11.5
C2-F3(20)-G(0)	C2			20	0
C2-F3(20)-G(6)				20	6
C2-F3(35)-G(0)	C2			35	0
C2-F3(35)-G(8)				35	8

4.2 LIMEWATER SUBMERGENCE TESTING

Limewater submergence testing (LST) consisted of submerging mortar bars in a saturated lime water solution and measuring length change over time. The LST of mortar bars used in this study is a modified version of ASTM C 1038. The mortar bars were proportioned, mixed and cured in accordance with the same specifications outlined in ASTM C 1012 with the exception that the water to cement ratio was a constant 0.485 for all mixtures. For each mixture, 4 mortar bars (3 for measuring length change, and 1 for x-ray diffraction analysis) and 6-9 mortar cubes (for compressive strength testing) were prepared. After the mortar cured for one day at 35 ± 3ºC (95 ± 5 ºF), the forms were stripped, an initial length measurement was taken, the mortar bars were placed in a saturated lime water solution, and the mortar cubes were tested for their compressive strength. Subsequent length change measurements were taken at 1, 3, 7, 14, 21, 28, 56,91, and 105 days. Compressive strength was tested until the mortar reached a compressive strength of 20 ± 1 MPa (2900 ± 145 psi). The mixture proportions for LST are presented in **Table 4.3.**

Table 4.3. Mixture proportions for LST and Isothermal Calorimetry.

Mix ID	Gypsum Admixture Dosages (%)							
C1-F1(20)	0	2	4	6	8	10	12	15
C1-F1(35)	0	2	4	6	8	10	12	15
C1-F2(20)	0	2	4	6	8	10	12	15
C1-F2(35)	0	2	4	6	8	10	12	15
C1-F3(20)	0	2	4	6	8	10	12	15
C1-F3(35)	0	2	4	6	8	10	12	15
C2-F1(20)	0	2	4	6	8	10	12	15
C2-F1(35)	0	2	4	6	8	10	12	15
C2-F2(20)	0	2	4	6	8	10	12	15
C2-F2(35)	0	2	4	6	8	10	12	15
C2-F3(20)	0	2	4	6	8	10	12	15
C2-F3(35)	0	2	4	6	8	10	12	15

4.3 ISOTHERMAL CALORIMETRY

Mixture proportions for isothermal calorimetry testing are shown in **Table 4.3**. Neat cement paste (cement, fly ash, de-ionized water, and gypsum) was used for this testing regime. Cement pastes were prepared with a water to cement ratio of 0.38. All dry ingredients were kept in a temperature-controlled room allowing for temperature equilibrium of 23 $^{\circ}$C (73 $^{\circ}$F) between the constituents to be met prior to mixing. The dry ingredients were placed in an ADIACAL TC isothermal calorimeter container cup, and thoroughly combined using a vibrating table for 90 seconds, thereafter water was added to make a paste. The cement paste was stirred by hand using a glass stir for 60 seconds, then mixed on the vibrating table for an additional 60 seconds. After all the mixing took place the specimens were immediately placed in a Grace ADIACAL TC isothermal calorimeter where the heat of hydration was measured every 60 seconds for a period of 7 days (168 hours).

4.4 X-RAY DIFFRACTION AND RIETVELD REFINEMENT

X-Ray diffraction analysis was performed on fragments of mortar bars that were extracted from LST at two different ages. Once an average of two mortar cubes from a respective mixture achieved a compressive strength of 20 MPa (2900 psi) a mortar bar was selected from the mix and broken in two equal halves; thereafter an approximate 50 mm (2 inch) portion was removed from one of the halves of the mortar bar for XRD analysis. The remaining pieces of the mortar bar were placed back in the saturated limewater solution. At 28 days after casting, the larger half of the remaining mortar bar was removed from the saturated limewater solution, broken in two more halves, and an approximate 50 mm (2 inch) portion was removed for additional XRD analysis.

The XRD analysis for LST was performed on a Siemens D500 Diffractometer with scanning parameters of 5^{O} to 60^{O} 2θ degrees, with a step of 0.02, and 6 second dwell time. Rietveld refinement was performed on the XRD scans using TOPAS academic V4.1 software. Sample preparation for XRD included grinding a respective 50 mm (2 inch) sample in a mortar and pestle into a fine powder, passing the powder through a number 140 sieve, placing the powder in sealed container and then a desiccator to fully dehydrate the sample of moisture for a period of at least one week, removing the sample from the desiccator and adding rutile as an internal standard at a constant value of approximately 10 ±0.01%, thoroughly mixing and grinding the rutile and powder into a slurry using 99.5% pure isopropanol, and allowing the slurry to completely dry into a powder. Final sample preparation included placing the powder into the sample holder with a razor blade and leveling the sample with a glass plate.

5.0 Results and Discussion

The tests conducted as part of this research study were carried out to meet two goals, both of which include using high calcium fly ash as partial replacement of a cement binder. The first goal was to confirm the effectiveness of a method of sulfate attack mitigation developed [7] and tested by previous researchers [8, 9]. The second goal was to develop a short-term testing method by which the proper amount of sulfate (gypsum) dosage could be determined such that the sulfate attack mechanism in cement binders containing high calcium fly ash would be mitigated.

5.1 EXPOSURE CONDITIONS

Deterioration to concrete due to sulfate attack is the result of the type of exposure to which the concrete element is subjected. The American Concrete Institute (ACI) has defined sulfate exposure conditions which are shown in **Table 5.1**.

Table 5.1. Defined Exposure Conditions per ACI Table 19.3.1.1.

	Class	Water-soluble sulfate (SO_4^{2-}) in soil, percent by mass [1]	Dissolved sulfate (SO_4^{2-}) in water, ppm [2]
Sulfate (S)	S0	$SO_4^{2-} < 0.10$	$SO_4^{2-} < 150$
	S1	$0.10 \leq SO_4^{2-} < 0.20$	$150 \leq SO_4^{2-} < 1{,}500$ or seawater
	S2	$0.20 \leq SO_4^{2-} < 2.00$	$1{,}500 \leq SO_4^{2-} < 10{,}000$
	S3	$SO_4^{2-} > 2.00$	$SO_4^{2-} > 10{,}000$

[1] Percent sulfate by mass in soil shall be determined by ASTM C1580.

[2] Concentration of dissolved sulfates in water, in ppm, shall be determined by ASTM D516 or ASTM D4130.

5.2 LIMEWATER SUBMERGENCE TESTING

5.2.1 Results

Limewater submergence testing (LST) was performed to determine effects that gypsum imposed on the cement binder and/or mortar. Of primary interest was assessing volume stability and identifying hydration products that formed during the early ages (within 28 days). Expansion results from the LST are shown in **Tables 5.2-5.5**. In the interest of being concise, the table only includes expansion data for 3, 7, 14, 28, and 105 days. Measurements taken at 105 days indicated that the mortar bars were no longer expanding. The data table includes **bolded** values, which are meant to indicate when a mortar bar expanded beyond 0.10% (the expansion limit imposed by ASTM C 1012). Additionally, the expansion results are plotted in **Figures 5.1-5.4** to provide a graphical representation of the results. Note that the leader lines in the plots indicate the gypsum dosage for the given mixture.

Table 5.2. LST results for cement C1 with 35% replacement of ashes F1-F3.

Mix ID	Gypsum [%]	Expansion [days]				
		3	7	14	28	105
C1-F1(35)	0	0.013%	-0.001%	-0.015%	0.006%	0.007%
	2	0.011%	0.026%	0.020%	0.010%	0.006%
	4	0.013%	0.014%	0.013%	0.008%	0.004%
	6	0.013%	0.010%	0.012%	0.008%	0.003%
	8	0.047%	0.057%	0.054%	0.047%	0.040%
	10	0.054%	0.092%	0.096%	0.095%	0.087%
	12	0.061%	**0.102%**	**0.134%**	**0.162%**	**0.152%**
	15	0.050%	0.091%	**0.138%**	**0.234%**	**0.454%**
C1-F2(35)	0	-0.008%	-0.009%	-0.010%	-0.008%	0.009%
	2	-0.009%	-0.013%	-0.017%	-0.008%	-0.010%
	4	-0.002%	-0.002%	-0.002%	-0.003%	-0.005%
	6	0.000%	-0.009%	-0.019%	-0.003%	-0.002%
	8	0.057%	0.059%	0.061%	0.056%	0.054%
	10	0.047%	0.097%	**0.146%**	**0.143%**	**0.135%**
	12	0.042%	**0.109%**	**0.175%**	**0.265%**	**0.257%**
	15	0.053%	**0.123%**	**0.193%**	**0.356%**	**0.783%**
C1-F3(35)	0	0.009%	0.002%	0.006%	0.005%	0.010%
	2	0.001%	0.001%	0.005%	0.004%	0.008%
	4	0.006%	0.001%	0.005%	0.004%	0.008%
	6	0.001%	0.001%	0.004%	0.003%	0.006%
	8	0.031%	0.027%	0.030%	0.028%	0.033%
	10	0.055%	**0.109%**	**0.113%**	**0.110%**	**0.111%**
	12	0.055%	**0.119%**	**0.171%**	**0.170%**	**0.171%**
	15	0.045%	0.081%	**0.132%**	**0.241%**	**0.678%**

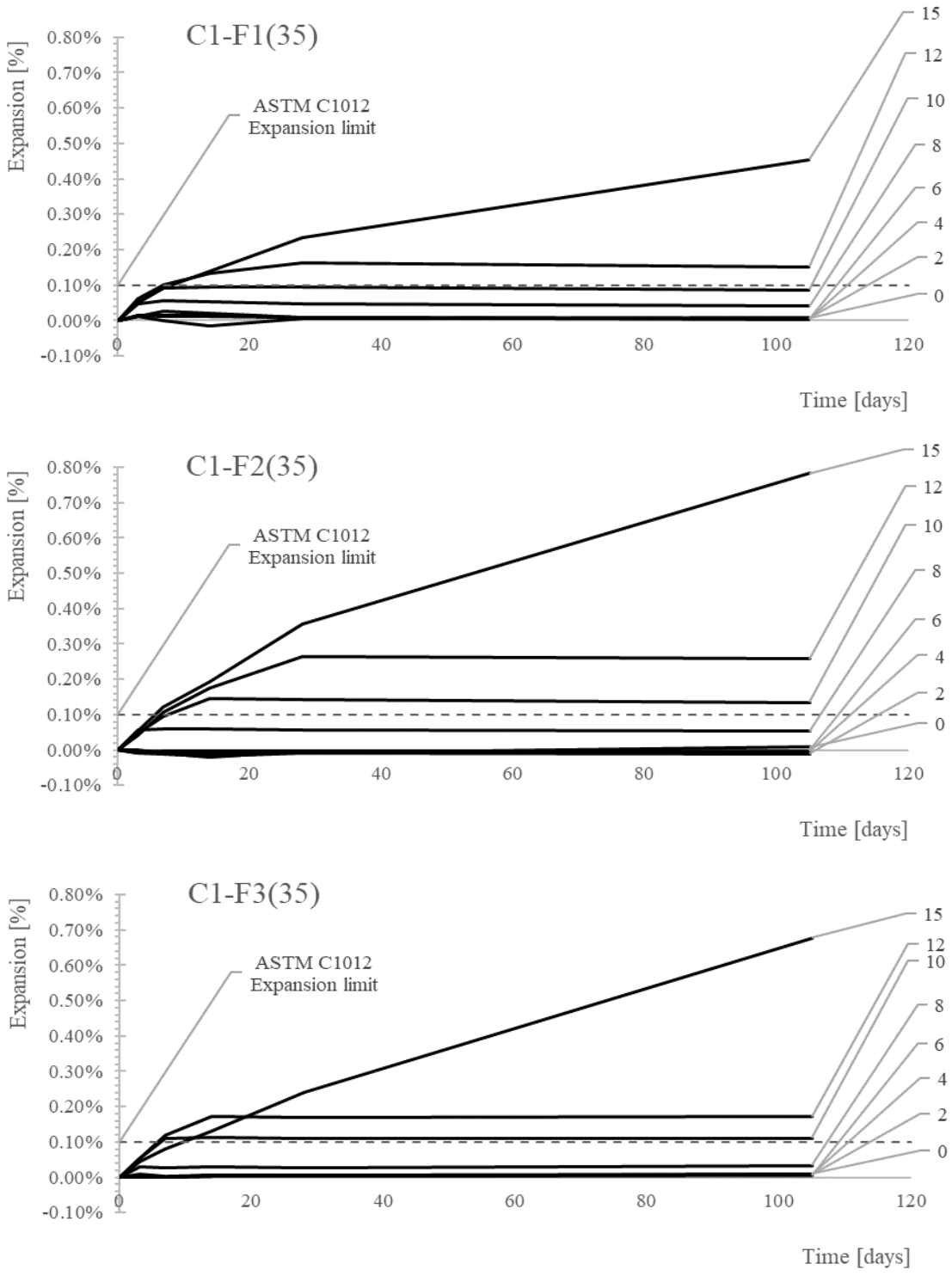

Figure 5.1. LST results for cement C1 with 35% replacement of ashes F1-F3.

Table 5.3. LST results for cement C1 with 20% replacement of ashes F1-F3.

Mix ID	Gypsum [%]	Expansion [days]				
		3	7	14	28	105
C1-F1(20)	0	-0.010%	-0.007%	-0.009%	-0.012%	-0.005%
	2	-0.009%	-0.012%	-0.012%	-0.015%	-0.007%
	4	0.001%	-0.002%	-0.003%	-0.005%	0.001%
	6	-0.004%	-0.007%	-0.007%	-0.008%	-0.001%
	8	0.028%	0.036%	0.037%	0.035%	0.043%
	10	0.010%	0.028%	0.048%	0.078%	0.092%
	12	0.015%	0.031%	0.056%	**0.101%**	**0.243%**
	15	0.012%	0.029%	0.057%	**0.108%**	**0.480%**
C1-F2(20)	0	-0.002%	-0.001%	0.001%	0.001%	0.004%
	2	0.007%	-0.004%	0.000%	0.001%	0.002%
	4	0.002%	0.006%	0.007%	0.005%	0.006%
	6	0.016%	0.014%	0.019%	0.014%	0.016%
	8	0.032%	0.067%	0.069%	0.071%	0.074%
	10	0.028%	0.057%	0.096%	**0.131%**	**0.134%**
	12	0.032%	0.064%	0.092%	**0.159%**	**0.386%**
	15	0.035%	0.069%	**0.101%**	**0.174%**	**0.632%**
C1-F3(20)	0	0.004%	0.002%	0.008%	0.002%	-0.005%
	2	0.009%	0.006%	0.006%	-0.001%	-0.008%
	4	0.005%	0.005%	0.011%	0.006%	0.000%
	6	0.011%	0.012%	0.009%	0.003%	-0.006%
	8	0.023%	0.042%	0.047%	0.046%	0.041%
	10	0.021%	0.038%	0.064%	0.096%	0.096%
	12	0.017%	0.030%	0.050%	**0.119%**	**0.336%**
	15	0.019%	0.040%	0.060%	**0.112%**	**0.459%**

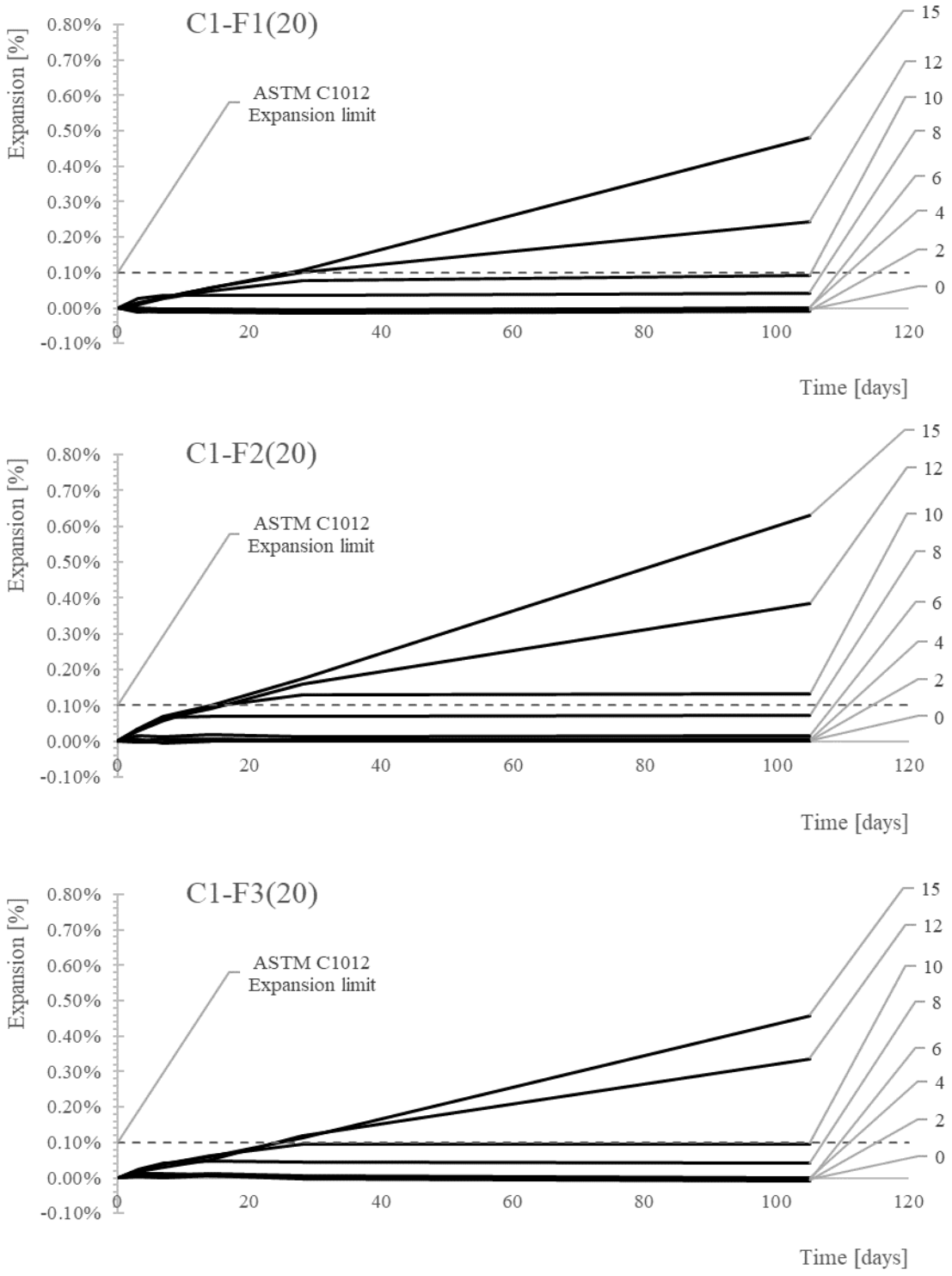

Figure 5.2. LST results for cement C1 with 20% replacement of ashes F1-F3.

Table 5.4. LST results for cement C2 with 35% replacement of ashes F1-F3.

Mix ID	Gypsum [%]	Expansion [days]				
		3	7	14	28	105
C2-F1(35)	0	-0.008%	-0.010%	-0.011%	0.001%	-0.005%
	2	-0.004%	-0.006%	-0.006%	0.004%	-0.002%
	4	-0.002%	-0.004%	-0.004%	0.010%	-0.002%
	6	-0.003%	-0.005%	-0.002%	0.007%	-0.001%
	8	0.022%	0.019%	0.021%	0.028%	0.021%
	10	0.025%	0.043%	0.052%	0.061%	0.049%
	12	0.028%	0.051%	0.073%	0.098%	0.088%
	15	0.024%	0.045%	0.085%	**0.153%**	**0.261%**
C2-F2(35)	0	-0.009%	-0.012%	-0.012%	-0.004%	-0.007%
	2	0.002%	0.000%	-0.001%	0.005%	0.003%
	4	0.004%	0.018%	0.001%	0.005%	0.005%
	6	0.005%	0.016%	0.003%	0.014%	0.008%
	8	0.044%	0.048%	0.044%	0.054%	0.046%
	10	0.055%	0.094%	**0.103%**	**0.104%**	**0.101%**
	12	0.037%	0.069%	**0.114%**	**0.221%**	**0.494%**
	15	0.055%	0.096%	**0.147%**	**0.250%**	**0.532%**
C2-F3(35)	0	-0.005%	-0.004%	-0.002%	0.000%	0.006%
	2	-0.005%	-0.004%	-0.001%	-0.001%	0.005%
	4	-0.004%	-0.002%	0.000%	0.001%	0.005%
	6	-0.001%	0.000%	0.003%	0.003%	0.008%
	8	0.019%	0.020%	0.023%	0.022%	0.028%
	10	0.035%	0.064%	0.068%	0.068%	0.072%
	12	0.037%	0.071%	**0.111%**	**0.118%**	**0.121%**
	15	0.033%	0.062%	**0.102%**	**0.193%**	**0.398%**

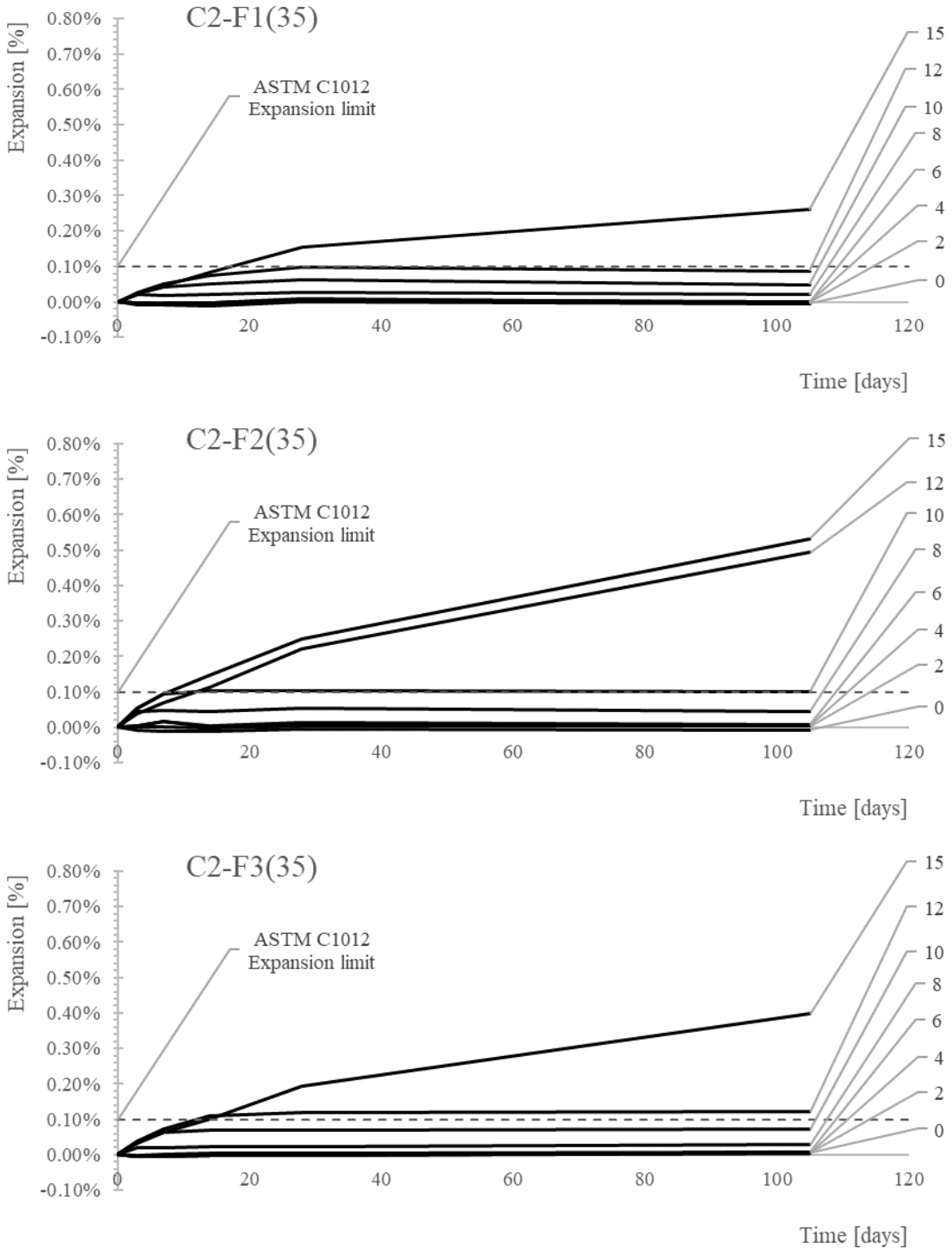

Figure 5.3. LST results for cement C2 with 35% replacement of ashes F1-F3.

Table 5.5. LST results for cement C2 with 20% replacement of ashes F1-F3.

Mix ID	Gypsum [%]	Expansion [days]				
		3	7	14	28	105
C2-F1(20)	0	-0.002%	-0.002%	-0.004%	-0.002%	-0.001%
	2	-0.002%	-0.005%	0.000%	-0.001%	0.000%
	4	0.002%	0.003%	0.000%	0.002%	0.004%
	6	0.006%	0.005%	0.011%	0.005%	0.009%
	8	0.019%	0.026%	0.027%	0.027%	0.030%
	10	0.015%	0.026%	0.042%	0.056%	0.056%
	12	0.014%	0.028%	0.038%	0.066%	**0.139%**
	15	0.016%	0.036%	0.049%	0.086%	**0.240%**
C2-F2(20)	0	-0.004%	-0.006%	-0.008%	-0.005%	-0.008%
	2	-0.005%	-0.004%	-0.003%	-0.017%	-0.007%
	4	-0.006%	-0.006%	-0.007%	-0.007%	-0.006%
	6	0.001%	-0.001%	-0.002%	-0.008%	-0.002%
	8	0.021%	0.026%	0.030%	0.014%	0.025%
	10	0.014%	0.045%	0.077%	0.050%	0.056%
	12	0.016%	0.040%	0.064%	0.081%	**0.120%**
	15	0.015%	0.037%	0.059%	0.096%	**0.329%**
C2-F3(20)	0	-0.009%	-0.009%	-0.014%	-0.007%	-0.005%
	2	-0.009%	-0.002%	-0.010%	-0.003%	0.000%
	4	-0.008%	-0.004%	-0.008%	-0.002%	0.001%
	6	-0.009%	-0.003%	-0.007%	0.000%	0.001%
	8	-0.013%	0.000%	-0.007%	0.001%	0.002%
	10	0.001%	0.023%	0.032%	0.061%	0.066%
	12	0.005%	0.025%	0.038%	0.074%	**0.119%**
	15	0.012%	0.031%	0.044%	0.084%	**0.270%**

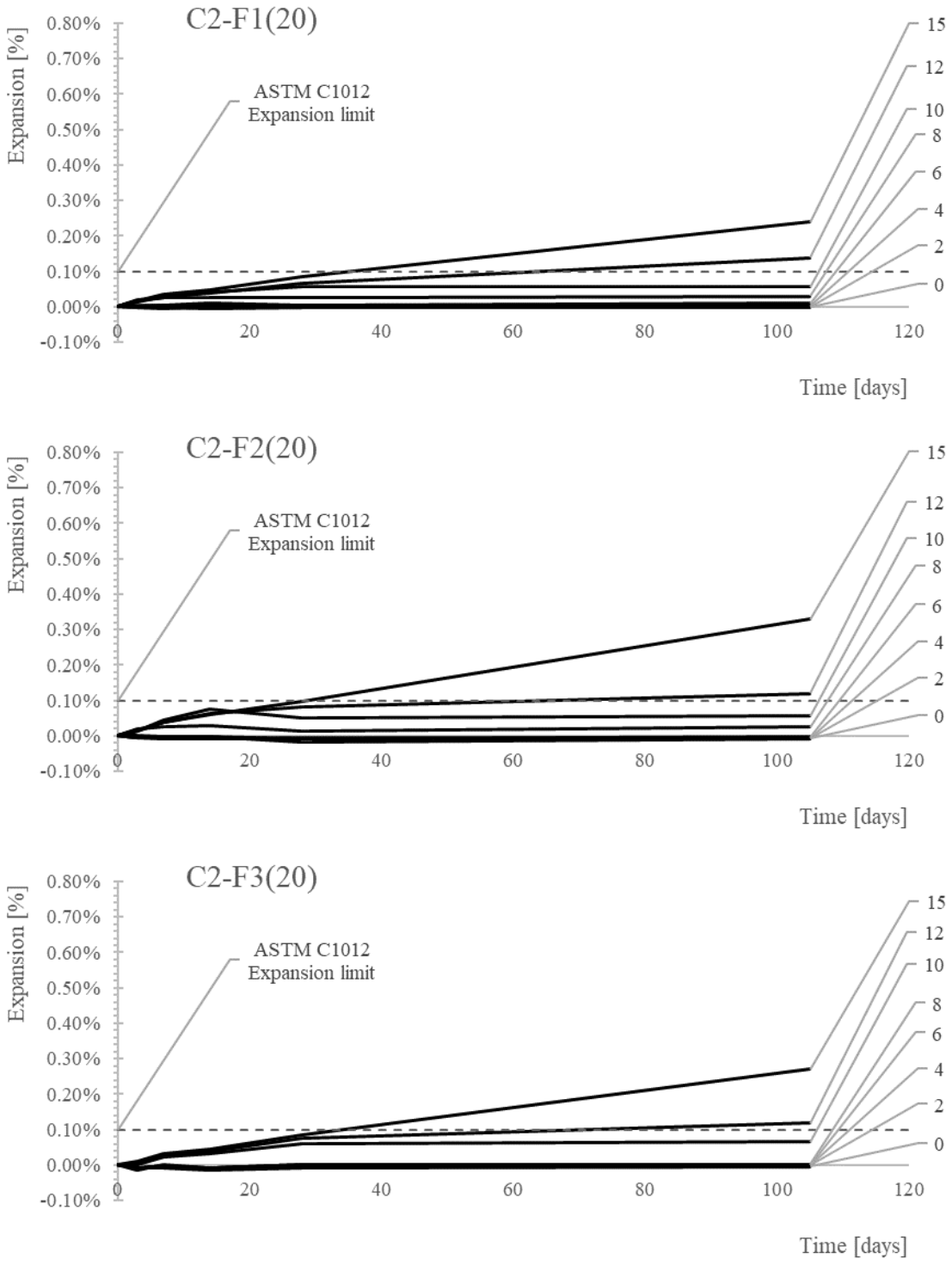

Figure 5.4. LST results for cement C2 with 20% replacement of ashes F1-F3.

5.2.2 Discussion

The results shown in **Tables 5.2-5.5** and plotted in **Figures 5.1-5.4** indicate a clear effect of the gypsum additive on the mortar. As the gypsum quantities are increased the expansion of the mortar also increases. In general, once the gypsum quantities exceed 6%-8% the mortar bars showed an increase in expansion.

The types of cement used in the mixture affected the expansion results; mixtures containing cement C1 expanded more than mixtures containing C2. The increase in expansion may be due to the increase in available sulfates. The XRF results shown in **Table 2.2** indicate an approximate 35% difference in SO_3 content between the two cements used in this study.

The type of fly ash and level of replacement affected the expansion results of LST. mixtures containing fly ash F2 expanded more than mixtures containing ash F3, both of which (generally) expanded more than mixture containing ash F1. In terms of mixture proportions, mixtures containing 35% fly ash replacement (of either C1 or C2) showed a higher likelihood of expanding beyond the 0.1% than those mixtures which contained 20% replacement. As with the cements, the increase in expansion (based on the ash used) is likely due to the sulfate content within the ash. The XRF data shown in **Table 2.1** indicates that the SO_3 content in ascending order is F1< F3 < F2. Additionally, the quantity of amorphous SO_3 of the respective fly as shown in **Figure 3.1** follows a similar trend and may have been a contributing factor.

As stated previously the expansions that occurred are all likely due to the total sulfate content. The sulfates are reacting with C_3A to form AFt and AFm phases. The formation of AFt and AFm as a function of gypsum content will be investigated in the following sections of this thesis.

5.3 ISOTHERMAL CALORIMETRY AND MAXIMUM HEAT

The heat evolution (heat of hydration) curve of cement binders is often sub-divided into five stages which are numbered in **Figure 5.5** and briefly described here:

1. Initial period: dissolution; ettringite (AFt) formation
2. Induction period: increase in Ca^{2+} concentration
3. Acceleration period: rapid formation of C-S-H and CH
4. Retardation period: monosulfoaluminate (AFm) formation and gypsum depletion.
5. Steady State period: continuation of hydration product formation

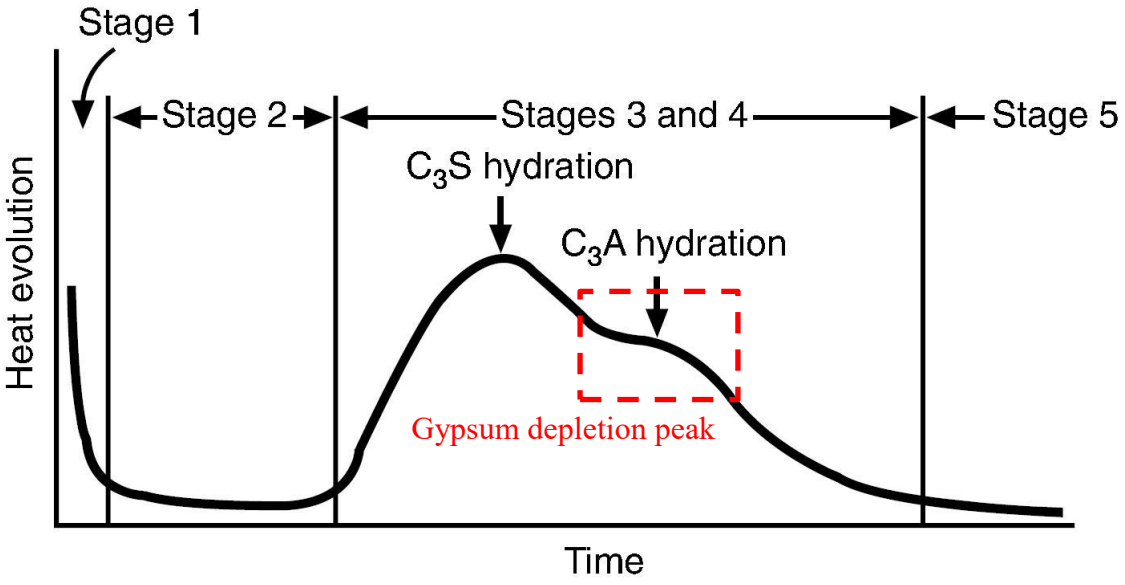

Figure 5.5. Heat evolution as a function of time [2]. Additional annotations (in red) by the author of this thesis.

5.3.1 Results

Isothermal calorimetry was performed to determine the effects of the gypsum on the heat of hydration, and cumulative heat produced by the neat cement paste. The goal was to examine the point of sulfate depletion (on the heat of hydration curve) and cumulative heat (area under the heat of hydration curve), and thereafter find correlations to the expansion results from LST and hydration product formation using XRD analysis. The heat of hydration and maximum heat produced of each mix are presented in **Figures 5.7-5.18**. The heat of hydration curves exhibited variable behavior in terms of the location of sulfate depletion peak; therefore, the results that follow only include heat of hydration data for mixtures in which the sulfate depletion peak was observable within 7 days. Additionally, the heat of hydration curves do not show the first three hours of hydration that were recorded by the calorimeter. Typical heat of hydration and cumulative heat curves will be shown and discussed in correlation to the results of this research study in this and proceeding sections.

The maximum heat curves were plotted by recording the value of power (in J/g) at 168 hours (the end of testing) from the cumulative heat curve (**Figure 5.6)** and plotting the value vs. the gypsum content of the respective mixture. An example of how the maximum heat curve is constructed will follow.

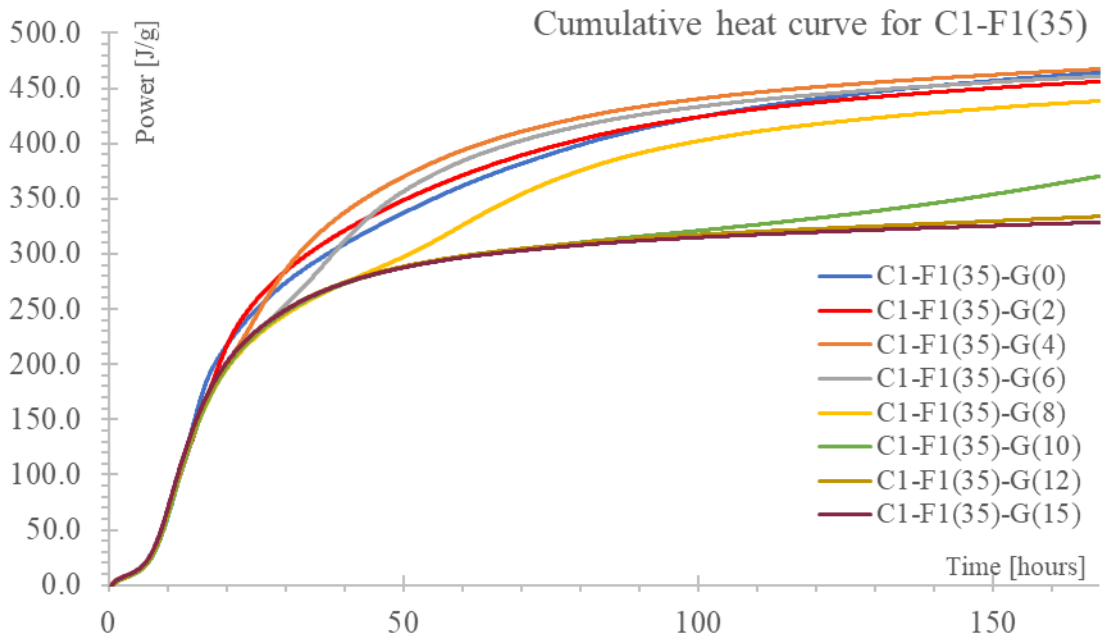

Figure 5.6. Cumulative heat results from isothermal calorimetry of mixture C1-F1(35).

From **Figure 5.6** above a table can be constructed (**Table 5.6**) which includes the heat output at the end of the test, and the gypsum content which produced the respective amount of heat. When the values are plotted (independent variable gypsum and dependent variable max heat) the maximum heat curve (**Figure 5.7**) results**.**

Table 5.6. Maximum heats and corresponding gypsum contents for mix C1-F1(35).

Mix ID: C1-F1(35)								
Gypsum [%]	0	2	4	6	8	10	12	15
Max heat [J/g]	462	454	465	459	436	368	331	327

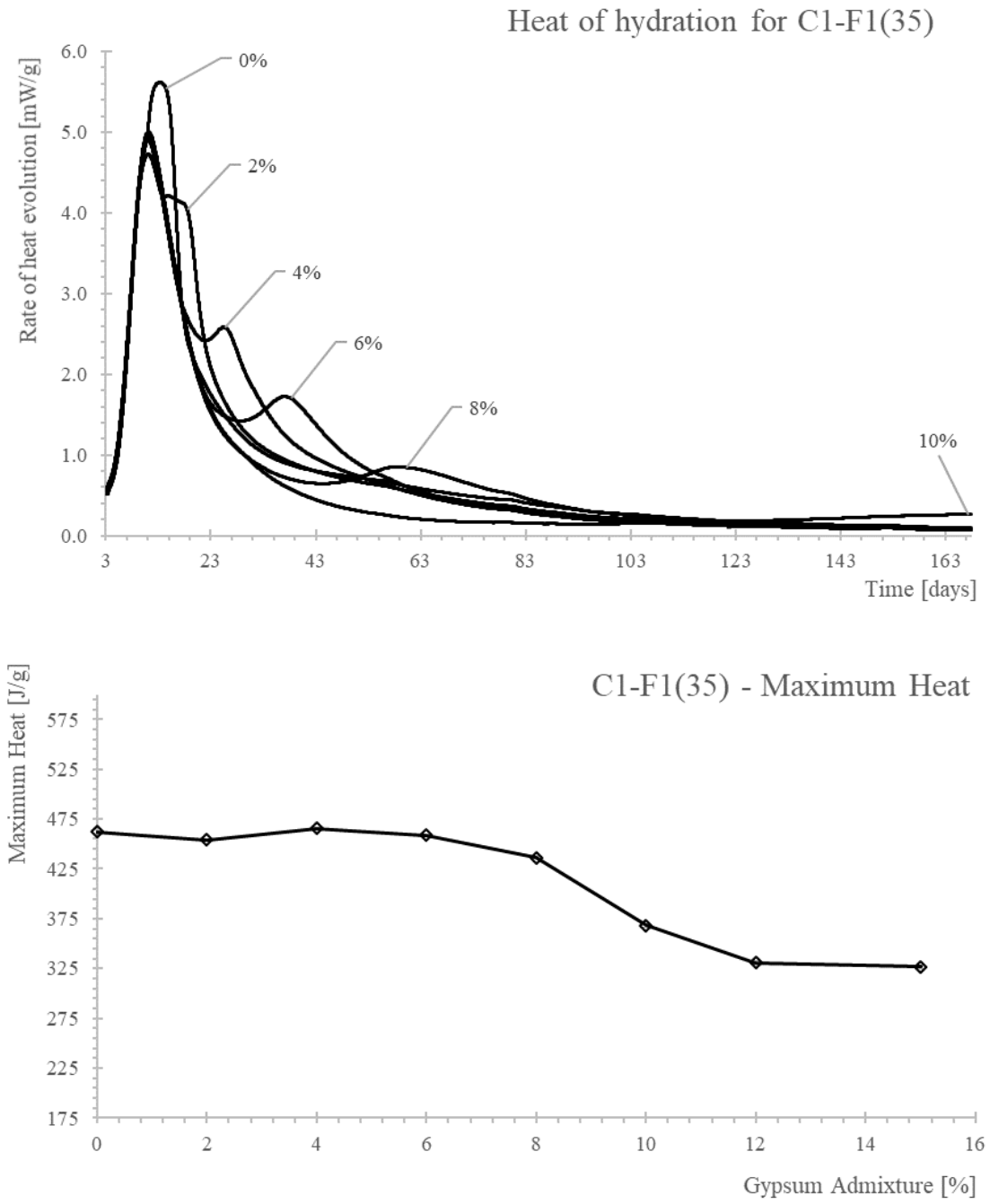

Figure 5.7. Heat of hydration and maximum heat curves for mixture C1-F1(35).

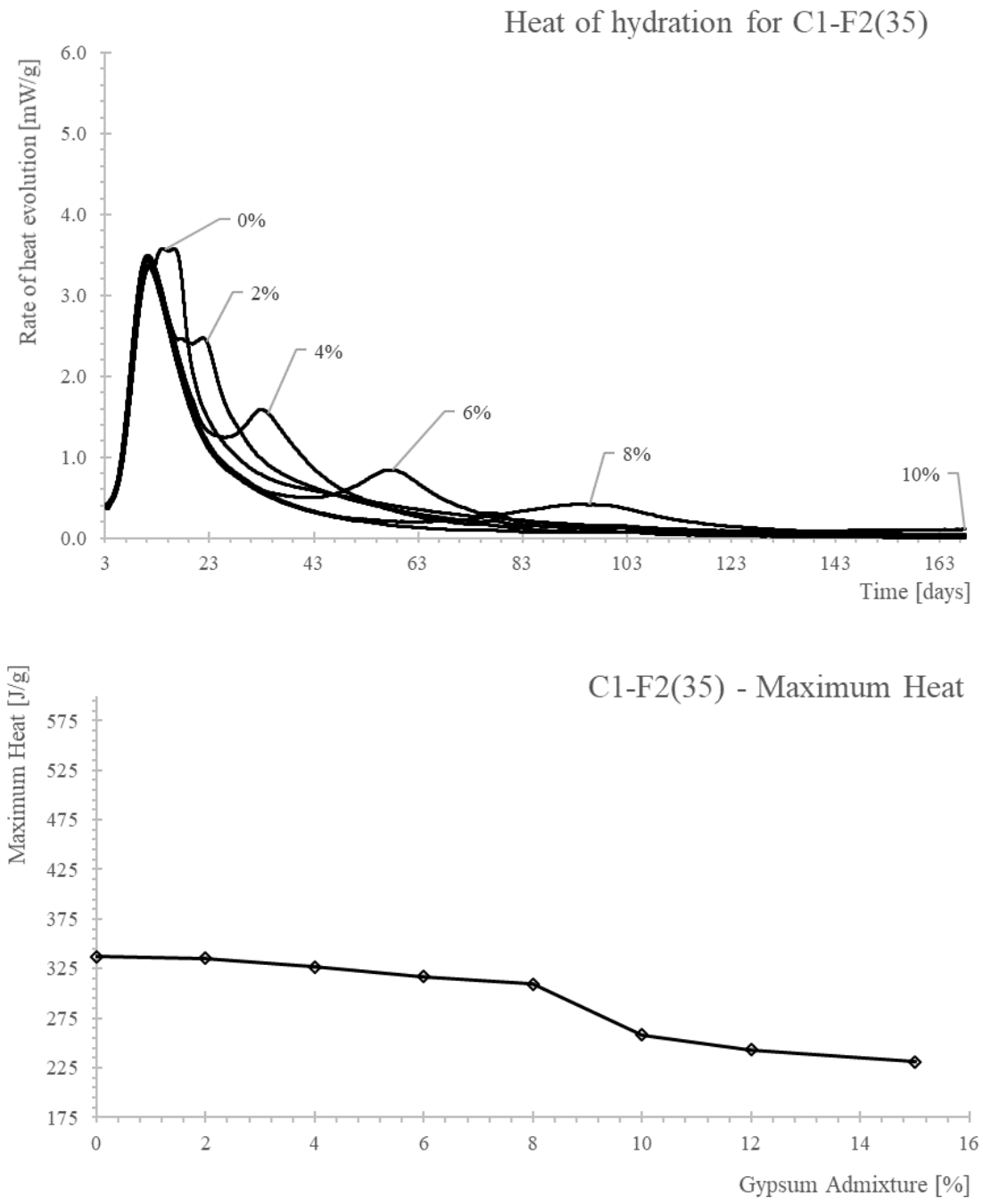

Figure 5.8. Heat of hydration and maximum heat curves for mixture C1-F2(35).

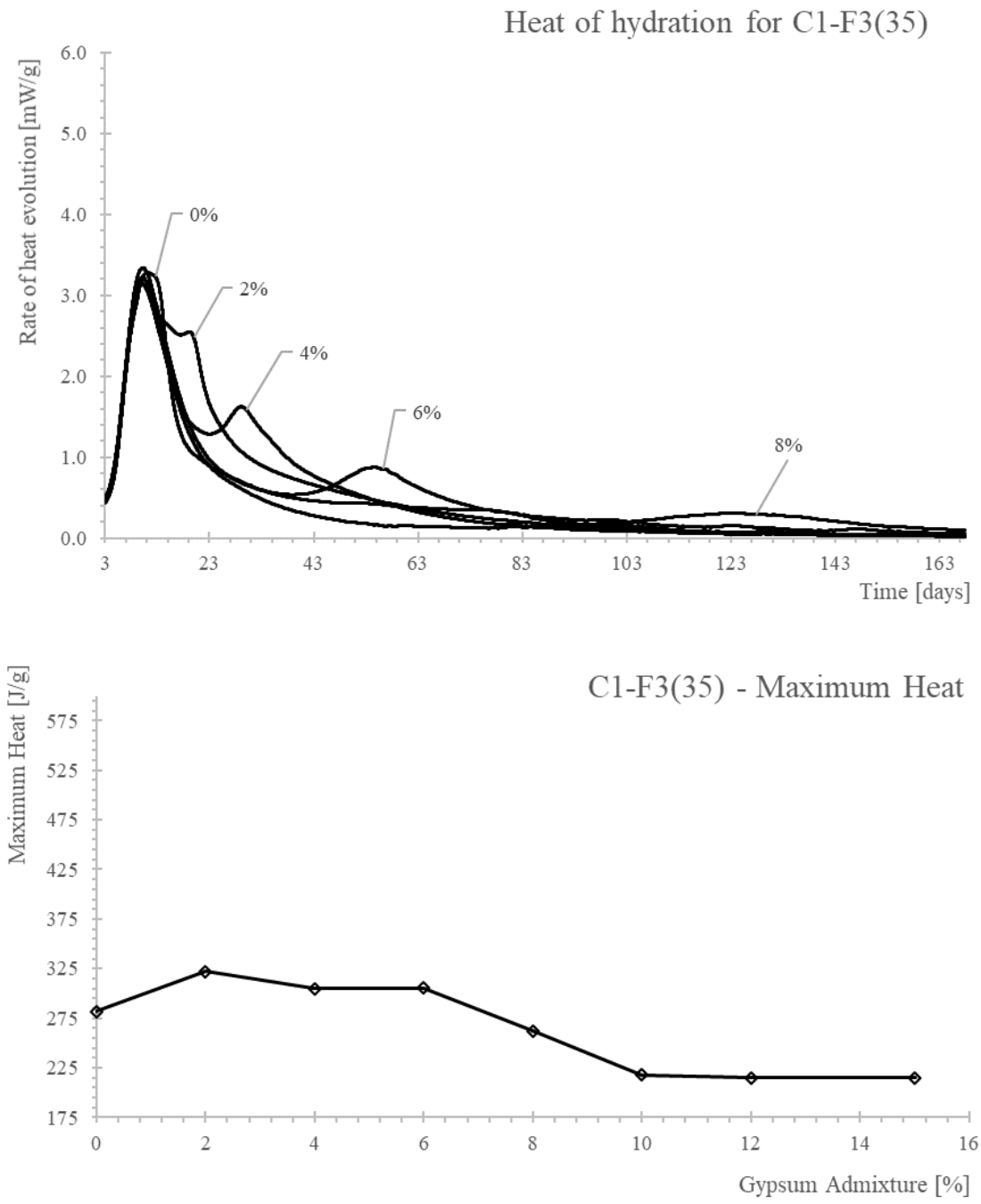

Figure 5.9. Heat of hydration and maximum heat curves for mixture C1-F3(35).

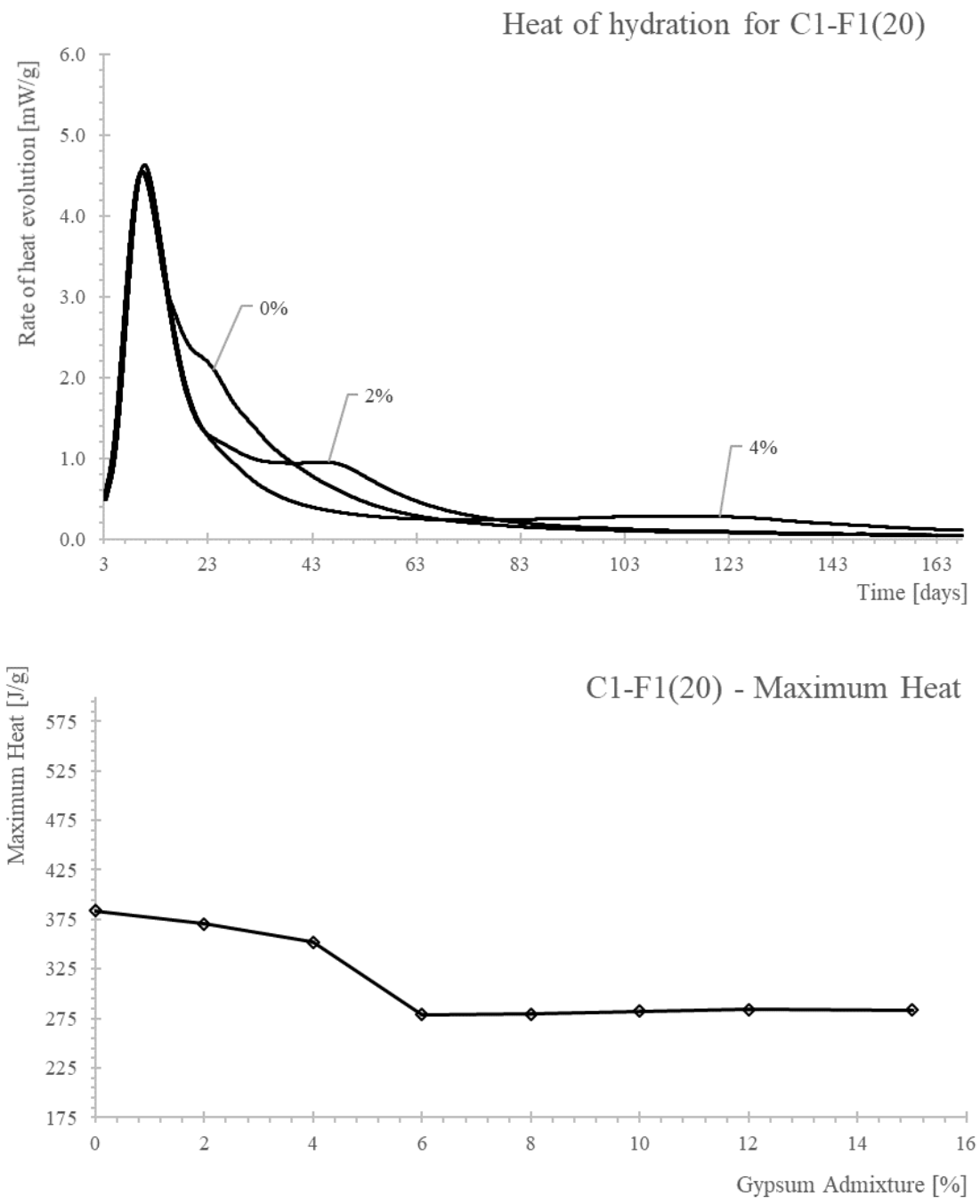

Figure 5.10. Heat of hydration and maximum heat curves for mixture C1-F1(20).

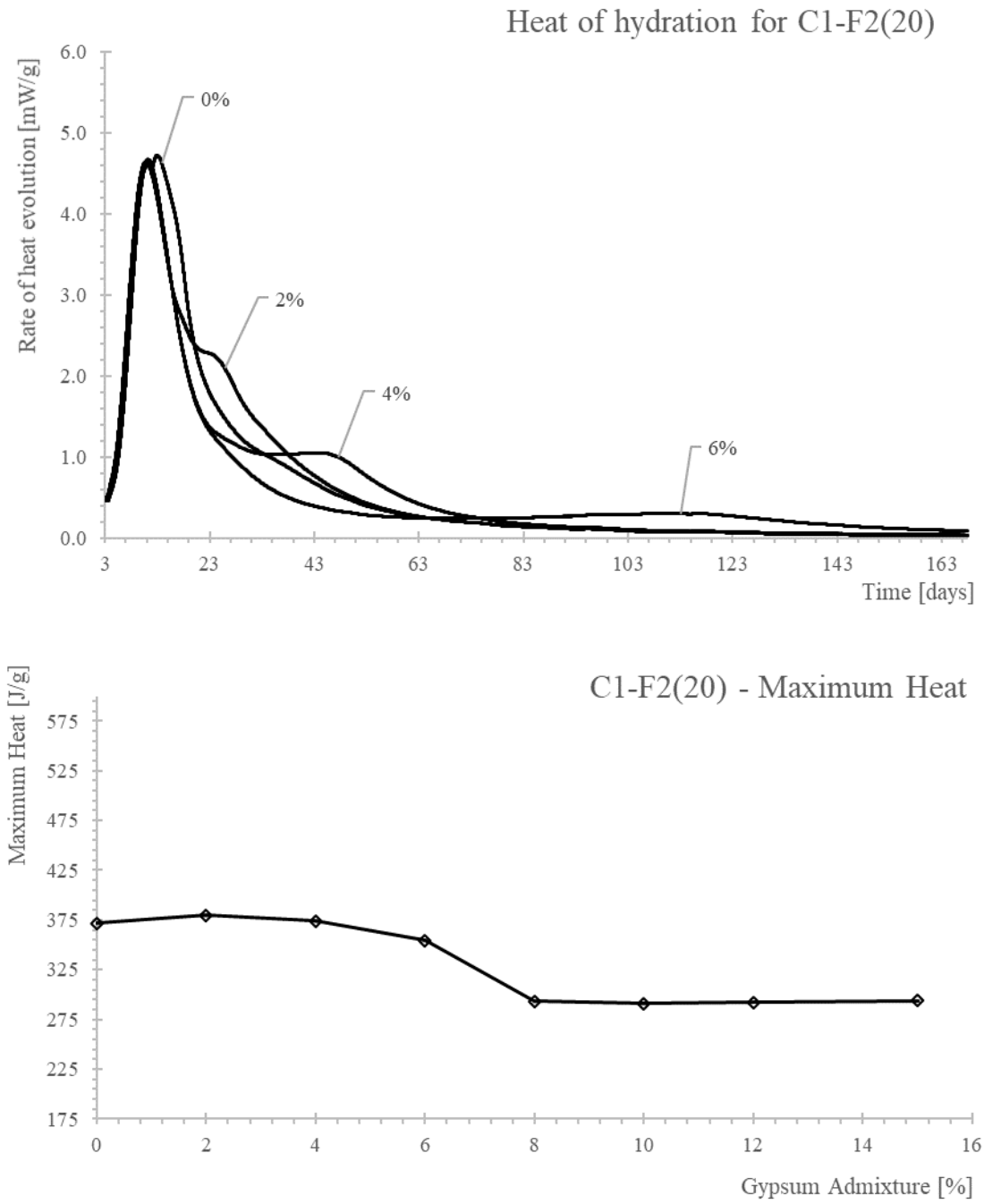

Figure 5.11. Heat of hydration and maximum heat curves for mixture C1-F2(20).

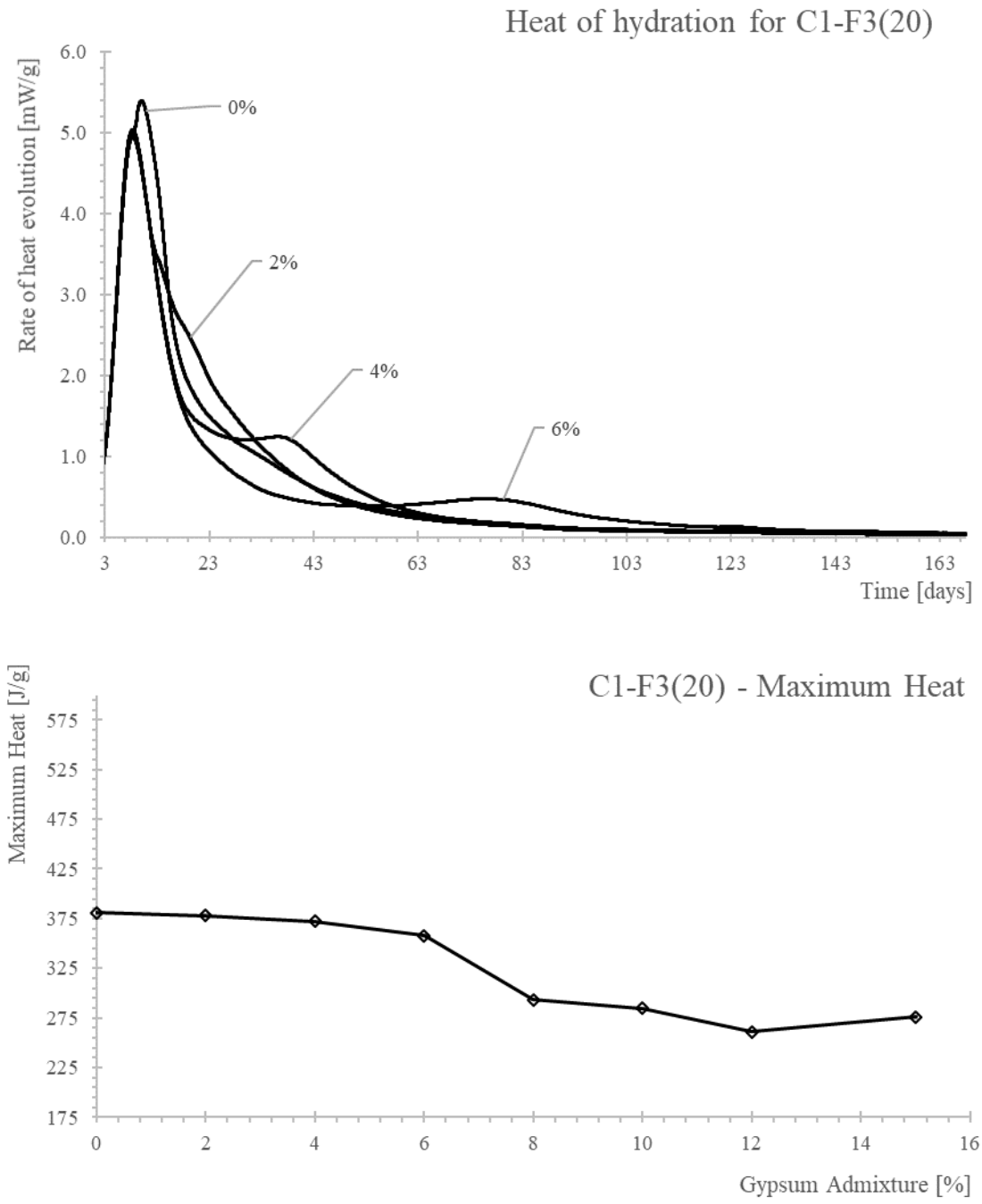

Figure 5.12. Heat of hydration and maximum heat curves for mixture C1-F3(20).

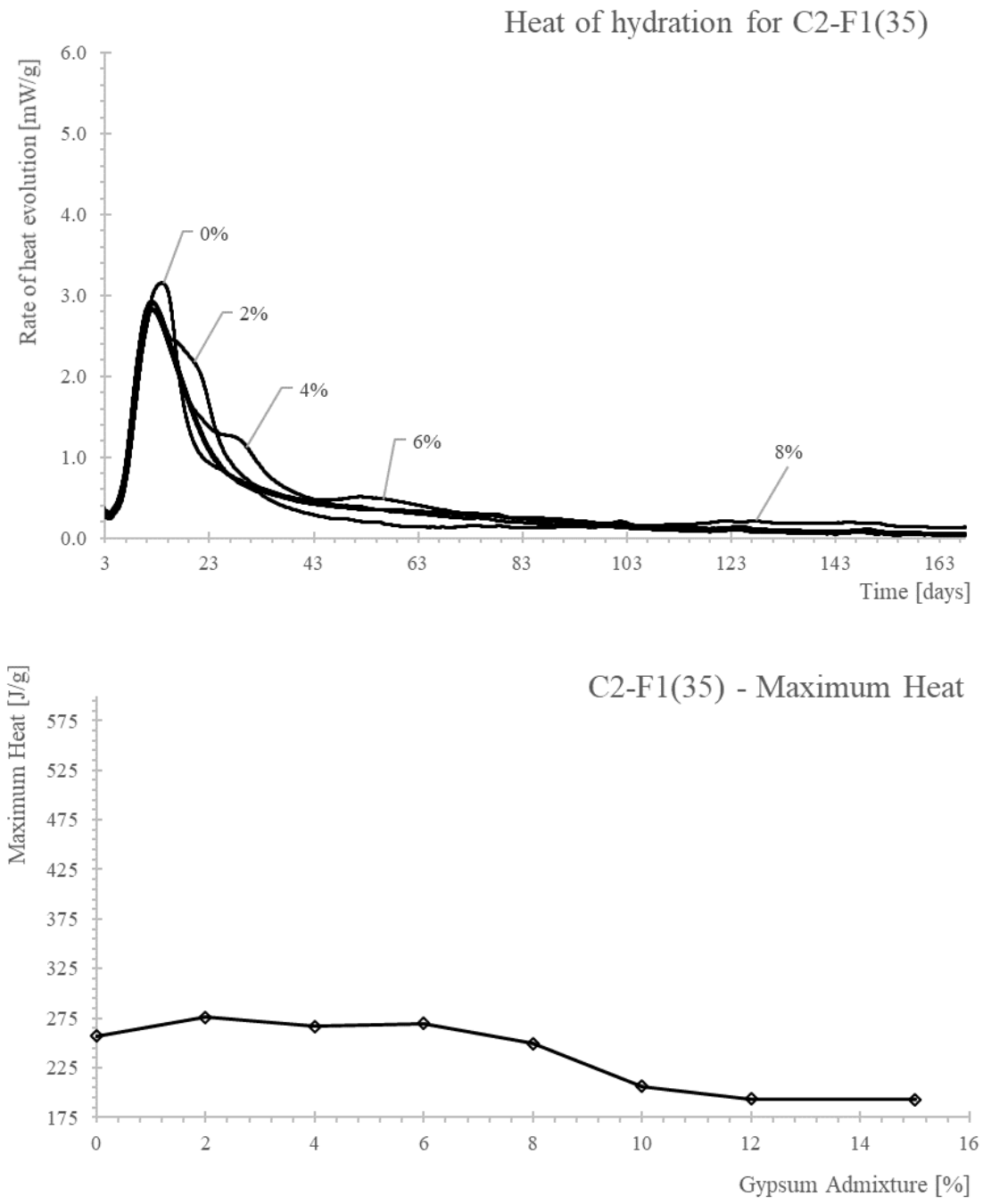

Figure 5.13. Heat of hydration and maximum heat curves for mixture C2-F1(35).

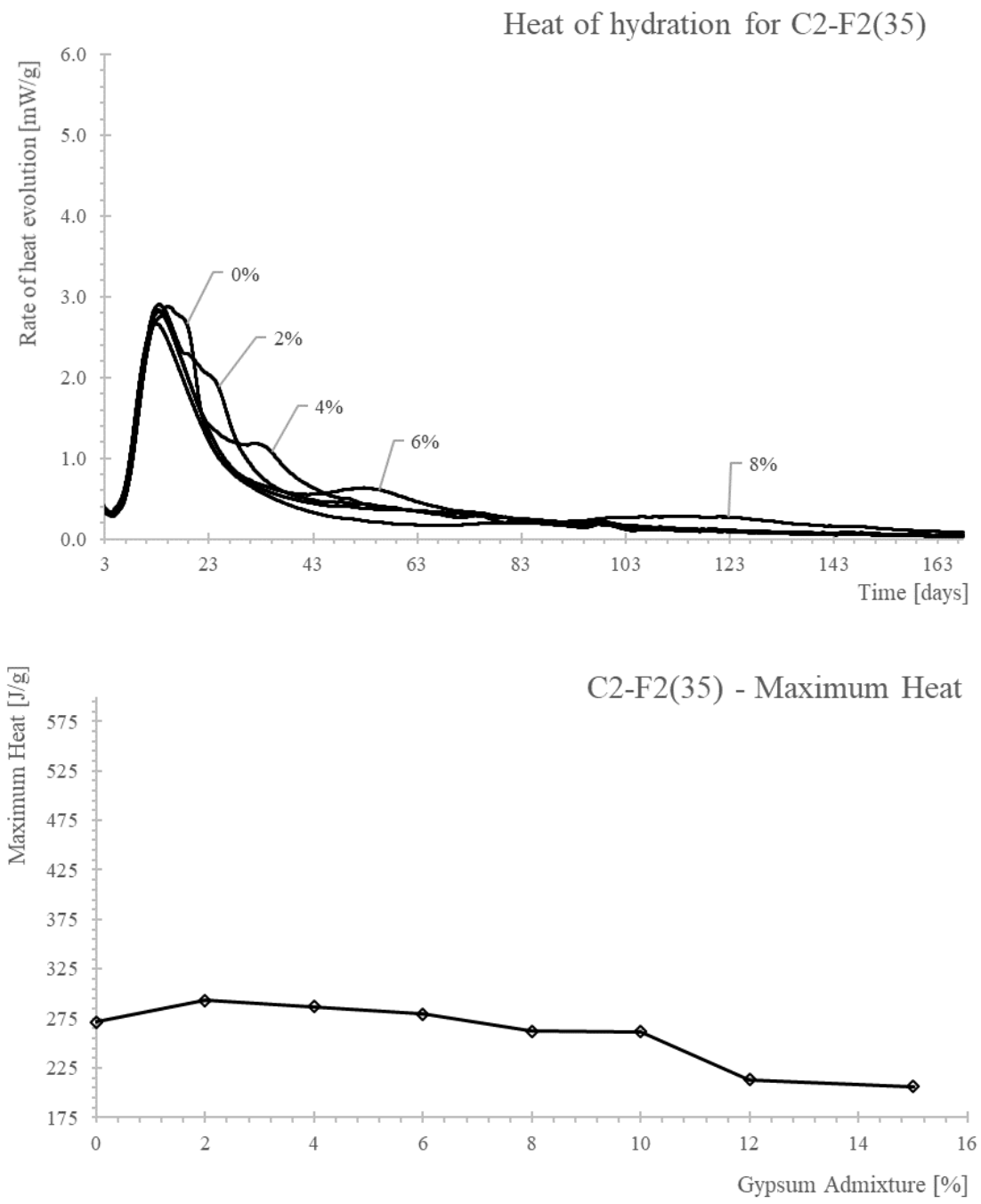

Figure 5.14. Heat of hydration and maximum heat curves for mixture C2-F2(35).

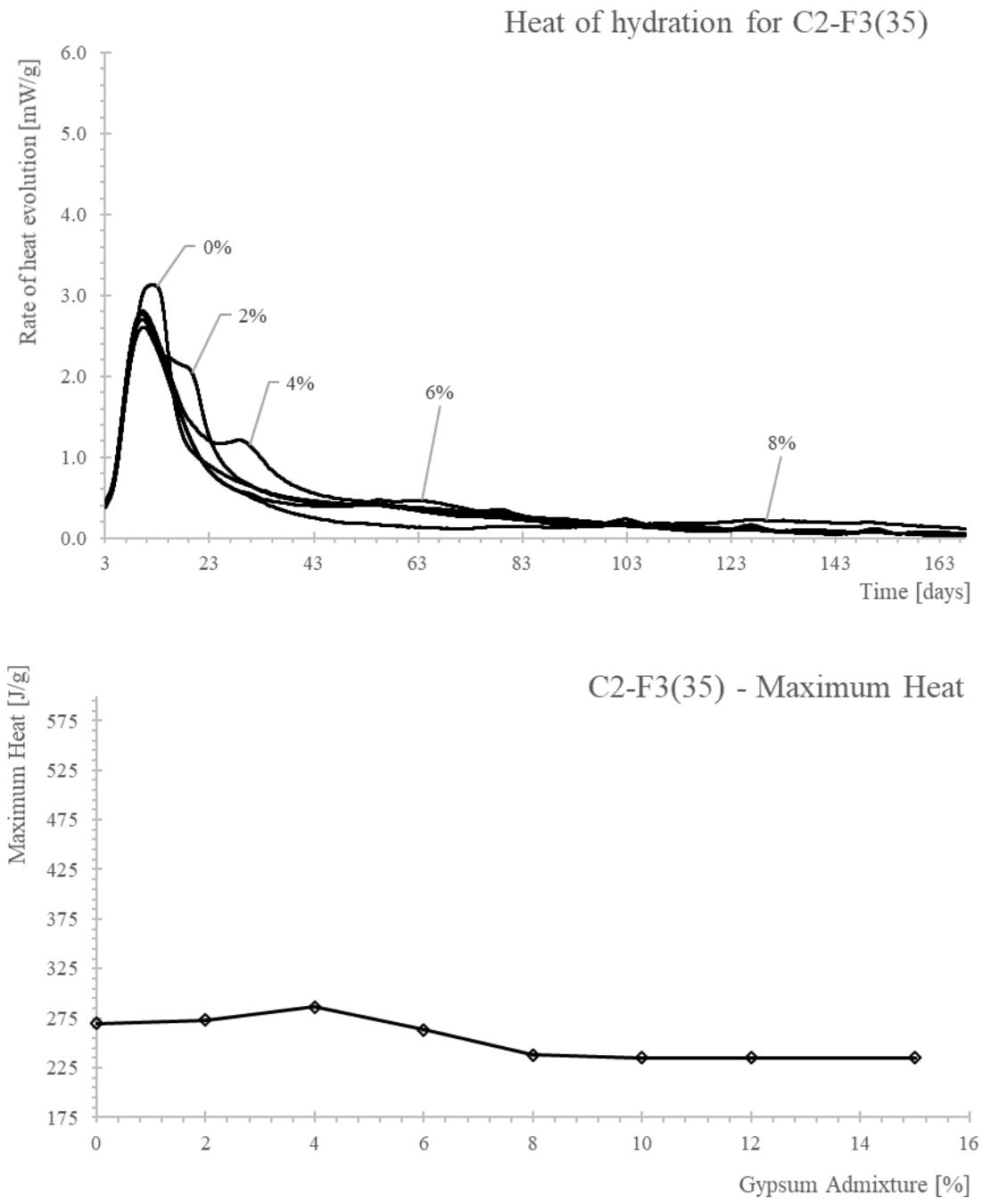

Figure 5.15. Heat of hydration and maximum heat curves for mixture C2-F3(35).

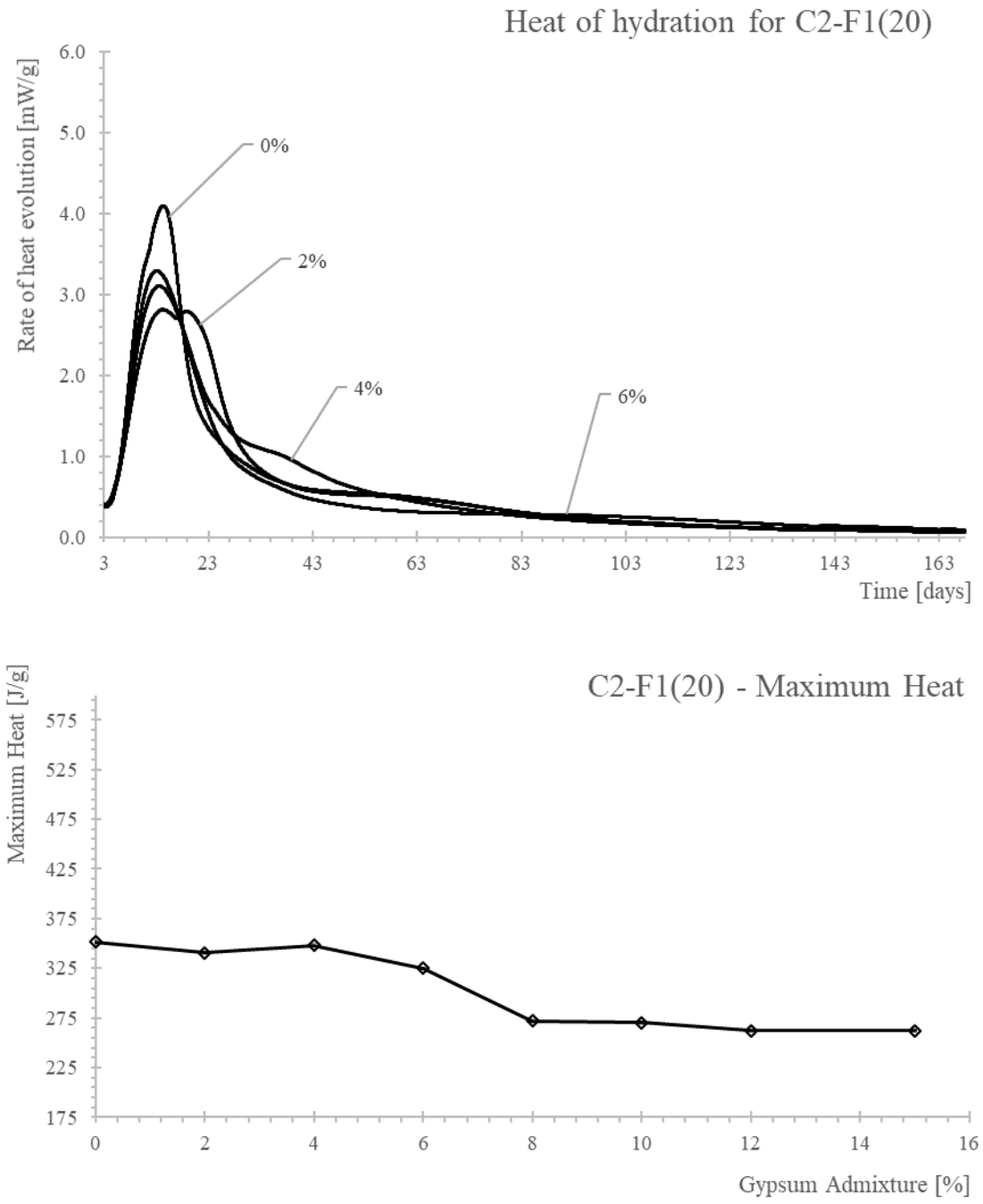

Figure 5.16. Heat of hydration and maximum heat curves for mixture C2-F1(20).

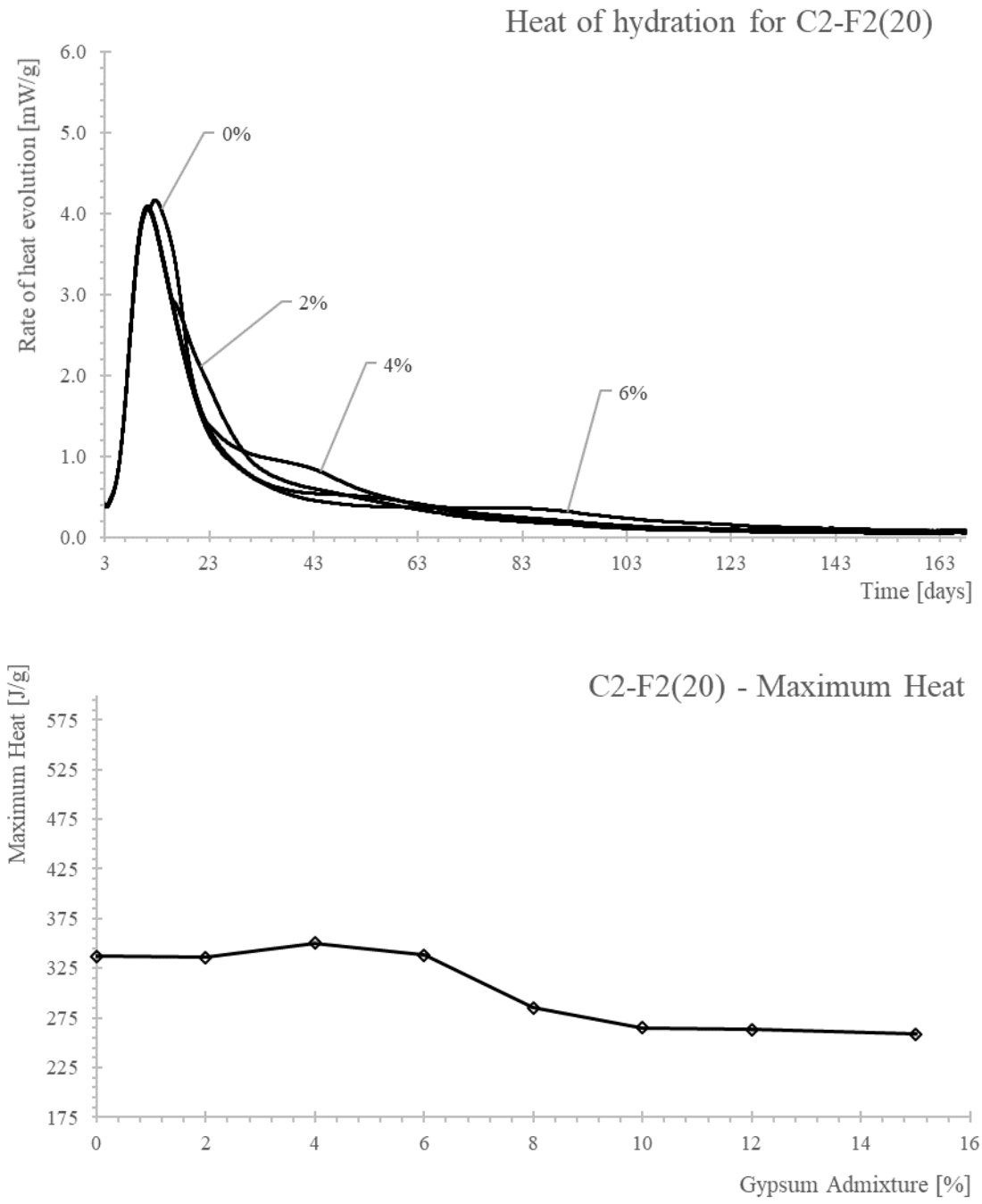

Figure 5.17. Heat of hydration and maximum heat curves for mixture C2-F2(20).

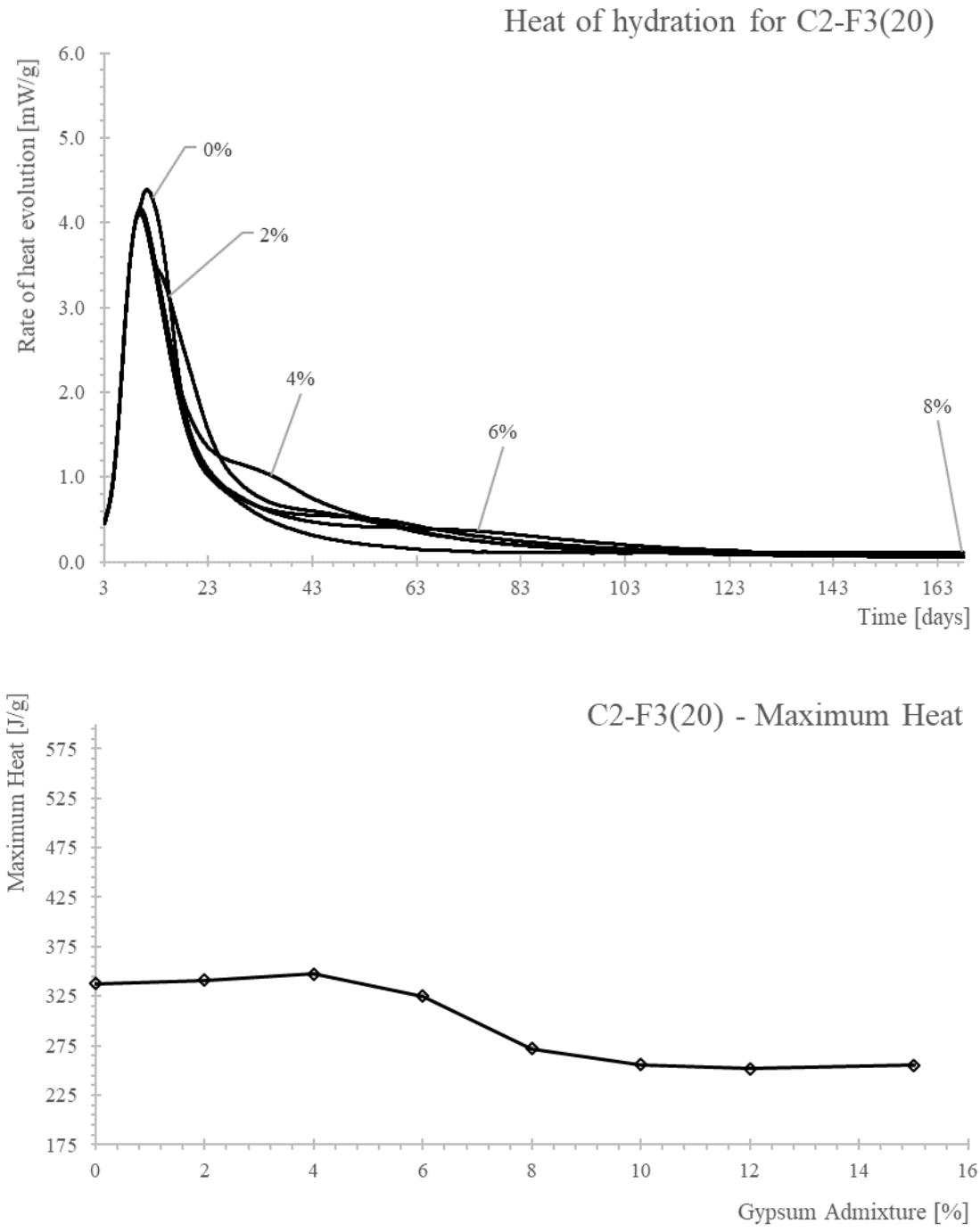

Figure 5.18. Heat of hydration and maximum heat curves for mixture C2-F3(20).

5.3.2 Discussion

Researchers have dedicated studies to the effects that SCM's [24] and gypsum [4, 25, 26] impart on the heat of hydration curve, noting a definitive impact on the characteristic shape of the curve and rate of heat evolution. Thus, the heat of hydration curves shown in **Figures 5.7-5.18** indicate multiple points of interest in relation to the aforementioned studies.

When gypsum and C_3A react during the early ages of cement hydration, the reaction produces a change to the shape of the heat of hydration curved (named by Lerch the "gypsum depletion peak") during stage 4 as shown in **Figure 5.5** as well as **Figures 5.19** and **5.20**.

Research [27, 28] has shown through in-situ QXRD in conjunction with heat of hydration testing that the time at which the gypsum depletion peak occurs is coincident with accelerated AFt precipitation and renewed dissolution of C_3A. With this study in mind, one can infer from **Figures 5.7-5.18** at what time the onset of renewed C_3A dissolution occurred and when the precipitation of AFm begins for the respective mixtures in this research study. The implication being that, one can simply analyze the heat of hydration curve, and determine when AFt and AFm phases in the mixture are forming.

Understanding the time at which AFt and AFm may form provides insight into how a mixture will perform in terms of sulfate resistance. If AFt forms at later ages (when the cement binder is completely set) damage in the form of expansive cracking to the paste matrix will likely be incurred, due to the expansive nature in which AFt forms. The expansive cracking from the late formation of AFt, may allow for the ingress of external sulfates and possibly exacerbate the layering effect researched by [17] that commonly occurs as part of the external sulfate attack mechanism.

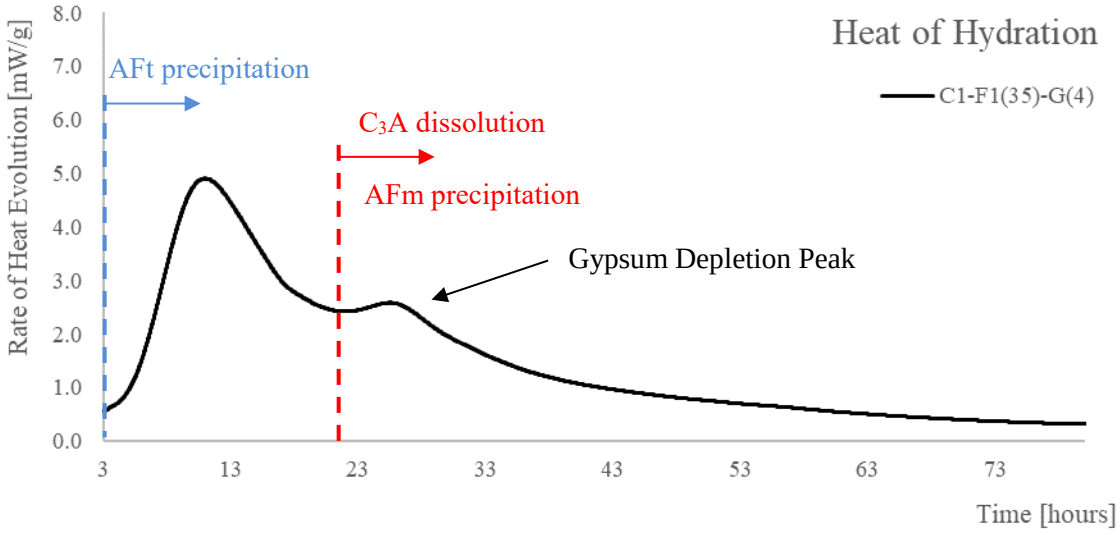

Figure 5.19. Typical Heat of hydration curve.

Lerch [25] in his early research on the study of the appropriate dosage of gypsum for a given cement/clinker stated the following:

> *A properly retarded cement can be considered as one which contains the minimum quantity of gypsum required to give a curve that shows two cycles of ascending and descending rates of heat liberation and that shows no appreciable change with larger additions of gypsum during the first 30 hours of hydration.*

A plot showing a mixture which meets Lerch's guidelines is shown below in **Figure 5.20**.

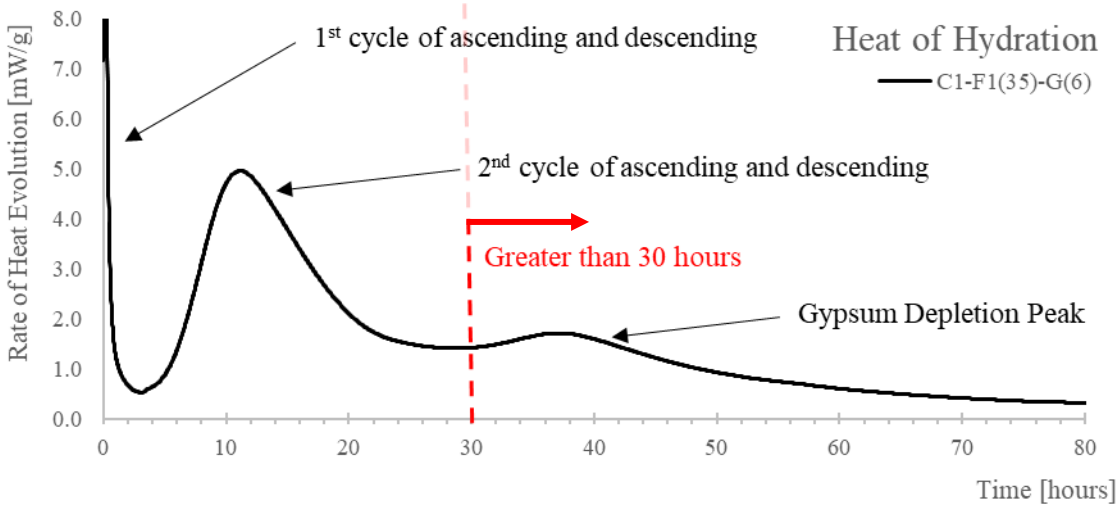

Figure 5.20. Heat of hydration curve meeting Lerch's guidelines.

Given Lerch's guidelines, **Table 5.7** has been prepared to show which mixtures in this study were under-sulfated (u), properly sulfated (**X**), or were over-sulfated (o). Given that mixtures used in this study were prepared in approximately even intervals of 2% gypsum additive, some of the properly sulfated mixtures may have fallen within a range, therefore this is reflected in the provided values shown in **Table 5.7**.

It has been stated by researchers [4] that modern cements differ from those in which Lerch was studying in terms of Blaine fineness (amongst other parameters). That is, most modern cements have a finer particle size than those which Lerch studied. Hydration kinetics are affected by the fineness of the cement (also shown by Lerch) thereby altering the shape of the heat of hydration curve. The author of this thesis has taken note of this and has nonetheless elected to analyze the data with Lerch's guidance in mind.

Table 5.7. Comparison of heat of hydration performance to Lerch's guidelines.

	Gypsum [%]	0	2	4	6	8	10	12	15
Mix ID	C1-F1(35)	u	u	u	**X**	**X**	o	o	o
	C1-F2(35)	u	u	u	**X**	o	o	o	o
	C1-F3(35)	u	u	u	**X**	o	o	o	o
	C1-F1(20)	u	**X**	**X**	o	o	o	o	o
	C1-F2(20)	u	u	**X**	**X**	o	o	o	o
	C1-F3(20)	u	u	**X**	**X**	o	o	o	o
	C2-F1(35)	u	u	**X**	**X**	o	o	o	o
	C2-F2(35)	u	u	**X**	**X**	o	o	o	o
	C2-F3(35)	u	u	**X**	**X**	o	o	o	o
	C2-F1(20)	u	u	**X**	**X**	o	o	o	o
	C2-F2(20)	u	u	**X**	**X**	o	o	o	o
	C2-F3(20)	u	u	**X**	**X**	o	o	o	o

Note: u = under-sulfated, **X** = properly sulfated, o = over-sulfated

From the data shown in **Table 5.7** it can be observed that according to Lerch the proper amount of gypsum addition for most mixtures would be in the range of 4% - 6% for the materials and replacement values used in this study. Mixtures deemed properly sulfated here will be analyzed in comparison with other data collected in this study to be discussed in later portions of this thesis.

An ascending (1), primary plateauing (2), descending (3), and secondary plateauing (4) pattern (example shown in **Figure 5.21**) emerges when examining the maximum heat curves shown in **Figures 5.7-5.18.** Researchers [26] have found that higher amounts of heat produced during hydration (from the cumulative heat curve) tend to correlate with higher strength gain at earlier ages. Thus, when observing the maximum heat curves shown in **Figures 5.7-5.18** one can assume mixtures with the highest relative heat for the given mixture are more likely to achieve higher early strength. Unfortunately, strength gain data was not properly collected and kept track of during this research and cannot be presented here. However, it is noted that mixtures containing nominally greater than 10% gypsum content generally took between 7-9 days to achieve a compressive strength of 20 ± 1 MPa (2900 ± 145 psi).

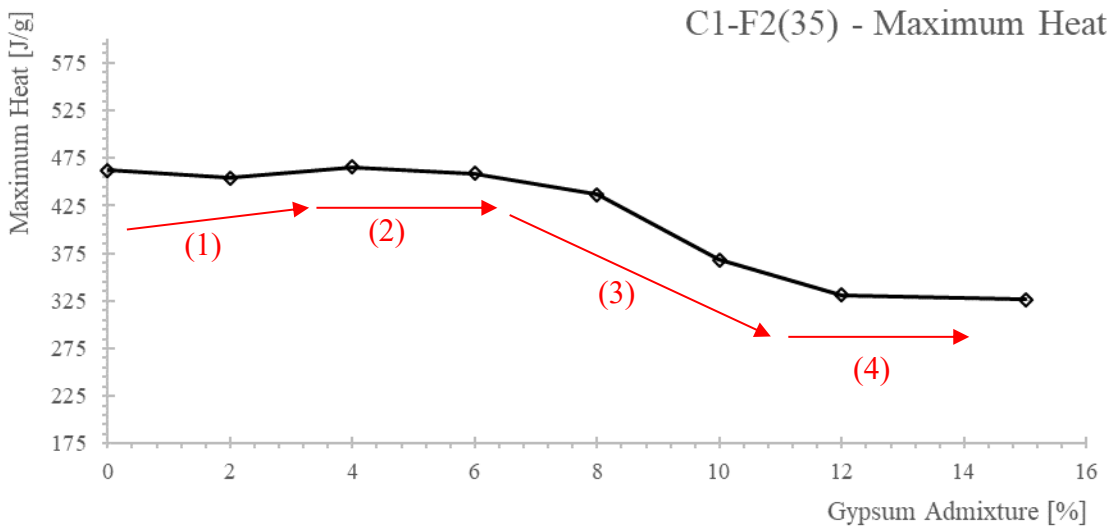

Figure 5.21. Typical behavior observed in the maximum heat curves.

An additional pattern emerged when correlating the maximum heat curve to the QXRD analysis, and LST results that will be discussed in section **5.6** of this thesis.

5.4 QUALITATIVE AND QUANTITATIVE X-RAY DIFFRACTION

This testing was performed to provide insight into the hydration product formation as a function of gypsum additive, and to possibly draw correlations between results from other testing performed as part of this research study.

Both qualitative and quantitative x-ray diffraction (QXRD) was performed on mortar bars of two different ages from LST. The first round of analysis was conducted on mortar samples after the given mortar mixture had achieved a compressive strength of 20± 1 MPa (2900 ± 145 psi), hereafter referred to in figures as 20 MPa. The rate of strength gain of the mixtures was variable, where it took mortars anywhere from 1-9 days to achieve the compressive strength of 20± 1 MPa (2900 ± 145 psi). The second round of testing was conducted when the mortar was 28 days old (hereafter referred to in figures as 28 day) relative to the date of casting the given mixture.

The results of this testing regime are divided into two groups – mixtures without gypsum and mixtures containing gypsum. This has been done to fully understand the implications of using gypsum as an additive for the testing herein.

5.4.1 Mortar Mixtures Containing No Gypsum

5.4.1.1 Results

To establish a baseline understanding of the hydration products formed in the absence of gypsum additive, QXRD analysis was performed on straight cement mortar mixtures to compare against mortar mixtures containing fly ash. **Figures 5.22-5.25** show the differences in AFt and AFm for the aforementioned mixtures. The maximum standard deviation between any one measurement was ± 1.5%, thus error bars of ± 1.5% have been broadly applied to all the data.

Table 5.8. Summary of AFt and AFm formation of two ages of mortar mixtures containing no gypsum for all mixtures with cement C1 and fly ash replacement amounts of and 35%.

Mix ID	Analysis at 20 MPa		Analysis at 28 days	
	AFt (%)	AFm (%)	AFt (%)	AFm (%)
C1	7.5	4.7	10.3	3.7
C1-F1(35)	2.6	2.4	1.4	10.7
C1-F2(35)	6.8	0.3	6.5	1.1
C1-F3(35)	5.7	2.8	2.9	3.2

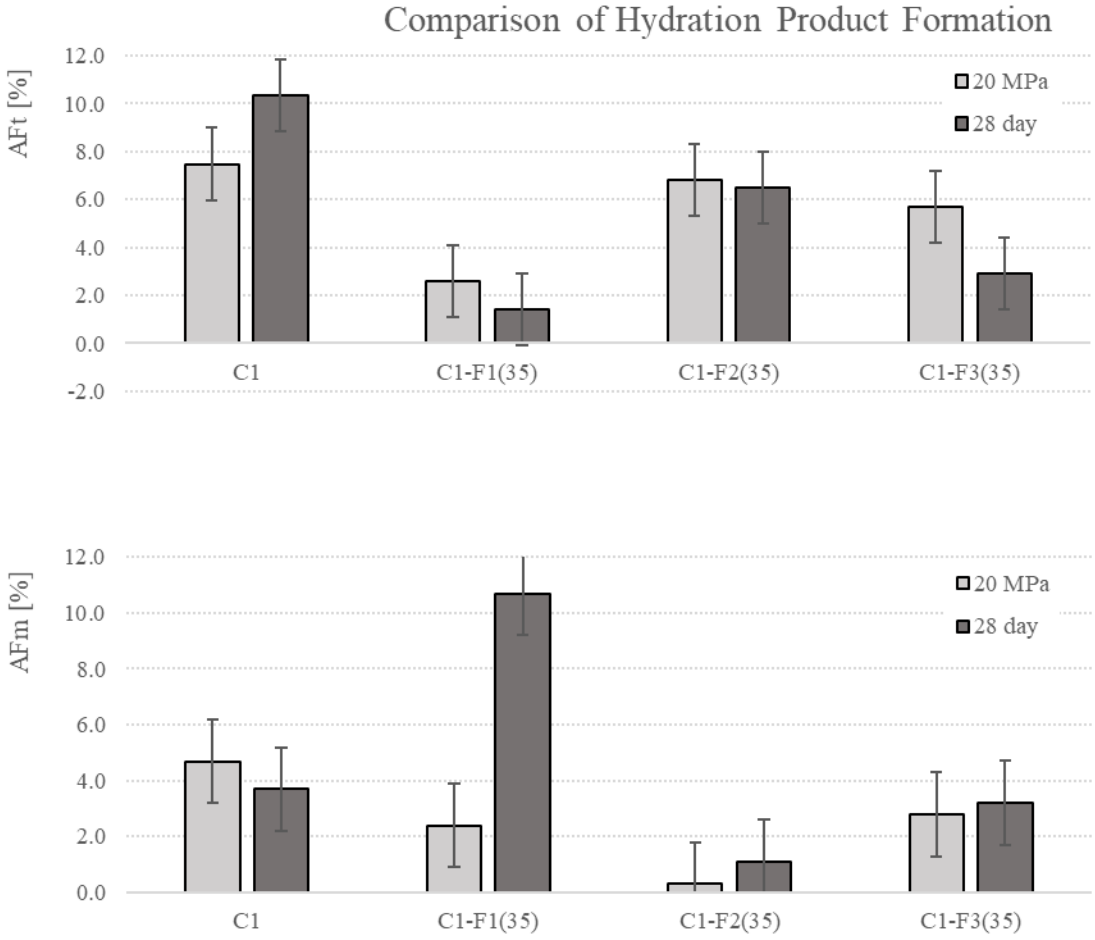

Figure 5.22. Comparison of AFt and AFm formation of two ages of mortar mixtures containing no gypsum for all mixtures with cement C1 and fly ash replacement amounts of 35%.

Table 5.9. Summary of AFt and AFm formation of two ages of mortar mixtures containing no gypsum for all mixtures with cement C1 and fly ash replacement amounts of and 20%.

Mix ID	Analysis at 20 MPa		Analysis at 28 days	
	AFt (%)	AFm (%)	AFt (%)	AFm (%)
C1	7.5	4.7	10.3	3.7
C1-F1(20)	3.8	2.1	3.5	5.3
C1-F2(20)	3.6	2.7	5.1	4.1
C1-F3(20)	3.6	2.8	3.2	5.7

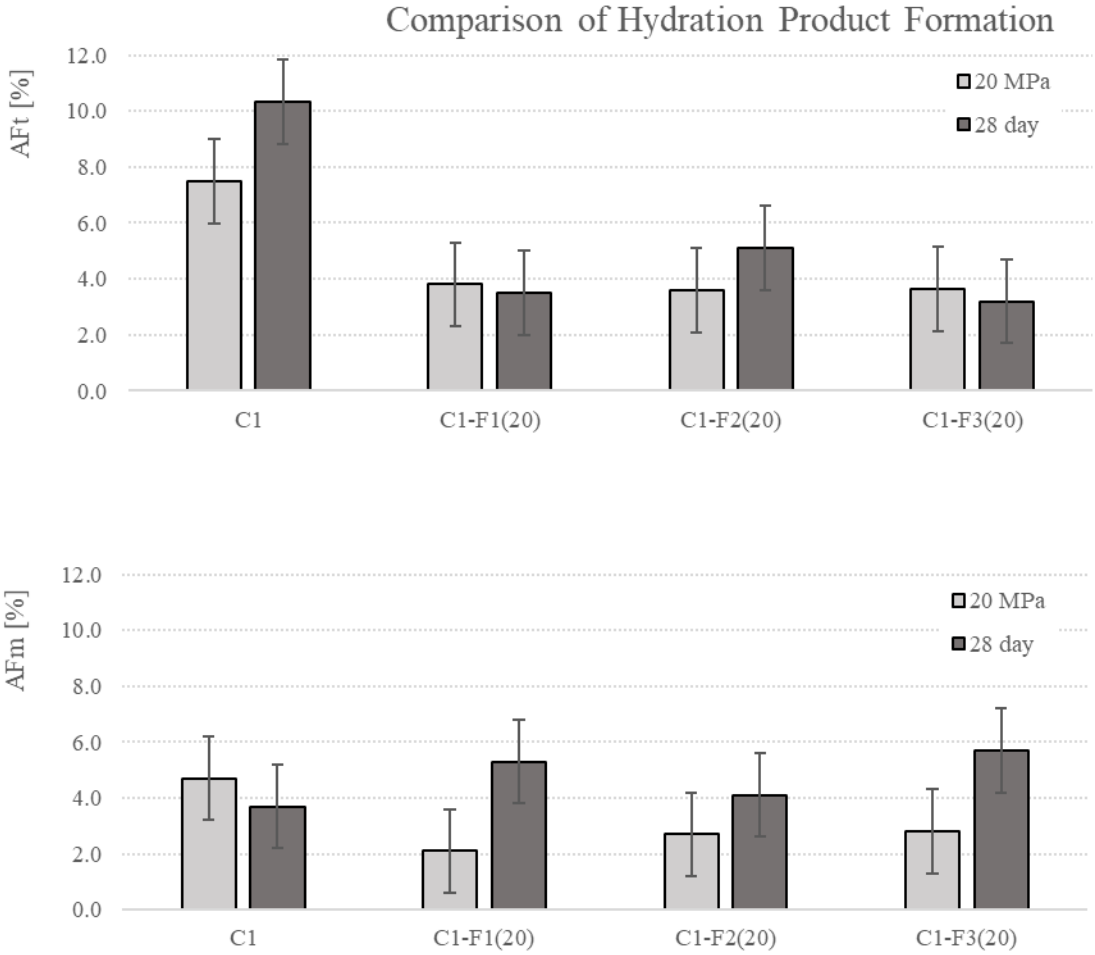

Figure 5.23. Comparison of AFt and AFm formation of two ages of mortar mixtures containing no gypsum for all mixtures with cement C1 and fly ash replacement amounts of 20%.

Table 5.10. Summary of AFt and AFm formation of two ages of mortar mixtures containing no gypsum for all mixtures with cement C2 and fly ash replacement amounts of and 35%.

Mix ID	Analysis at 20 MPa		Analysis at 28 days	
	AFt (%)	AFm (%)	AFt (%)	AFm (%)
C2	3.9	2.5	9.8	4.8
C2-F1(35)	6.2	2.1	4.8	4.9
C2-F2(35)	9.0	0.9	4.0	2.8
C2-F3(35)	5.5	1.9	3.6	3.5

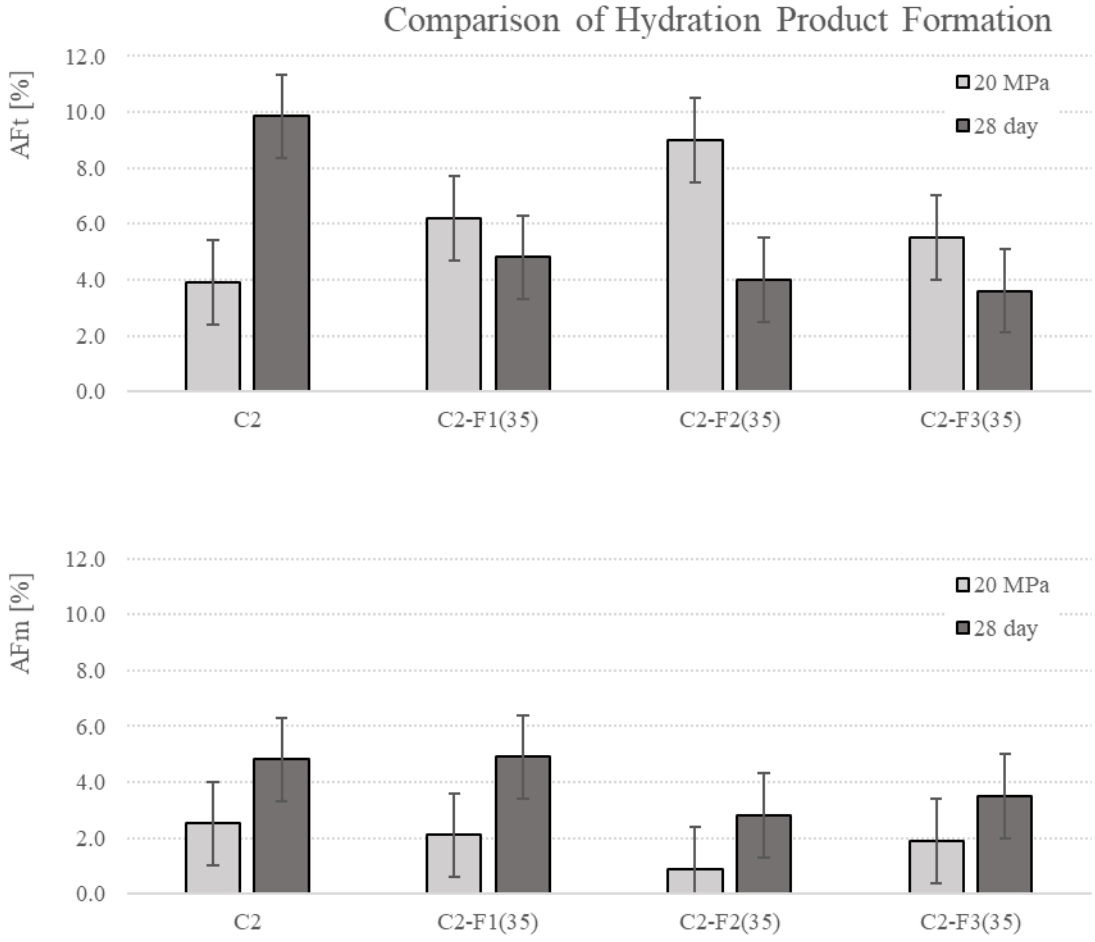

Figure 5.24. Comparison of AFt and AFm formation of two ages of mortar mixtures containing no gypsum for all mixtures with cement C2 and fly ash replacement amounts of 35%.

Table 5.11. Summary of AFt and AFm formation of two ages of mortar mixtures containing no gypsum for all mixtures with cement C2 and fly ash replacement amounts of and 20%.

Mix ID	Analysis at 20 MPa		Analysis at 28 days	
	AFt (%)	AFm (%)	AFt (%)	AFm (%)
C2	3.9	2.5	9.8	4.8
C2-F1(20)	7.0	3.7	7.5	7.9
C2-F2(20)	7.1	1.0	5.7	5.2
C2-F3(20)	4.8	3.3	5.1	10.4

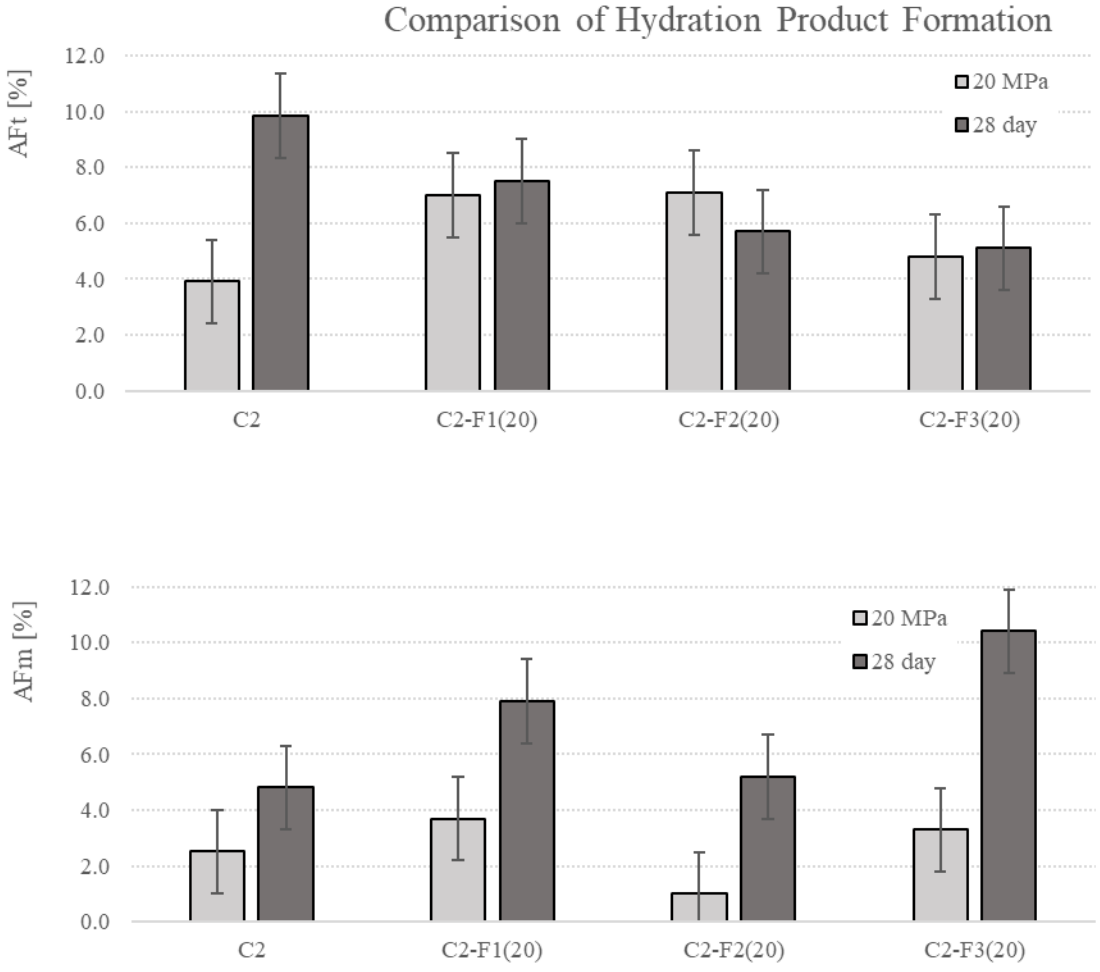

Figure 5.25. Comparison of AFt and AFm formation of two ages of mortar mixtures containing no gypsum for all mixtures with cement C2 and fly ash replacement amounts of 20%.

5.4.1.2 Discussion

The results from this testing show that the inclusion of fly ash affects the formation of AFt and AFm in early ages of the mortars in this study. The results indicate a difference between the hydration product formation between the two ages. The QXRD analysis of 20 MPa and 28 day samples exhibit AFt decreases and AFm increases. This is due to the formation of AFm at the expense of AFt.

It was expected that the C_3A content of the differing fly ashes would affect the outcome of the hydration products measured in QXRD analysis. Specifically, it was assumed that as the C_3A content of the ash increased, an increase in AFm would be observable between the mixtures. This assumption held true for mixtures containing 20% replacement (regardless of the cement type) but was not the case with mixtures containing 35% replacement (regardless of the cement type). It is noted here and in other portions of this thesis that the AFm phase was difficult to analyze with QXRD due to the solid solution nature of the substance.

It appears as though there is a correlation between the SO_3 content of the fly ashes and the amount of AFt formed. The fly ash containing the highest amount of SO_3 (from **Table 2.1**) content (F2 with 2.5% SO_3) generated more Aft three out of four times in this study, than the mixtures containing ashes F1 (SO_3 content of 1%) and F3 (SO_3 content of 1.5%). A similar trend between AFt formation and SO_3 content has been observed by other researchers [8].

5.4.2 Mortar Mixtures Containing Gypsum

5.4.2.1 Results

Both quantitative and qualitative XRD analysis is shown here to provide supporting evidence that Rietveld refinement conducted on the XRD scans was valid. The QXRD data consists of the average of two separate scans. The maximum standard deviation between any one measurement was ± 1.5%, thus error bars of ± 1.5% have been broadly applied to all the data. **Figures 5.26-5.37** show the side by side results for both forms of analysis. In order to capture and clearly delineate the presence of AFt, AFm, and gypsum that occur at the varying levels of gypsum additive dosage the quantitative results shown in the proceeding figures include the XRD 2θ phase spectrum between the angles of 8.5-12.5. Additionally, a summary of the results for each cement and fly ash replacement level is provided in **Table 5.12-5.15**.

Table 5.12. QXRD results for mixtures C1-F1(35), C1-F2(35), and C1-F3(35).

MIX ID	Gypsum Additive	AFt [20 Mpa]	AFt [28 days]	AFm [20 Mpa]	AFm [28 days]
	[%]	[%]	[%]	[%]	[%]
C1-F1(35)	0	2.6	1.4	2.4	10.7
	2	3.5	5.7	1.6	5.7
	4	5.4	7.0	2.0	7.5
	6	9.7	10.5	1.9	9.0
	8	14.6	15.7	2.1	2.8
	10	14.2	18.5	1.9	1.7
	12	14.3	21.9	1.8	1.5
	15	12.3	17.4	1.5	1.5
C1-F2(35)	0	6.8	6.5	0.3	1.1
	2	8.2	9.7	0.7	1.6
	4	12.4	14.1	0.3	2.8
	6	12.3	15.0	0.2	3.0
	8	14.6	18.1	0.4	1.0
	10	15.2	19.1	1.2	1.6
	12	16.9	24.3	0.5	1.7
	15	15.2	24.3	0.4	1.1
C1-F3(35)	0	5.7	2.9	2.8	3.2
	2	6.3	4.5	1.9	8.0
	4	9.3	7.4	3.2	4.8
	6	13.6	13.1	1.8	4.5
	8	16.2	13.5	2.4	2.6
	10	17.6	17.0	2.0	2.7
	12	15.1	21.9	2.7	2.1
	15	13.9	17.5	1.5	2.0

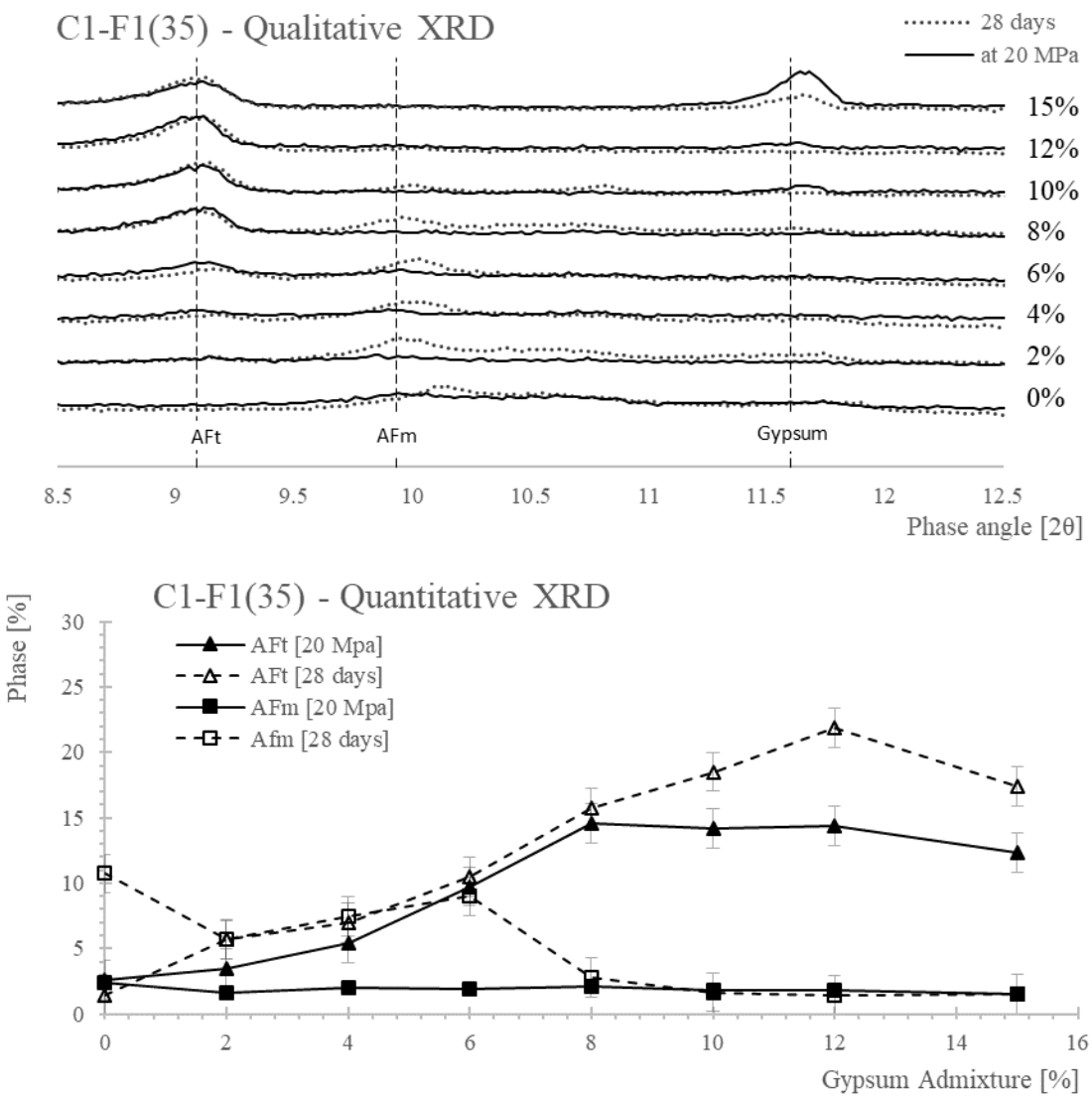

Figure 5.26. Qualitative and Quantitative XRD analysis for mixture C1-F1(35).

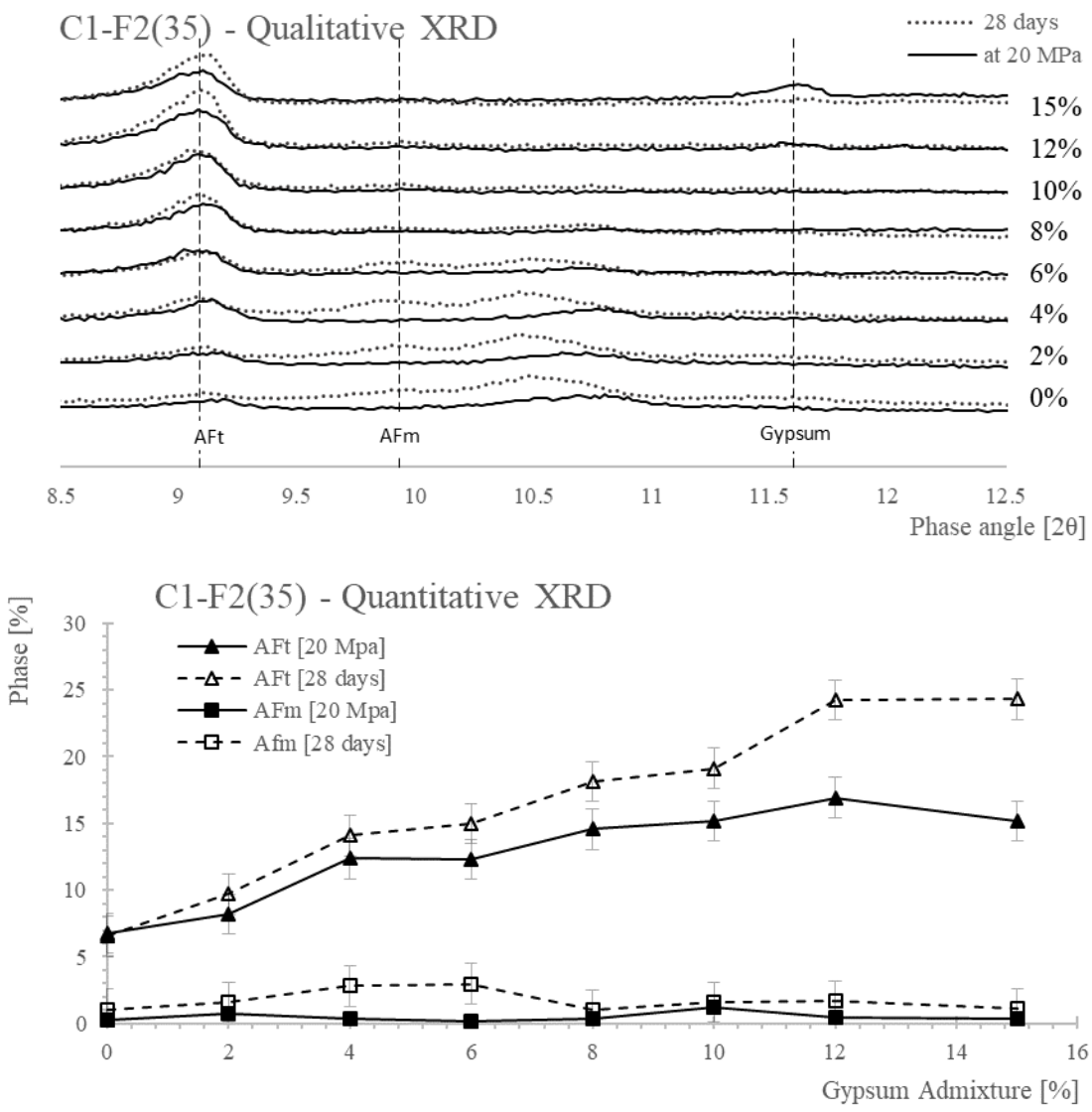

Figure 5.27. Qualitative and Quantitative XRD analysis for mixture C1-F2(35).

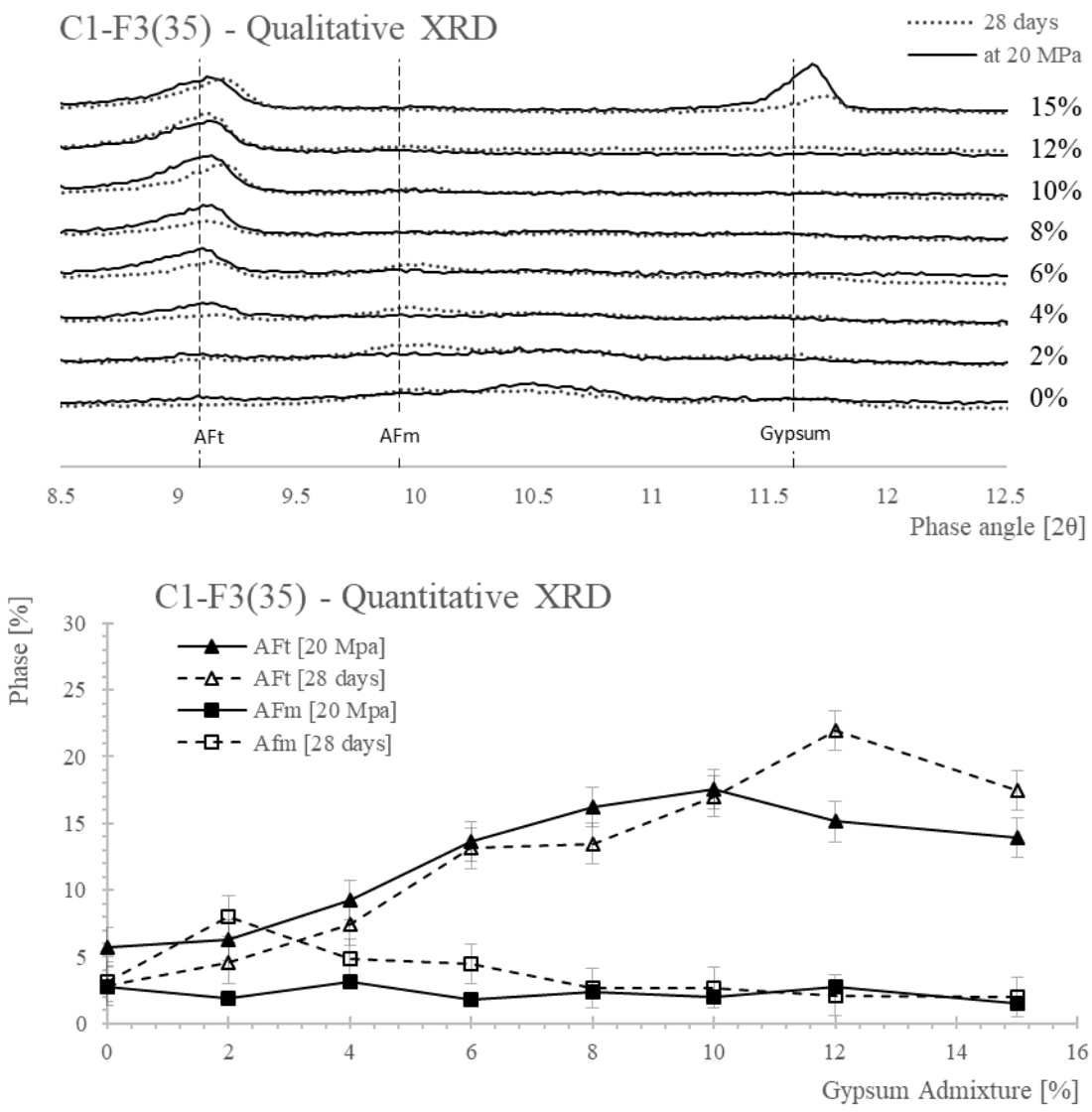

Figure 5.28. Qualitative and Quantitative XRD analysis for mixture C1-F3(35).

Table 5.13. QXRD results for mixtures C1-F1(20), C1-F2(20), and C1-F3(20).

MIX ID	Gypsum Additive	AFt [20 Mpa]	AFt [28 days]	AFm [20 Mpa]	AFm [28 days]
	[%]	[%]	[%]	[%]	[%]
C1-F1(20)	0	3.8	3.5	2.1	5.3
	2	5.2	6.9	3.1	5.3
	4	6.5	11.7	2.4	5.3
	6	13.1	17.5	2.6	6.0
	8	14.4	17.8	2.3	2.1
	10	11.6	18.8	2.3	2.8
	12	11.7	16.1	2.1	4.7
	15	10.9	16.6	2.6	5.8
C1-F2(20)	0	3.6	5.1	2.7	4.1
	2	8.6	5.6	3.3	5.3
	4	10.8	12.7	2.2	4.8
	6	11.2	16.0	1.9	4.1
	8	13.2	15.6	1.5	3.0
	10	15.6	19.3	2.3	2.0
	12	13.0	17.1	2.0	1.6
	15	13.1	15.7	1.4	3.3
C1-F2(20)	0	3.6	3.2	2.8	5.7
	2	5.5	4.4	2.8	2.0
	4	7.1	8.1	2.4	2.0
	6	10.7	12.7	2.6	2.4
	8	12.2	13.5	2.5	2.8
	10	13.0	9.6	2.1	1.7
	12	11.2	11.1	2.8	3.2
	15	12.8	10.5	2.6	2.7

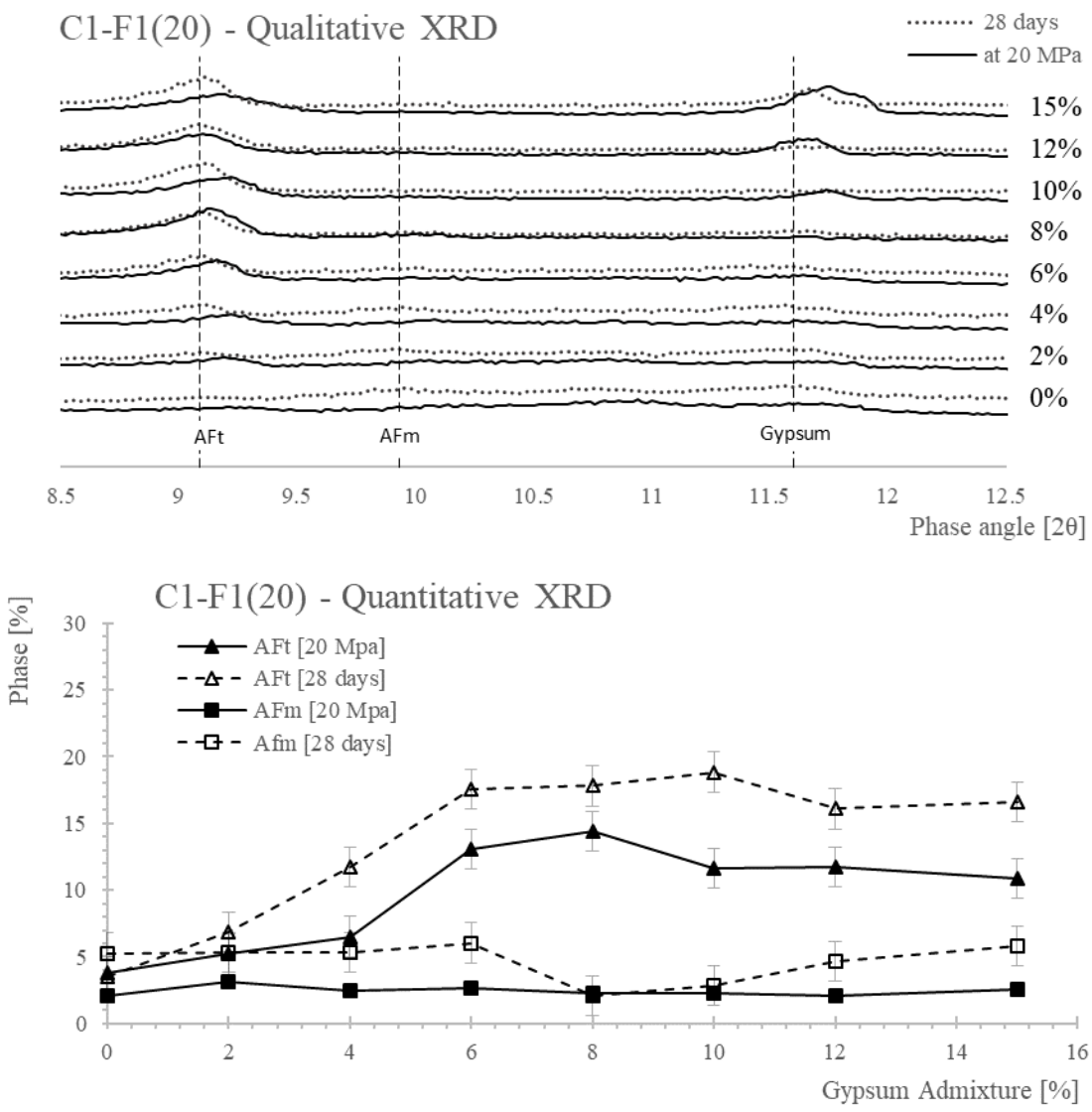

Figure 5.29. Qualitative and Quantitative XRD analysis for mixture C1-F1(20).

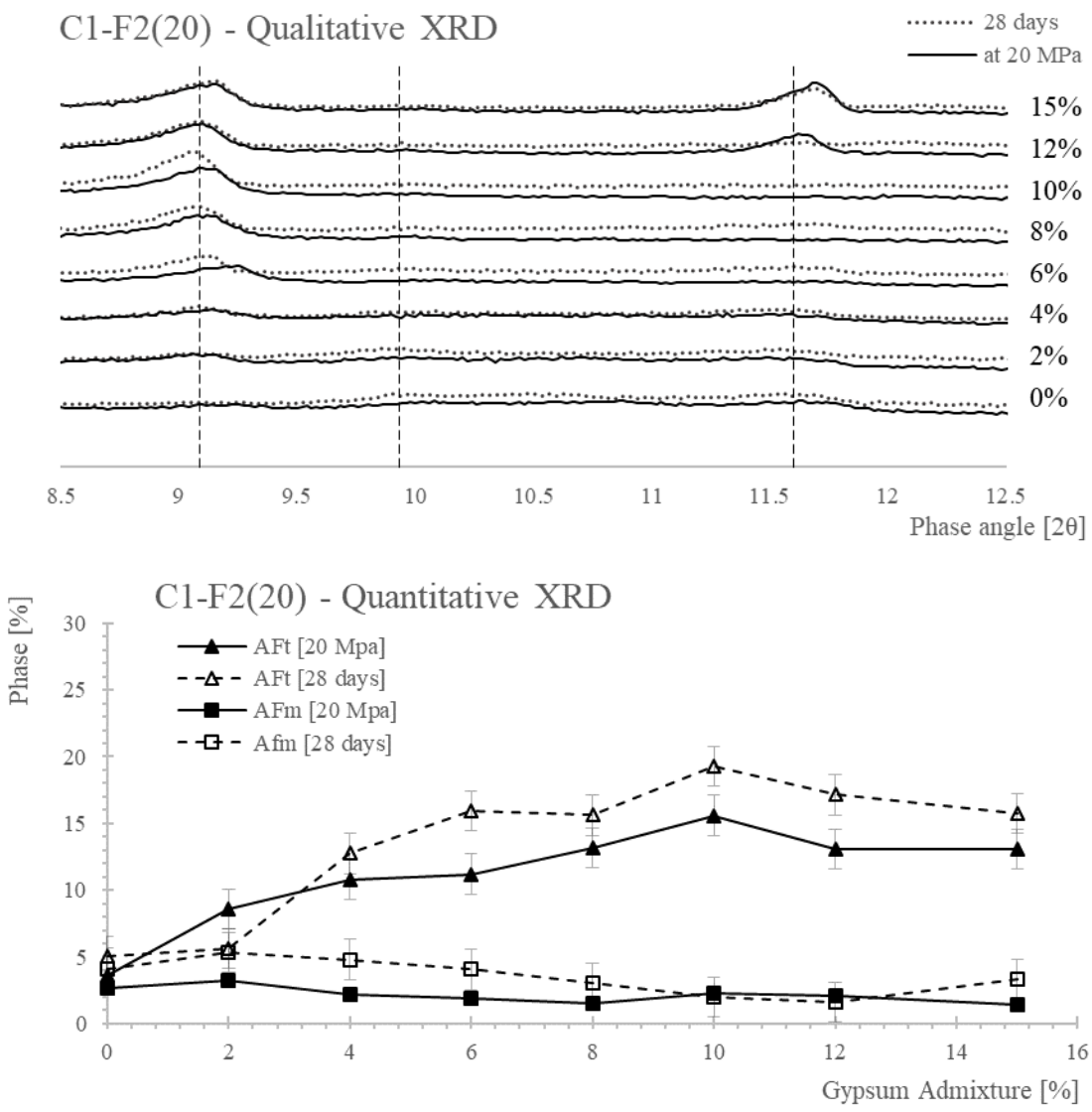

Figure 5.30. Qualitative and Quantitative XRD analysis for mixture C1-F2(20).

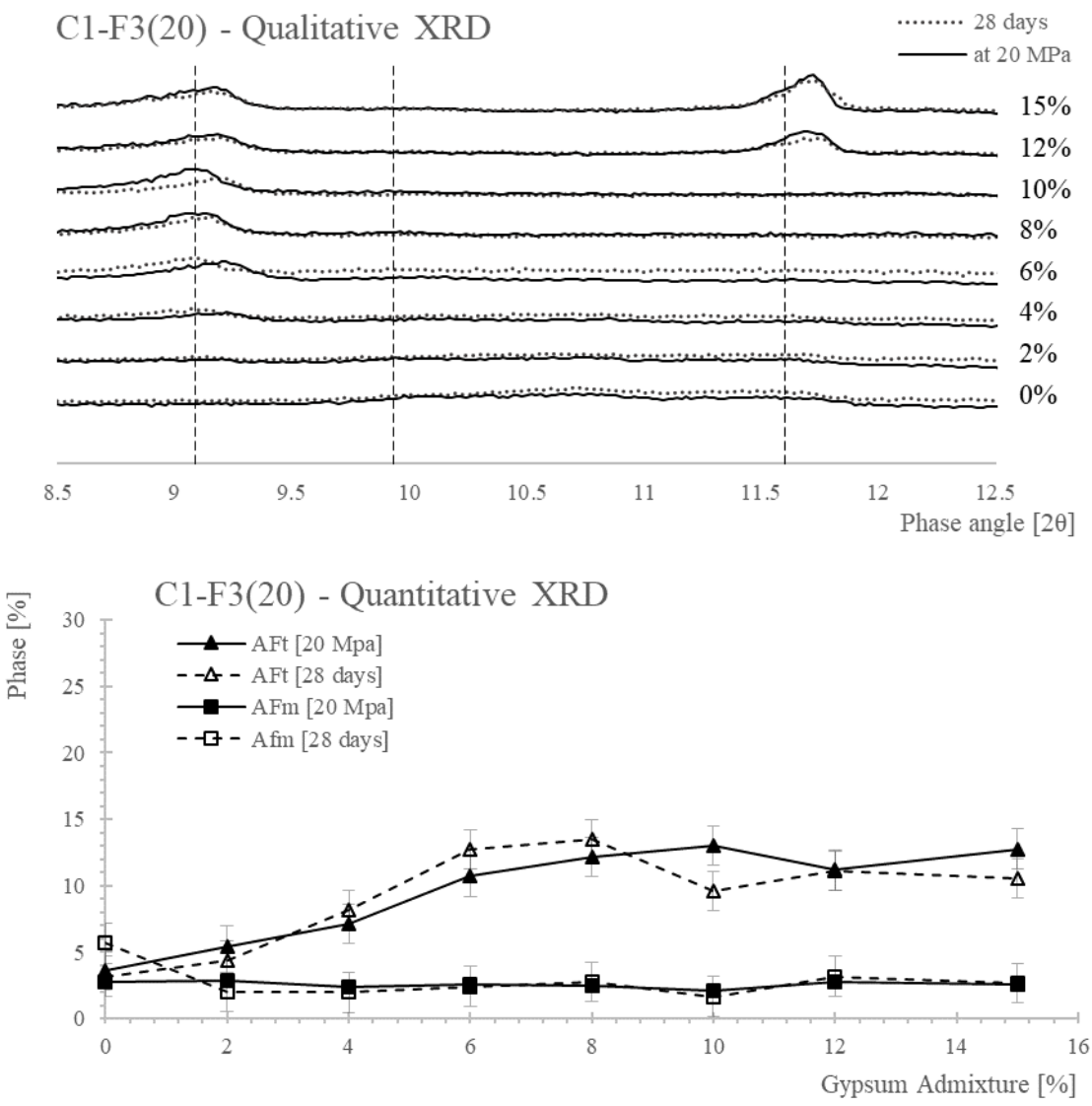

Figure 5.31. Qualitative and Quantitative XRD analysis for mixture C1-F3(20).

Table 5.14. QXRD results for mixtures C2-F1(35), C2-F2(35), and C2-F3(35).

MIX ID	Gypsum Additive	AFt [20 Mpa]	AFt [28 days]	AFm [20 Mpa]	AFm [28 days]
	[%]	[%]	[%]	[%]	[%]
C2-F1(35)	0	6.2	4.8	2.1	4.9
	2	7.7	7.6	2.9	4.5
	4	10.6	12.5	2.2	3.6
	6	12.8	16.0	2.7	3.7
	8	16.9	16.0	2.3	3.8
	10	16.4	19.1	2.2	1.8
	12	18.9	19.7	1.8	2.2
	15	18.3	19.8	1.4	2.1
C2-F2(35)	0	9.0	4.0	0.9	2.8
	2	9.6	11.0	1.6	3.2
	4	11.3	14.3	1.1	2.7
	6	14.5	13.1	0.8	1.7
	8	15.7	15.9	0.7	1.7
	10	18.6	18.0	0.8	1.3
	12	15.4	17.4	2.4	1.2
	15	11.9	20.1	1.1	1.7
C2-F3(35)	0	5.5	3.6	1.9	3.5
	2	6.8	5.1	1.9	4.0
	4	7.3	10.7	2.2	4.5
	6	12.7	14.5	5.6	4.1
	8	14.1	14.1	1.4	3.1
	10	15.5	15.3	1.3	2.7
	12	13.4	17.9	2.0	2.0
	15	13.5	17.5	1.6	1.5

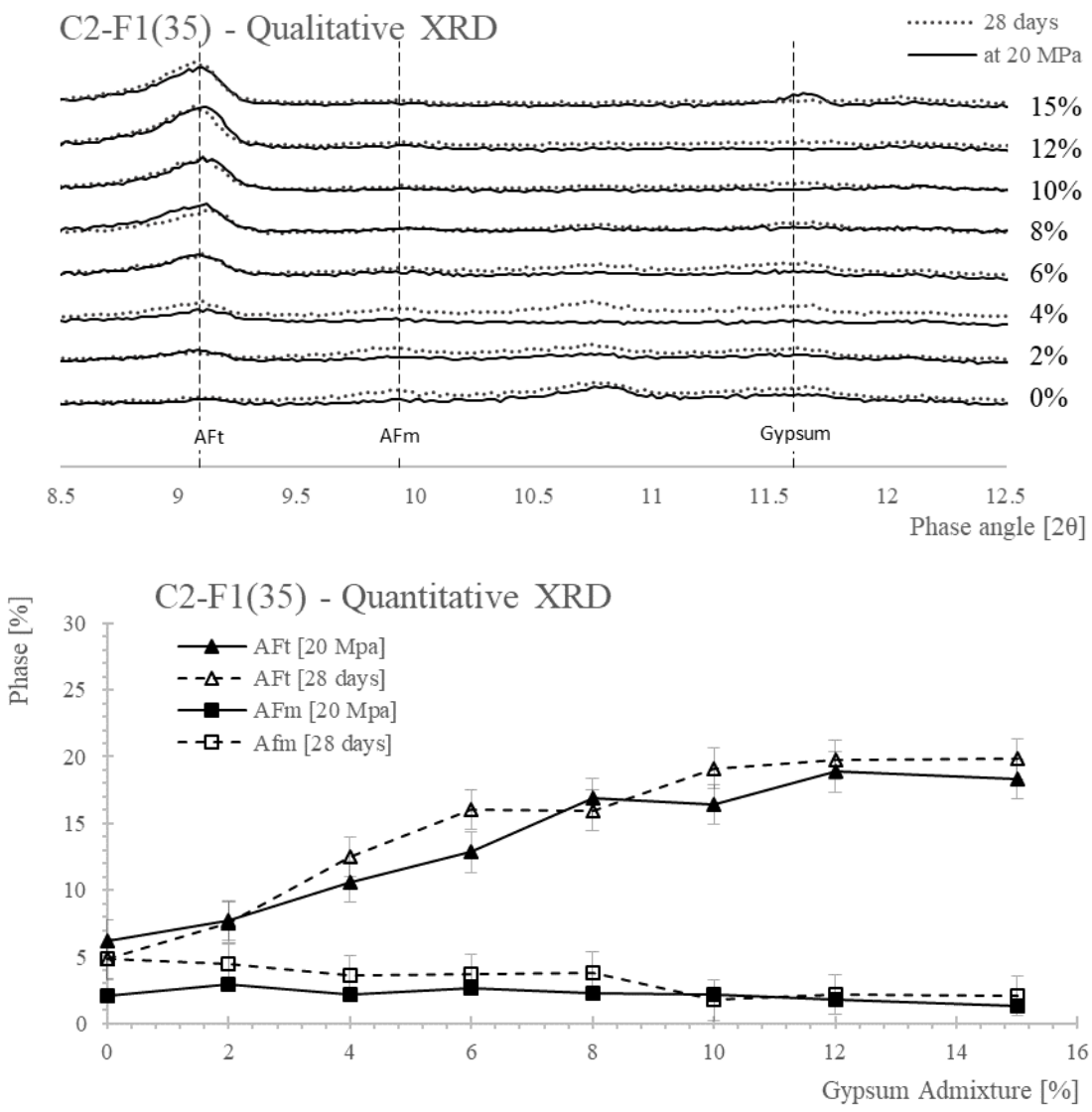

Figure 5.32. Qualitative and Quantitative XRD analysis for mixture C2-F1(35).

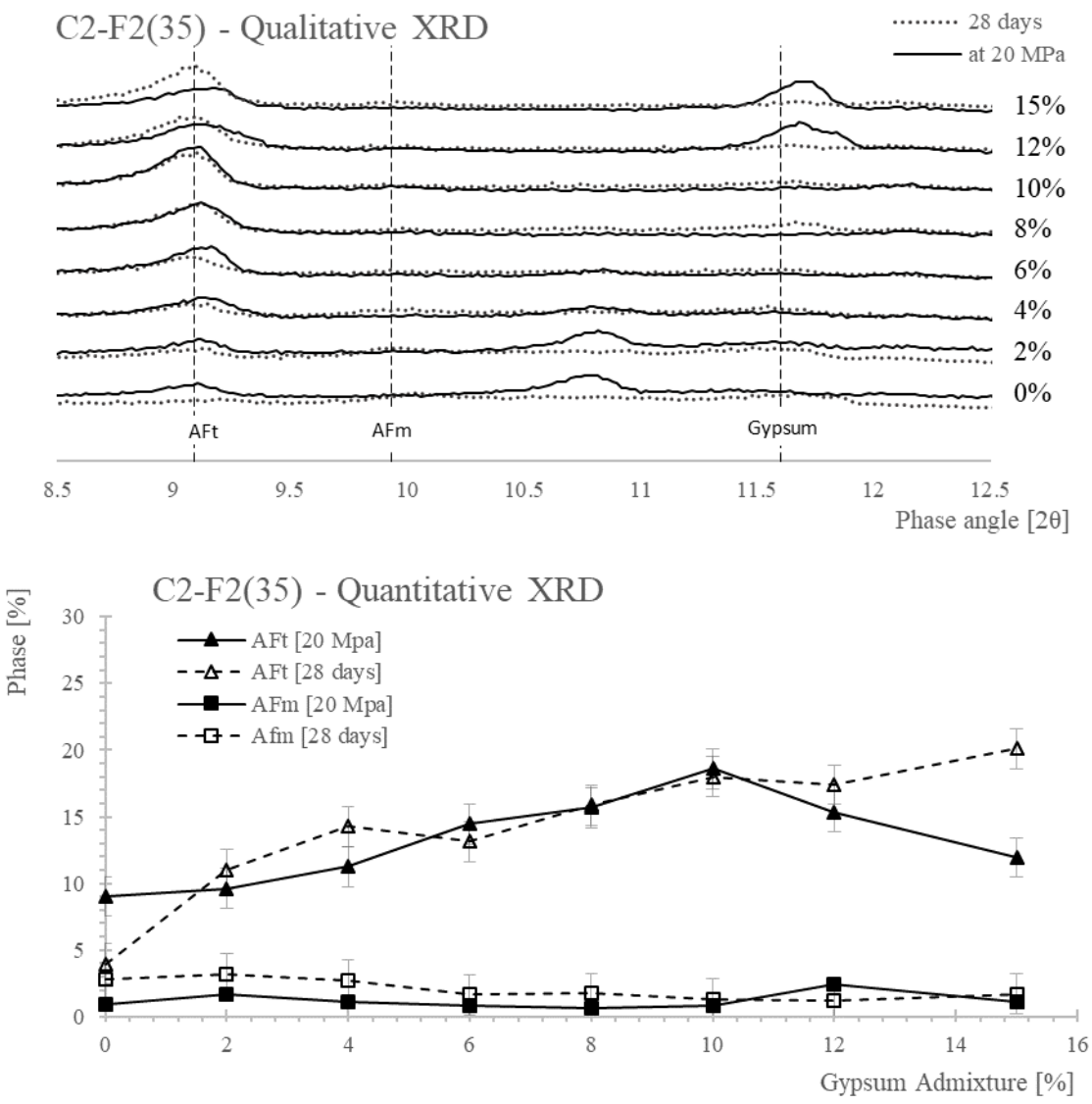

Figure 5.33. Qualitative and Quantitative XRD analysis for mixture C2-F2(35).

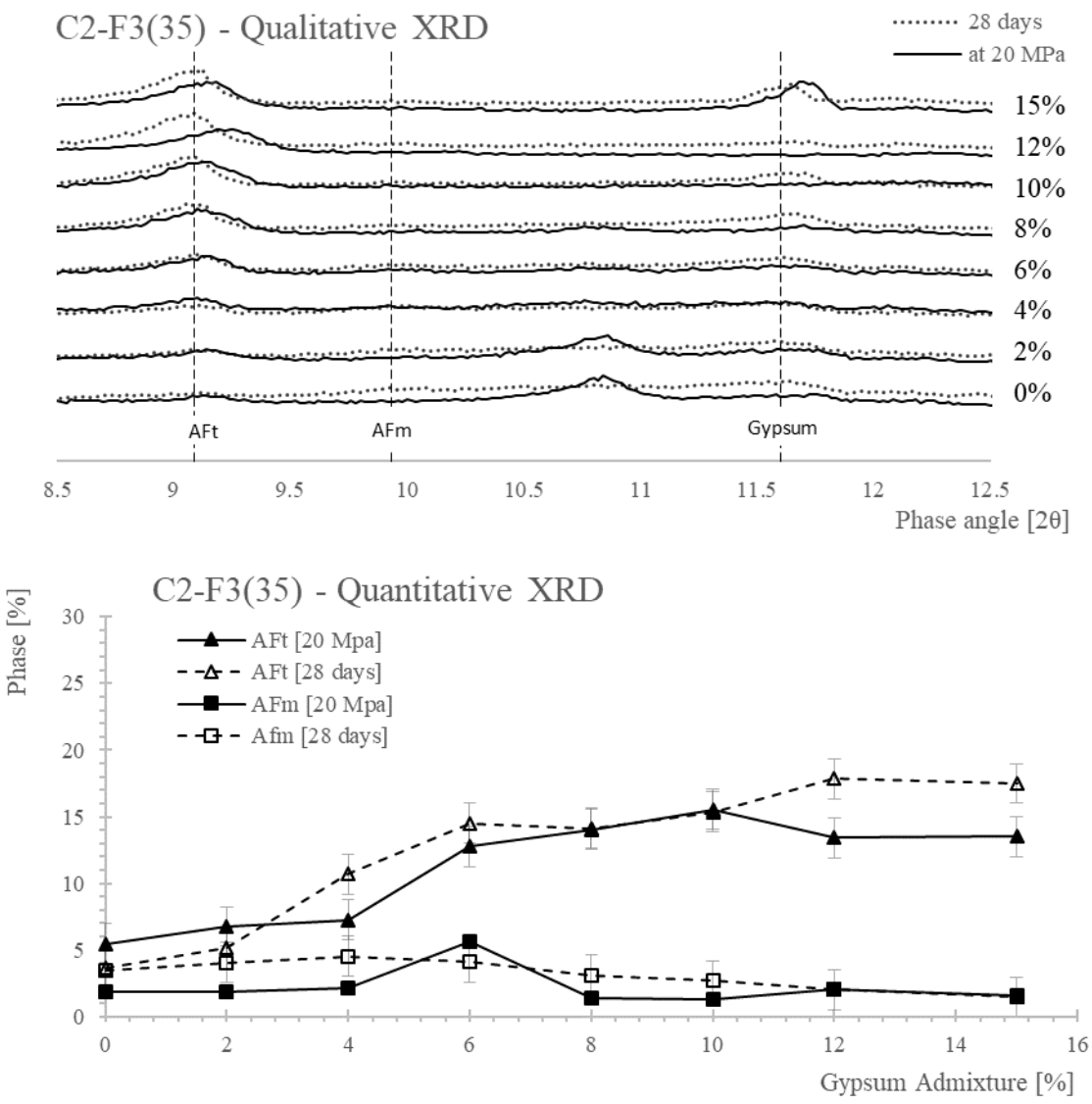

Figure 5.34. Qualitative and Quantitative XRD analysis for mixture C2-F3(35).

Table 5.15. QXRD results for mixtures C2-F1(20), C2-F2(20), and C2-F3(20).

MIX ID	Gypsum Additive	AFt [20 Mpa]	AFt [28 days]	AFm [20 Mpa]	AFm [28 days]
	[%]	[%]	[%]	[%]	[%]
C2-F1(20)	0	7.0	7.5	3.7	7.9
	2	9.6	8.3	4.3	10.5
	4	12.5	10.8	3.3	9.1
	6	13.3	13.5	2.4	5.8
	8	14.2	16.5	2.5	5.0
	10	12.3	16.5	1.7	3.5
	12	11.3	14.7	1.4	2.7
	15	13.9	15.5	2.3	2.0
C2-F2(20)	0	7.1	5.7	1.0	5.2
	2	9.3	8.6	5.3	13.6
	4	9.6	11.1	3.7	3.5
	6	17.1	16.7	2.3	2.8
	8	14.5	17.1	1.6	7.3
	10	14.4	18.3	0.7	3.9
	12	15.1	19.3	2.4	2.4
	15	13.0	15.0	1.8	2.2
C2-F3(20)	0	4.8	5.1	3.3	10.4
	2	6.4	8.3	3.9	7.9
	4	8.4	11.7	3.7	5.1
	6	9.7	13.3	4.1	7.3
	8	12.9	14.6	1.9	2.7
	10	12.0	14.6	1.8	1.4
	12	13.8	14.4	2.4	2.0
	15	12.0	14.9	2.4	2.9

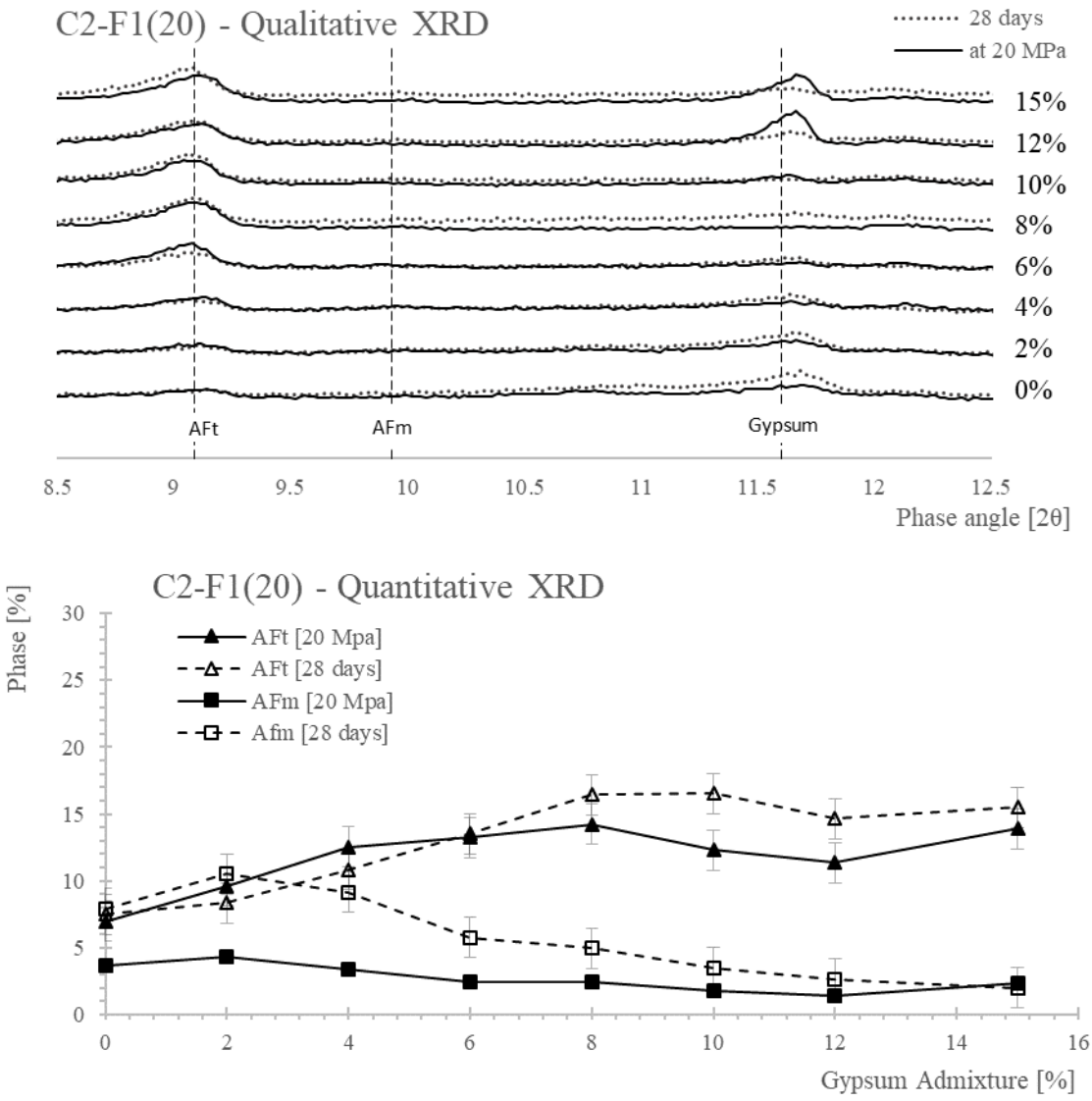

Figure 5.35. Qualitative and Quantitative XRD analysis for mixture C2-F1(20).

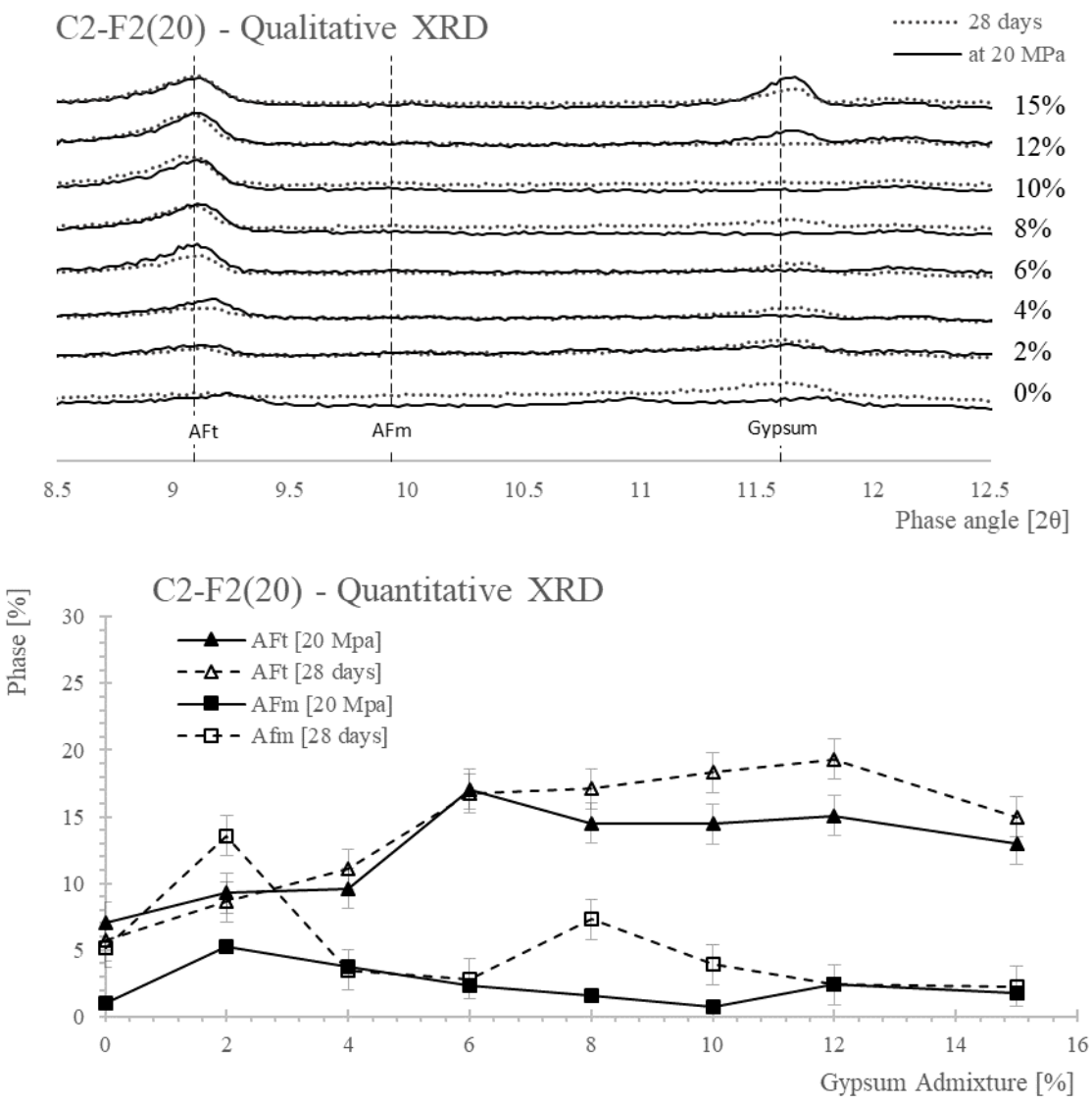

Figure 5.36. Qualitative and Quantitative XRD analysis for mixture C2-F2(20).

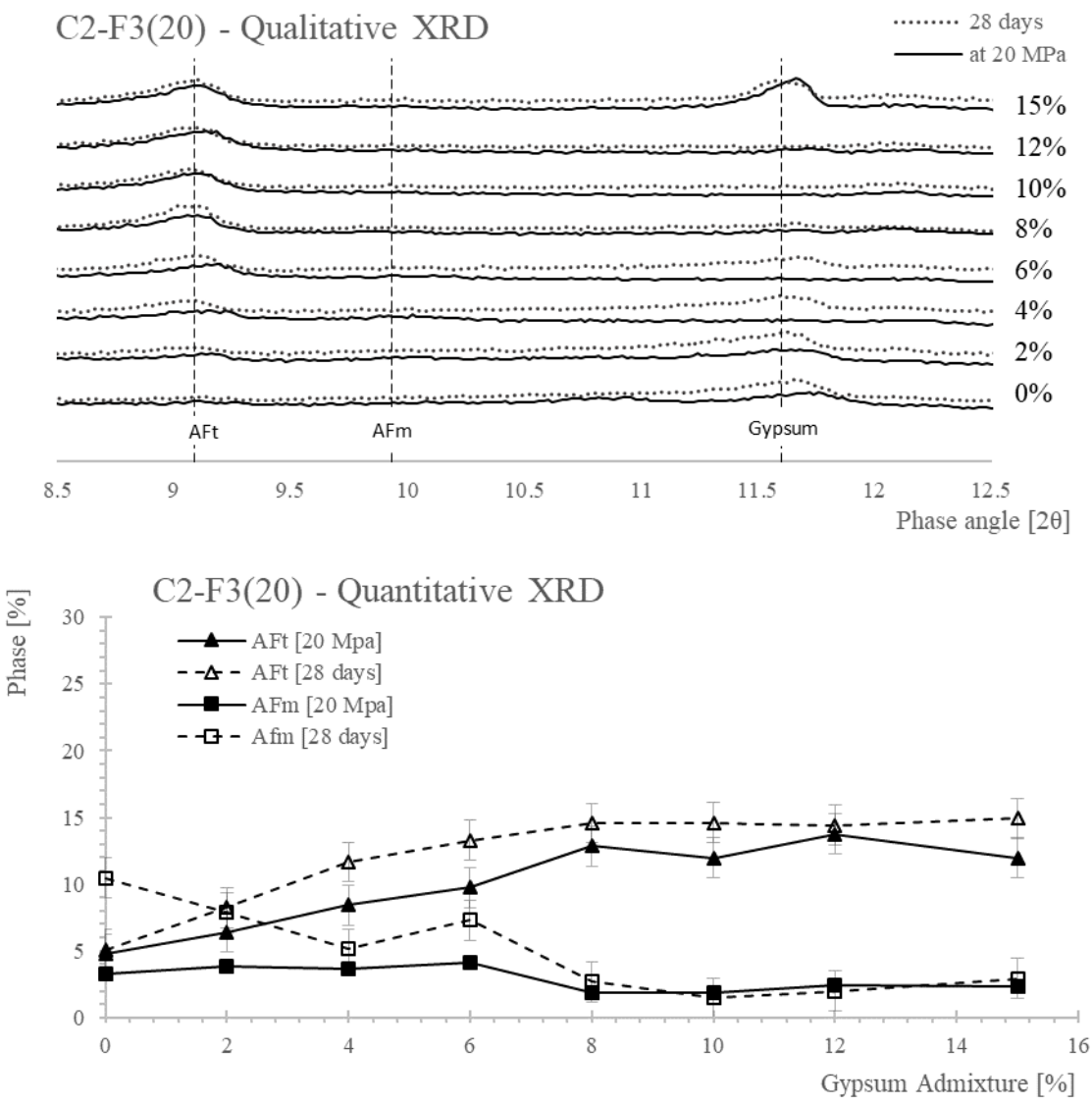

Figure 5.37. Qualitative and Quantitative XRD analysis for mixture C2-F3(20).

5.4.2.2 Discussion

The results shown in **Figures 5.26-5.37** provide insight into multiple points of interest. The following is a numbered list of observations and corresponding descriptions of common characteristics noted while analyzing the data. The numbered list corresponds to annotations shown in **Figure 5.38**, which was chosen as a good example to provide graphical representation of the observations.

(1) The 20 MPa curve in every mixture, regardless of cement type or fly ash replacement level exhibits a point of peak AFt formation.

(2) There is a general increase in AFt formation between the 20 MPa and 28 day curves, especially at higher gypsum dosages.

(3) There is an increase in the formation of AFt, followed by a slight decrease, accompanied by a plateau in the 20 MPa curve.

(4) The AFm phase in both the 20 MPa and 28 Day curves are approximately equal after peak AFt has occurred.

(5) Mixtures containing gypsum produced 2-5 times more AFt than mixtures without.

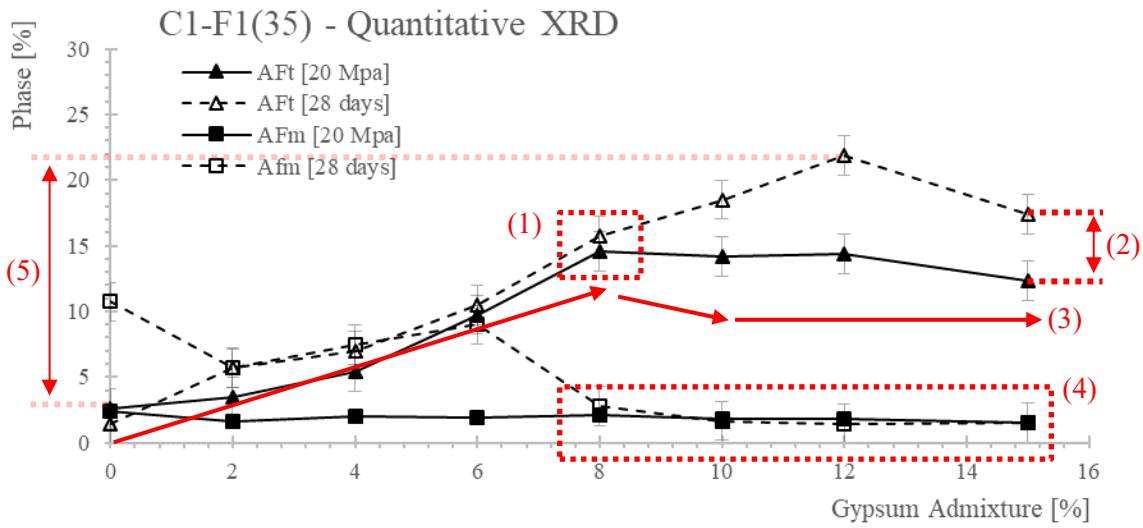

Figure 5.38. Annotated typical characteristics corresponding to numbered list of observations.

Peak AFt formation on the 20 MPa curve always occurred at gypsum dosages less than peak AFt on the 28 day curve. The difference between the peak AFt on the 20 MPa curve and peak AFt on the 28 day curve indicate that gypsum is limited in its effectiveness at producing AFt at early ages. This is a critical point to note because the formation of AFt at later ages is expansive and may result in degradation of the binder.

No analysis has been performed to understand why there is a decrease in AFt after peak AFt formation, and this question is left unanswered here.

The increase in AFm that occurs between the 20 MPa curve and 28 day curve is due to the mixture being under-sulfated. There is ample C_3A available for hydration, and not enough sulfate to stabilize the AFt phase. It is noted here that AFm was difficult to quantify using Rietveld refinement methods. The solid solution nature of AFm as documented by researchers [29] makes quantifying AFm difficult. When visually assessing the Rietveld curve, with respect to the AFm phase of the spectrum, the fit was at times poor. All QXRD data are included in the **Appendix** section of this thesis.

By far the most interesting observation of note is the benefit the gypsum additive is providing in the precipitation of AFt. With every mixture, regardless of cement type or fly ash replacement levels, an observable increase in AFt corresponds to increasing dosages of gypsum additive.

In proceeding sections of this thesis, a comparative analysis will be performed to show correlations between the formation of hydration products with the other testing methods performed as part of this research study.

5.5 ASTM C 1012 TESTING

The ASTM C 1012 test is an industry standard benchmark test for sulfate resistance. A passing result is required within the cement and concrete industry to prove that a cement or mortar mixture is sulfate resistant. The test is very aggressive (>33,000ppm SO_3) and is meant to serve as a quasi-short-term test by creating conditions that are considerably harsher than any sulfate exposure condition encountered in practice. The testing conditions are well in excess of the S3 exposure conditions per ACI-318 (as shown in **Table 5.1**). The test can run for a duration of 18 months, and results are accepted as passing if they meet expansion limit requirements in ASTM C 1157 performance specification for hydraulic cements as well as ASTM C 595 specification for blended cements. The expansion limit criteria in the aforementioned standards are:

Table 5.16. Summary of expansion limits imposed by ASTM C 1157 and C 595.

Classification	Maximum Expansion (%)	
	At 6 months	At 12 Months
Moderate sulfate-resistance, Type MS	0.1	-
High sulfate-resistance, Type HS	0.05	0.1

The ASTM C 1012 testing in this study was conducted in two phases. The first phase was to assess the validity of a sulfate attack mitigation strategy proposed by Tikalsky and Carrasquillo [7], which was later tested by Dhole [9], and Aguayo [8]. This strategy entailed making an assumption about the reactive phases of the fly ash based on chemical composition, followed by stoichiometrically solving for the amount of gypsum required to meet the assumed reactivity. The second phase of ASTM C 1012 testing had two goals: to prepare mixtures which correlated to passing results observed in the first phase of testing, and to prepare mixtures which correlated to those tested in LST, isothermal calorimetry, and XRD analysis. The second phase of testing is highlighted green in **Tables 5.17-5.28** to clearly delineate between the two phases.

5.5.1 Results

The plotted expansion results (**Figures 5.39-5.50**) are truncated at (0.8% expansion in figures) for clarity to the reader. Additionally, the tabulated form of the expansion results (**Tables 5.17-5.28**) include **bolded** values for expansion measurements in excess of 0.1% (fail), and highlighted values to clearly indicate which results have met (pass) requirements of sulfate-resistance categories indicated in **Table 5.16.**

Table 5.17. ASTM C1012 mortar bar expansion results for mixture C1-F1(35).

MIX ID	Exp % 7d	Exp % 14d	Exp % 28d	Exp % 105d	Exp % 6m	Exp % 12m
C1	0.006	0.006	0.017	0.091	**0.266**	-
C1-F1(35)-G(0)	0.013	0.021	0.032	-	-	-
C1-F1(35)-G(8)	0.019	0.038	0.042	0.062	0.092	
C1-F1(35)-G(10.5)	0.054	0.065	0.096	**0.245**	**0.462**	**0.875**
C1-F1(35)-G(11.8)	0.076	0.095	**0.148**	**0.418**	**0.829**	**1.484**
C1-F1(35)-G(14.0)	**0.119**	**0.195**	**0.297**	**0.663**	**0.988**	**1.897**
C1-F1(35)-G(14.7)	0.087	**0.207**	**0.399**	**0.834**	**1.178**	**2.194**

Note: "-" indicates mortar bar was not measurable
Note: empty portions of the table indicate no measurement taken

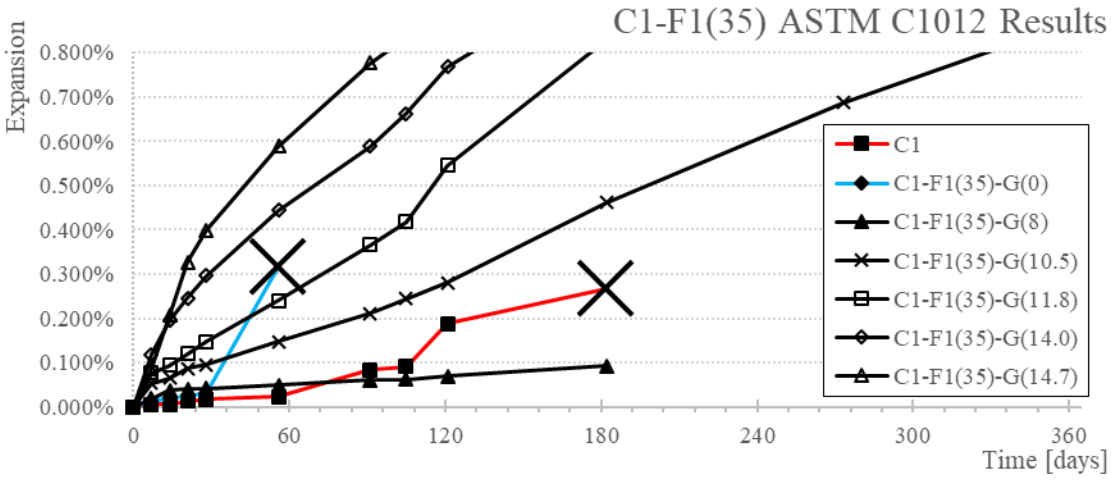

Figure 5.39. ASTM C1012 mortar bar expansion results for mixture C1-F1(35).

Table 5.18. ASTM C1012 mortar bar expansion results for mixture C1-F2(35).

MIX ID	Exp % 7d	Exp % 14d	Exp % 28d	Exp % 105d	Exp % 6m	Exp % 12m
C1	0.006	0.006	0.017	0.091	**0.266**	-
C1-F2(35)-G(0)	0.018	0.024	0.034	-	-	-
C1-F2(35)-G(8)	0.038	0.063	0.078	**0.143**	**0.217**	
C1-F2(35)-G(8.6)	0.008	0.010	0.012	0.023	0.026	0.051
C1-F2(35)-G(11.4)	0.083	**0.107**	**0.186**	**0.580**	**1.080**	**1.839**
C1-F2(35)-G(11.9)	0.098	**0.121**	**0.172**	**0.516**	**1.017**	**1.762**
C1-F2(35)-G(14.8)	**0.171**	**0.279**	**0.575**	**1.462**	**1.874**	**3.511**

Note: "-" indicates mortar bar was not measurable

Note: empty portions of the table indicate no measurement taken

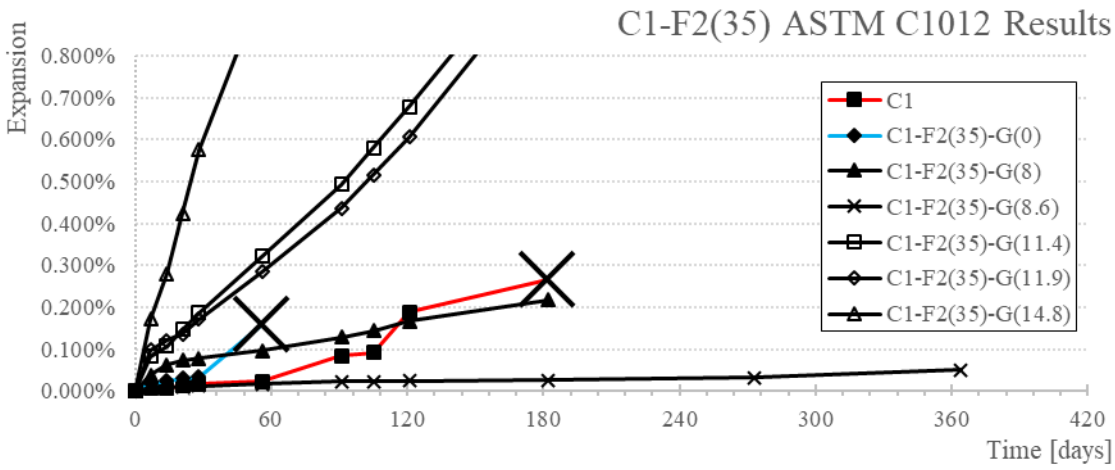

Figure 5.40. ASTM C1012 mortar bar expansion results for mixture C1-F2(35).

Table 5.19. ASTM C1012 mortar bar expansion results for mixture C1-F3(35).

MIX ID	Exp % 7d	Exp % 14d	Exp % 28d	Exp % 105d	Exp % 6m	Exp % 12m
C1	0.006	0.006	0.017	0.091	**0.266**	-
C1-F3(35)-G(0)	0.001	0.003	0.014	**0.120**	-	-
C1-F3(35)-G(8)	0.035	0.049	0.060	**0.143**	**0.249**	

Note: "-" indicates mortar bar was not measurable

Note: empty portions of the table indicate no measurement taken

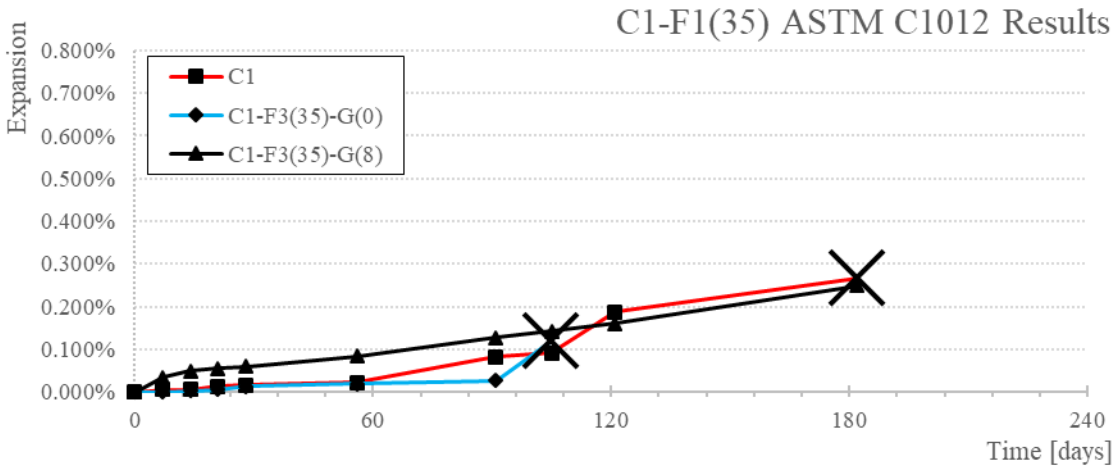

Figure 5.41. ASTM C1012 mortar bar expansion results for mixture C1-F3(35).

Table 5.20. ASTM C1012 mortar bar expansion results for mixture C1-F1(20).

MIX ID	Exp % 7d	Exp % 14d	Exp % 28d	Exp % 105d	Exp % 6m	Exp % 12m
C1	0.006	0.006	0.017	0.091	**0.266**	-
C1-F1(20)-G(0)	0.014	0.020	0.027	-	-	-
C1-F1(20)-G(6)	0.055	0.063	0.084	**0.158**	**0.253**	
C1-F1(20)-G(8.7)	0.042	0.050	0.071	**0.334**	**0.769**	**1.588**
C1-F1(20)-G(11.6)	0.044	**0.106**	**0.247**	**0.735**	**1.265**	**2.190**
C1-F1(20)-G(12.2)	0.085	**0.150**	**0.419**	**0.883**	**1.592**	**2.204**
C1-F1(20)-G(15.2)	0.043	**0.118**	**0.278**	**0.871**	**1.421**	**2.302**

Note: "-" indicates mortar bar was not measurable

Note: empty portions of the table indicate no measurement taken

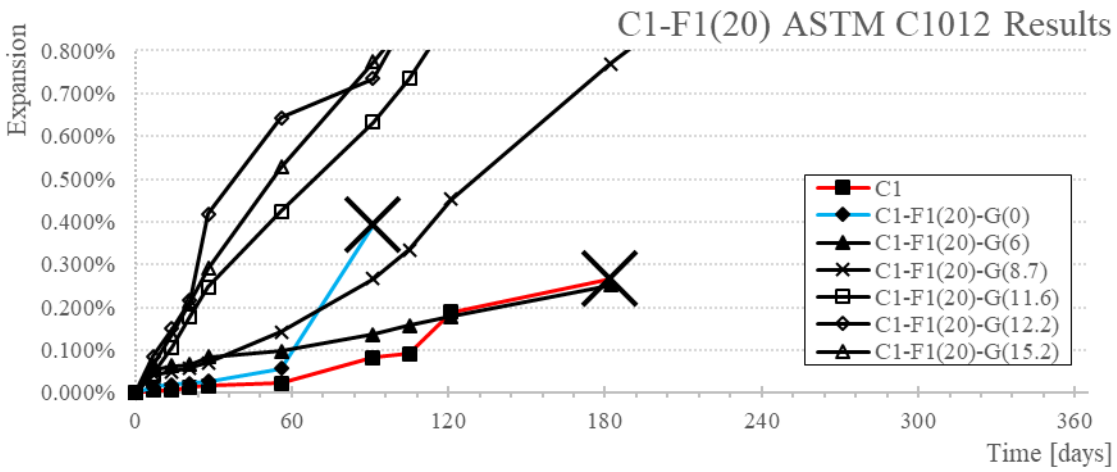

Figure 5.42. ASTM C1012 mortar bar expansion results for mixture C1-F1(20).

Table 5.21. ASTM C1012 mortar bar expansion results for mixture C1-F2(20).

MIX ID	Exp % 7d	Exp % 14d	Exp % 28d	Exp % 105d	Exp % 6m	Exp % 12m
C1	0.006	0.006	0.017	0.091	**0.266**	-
C1-F2(20)-G(0)	0.036	0.041	0.039	-	-	-
C1-F2(20)-G(6)	0.050	0.065	0.078	**0.177**	**0.307**	
C1-F2(20)-G(7.6)	0.019	0.039	0.060	**0.260**	**0.578**	**1.662**
C1-F2(20)-G(10.2)	0.052	**0.121**	**0.221**	**0.758**	**1.184**	**1.923**
C1-F2(20)-G(10.7)	0.056	**0.123**	**0.233**	**0.682**	**1.105**	**1.751**
C1-F2(20)-G(13.4)	0.065	**0.137**	**0.291**	**0.874**	**1.307**	**2.484**

Note: "-" indicates mortar bar was not measurable

Note: empty portions of the table indicate no measurement taken

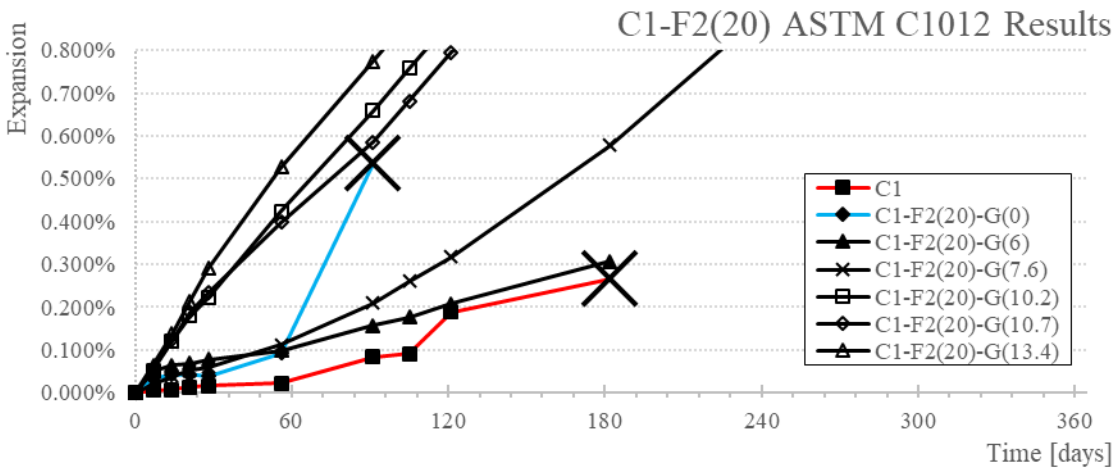

Figure 5.43. ASTM C1012 mortar bar expansion results for mixture C1-F2(20).

Table 5.22. ASTM C1012 mortar bar expansion results for mixture C1-F3(20).

MIX ID	Exp % 7d	Exp % 14d	Exp % 28d	Exp % 105d	Exp % 6m	Exp % 12m
C1	0.006	0.006	0.017	0.091	**0.266**	-
C1-F3(20)-G(0)	-0.003	0.009	0.013	**0.396**	-	-
C1-F3(20)-G(6)	0.014	0.022	0.050	**0.122**	**0.240**	

Note: "-" indicates mortar bar was not measurable

Note: empty portions of the table indicate no measurement taken

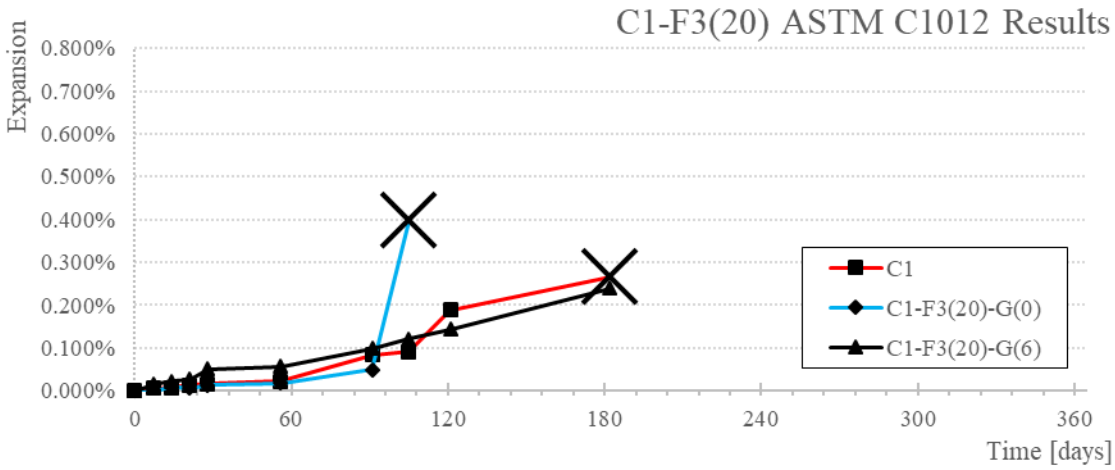

Figure 5.44. ASTM C1012 mortar bar expansion results for mixture C1-F3(20).

Table 5.23. ASTM C1012 mortar bar expansion results for mixture C2-F1(35).

MIX ID	Exp % 7d	Exp % 14d	Exp % 28d	Exp % 105d	Exp % 6m	Exp % 12m
C2	0.005	0.005	0.013	0.031	0.085	**0.768**
C2-F1(35)-G(0)	0.023	0.030	0.037	**0.133**	-	-
C2-F1(35)-G(6.0)	0.019	0.024	0.028	0.040	0.031	0.039
C2-F1(35)-G(8.0)	0.031	0.038	0.043	0.056	0.056	0.073
C2-F1(35)-G(8)	0.008	0.016	0.031	0.036	0.053	
C2-F1(35)-G(11.8)	0.075	0.079	0.095	**0.126**	**0.234**	**0.306**
C2-F1(35)-G(14.7)	0.061	0.099	**0.123**	**0.348**	**0.690**	**1.433**

Note: "-" indicates mortar bar was not measurable

Note: empty portions of the table indicate no measurement taken

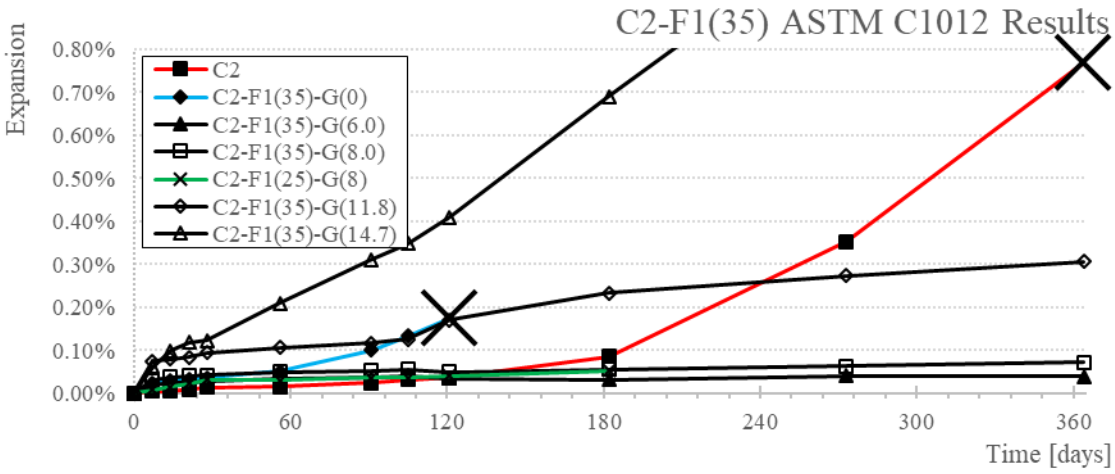

Figure 5.45. ASTM C1012 mortar bar expansion results for mixture C2-F1(35).

Table 5.24. ASTM C1012 mortar bar expansion results for mixture C2-F2(35).

MIX ID	Exp % 7d	Exp % 14d	Exp % 28d	Exp % 105d	Exp % 6m	Exp % 12m
C2	0.005	0.005	0.013	0.031	0.085	**0.768**
C2-F2(35)-G(0)	0.008	0.013	0.029	**0.271**	-	-
C2-F2(35)-G(4.1)	0.050	0.057	0.062	0.074	0.083	**0.117**
C2-F2(35)-G(5.4)	0.044	0.051	0.071	0.068	0.075	0.090
C2-F2(35)-G(8)	0.039	0.063	0.074	0.089	**0.109**	
C2-F2(35)-G(9.2)	0.022	0.032	0.041	0.084	**0.137**	**0.233**
C2-F2(35)-G(11.5)	0.033	0.045	0.062	**0.229**	**0.443**	**0.786**

Note: "-" indicates mortar bar was not measurable

Note: empty portions of the table indicate no measurement taken

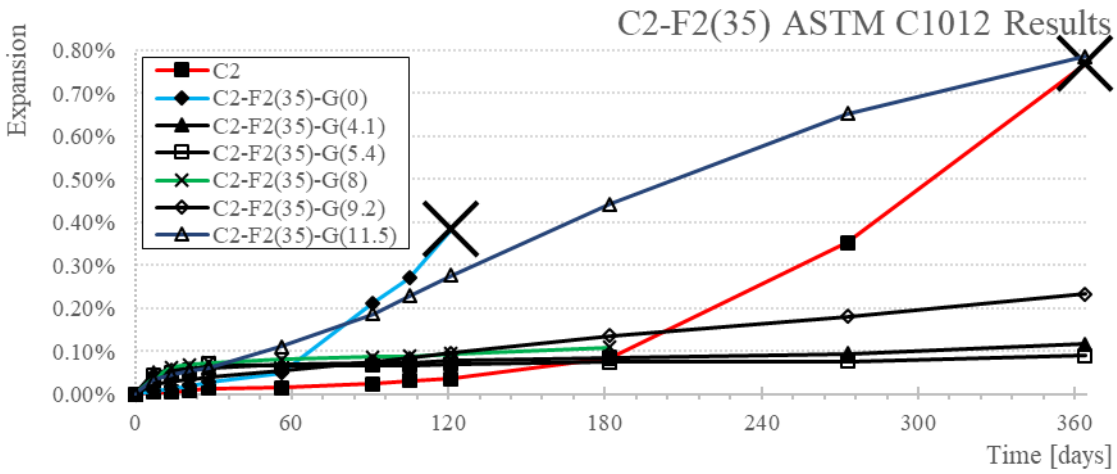

Figure 5.46. ASTM C1012 mortar bar expansion results for mixture C2-F2(35).

Table 5.25. ASTM C1012 mortar bar expansion results for mixture C2-F3(35).

MIX ID	Exp % 7d	Exp % 14d	Exp % 28d	Exp % 105d	Exp % 6m	Exp % 12m
C2	0.005	0.005	0.013	0.031	0.085	**0.768**
C2-F3(35)-G(0)	-0.002	0.001	0.014	0.046	0.077	-
C2-F3(35)-G(8)	0.012	0.024	0.029	0.050	0.093	

Note: "-" indicates mortar bar was not measurable

Note: empty portions of the table indicate no measurement taken

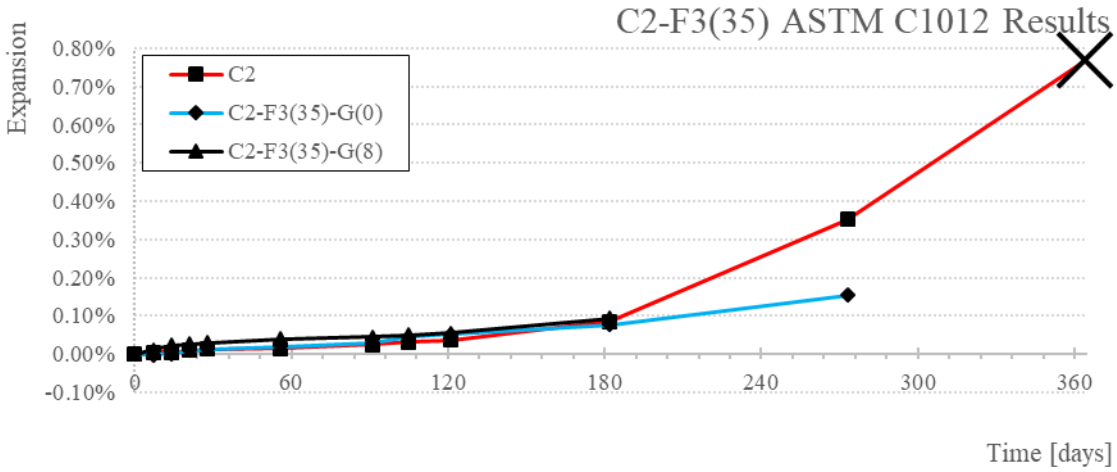

Figure 5.47. ASTM C1012 mortar bar expansion results for mixture C2-F3(35).

Table 5.26. ASTM C1012 mortar bar expansion results for mixture C2-F1(20).

MIX ID	Exp % 7d	Exp % 14d	Exp % 28d	Exp % 105d	Exp % 6m	Exp % 12m
C2	0.005	0.005	0.013	0.031	0.085	**0.768**
C2-F1(20)-G(0)	0.014	0.018	0.016	0.076	**0.247**	-
C2-F1(20)-G(3.2)	0.019	0.023	0.025	0.042	0.062	**0.160**
C2-F1(20)-G(4.3)	0.020	0.026	0.031	0.052	0.092	**0.185**
C2-F1(20)-G(6)	0.010	0.040	0.078	0.088	**0.125**	
C2-F1(20)-G(9.0)	0.015	0.022	0.039	**0.136**	**0.353**	**0.759**
C2-F1(20)-G(11.2)	0.029	0.048	0.071	**0.274**	**0.533**	**1.281**

Note: "-" indicates mortar bar was not measurable

Note: empty portions of the table indicate no measurement taken

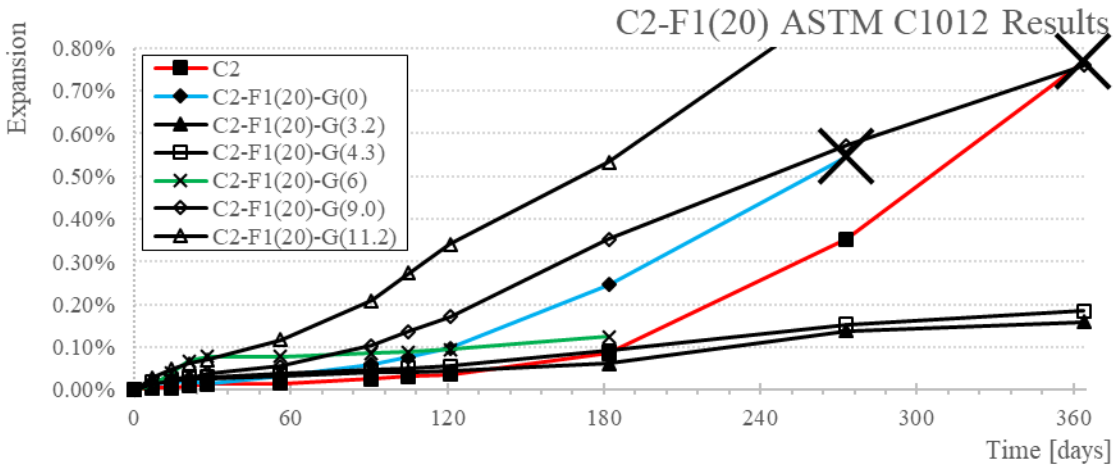

Figure 5.48. ASTM C1012 mortar bar expansion results for mixture C2-F1(20).

Table 5.27. ASTM C1012 mortar bar expansion results for mixture C2-F2(20).

MIX ID	Exp % 7d	Exp % 14d	Exp % 28d	Exp % 105d	Exp % 6m	Exp % 12m
C2	0.005	0.005	0.013	0.031	0.085	**0.768**
C2-F2(20)-G(0)	0.004	0.017	0.022	0.080	**0.315**	-
C2-F2(20)-G(2.1)	0.012	0.019	0.024	0.046	0.076	**0.297**
C2-F2(20)-G(2.8)	0.010	0.017	0.022	0.039	0.067	**0.204**
C2-F2(20)-G(6)	0.008	0.021	0.023	0.040	0.060	
C2-F2(20)-G(7.5)	0.023	0.028	0.040	**0.122**	**0.228**	**0.491**
C2-F2(20)-G(9.4)	0.035	0.047	0.061	**0.240**	**0.562**	**1.097**

Note: "-" indicates mortar bar was not measurable

Note: empty portions of the table indicate no measurement taken

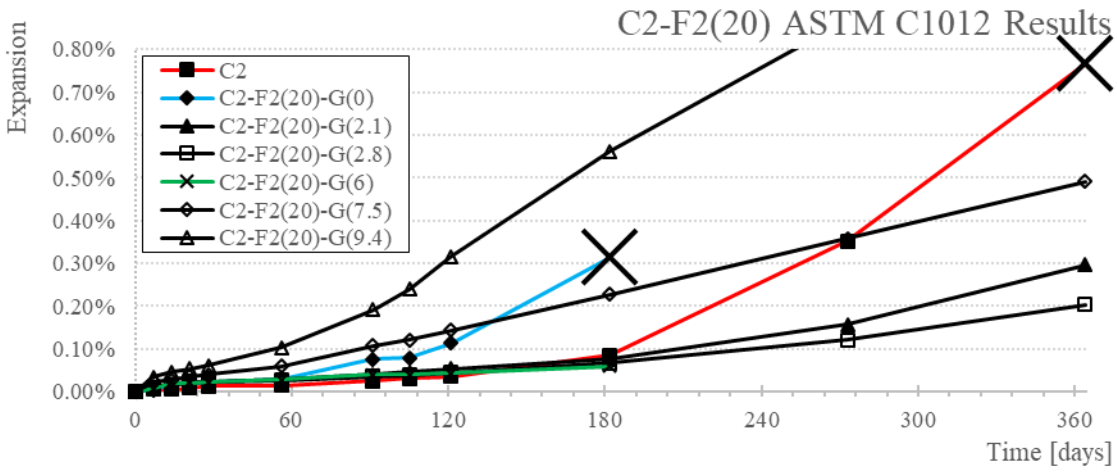

Figure 5.49. ASTM C1012 mortar bar expansion results for mixture C2-F2(20).

Table 5.28. ASTM C1012 mortar bar expansion results for mixture C2-F3(20).

MIX ID	Exp % 7d	Exp % 14d	Exp % 28d	Exp % 105d	Exp % 6m	Exp % 12m
C2	0.005	0.005	0.013	0.031	0.085	**0.768**
C2-F3(20)-G(0)	0.000	0.007	0.015	0.028	0.039	
C2-F3(20)-G(6)	0.012	0.017	0.021	0.046	0.083	

Note: "-" indicates mortar bar was not measurable
Note: empty portions of the table indicate no measurement taken

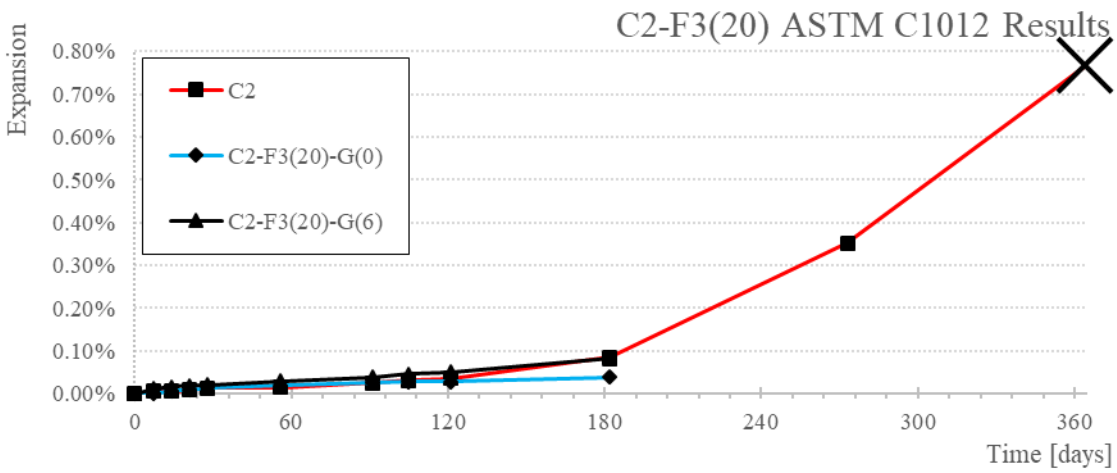

Figure 5.50. ASTM C1012 mortar bar expansion results for mixture C2-F3(20).

Table 5.29. Complete summary of ASTM C 1012 mortar bar expansion results for all 56 mixtures tested in this research study.

MIX ID	Exp % 6m	Exp % 12m
C1	**0.266**	-
C1-F1(35)-G(0)	-	-
C1-F1(35)-G(8)	0.092	
C1-F1(35)-G(10.5)	**0.462**	**0.875**
C1-F1(35)-G(11.8)	**0.829**	**1.484**
C1-F1(35)-G(14.0)	**0.988**	**1.897**
C1-F1(35)-G(14.7)	**1.178**	**2.194**
C1-F2(35)-G(0)	-	-
C1-F2(35)-G(8)	**0.217**	
C1-F2(35)-G(8.6)	0.026	0.051
C1-F2(35)-G(11.4)	**1.080**	**1.839**
C1-F2(35)-G(11.9)	**1.017**	**1.762**
C1-F2(35)-G(14.8)	**1.874**	**3.511**
C1-F3(35)-G(0)	-	-
C1-F3(35)-G(8)	**0.249**	
C1-F1(20)-G(0)	-	-
C1-F1(20)-G(6)	**0.253**	
C1-F1(20)-G(8.7)	**0.769**	**1.588**
C1-F1(20)-G(11.6)	**1.265**	**2.190**
C1-F1(20)-G(12.2)	**1.592**	**2.204**
C1-F1(20)-G(15.2)	**1.421**	**2.302**
C1-F2(20)-G(0)	-	-
C1-F2(20)-G(6)	**0.307**	
C1-F2(20)-G(7.6)	**0.578**	**1.662**
C1-F2(20)-G(10.2)	**1.184**	**1.923**
C1-F2(20)-G(10.7)	**1.105**	**1.751**
C1-F2(20)-G(13.4)	**1.307**	**2.484**
C1-F3(20)-G(0)	-	-
C1-F3(20)-G(6)	**0.240**	

MIX ID	Exp % 6m	Exp % 12m
C2	0.085	**0.768**
C2-F1(35)-G(0)	-	-
C2-F1(35)-G(6.0)	0.031	0.039
C2-F1(35)-G(8.0)	0.056	0.073
C2-F1(25)-G(8)	0.053	
C2-F1(35)-G(11.8)	**0.234**	**0.306**
C2-F1(35)-G(14.7)	**0.690**	**1.433**
C2-F2(35)-G(0)	-	-
C2-F2(35)-G(4.1)	0.083	**0.117**
C2-F2(35)-G(5.4)	0.075	0.090
C2-F2(35)-G(8)	**0.109**	
C2-F2(35)-G(9.2)	**0.137**	**0.233**
C2-F2(35)-G(11.5)	**0.443**	**0.786**
C2-F3(35)-G(0)	0.077	-
C2-F3(35)-G(8)	0.093	
C2-F1(20)-G(0)	**0.247**	
C2-F1(20)-G(3.2)	0.062	**0.160**
C2-F1(20)-G(4.3)	0.092	**0.185**
C2-F1(20)-G(6)	**0.125**	
C2-F1(20)-G(9.0)	**0.353**	**0.759**
C2-F1(20)-G(11.2)	**0.533**	**1.281**
C2-F2(20)-G(0)	**0.315**	
C2-F2(20)-G(2.1)	0.076	**0.297**
C2-F2(20)-G(2.8)	0.067	**0.204**
C2-F2(20)-G(6)	0.060	
C2-F2(20)-G(7.5)	**0.228**	**0.491**
C2-F2(20)-G(9.4)	**0.562**	**1.097**
C2-F3(20)-G(0)	0.039	
C2-F3(20)-G(6)	0.083	

Note: "-" indicates mortar bar was not measurable.

Note: empty portions of the table indicate no measurement taken.

5.5.2 Discussion

In total, 16 of the 56 mixtures passed ASTM C 1012 by meeting the expansion limits of ASTM C 1157 and C 595 (as shown in **Table 5.16**), not including the straight cement mixture containing C2 (a Type I/II sulfate-resistant cement). Mixtures which consisted of straight cement and cement with fly ash, as well as the mixtures which did not contain gypsum, degraded rapidly with a complete loss of cohesion.

Mortar bars that failed ASTM C 1012 that contained less than nominally 10% gypsum additive degraded in the same way as the straight cement mixtures, but always took a longer period of time to fail. When the mortar bars began to fail, cracking and degradation would start at the corners, which would be followed by cracking of the cross-section, then complete loss of cohesion and crumbling.

A limited number of mixtures (2) containing cement C1 passed. Mixtures C1-F1(35)-G(8) and C1-F2(35)-G(8.6) can be classified as exhibiting a moderate sulfate resistance. One of the passing mixtures, C1-F2(35)-G(8.6), was from phase 1. As part of phase 2, a replicate mixture was prepared, C1-F2(35)-G(8), to show repeatable results. Unfortunately, the results from phase 1 could not be repeated. The discrepancy in behavior between the two mixtures is potentially due to a prolonged curing period that mixture C1-F2(35)-G(8.6), which cured for 1 day too many (having achieved strength on a Sunday during a holiday weekend) and was placed in Na_2SO_4 1 day later than the replicate mixture C1-F2(35)-G(8). The occurrence of C1-F1(35)-G(8.6) having cured too long was a mistake made early on this research project which was not repeated.

Mixtures containing cement C2 performed better relative to mixtures containing cement C1. In total, 15 mixtures passed at 6 months. Cement C2 is a sulfate resisting cement which made it more likely for mixtures in which was used to perform better. In

general, mixtures containing C2 which passed also contained less gypsum (nominally less than 6 - 8%).

In analyzing the ASTM C 1012 data, a pattern emerged with respect to gypsum dosages. Mixtures using either cement C1 or C2 having contained gypsum quantities greater than or equal 10% typically showed:

a. Slow strength gain, often taking nominally 5-9 days for the mortar cubes to achieve a compressive strength of 20 MPa. These results imply the mixtures will not be feasible for practical use in construction.
b. High (nominally greater than 0.5%) expansion levels at 6 months.
c. Mortar bars were still intact even though expansion levels were excessive.
d. Degradation of the mortar bars differed in appearance from mixtures containing lower amounts of gypsum. Mortar bars containing greater than 10% gypsum showed very high levels of expansion, with no cracking at one year. However, the mortar bars were often warped, taking on a banana shaped appearance, having a noticeable curvature.

The results of this study indicate that mortars containing the amount of gypsum required by the guidance of Tikalsky and Carrasquillo [7] create mortars which expand well beyond limits imposed by ASTM. Other research studies [8, 9] have come to the same conclusion. The mortars in this study which contain the gypsum required to meet the guidance outlined by Tikalsky and Carrasquillo did not fail, by a complete lack of cohesion, but showed excessive levels of expansion (nominally greater than 0.5% at 6 months). Given previous research, in conjunction with the results of this study it is concluded here that the underlying assumptions presented by Tikalsky and Carrasquillo in proportioning the correct dosages of gypsum as an additive in binary blends of high calcium fly ash as a replacement for cements will not yield mortars that will meet ASTM standards.

5.6 Comparative Analysis of All Testing

The following presents a comparison between the data collected from all the testing methods performed in this research study. A pattern emerges when the data from each of the tests is overlaid, thus **Figures 5.51-5.62** have been prepared to show this pattern. The independent variable for all the figures shown is gypsum. The comparison of the data will be used to provide analysis pertaining to the passing or failing results obtained in ASTM C 1012 testing. The findings of this study appear to indicate that a comparison like the ones shown in the proceeding section can be used in future research as a means for developing a method for predicting the sulfate resistance of a given mixture. The comparative analysis results will also be examined against Lerch's criteria.

5.6.1 Results

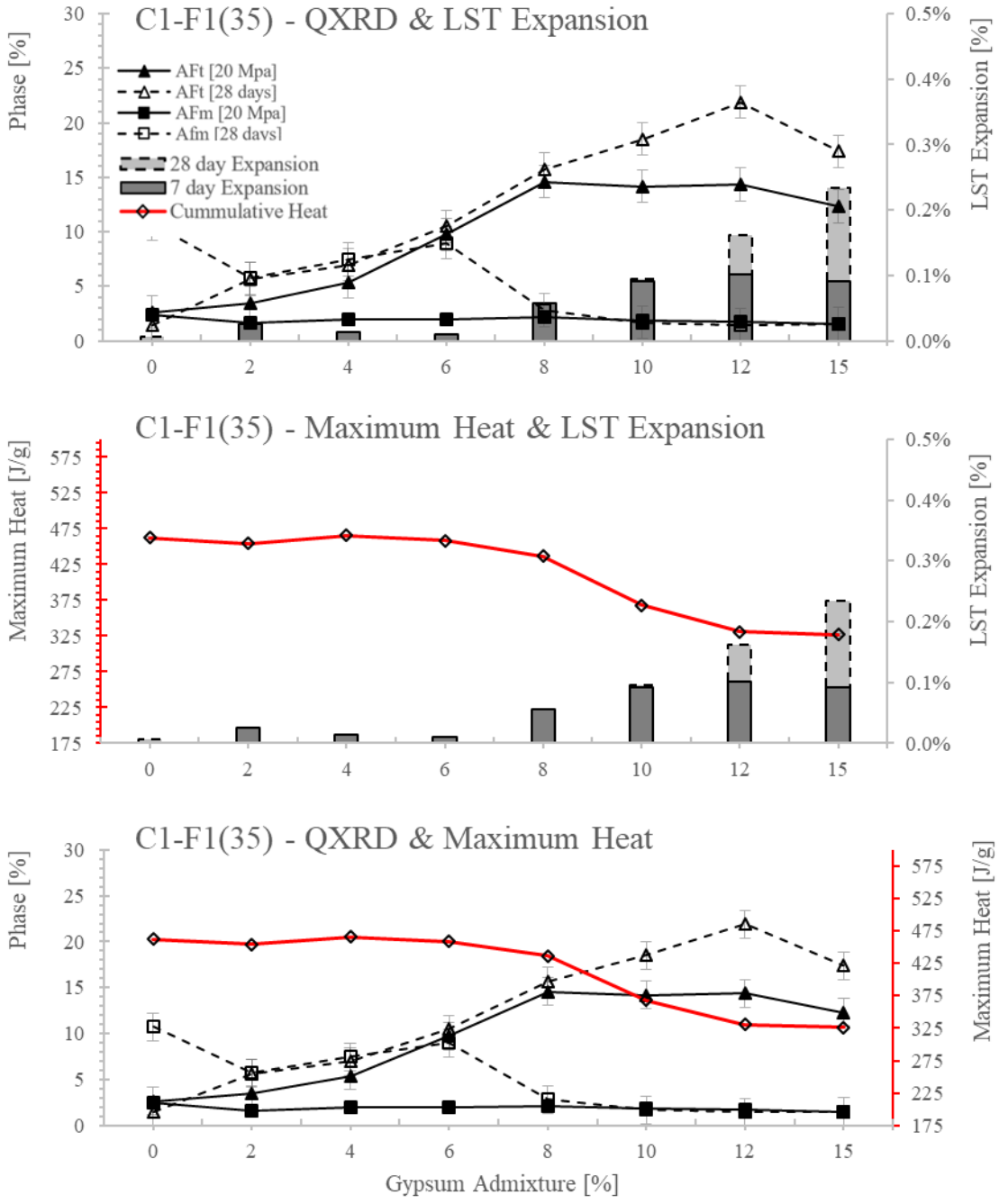

Figure 5.51. Comparison of expansion data from LST, QXRD analysis, and maximum heat curves for mixture C1-F1(35).

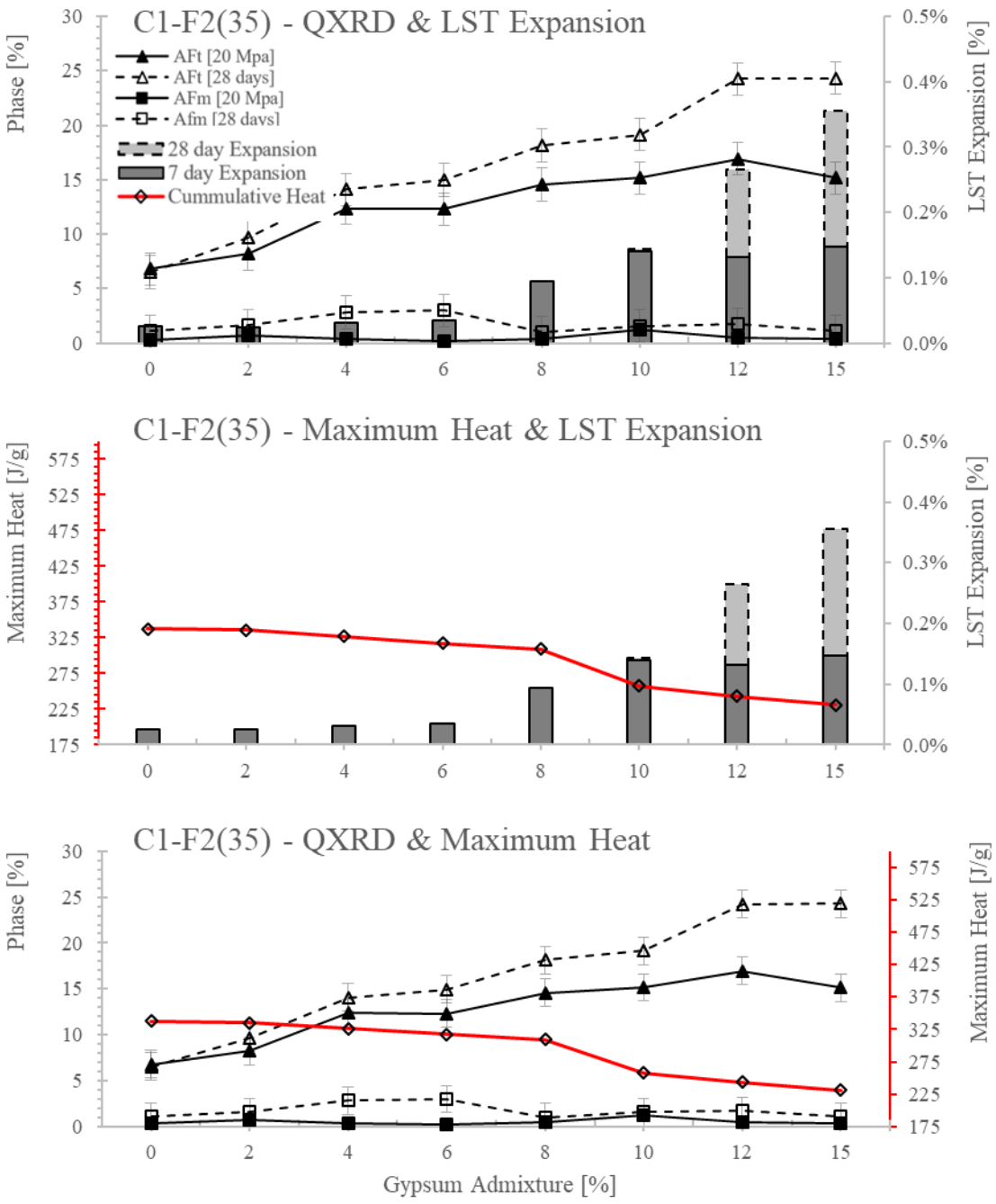

Figure 5.52. Comparison of expansion data from LST, QXRD analysis, and maximum heat curves for mixture C1-F2(35).

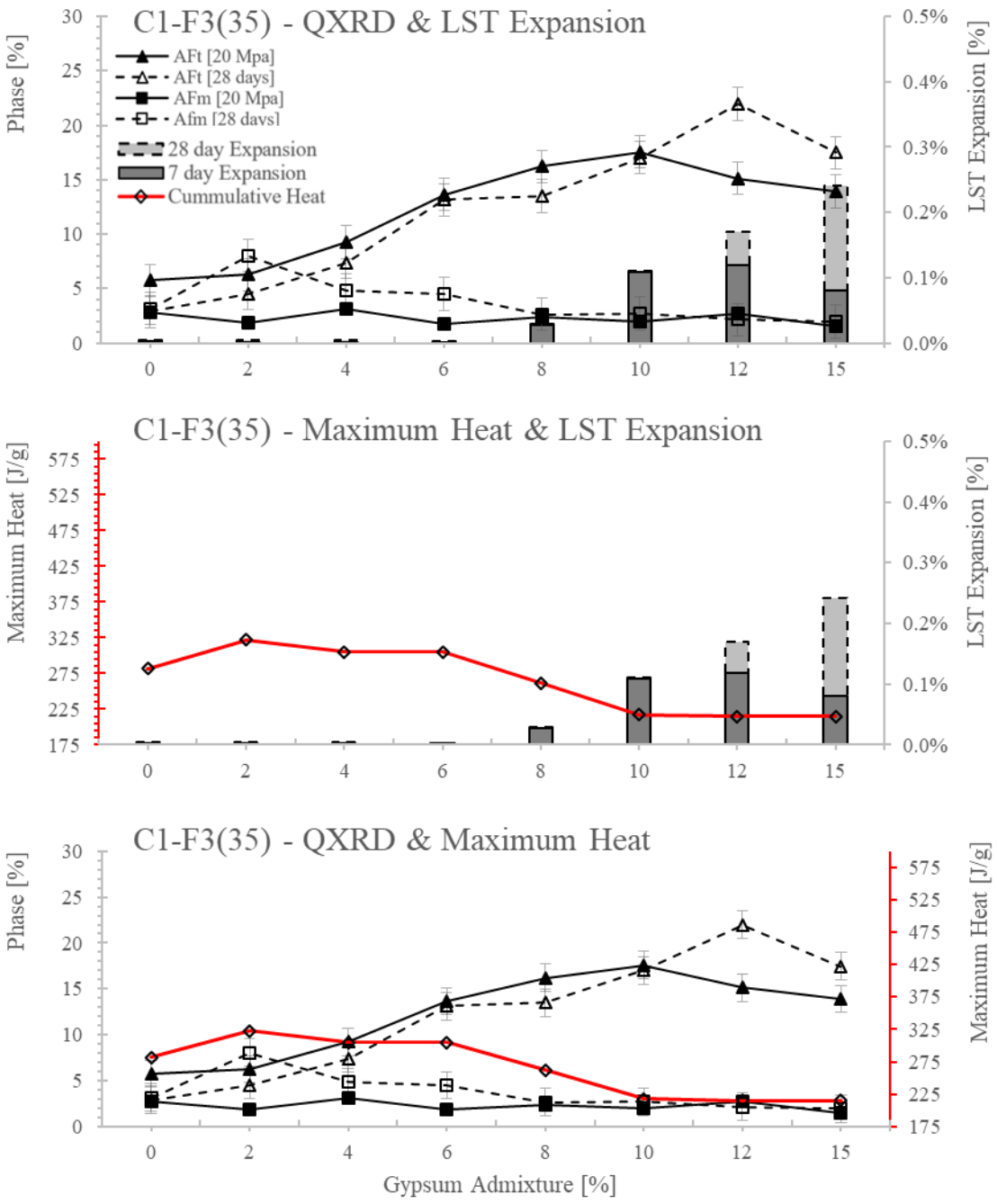

Figure 5.53. Comparison of expansion data from LST, QXRD analysis, and maximum heat curves for mixture C1-F3(35).

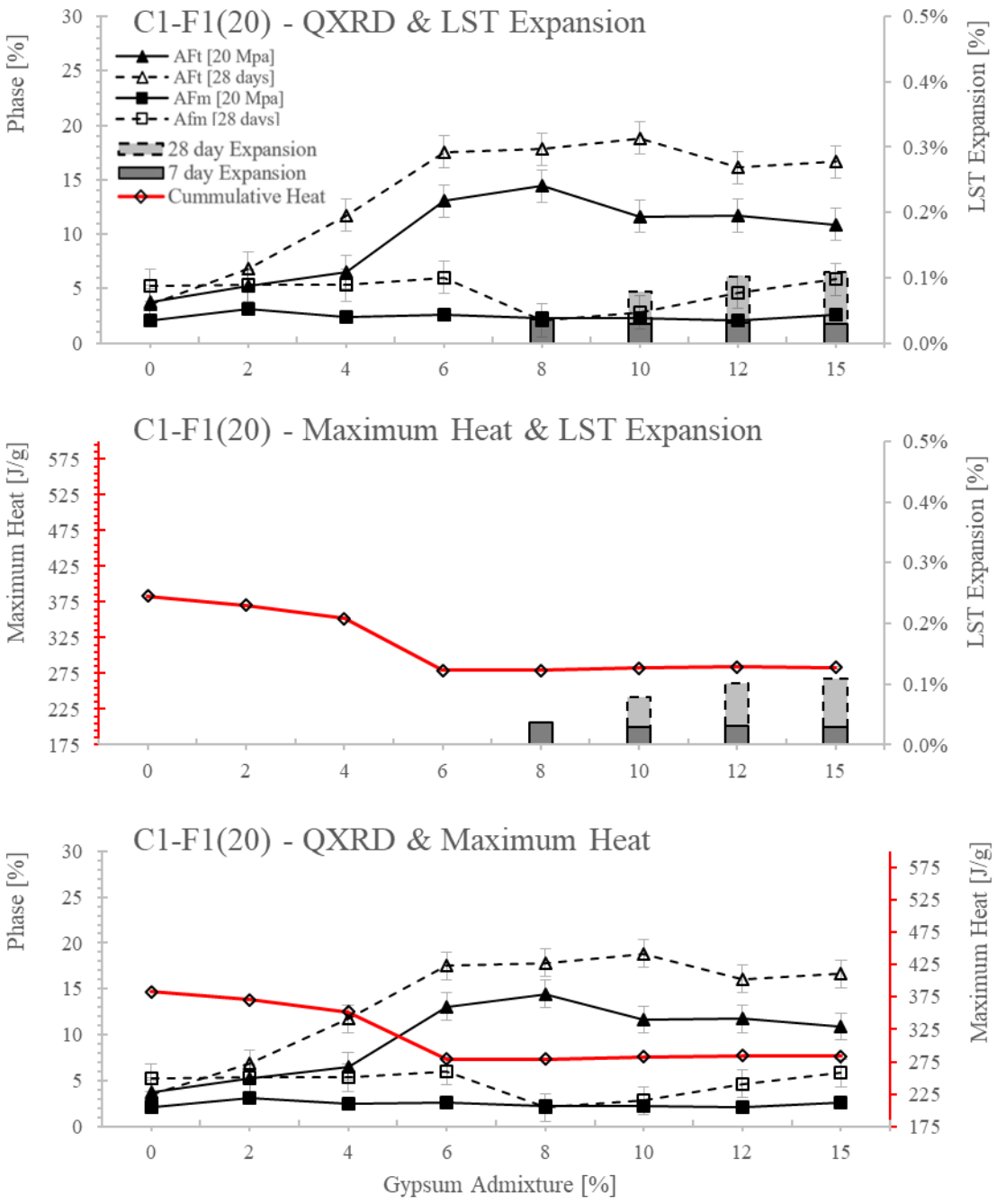

Figure 5.54. Comparison of expansion data from LST, QXRD analysis, and maximum heat curves for mixture C1-F1(20).

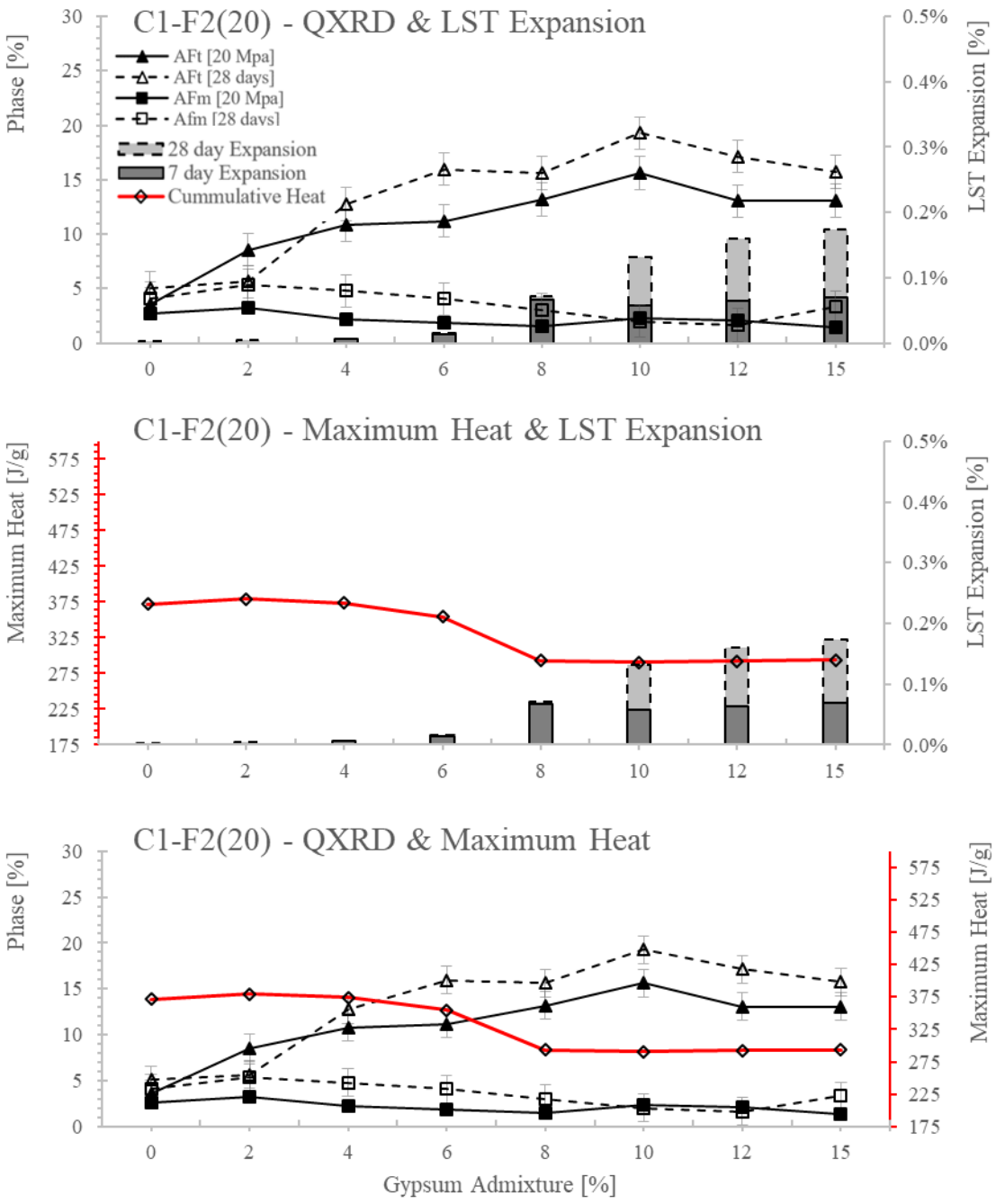

Figure 5.55. Comparison of expansion data from LST, QXRD analysis, and maximum heat curves for mixture C1-F2(20).

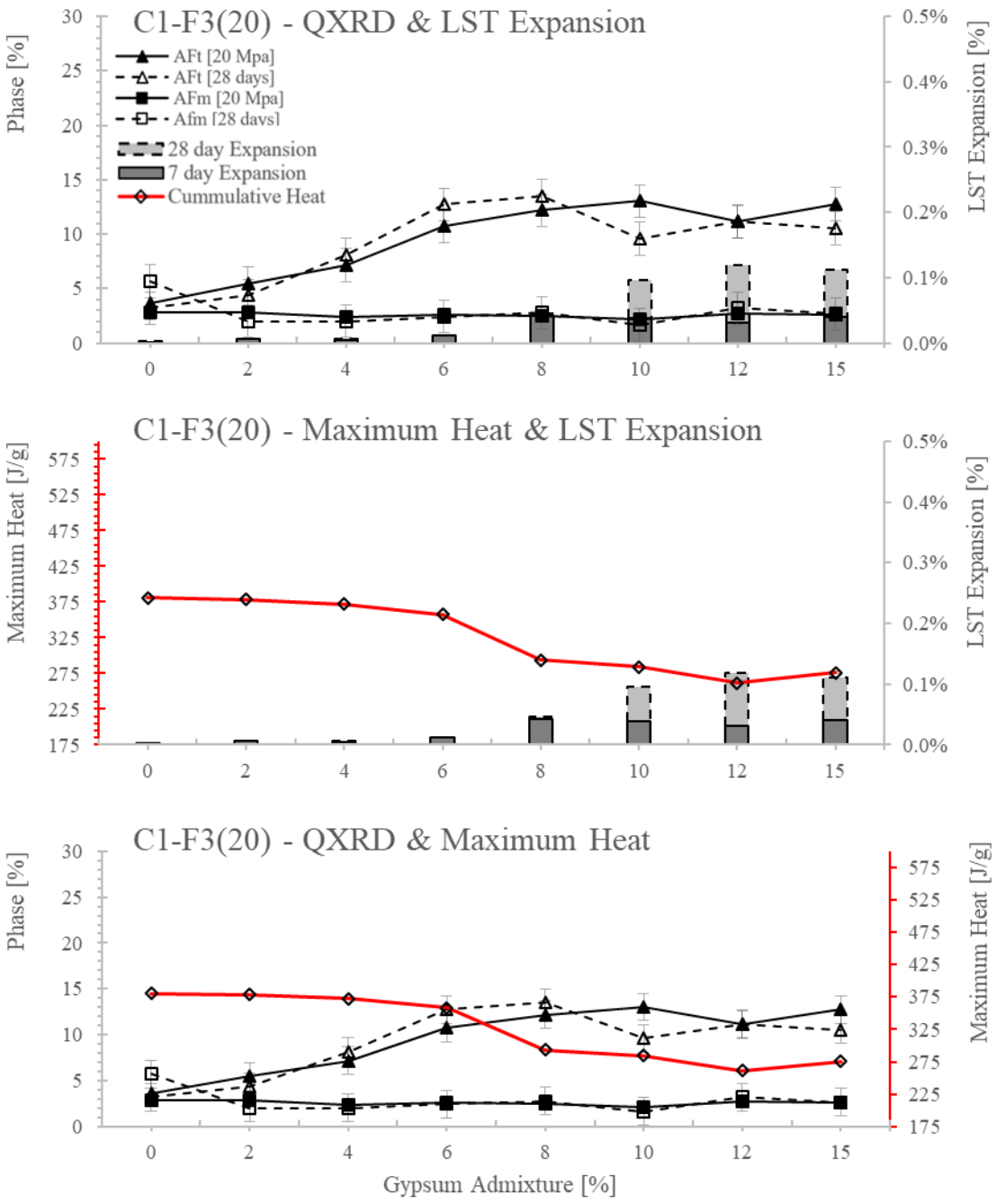

Figure 5.56. Comparison of expansion data from LST, QXRD analysis, and maximum heat curves for mixture C1-F3(20).

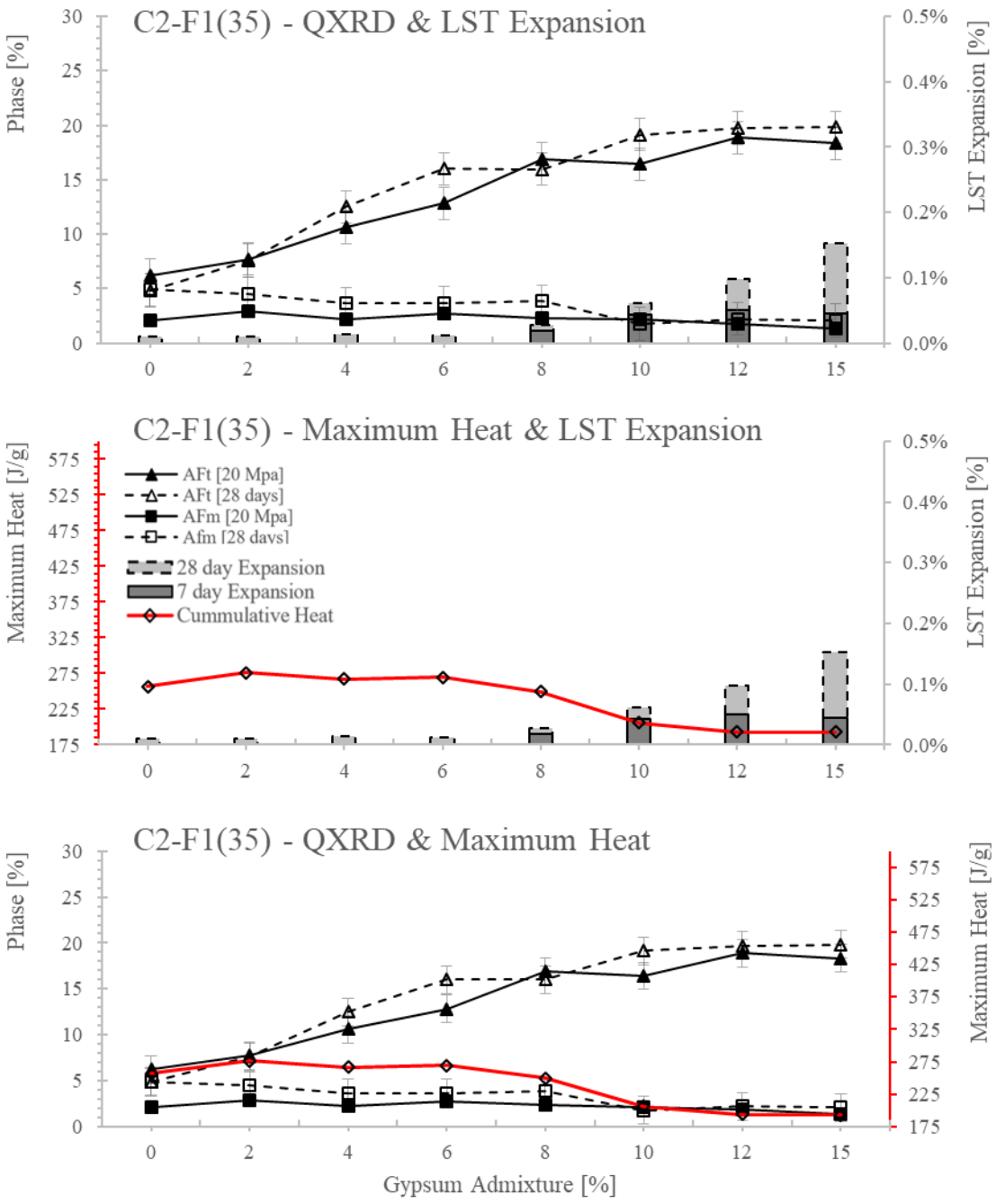

Figure 5.57. Comparison of expansion data from LST, QXRD analysis, and maximum heat curves for mixture C2-F1(35).

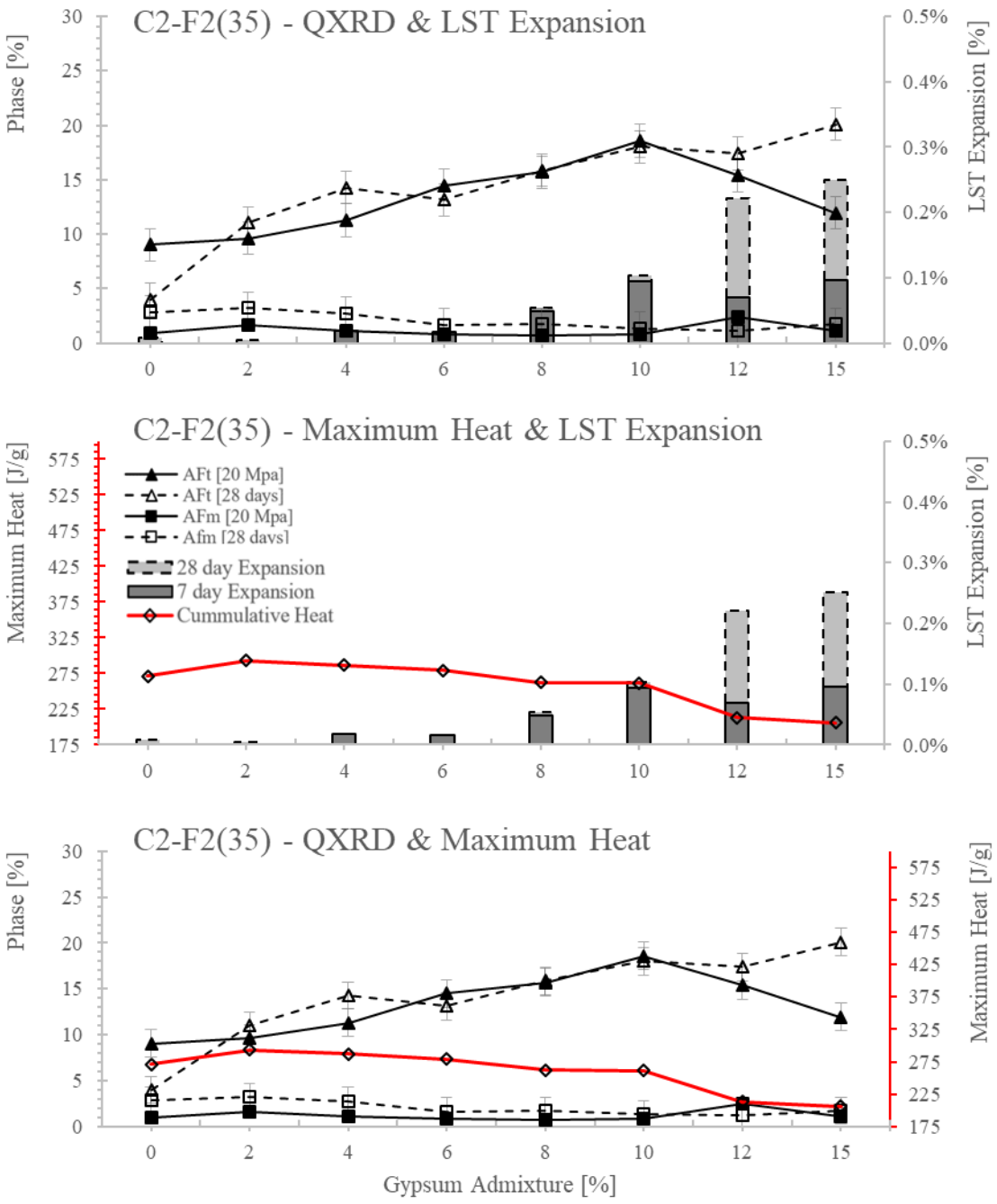

Figure 5.58. Comparison of expansion data from LST, QXRD analysis, and maximum heat curves for mixture C2-F2(35).

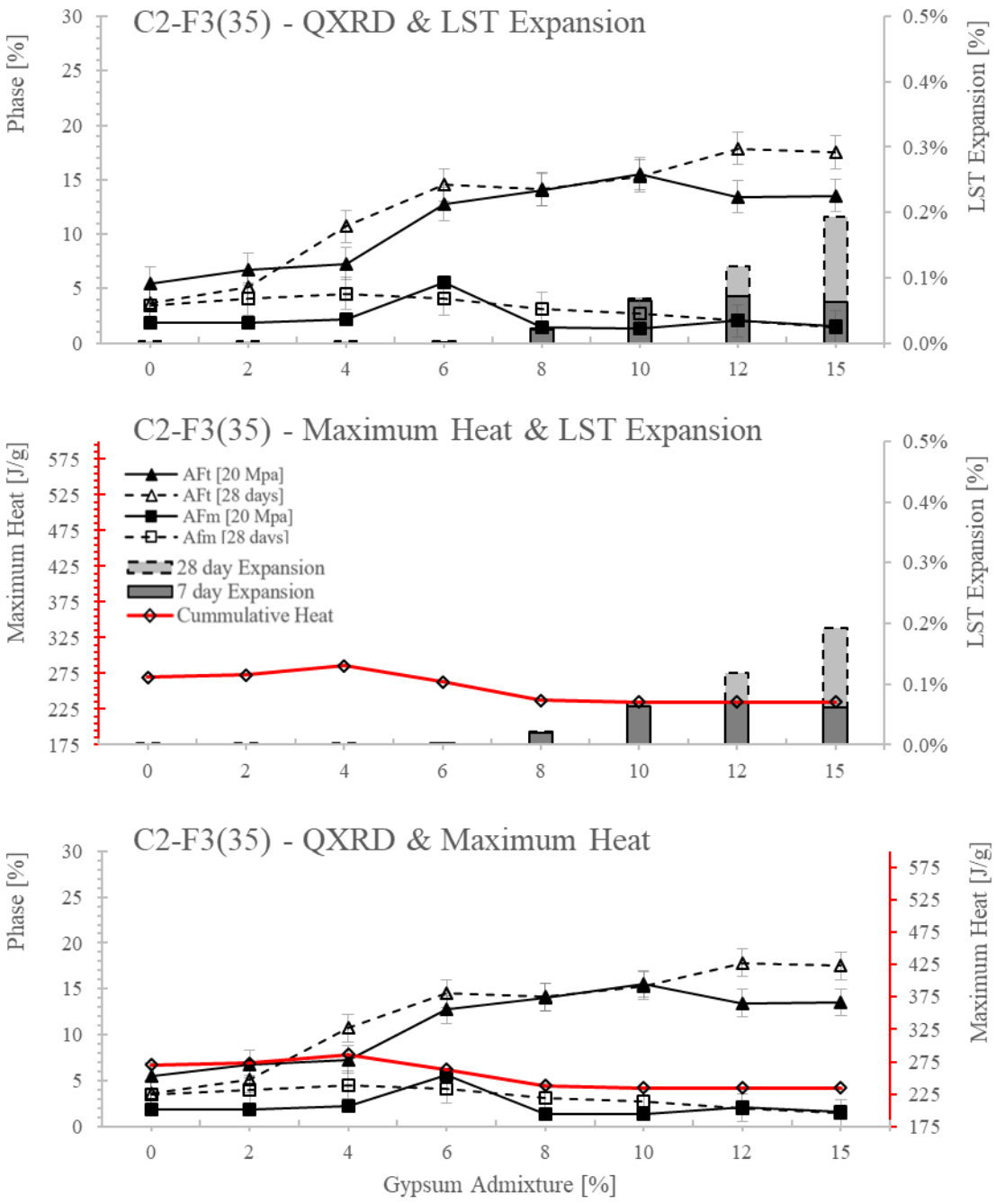

Figure 5.59. Comparison of expansion data from LST, QXRD analysis, and maximum heat curves for mixture C2-F3(35).

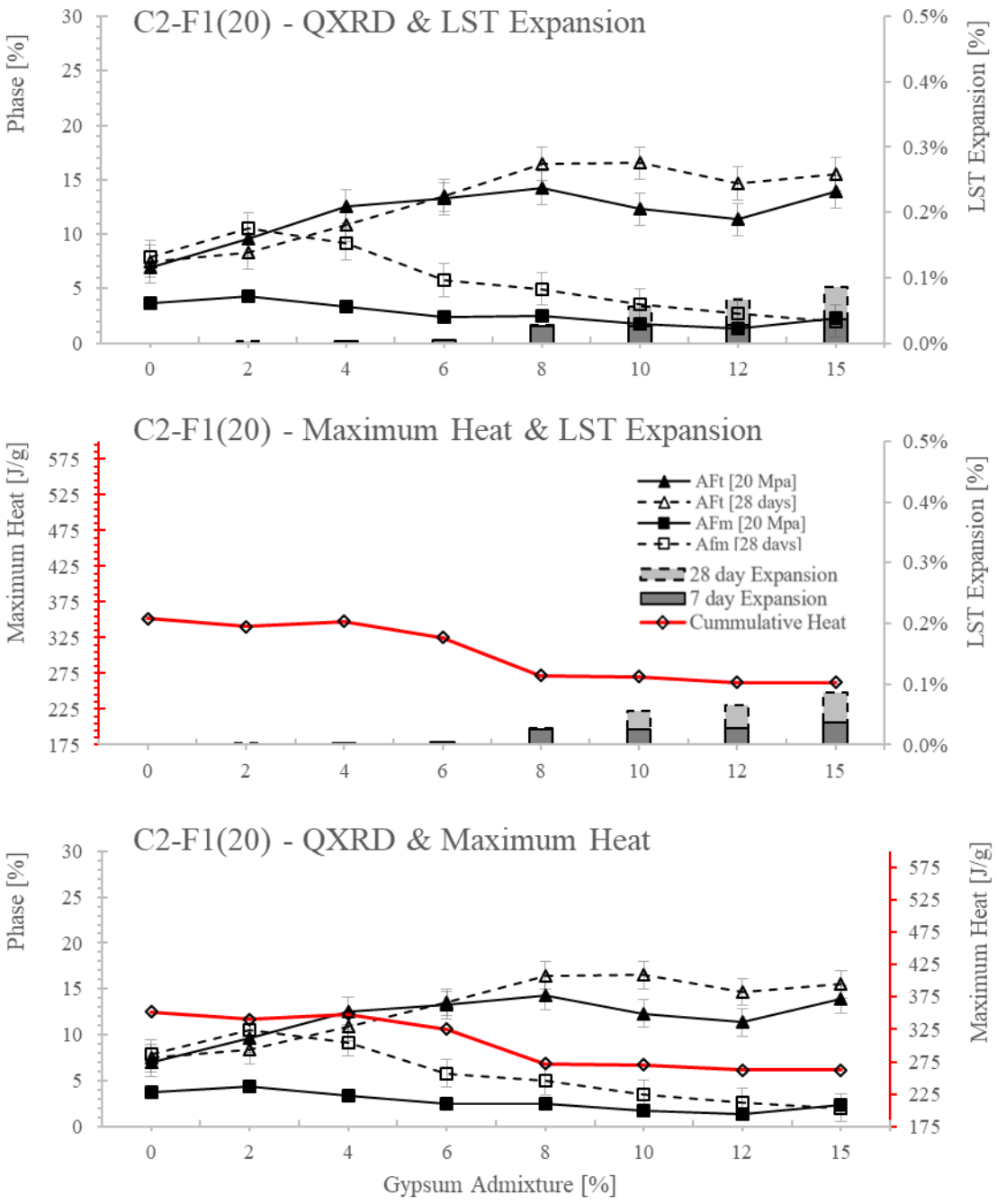

Figure 5.60. Comparison of expansion data from LST, QXRD analysis, and maximum heat curves for mixture C2-F1(20).

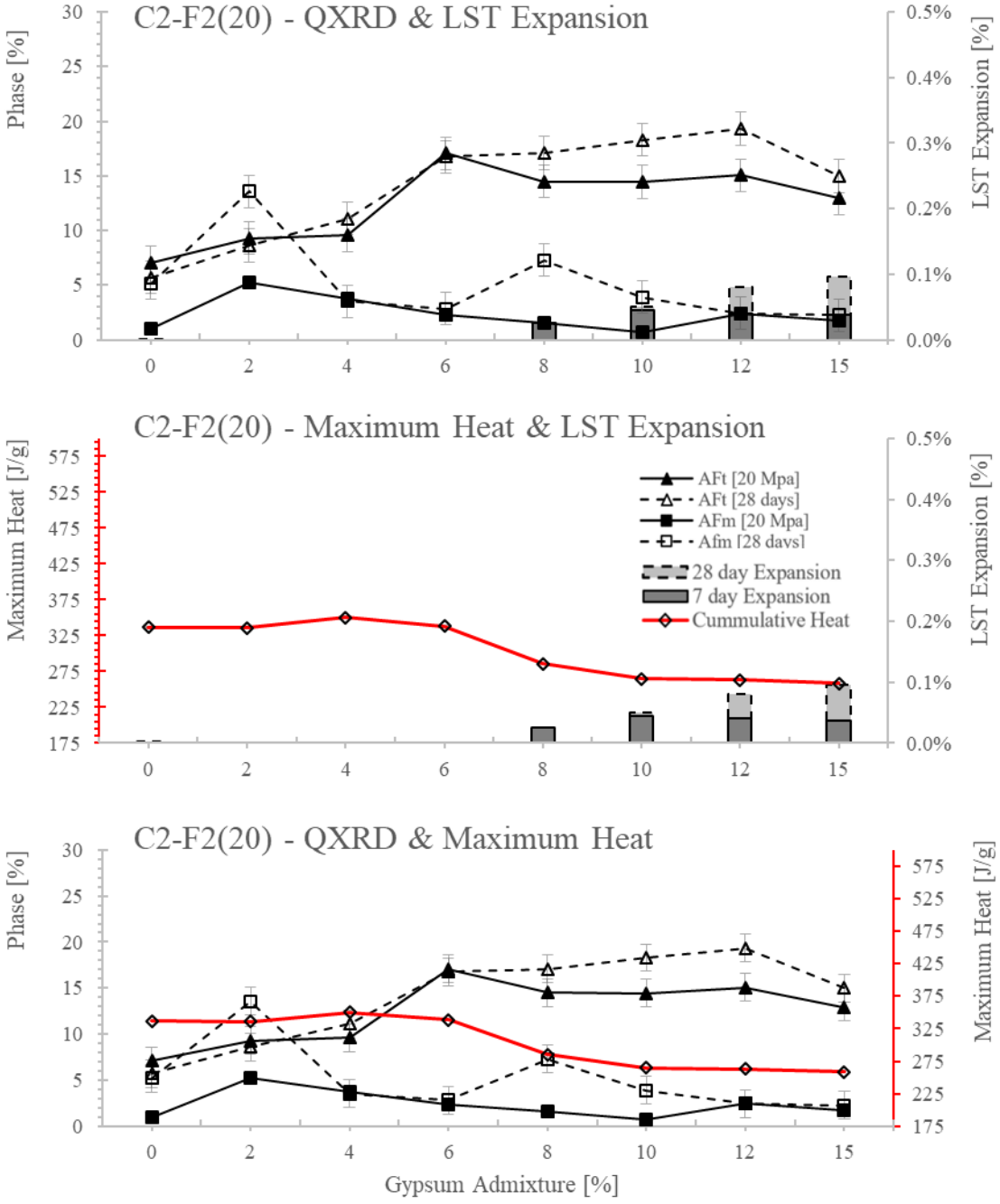

Figure 5.61. Comparison of expansion data from LST, QXRD analysis, and maximum heat curves for mixture C2-F2(20).

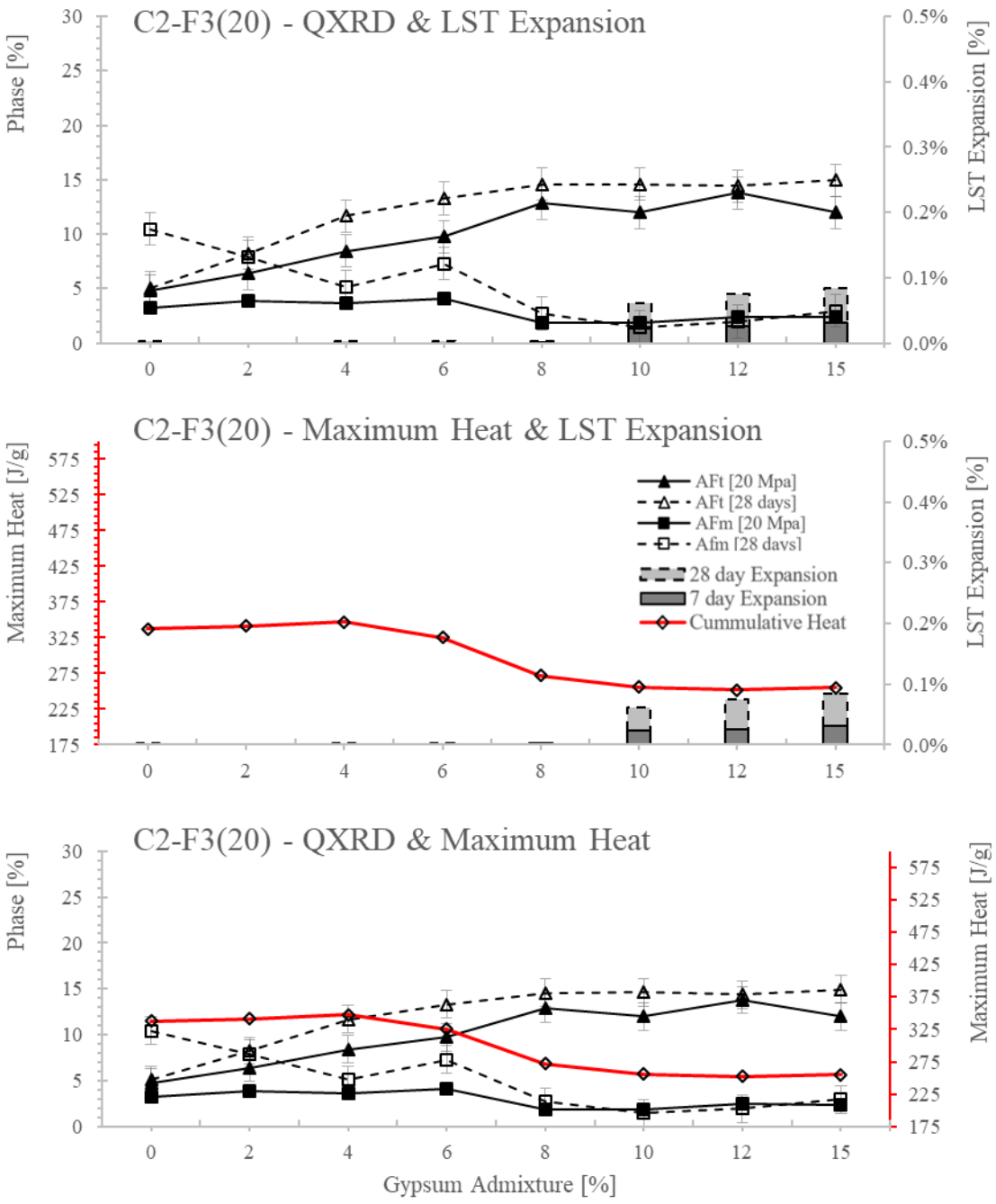

Figure 5.62. Comparison of expansion data from LST, QXRD analysis, and maximum heat curves for mixture C2-F3(20).

5.6.2 Discussion

The comparative analysis results shown in **Figures 5.51-5.62** indicate two important points of interest which include:

1. A drop in maximum heat is coincident with an increase in expansion at 7 days, and peak AFt formation on the 20 MPa curve.
2. The secondary plateau of the maximum heat curve is coincident with peak AFt formation on the 28 day curve and increased early age expansion.

These results are showing a correlation between the heat of hydration, early age expansion, and hydration product formation. One can infer from the results that when a large drop in maximum heat is recorded in isothermal calorimetry testing, that early age expansion (not due to external sulfate attack) will occur. Additionally, the drop in maximum heat indicates that the most benefit from gypsum addition with respect to C_3A dissolution has been achieved, thus forming the maximum amount of AFt possible at early ages of the binder's life (while it is still relatively plastic).

A comparison of mixtures which passed ASTM C 1012 to those which meet Lerch's guidance provides insight into a possible short-term method for determining the sulfate resistance of a cement binder. Mixtures that passed ASTM C 1012 testing and meet Lerch's guidance for a properly retarded cement are presented in **Table 5.30**.

Table 5.30. Summary of passing results of ASTM C 1012 testing that meet Lerch's recommendations for a properly retarded cement.

MIX ID	Exp % 6m	Exp % 12m
C1-F1(35)-G(8)	0.092	
C2-F1(35)-G(6.0)	0.031	0.039
C2-F2(35)-G(4.1)	0.083	**0.117**
C2-F2(35)-G(5.4)	0.075	0.090
C2-F1(20)-G(4.3)	0.092	**0.185**
C2-F2(20)-G(6)	0.060	
C2-F3(20)-G(6)	0.083	

When comparing the mixtures which passed ASTM C 1012 testing and those which meet Lerch's guidance it becomes clear that mixtures containing nominally less than 6% gypsum yield the best results. In total, 7 of the 16 passing results from ASTM C 1012 meet Lerch's criteria, while the remaining 9 mixtures that passed ASTM C 1012 include mixture proportion that include gypsum dosages within nominally ±2% of Lerch's guidance. Interestingly, research conducted at the University of Texas at Austin [9] using fly ashes F2 and F3, with similar replacement quantities as those used in this research, also achieved passing results with gypsum quantities that also appear to agree with Lerch's guidance.

While it would be seemingly advantageous to try and utilize gypsum additions that achieve the most amount of AFt possible, thereby mitigating the likelihood of sulfate attack, doing so generates excessive early age expansion and low maximum heat. This is a two-fold practical problem: the excessive early age expansion generated by high levels of gypsum would yield concrete and/or mortar elements that do not exhibit the volume stability required by the construction industry, and the low maximum heat does not produce concrete and/or mortar with adequate levels of strength gain that meet the time sensitive demands of construction.

6.0 Conclusions

Based on a review of literature, testing performed by other researchers, the characteristics and chemical composition of the materials used as part of this testing, the testing performed as part of this research study, and an analysis of the results yielded from the testing herein, conclusions of this research indicate:

- The use of gypsum is an effective method at mitigating external sulfate attack in binary blends of Type I or Type I/II cements with high calcium fly ash as a replacement for cement.
- The method developed by researchers [7] for determining adequate gypsum content to mitigate sulfate attack in binary blends of Type I or Type I/II cements with high calcium fly ash as a replacement for cement will yield a material that does not meet ASTM requirements.
- Mixtures containing C2 (a Type I/II cement) generated better sulfate resistant blends in this study, than mixtures containing C1 (a Type I cement).
- It appears possible to run a series of short term tests as indices for predicting the sulfate resistance of binary blends of Type I or Type I/II cements with high calcium fly ash as a replacement for cement which include: isothermal calorimetry, early expansion testing (likely ASTM C 1038), and QXRD.

7.0 Appendix

C1-F1(35)-G(0A)

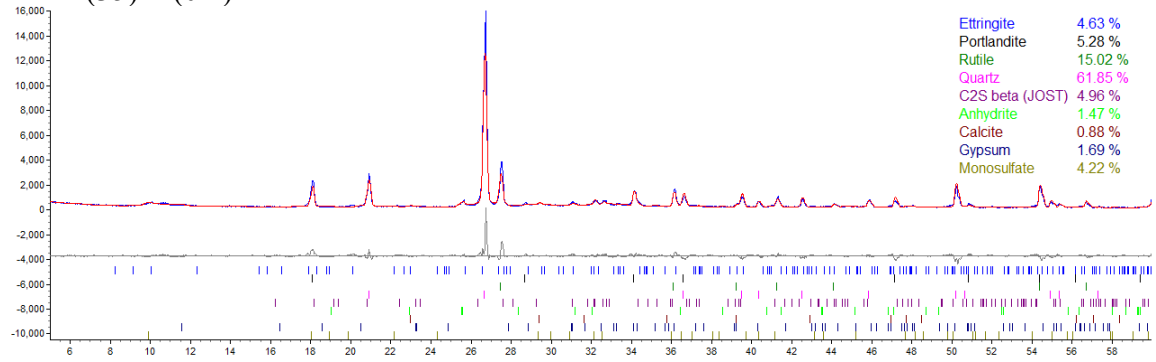

C1-F1(35)-G(0B)

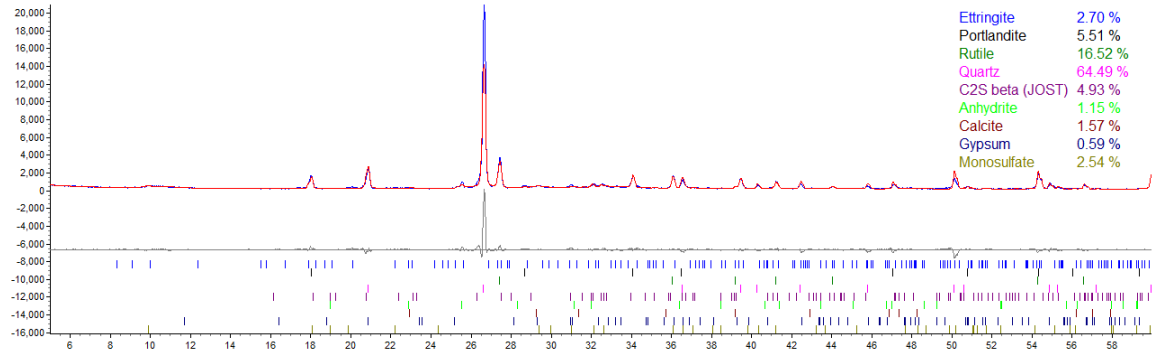

Figure A1. X-ray diffraction pattern and Rietveld refinement: C1-F1(35)-G(0).

C1-F1(35)-G(2A)

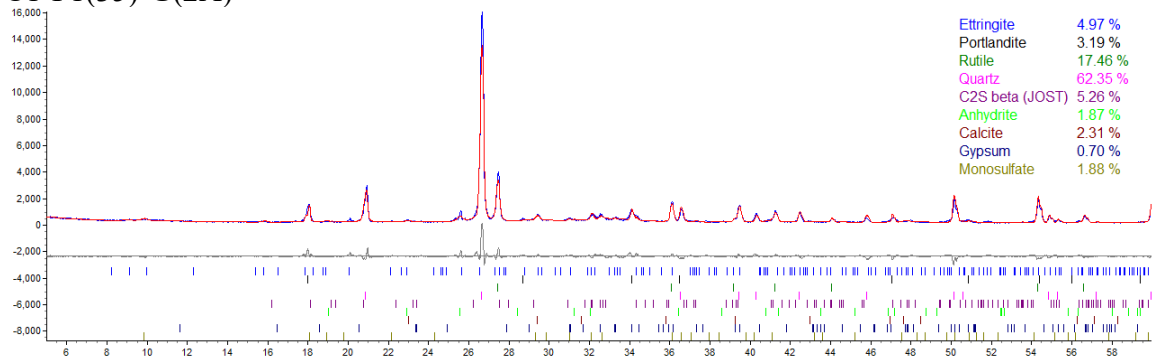

C1-F1(35)-G(2B)

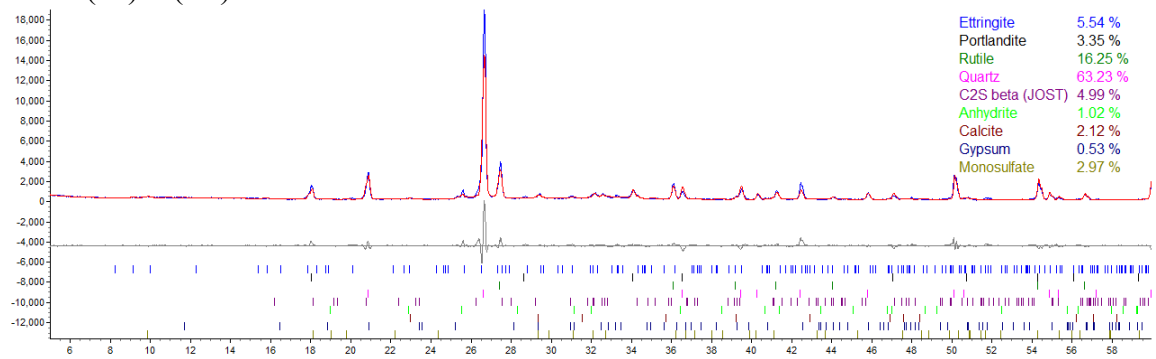

Figure A2. X-ray diffraction pattern and Rietveld refinement: C1-F1(35)-G(2).

C1-F1(35)-G(4A)

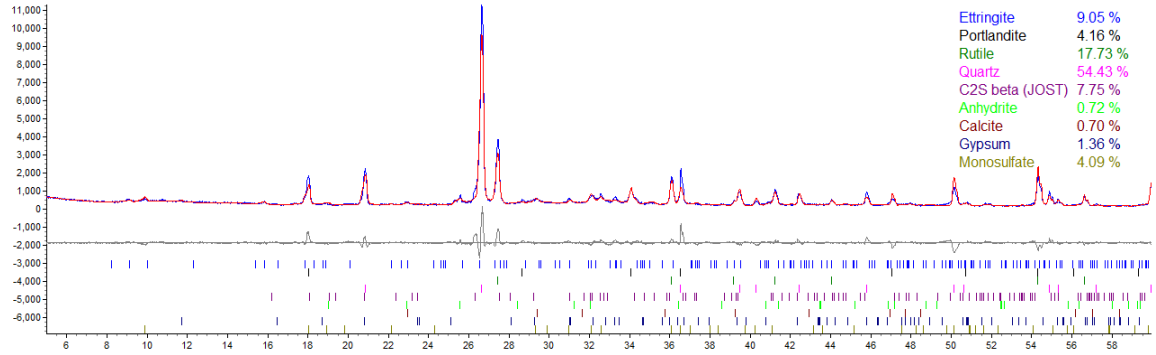

C1-F1(35)-G(4B)

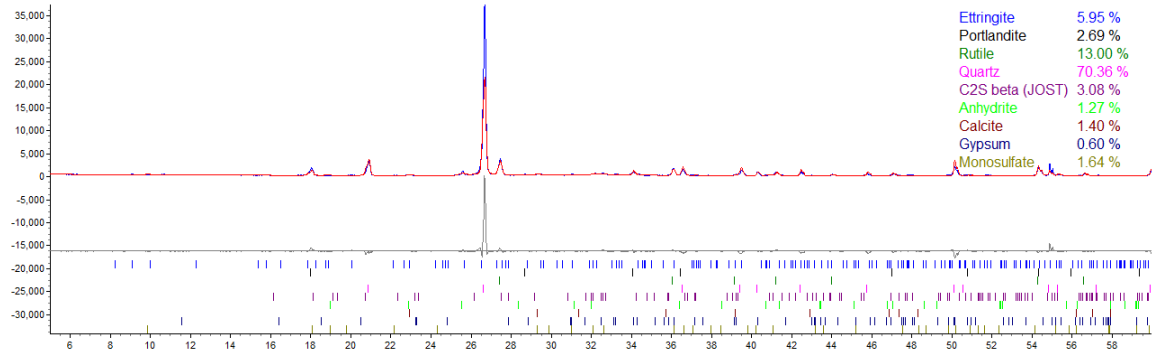

Figure A3. X-ray diffraction pattern and Rietveld refinement: C1-F1(35)-G(4).

C1-F1(35)-G(6A)

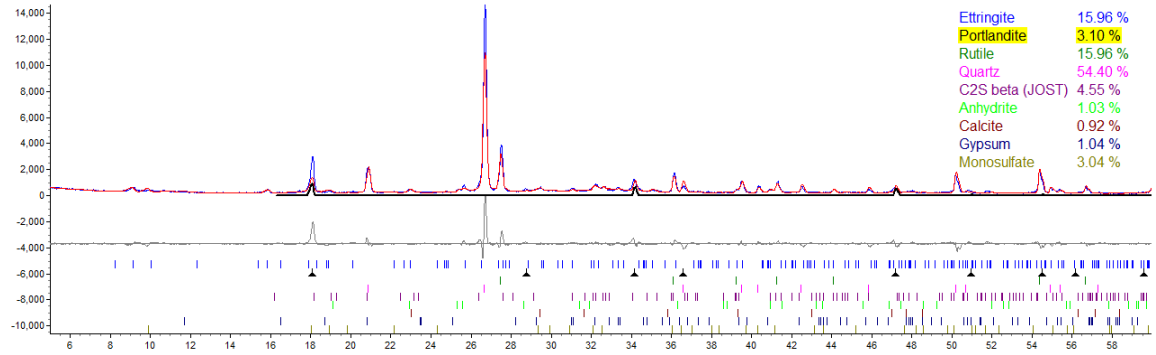

C1-F1(35)-G(6B)

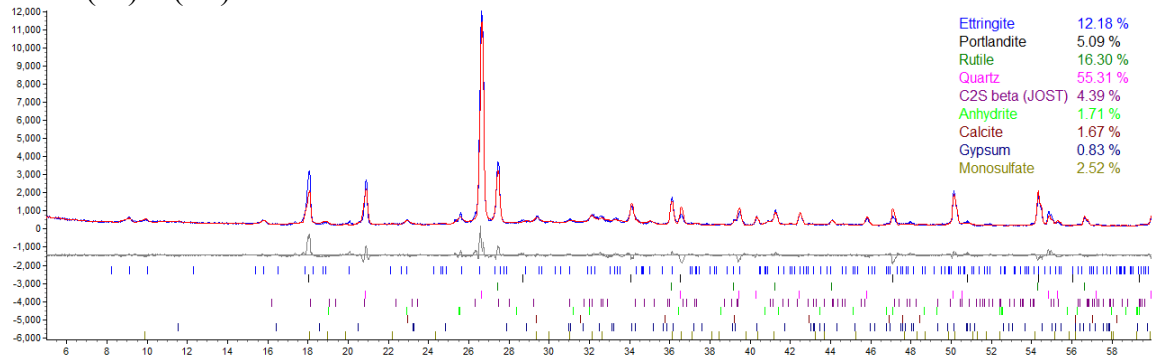

Figure A4. X-ray diffraction pattern and Rietveld refinement: C1-F1(35)-G(6).

C1-F1(35)-G(8A)

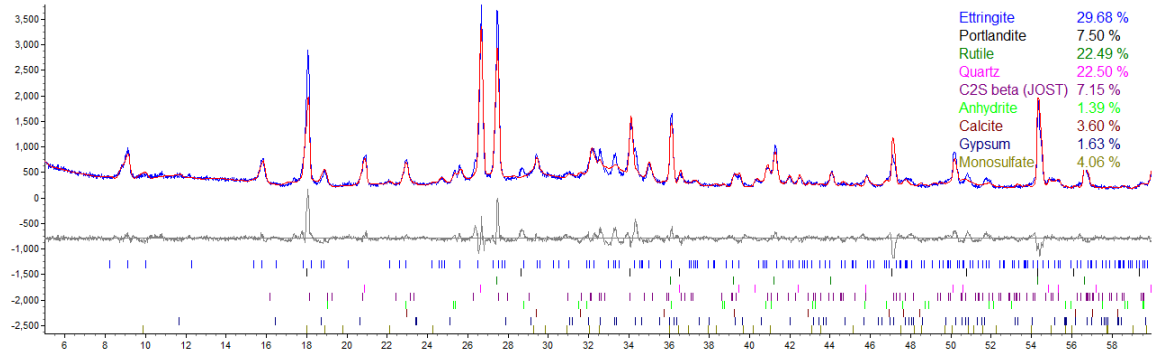

C1-F1(35)-G(8B)

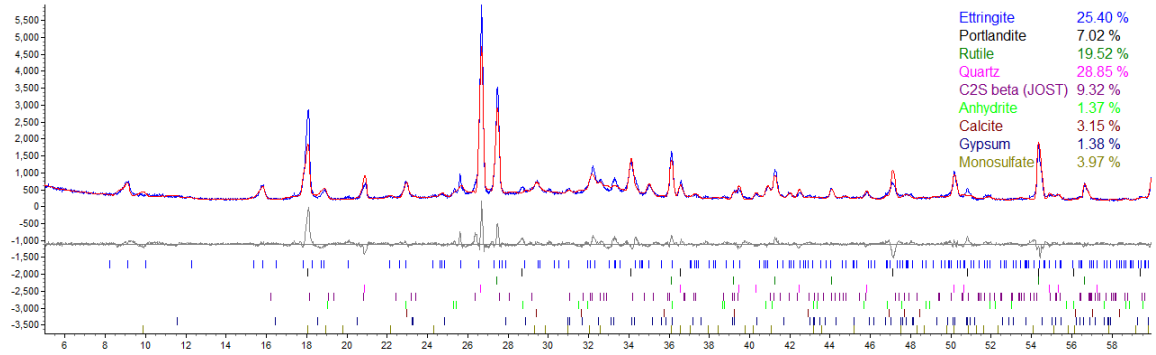

Figure A5. X-ray diffraction pattern and Rietveld refinement: C1-F1(35)-G(8).

C1-F1(35)-G(10A)

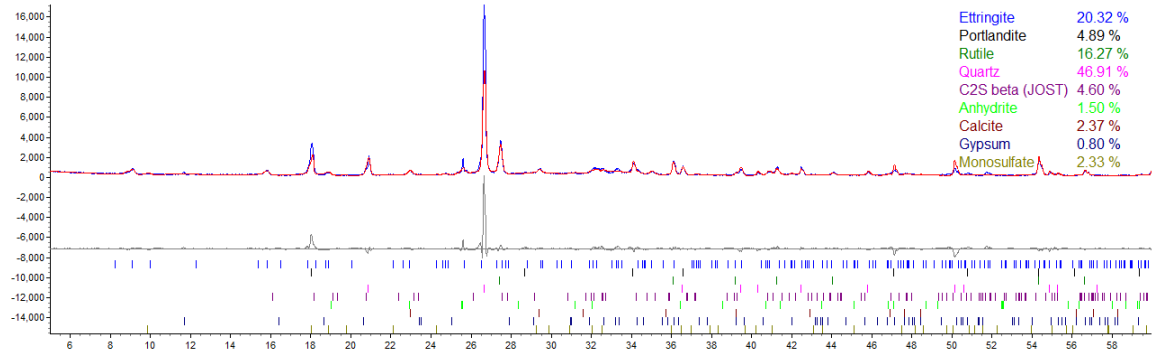

C1-F1(35)-G(10B)

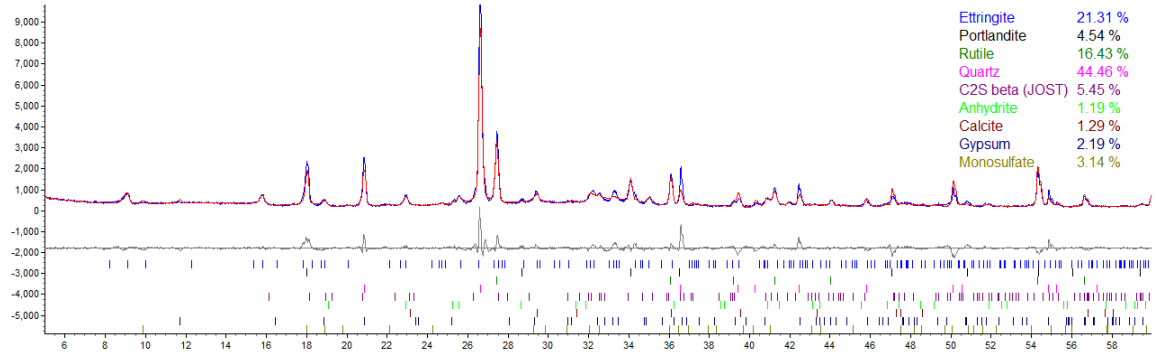

Figure A6. X-ray diffraction pattern and Rietveld refinement: C1-F1(35)-G(10).

C1-F1(35)-G(12A)

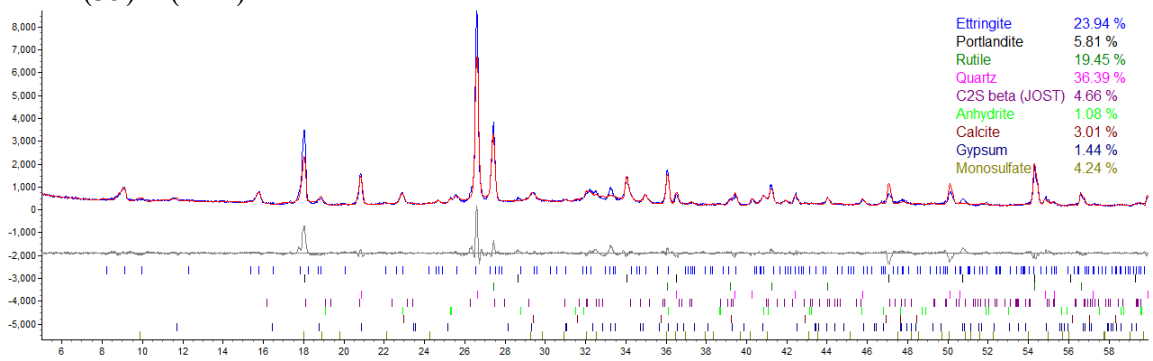

C1-F1(35)-G(12B)

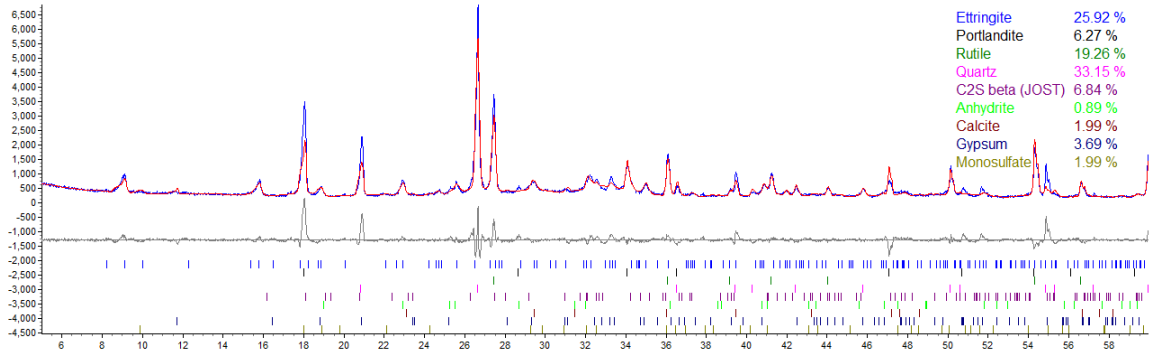

Figure A7. X-ray diffraction pattern and Rietveld refinement: C1-F1(35)-G(12).

C1-F1(35)-G(15A)

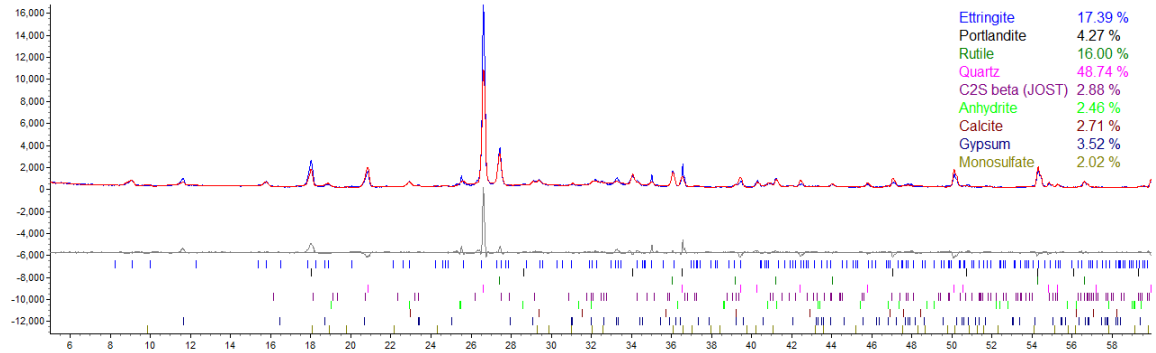

C1-F1(35)-G(15B)

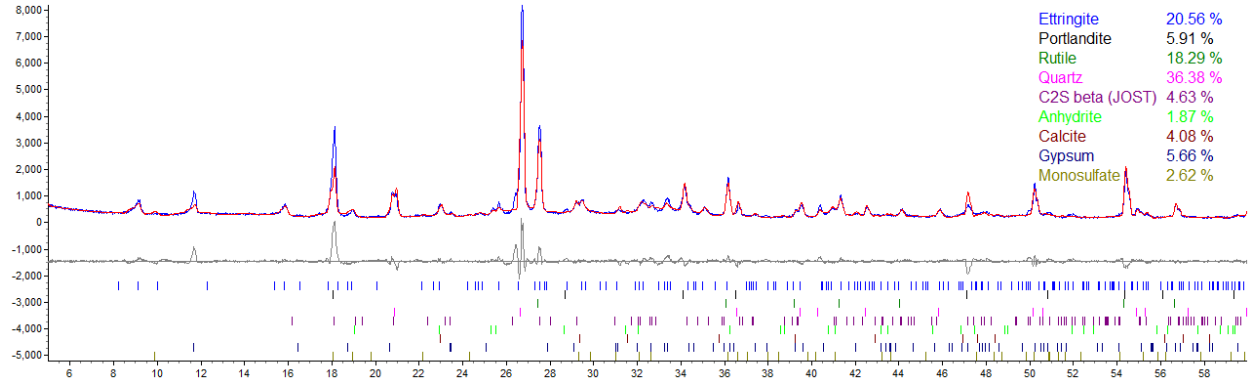

Figure A8. X-ray diffraction pattern and Rietveld refinement: C1-F1(35)-G(15).

28 Days - C1-F1(35)-G(0A)

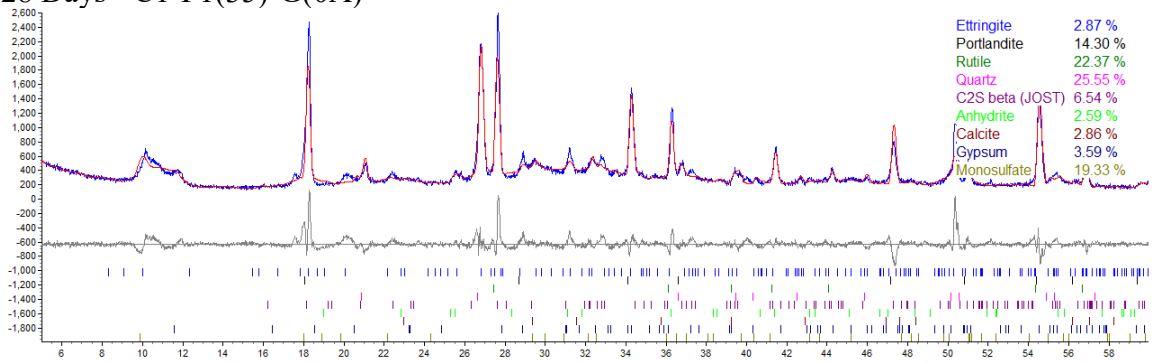

28 Days - C1-F1(35)-G(0B)

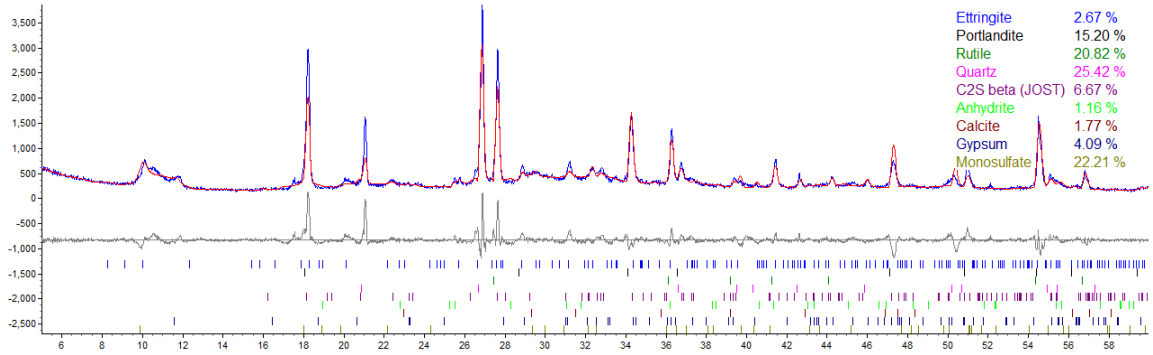

Figure A9. X-ray diffraction pattern and Rietveld refinement: C1-F1(35)-G(0) at 28 days.

28 Days - C1-F1(35)-G(2A)

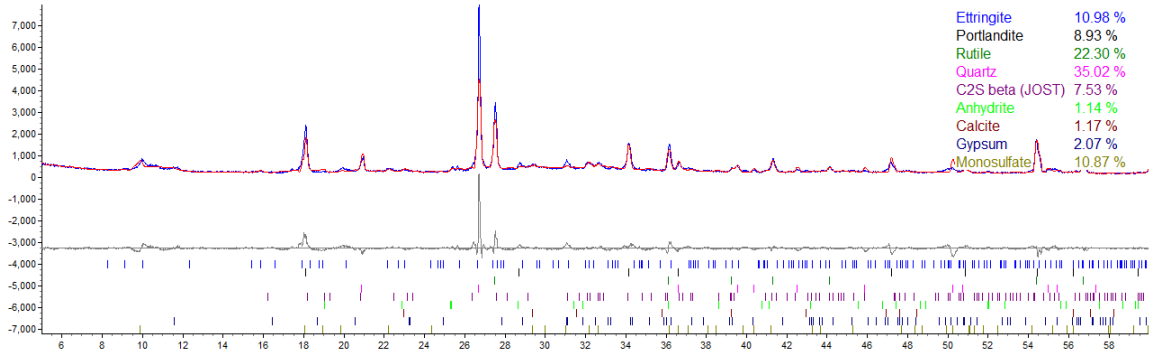

28 Days - C1-F1(35)-G(2C)

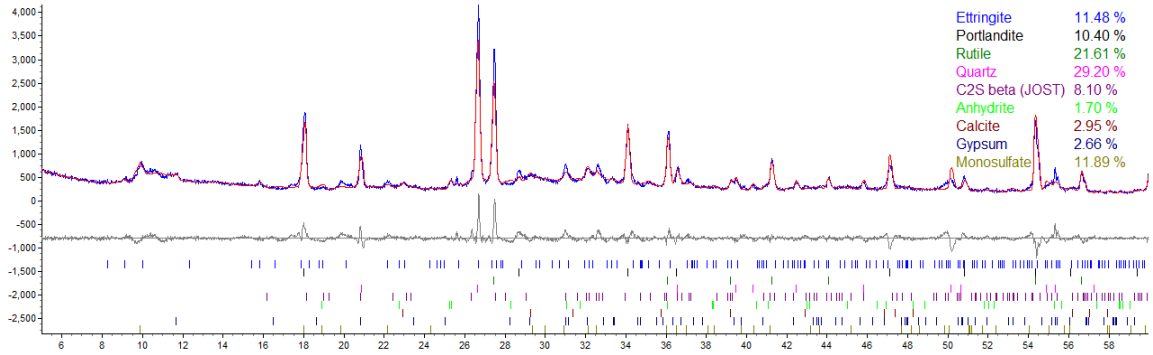

Figure A10. X-ray diffraction pattern and Rietveld refinement: C1-F1(35)-G(2) at 28 days.

28 Days - C1-F1(35)-G(4A)

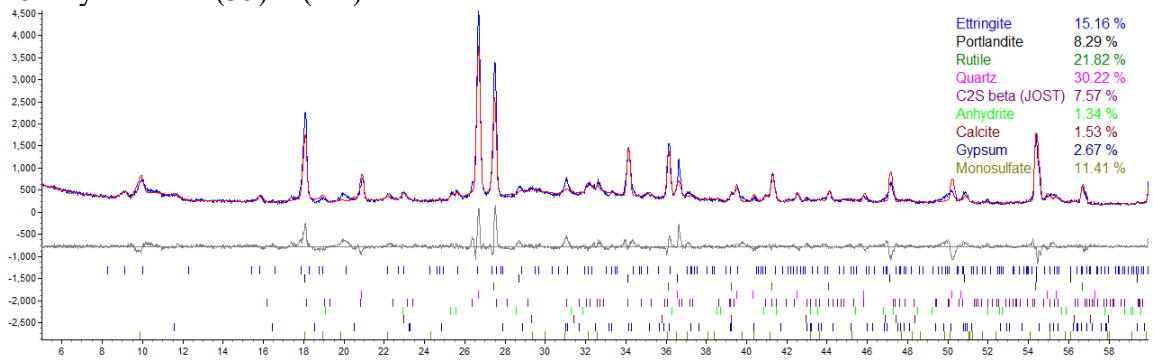

28 Days - C1-F1(35)-G(4B)

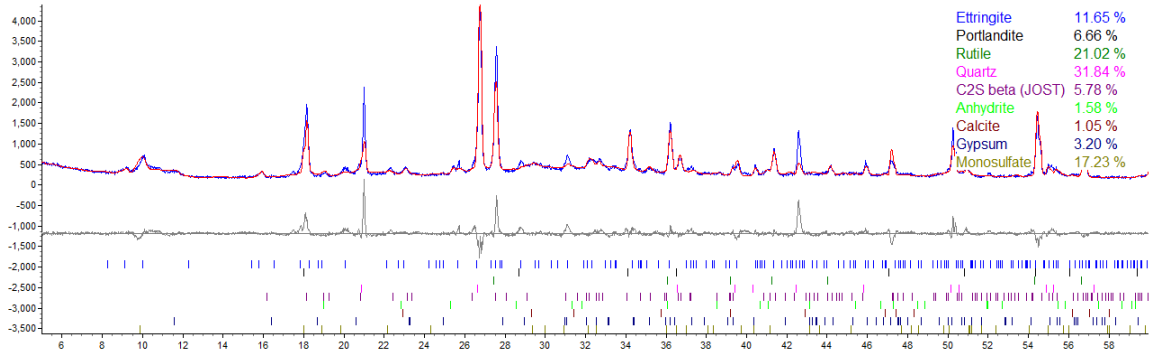

Figure A11. X-ray diffraction pattern and Rietveld refinement: C1-F1(35)-G(4) at 28 days.

28 Days - C1-F1(35)-G(6A)

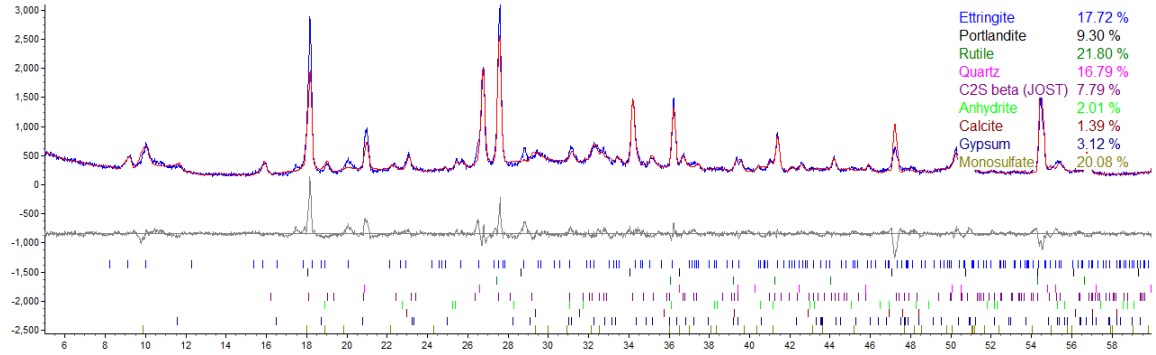

28 Days - C1-F1(35)-G(6B)

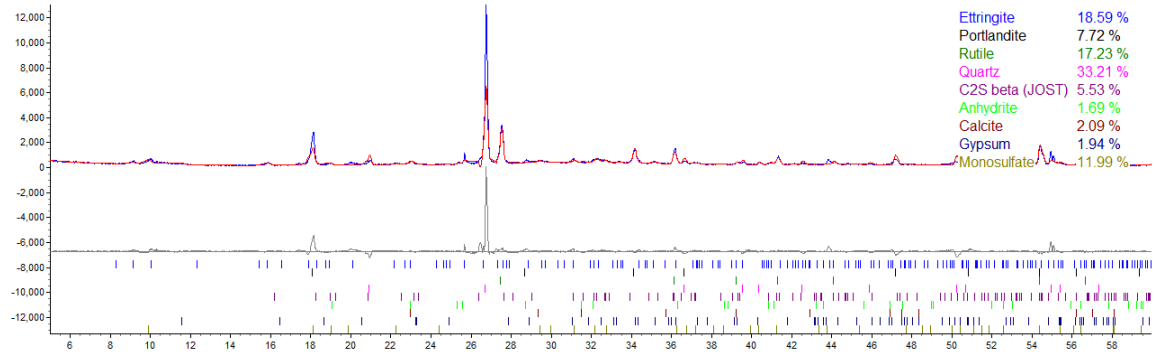

Figure A12. X-ray diffraction pattern and Rietveld refinement: C1-F1(35)-G(6) at 28 days.

28 Days - C1-F1(35)-G(8A)

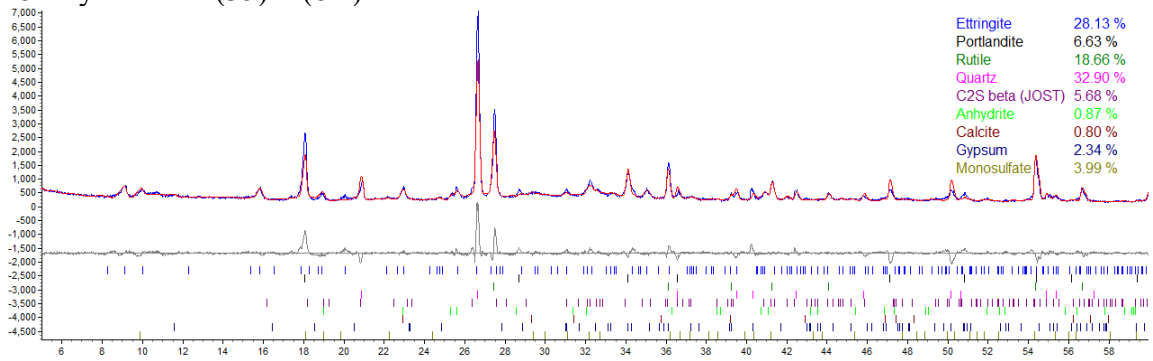

28 Days - C1-F1(35)-G(8B)

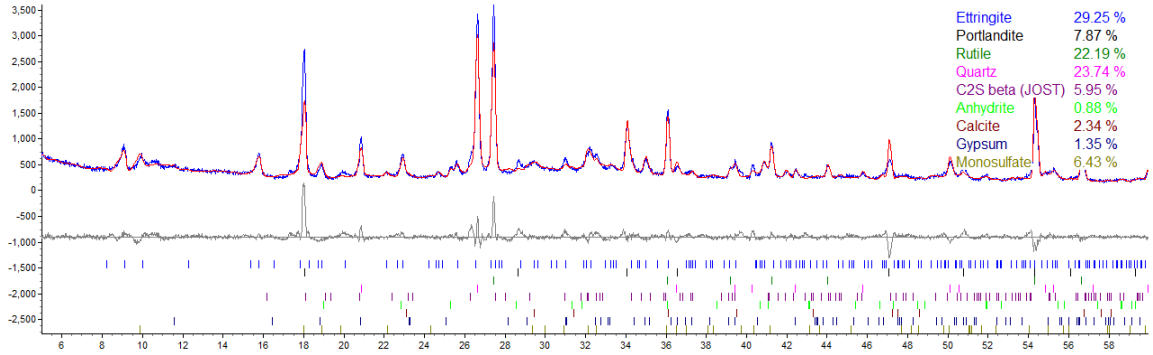

Figure A13. X-ray diffraction pattern and Rietveld refinement: C1-F1(35)-G(8) at 28 days.

28 Days - C1-F1(35)-G(10A)

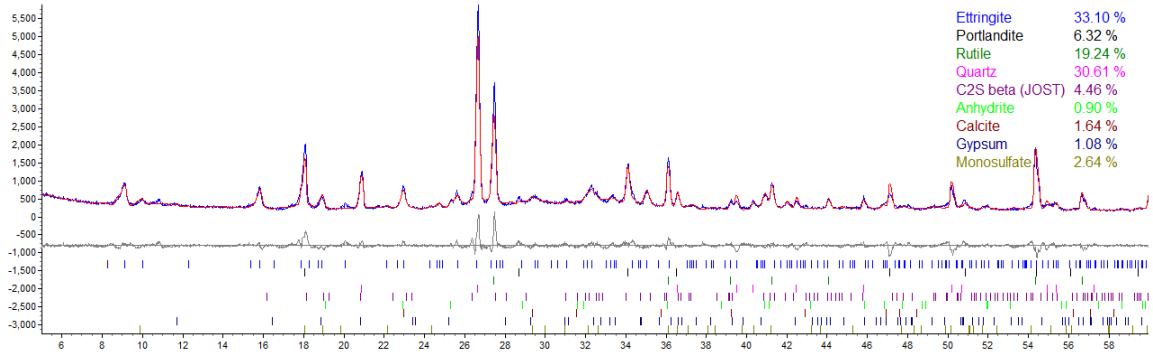

28 Days - C1-F1(35)-G(10B)

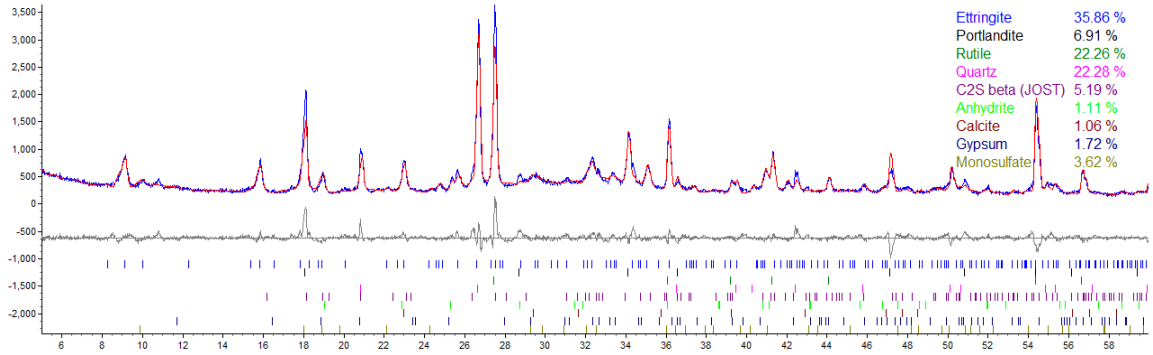

Figure A14. X-ray diffraction pattern and Rietveld refinement: C1-F1(35)-G(10) at 28 days.

28 Days - C1-F1(35)-G(12A)

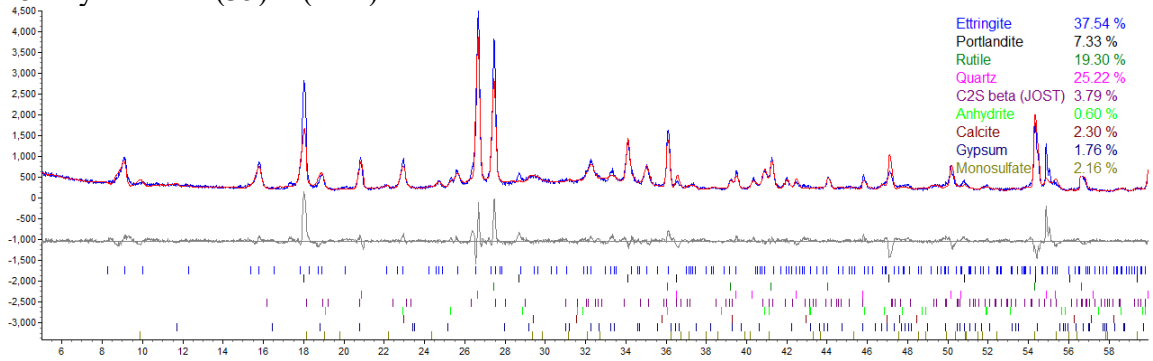

28 Days - C1-F1(35)-G(12B)

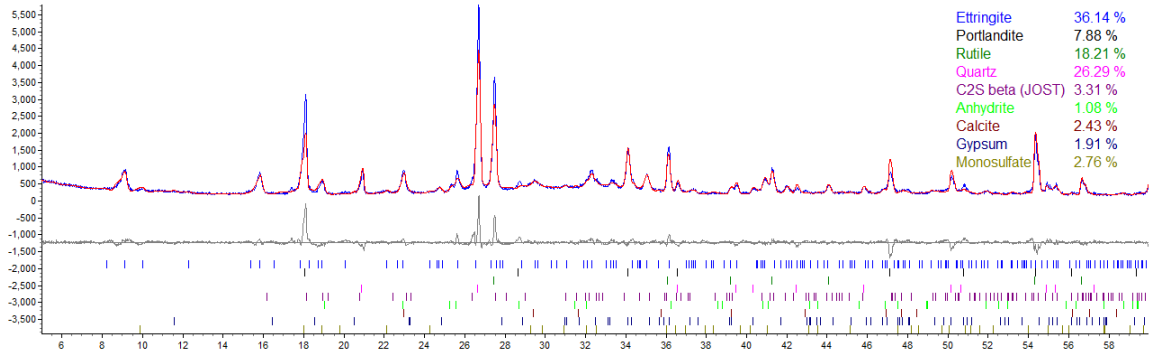

Figure A15. X-ray diffraction pattern and Rietveld refinement: C1-F1(35)-G(12) at 28 days.

28 Days - C1-F1(35)-G(15A)

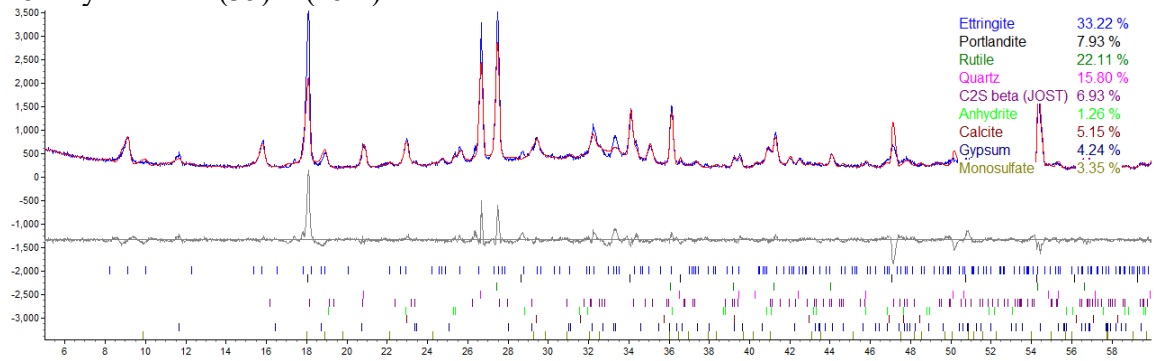

28 Days - C1-F1(35)-G(15B)

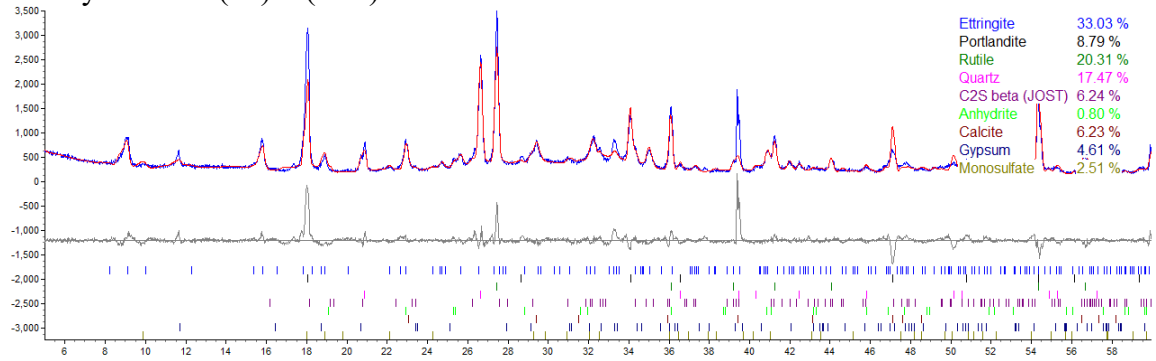

Figure A16. X-ray diffraction pattern and Rietveld refinement: C1-F1(35)-G(15) at 28 days.

C1-F2(35)-G(0A)

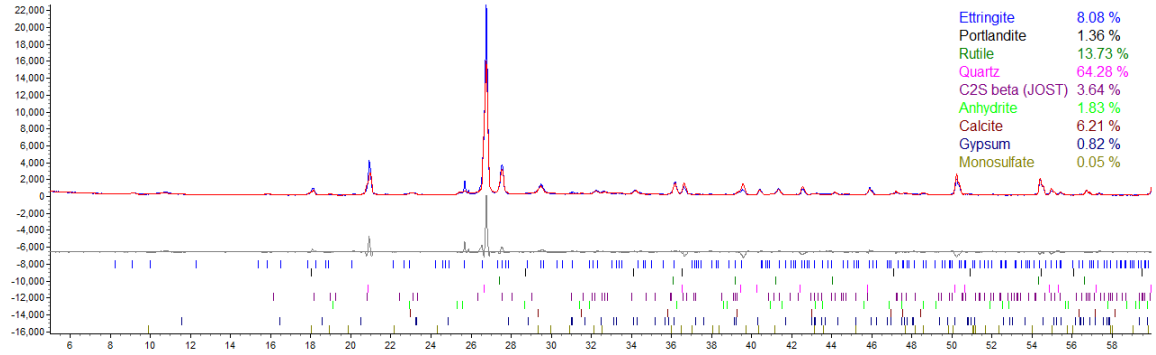

C1-F2(35)-G(0B)

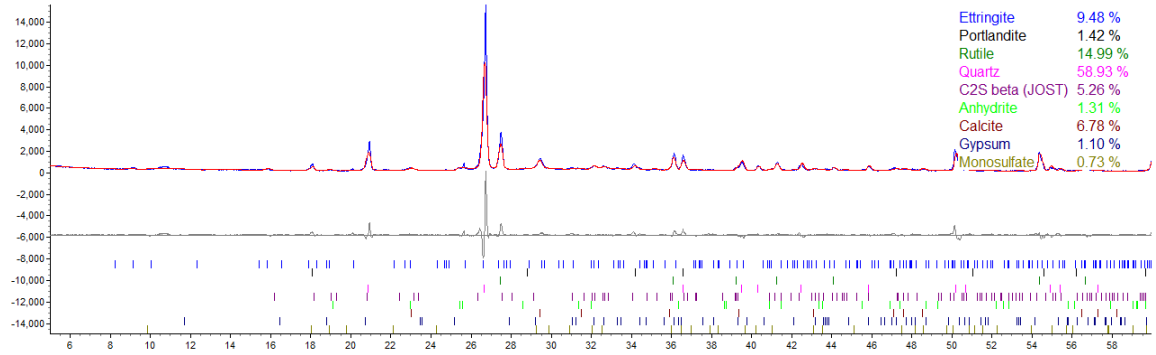

Figure A17. X-ray diffraction pattern and Rietveld refinement: C1-F2(35)-G(0).

C1-F2(35)-G(2A)

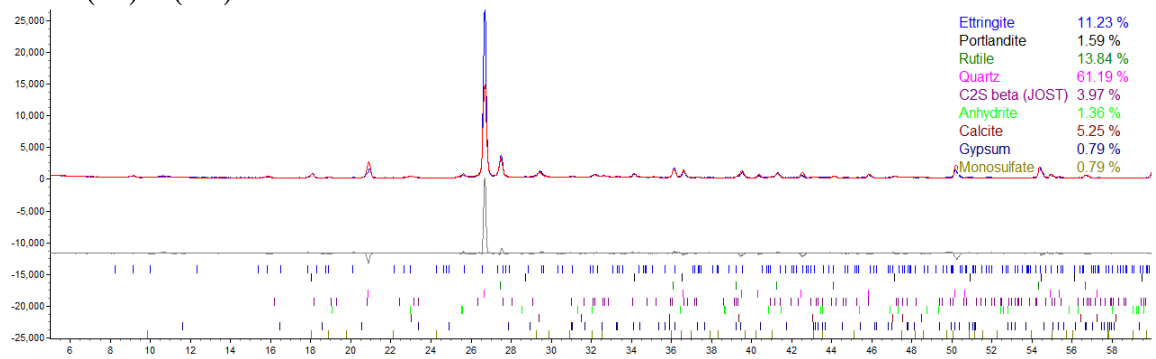

C1-F2(35)-G(2B)

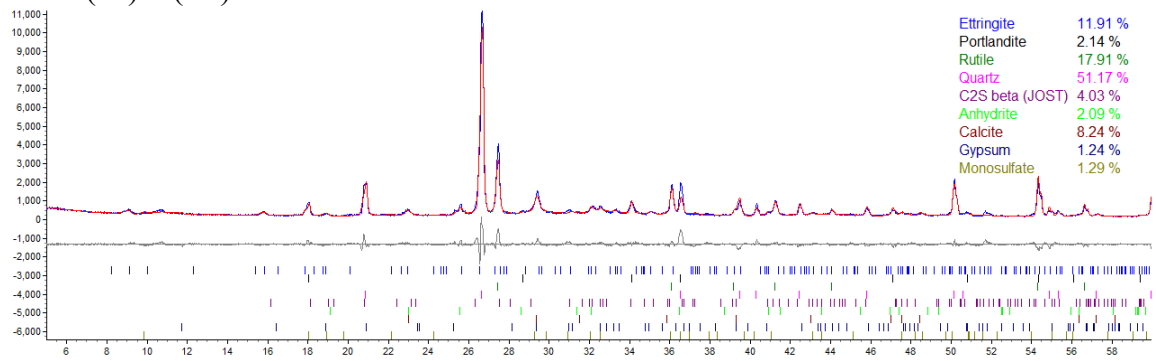

Figure A18. X-ray diffraction pattern and Rietveld refinement: C1-F2(35)-G(2).

C1-F2(35)-G(4A)

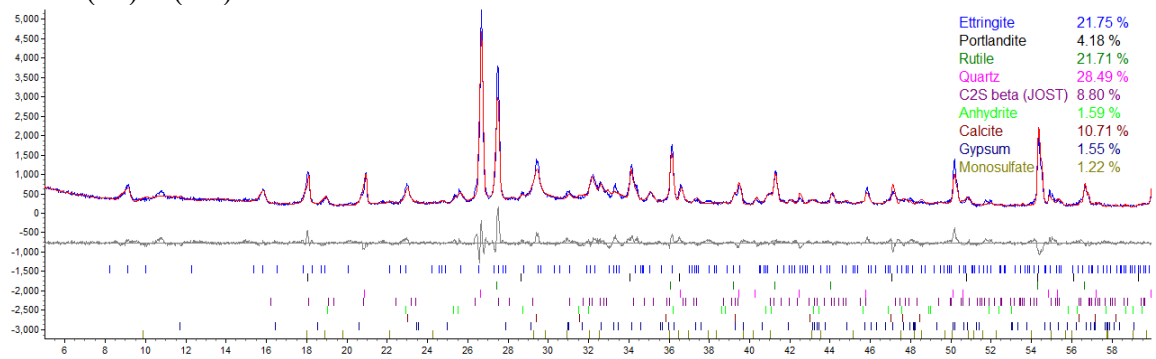

C1-F2(35)-G(4B)

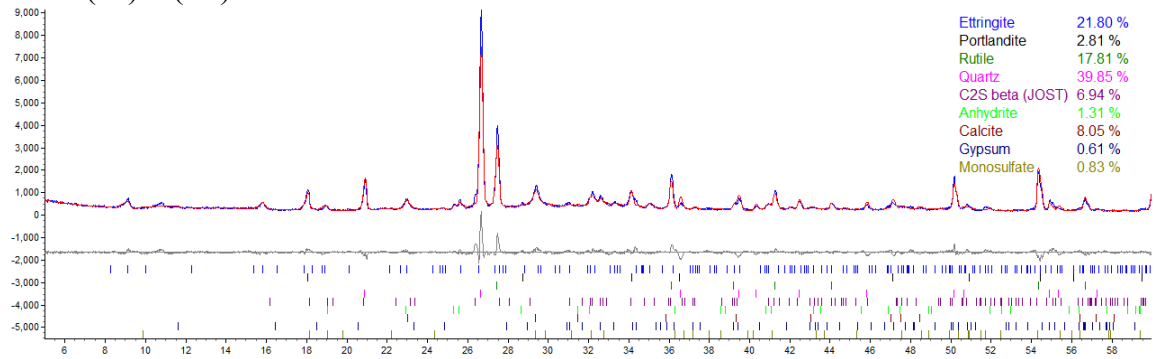

Figure A19. X-ray diffraction pattern and Rietveld refinement: C1-F2(35)-G(4).

C1-F2(35)-G(6A)

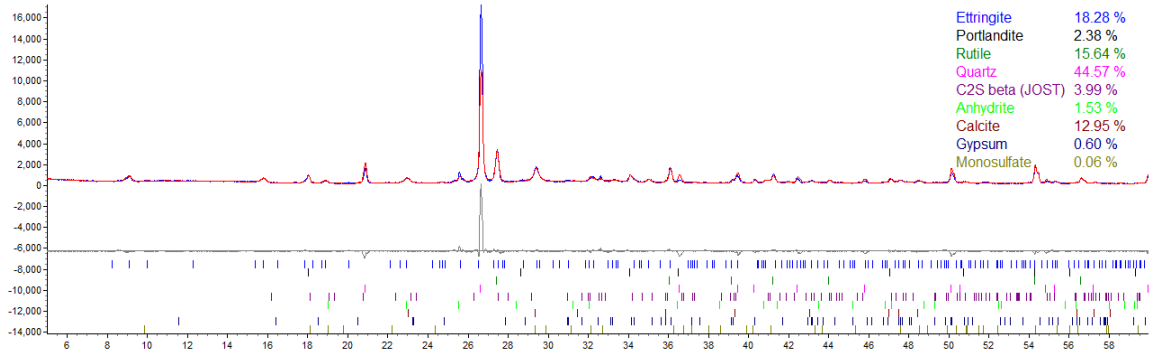

C1-F2(35)-G(6B)

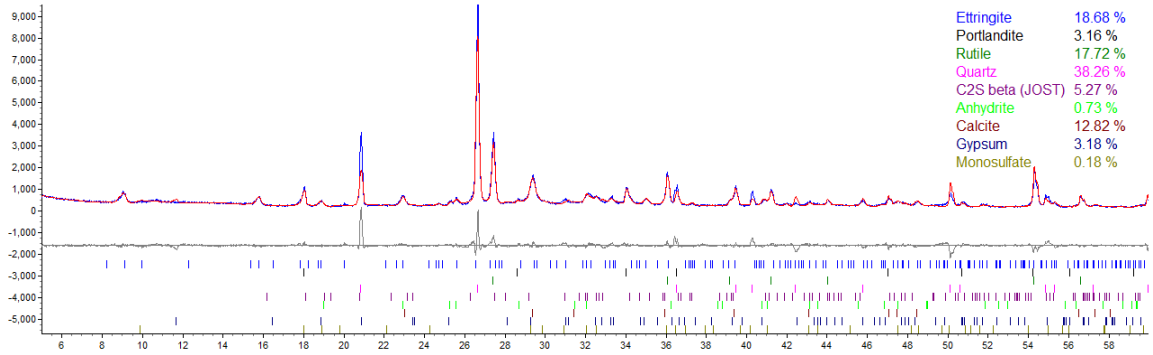

Figure A20. X-ray diffraction pattern and Rietveld refinement: C1-F2(35)-G(6).

C1-F2(35)-G(8A)

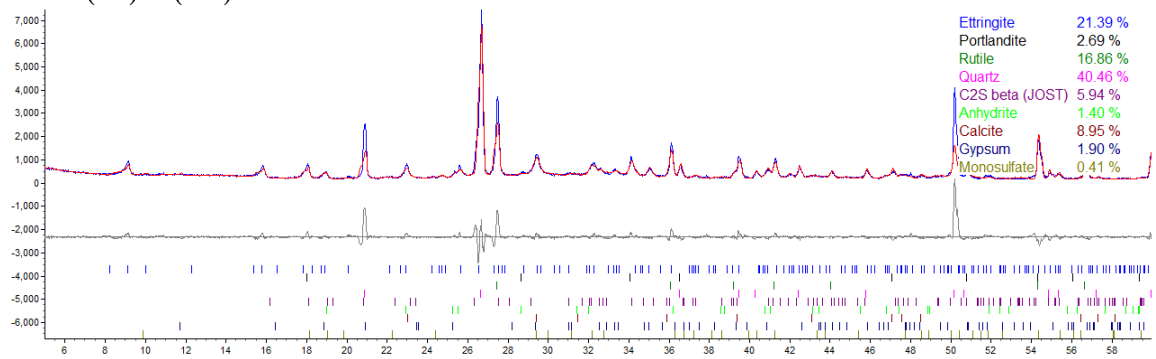

C1-F2(35)-G(8B)

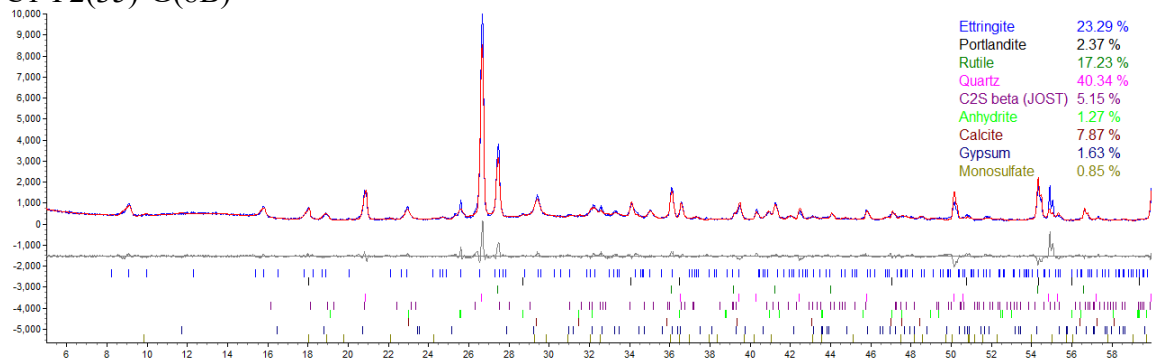

Figure A21. X-ray diffraction pattern and Rietveld refinement: C1-F2(35)-G(8).

C1-F2(35)-G(10A)

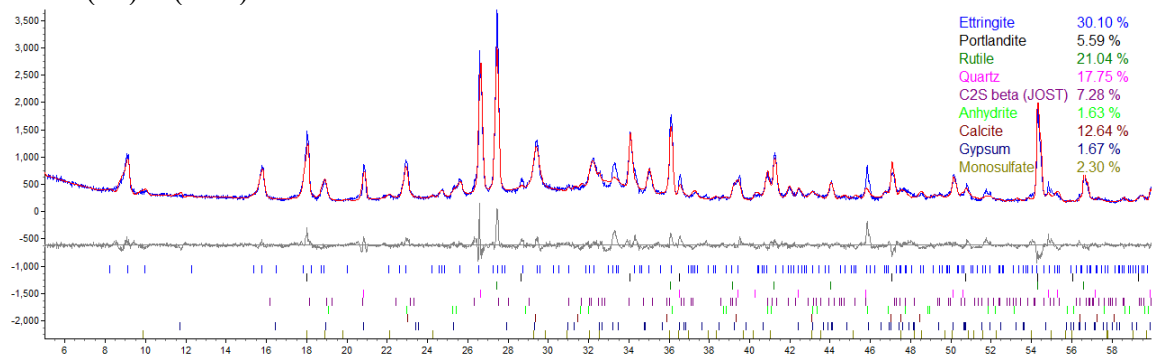

C1-F2(35)-G(10B)

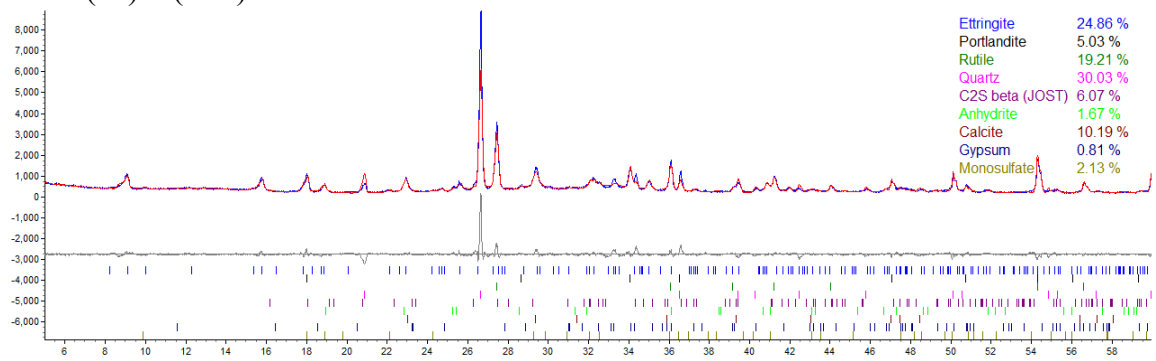

Figure A22. X-ray diffraction pattern and Rietveld refinement: C1-F2(35)-G(10).

C1-F2(35)-G(12A)

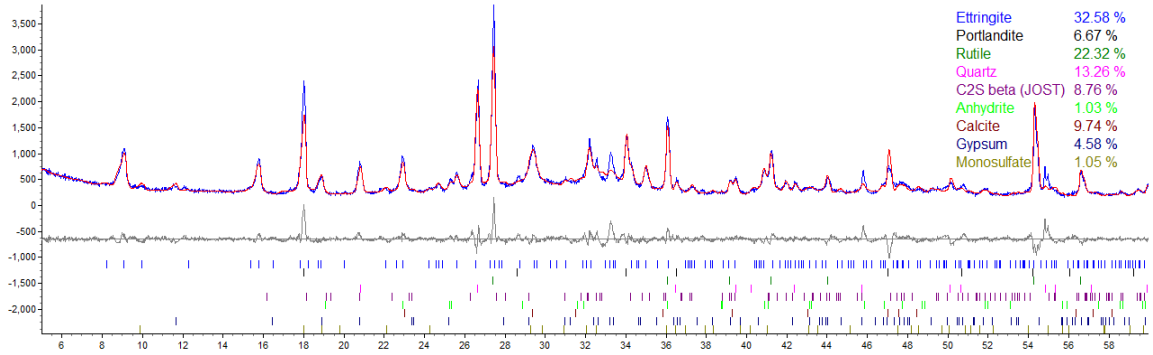

C1-F2(35)-G(12B)

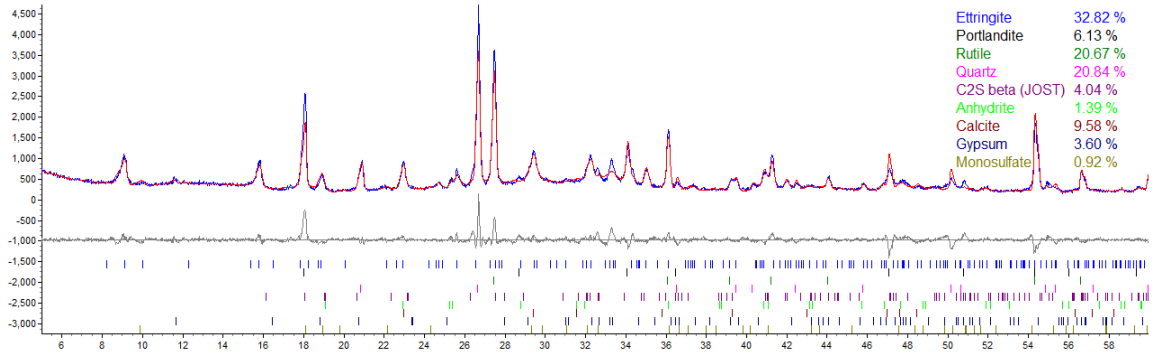

Figure A23. X-ray diffraction pattern and Rietveld refinement: C1-F2(35)-G(12).

C1-F2(35)-G(15A)

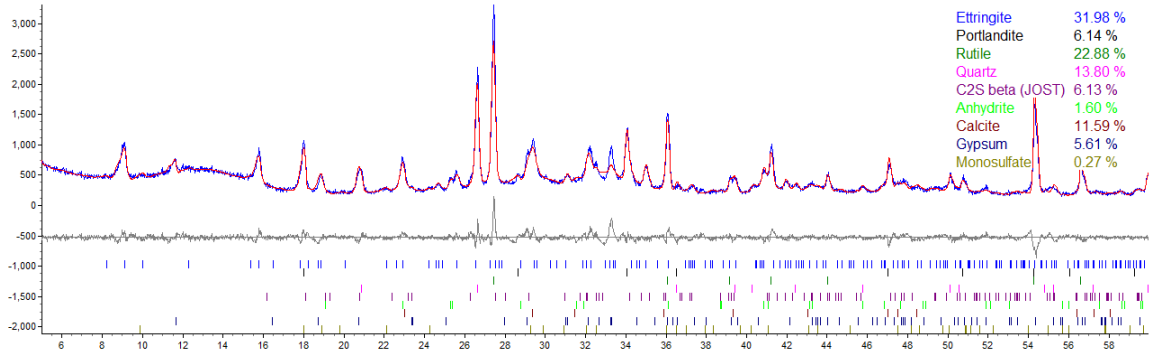

C1-F2(35)-G(15B)

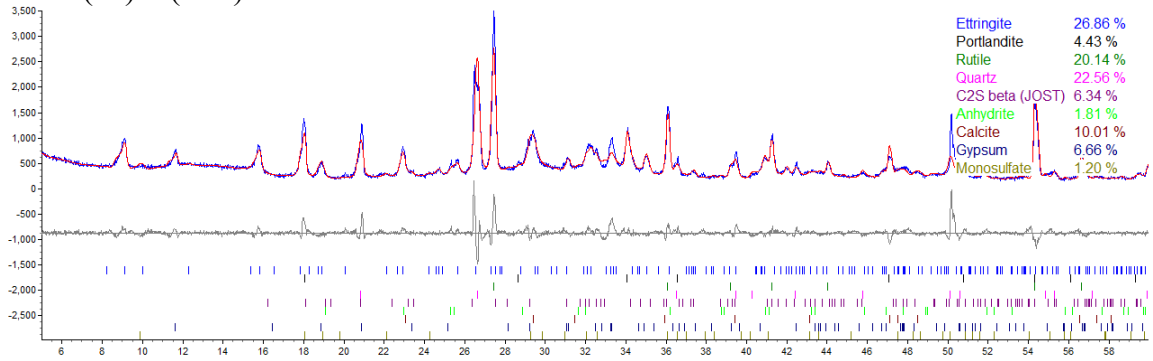

Figure A24. X-ray diffraction pattern and Rietveld refinement: C1-F2(35)-G(15).

28 Days C1-F2(35)-G(0A)

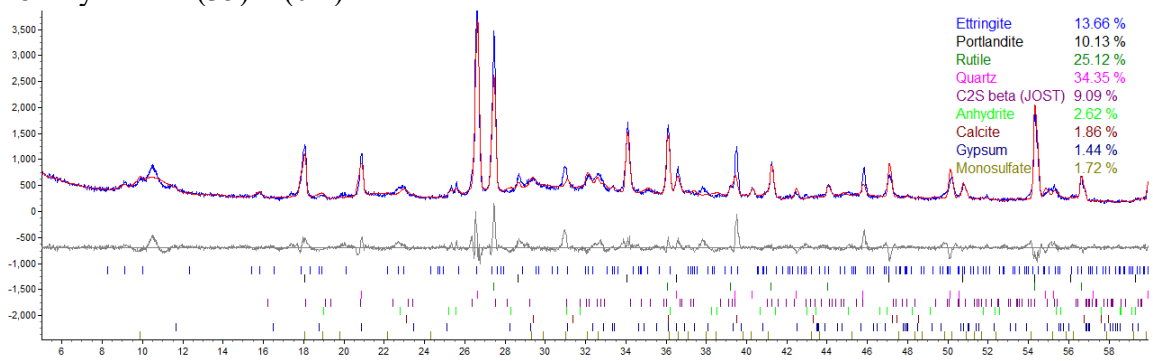

28 Days C1-F2(35)-G(0B)

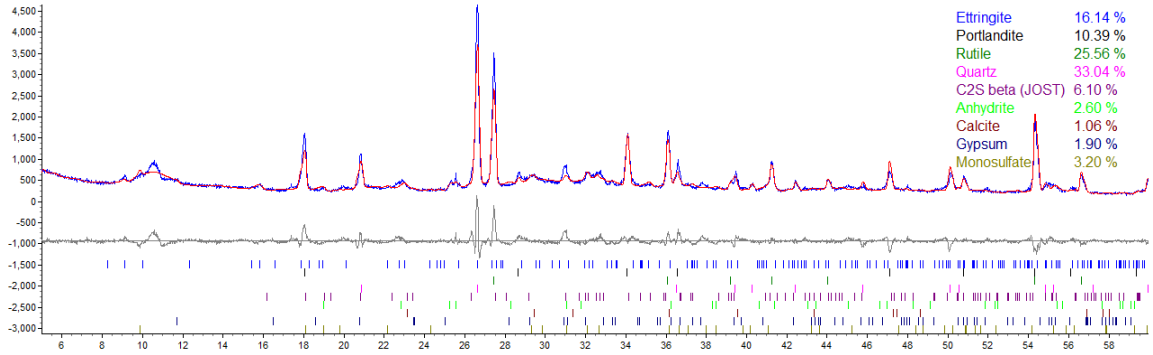

Figure A25. X-ray diffraction pattern and Rietveld refinement: C1-F2(35)-G(0) at 28 days.

28 Days C1-F2(35)-G(2A)

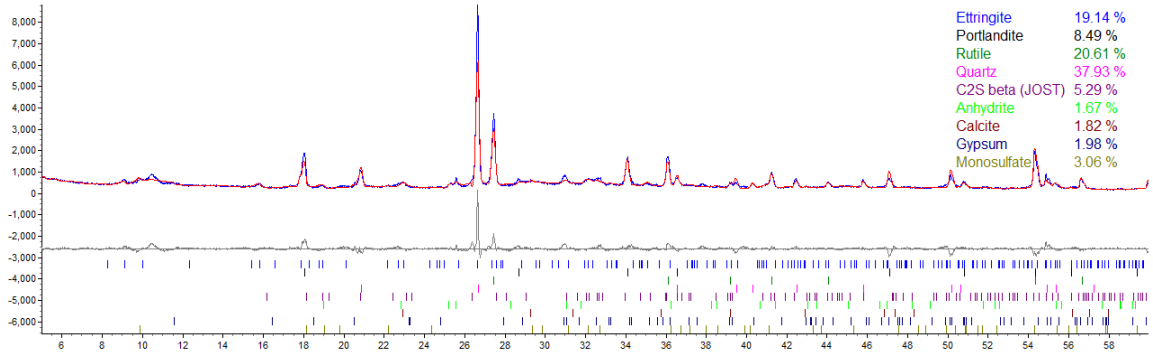

28 Days C1-F2(35)-G(2B)

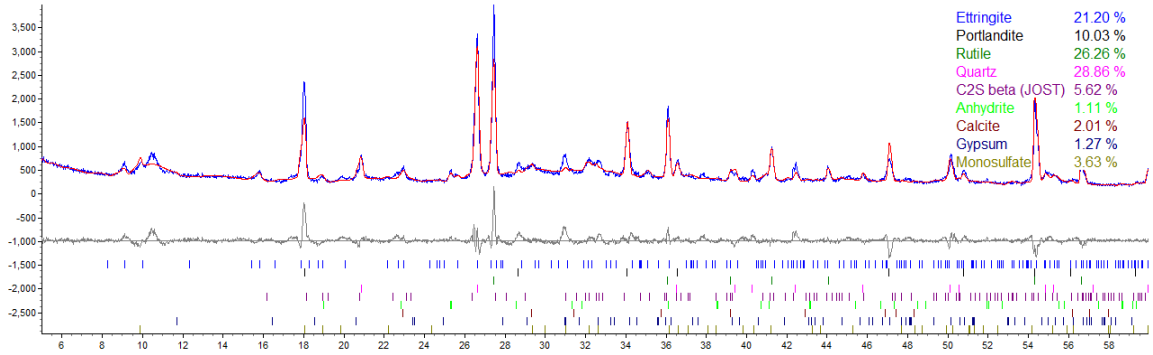

Figure A26. X-ray diffraction pattern and Rietveld refinement: C1-F2(35)-G(2) at 28 days.

28 Days C1-F2(35)-G(4A)

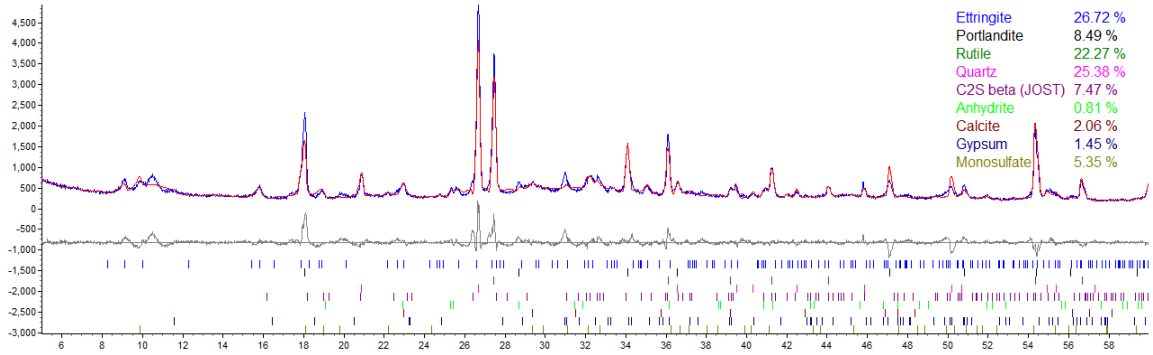

28 Days C1-F2(35)-G(4B)

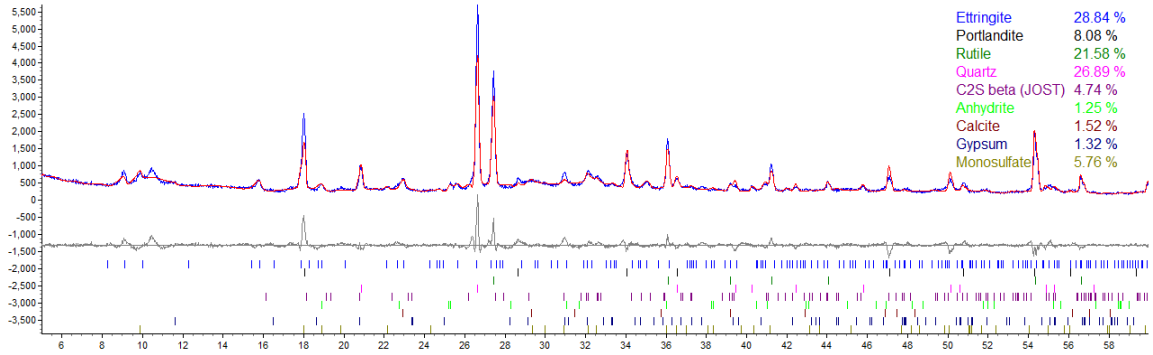

Figure A27. X-ray diffraction pattern and Rietveld refinement: C1-F2(35)-G(4) at 28 days.

28 Days C1-F2(35)-G(6A)

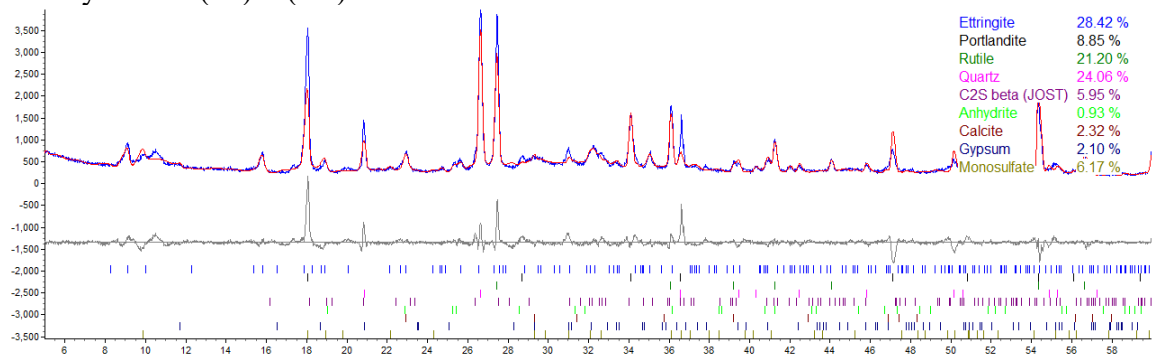

28 Days C1-F2(35)-G(6B)

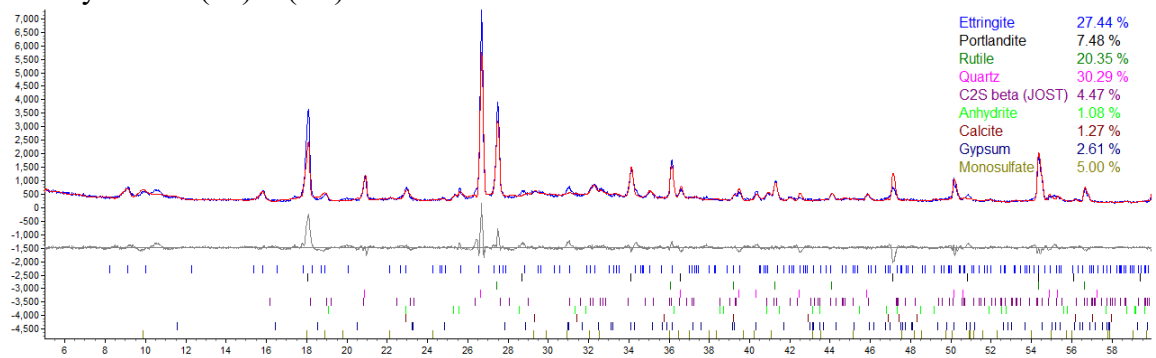

Figure A28. X-ray diffraction pattern and Rietveld refinement: C1-F2(35)-G(6) at 28 days.

28 Days C1-F2(35)-G(8A)

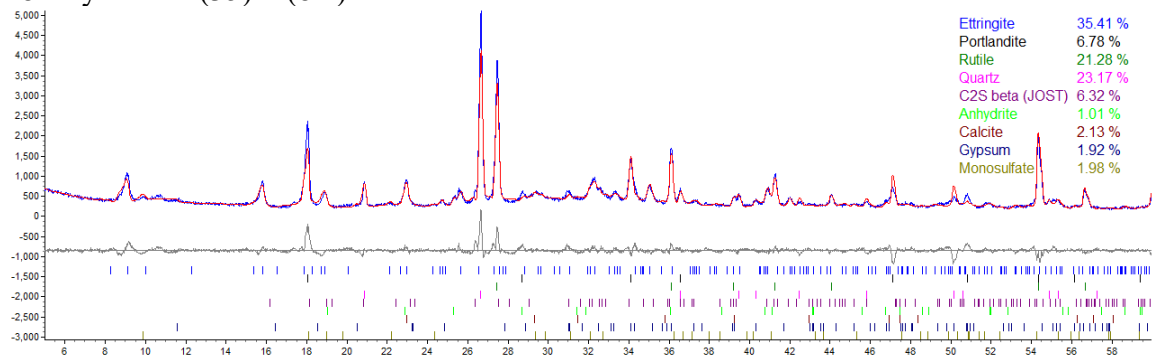

28 Days C1-F2(35)-G(8B)

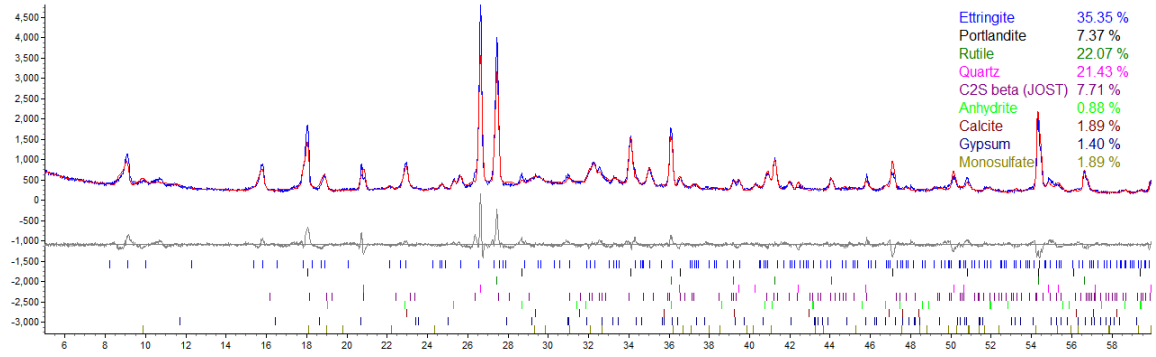

Figure A29. X-ray diffraction pattern and Rietveld refinement: C1-F2(35)-G(8) at 28 days.

28 Days C1-F2(35)-G(10A)

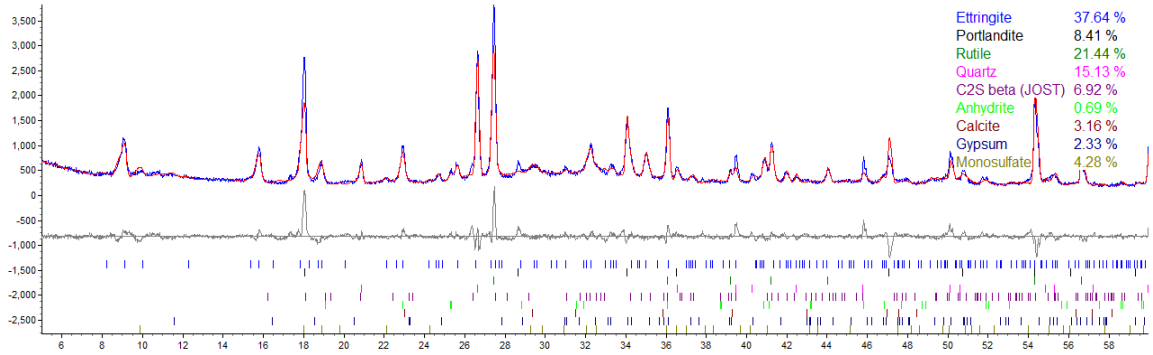

28 Days C1-F2(35)-G(10B)

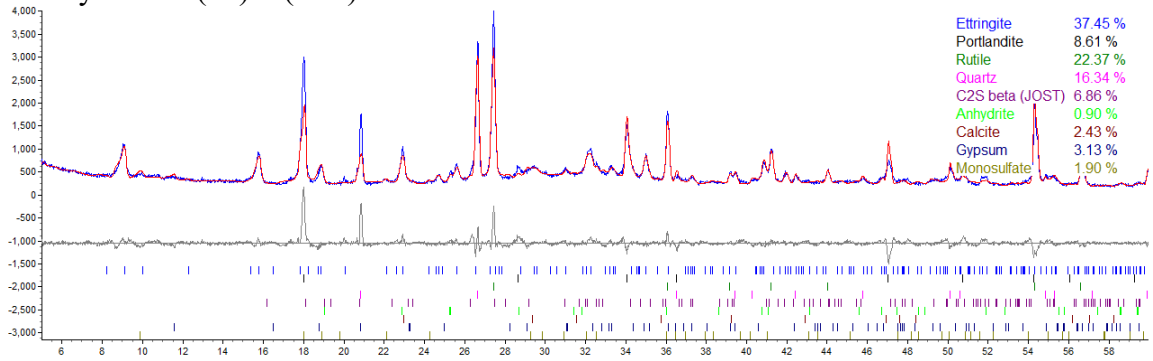

Figure A30. X-ray diffraction pattern and Rietveld refinement: C1-F2(35)-G(10) at 28 days.

28 Days C1-F2(35)-G(12A)

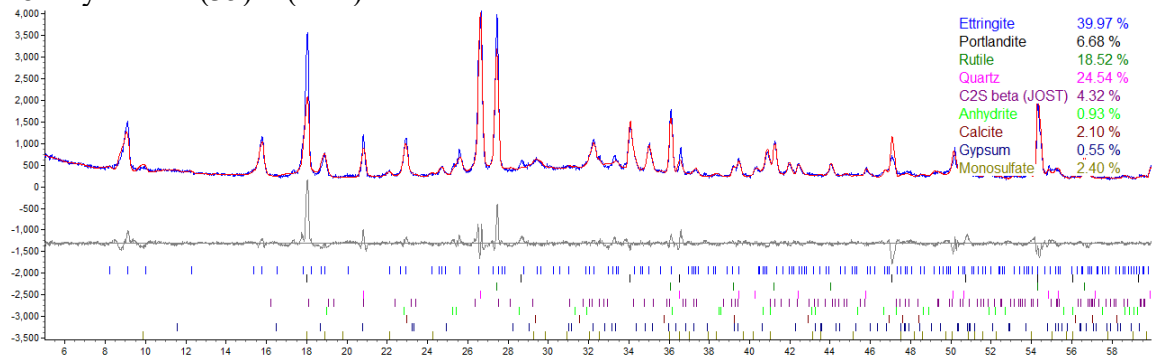

28 Days C1-F2(35)-G(12B)

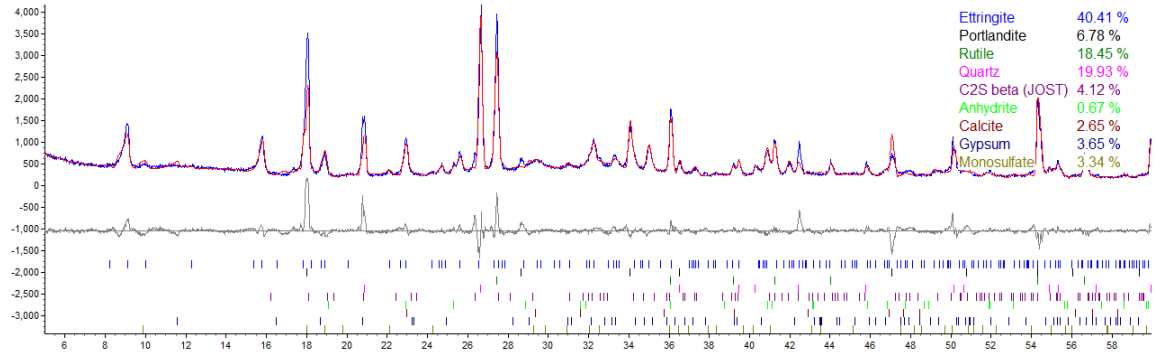

Figure A31. X-ray diffraction pattern and Rietveld refinement: C1-F2(35)-G(12) at 28 days.

28 Days C1-F2(35)-G(15A)

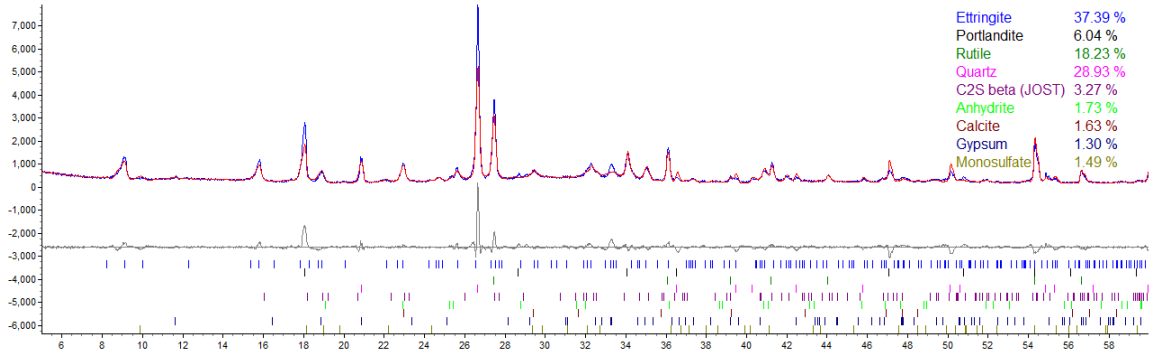

28 Days C1-F2(35)-G(15B)

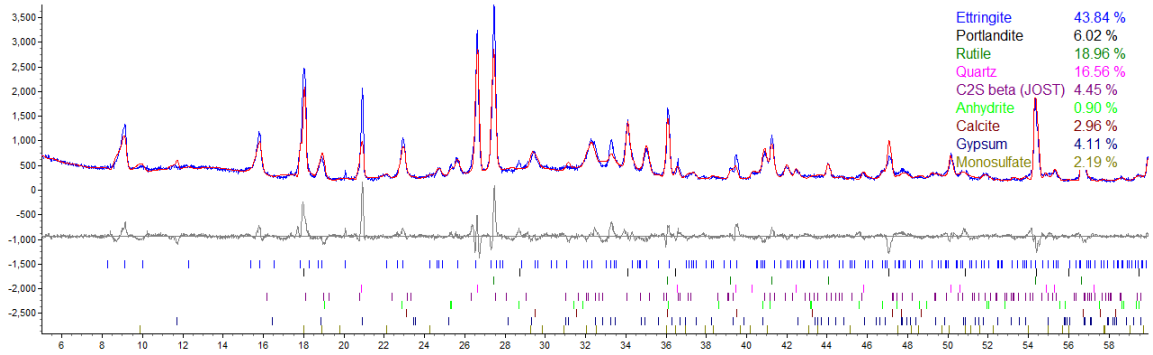

Figure A32. X-ray diffraction pattern and Rietveld refinement: C1-F2(35)-G(15) at 28 days.

C1-F3(35)-G(0A)

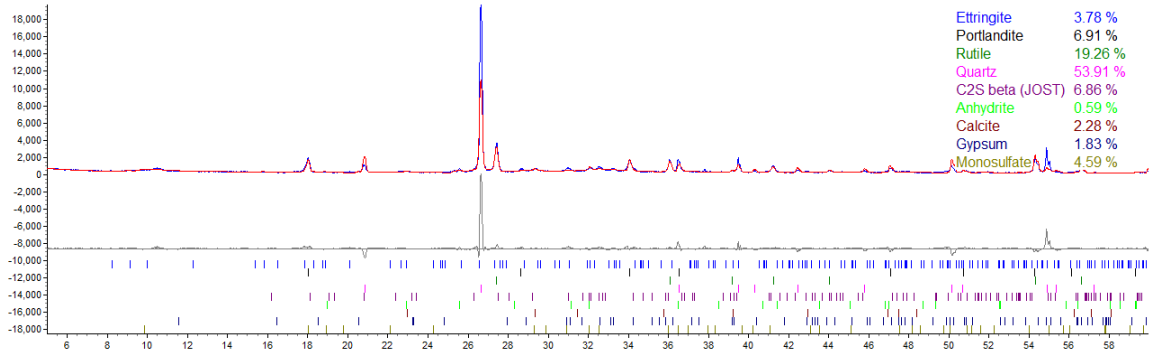

C1-F3(35)-G(0B)

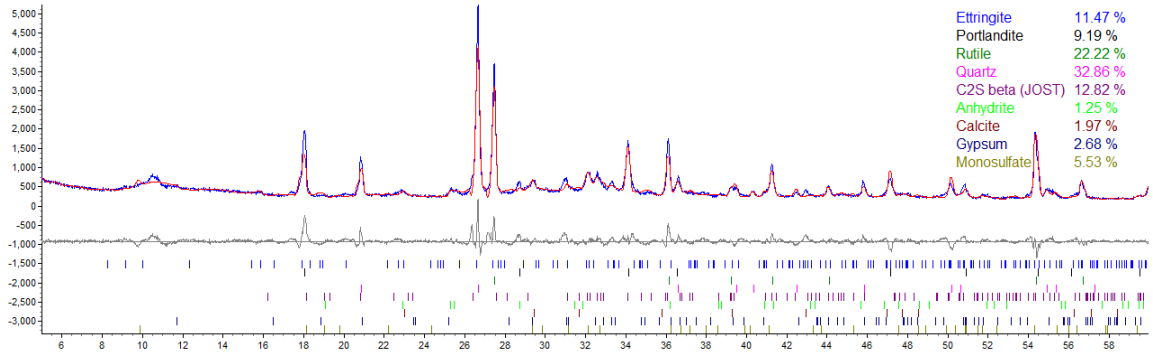

Figure A33. X-ray diffraction pattern and Rietveld refinement: C1-F3(35)-G(0).

C1-F3(35)-G(2A)

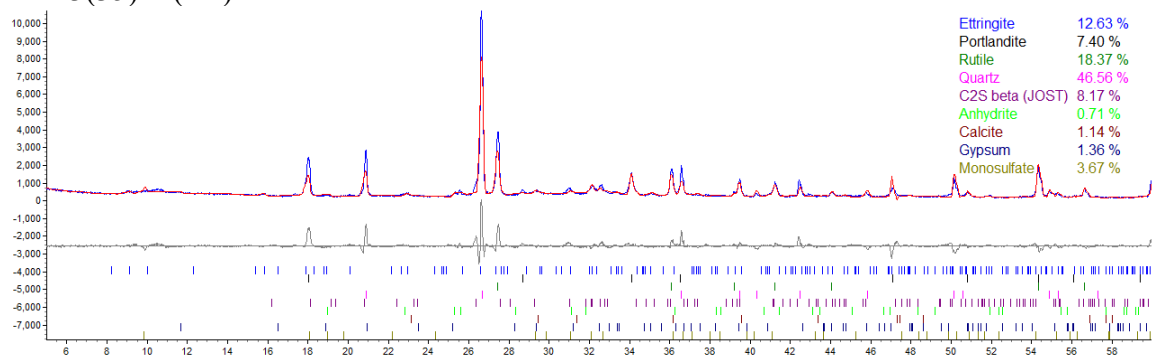

C1-F3(35)-G(2B)

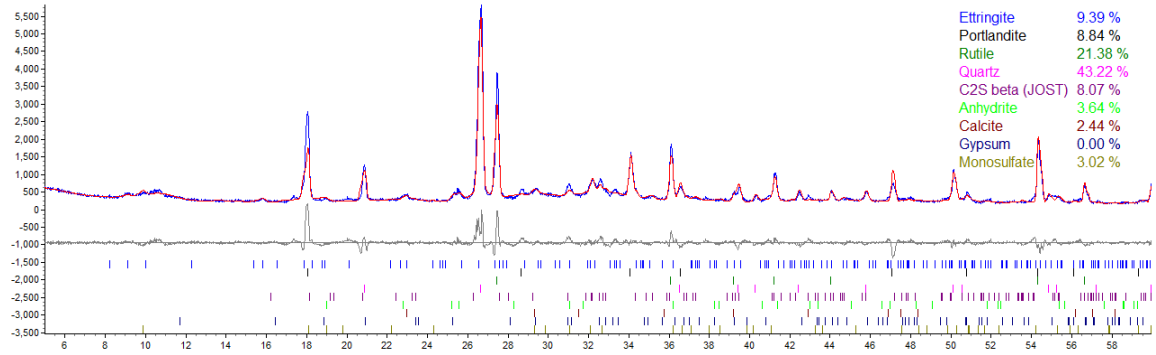

Figure A34. X-ray diffraction pattern and Rietveld refinement: C1-F3(35)-G(2).

C1-F3(35)-G(4A)

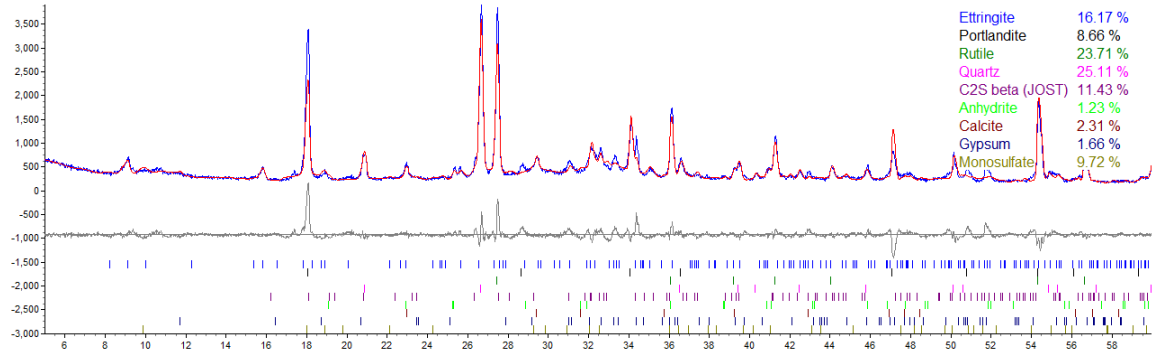

C1-F3(35)-G(4B)

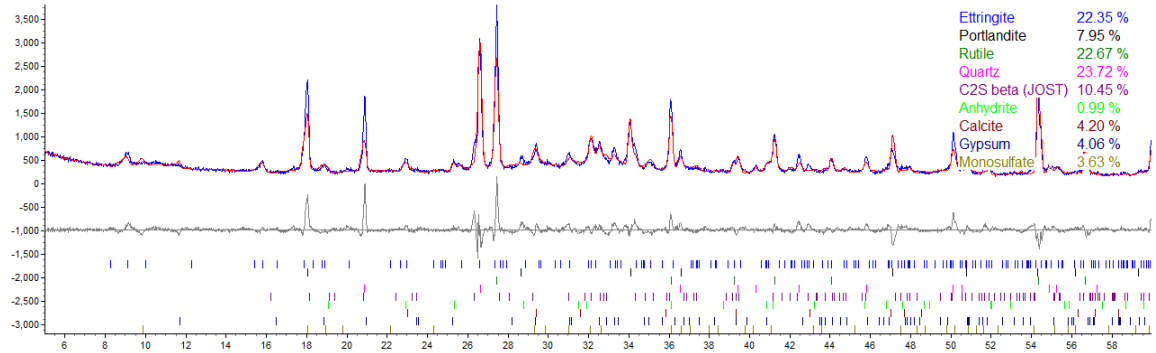

Figure A35. X-ray diffraction pattern and Rietveld refinement: C1-F3(35)-G(4).

C1-F3(35)-G(6A)

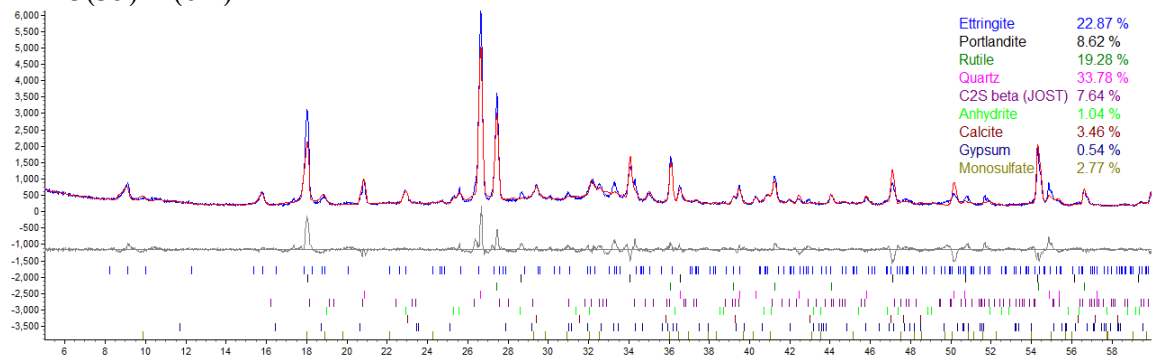

C1-F3(35)-G(6B)

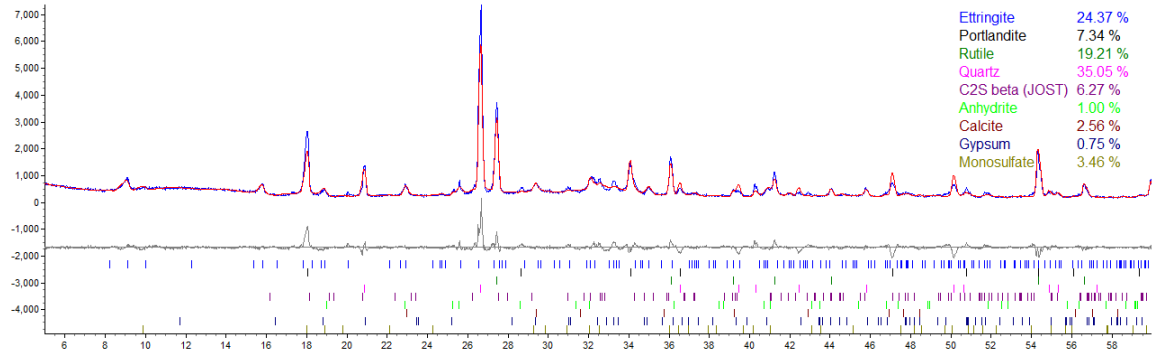

Figure A36. X-ray diffraction pattern and Rietveld refinement: C1-F3(35)-G(6).

C1-F3(35)-G(8A)

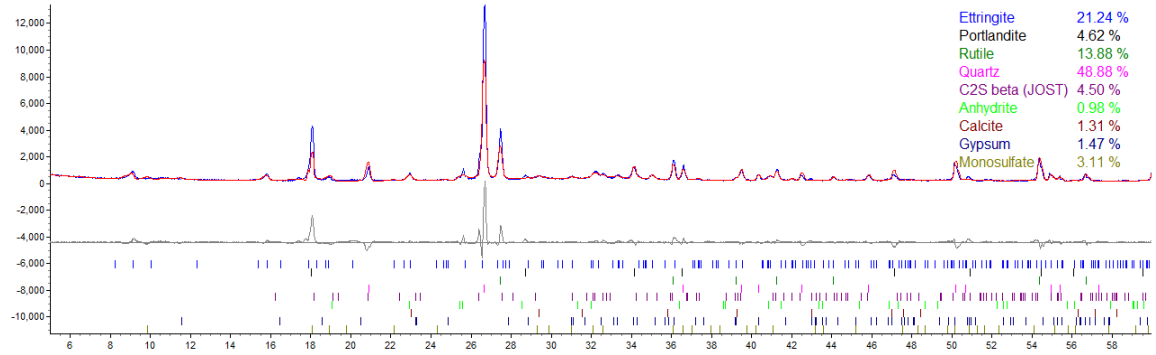

C1-F3(35)-G(8B)

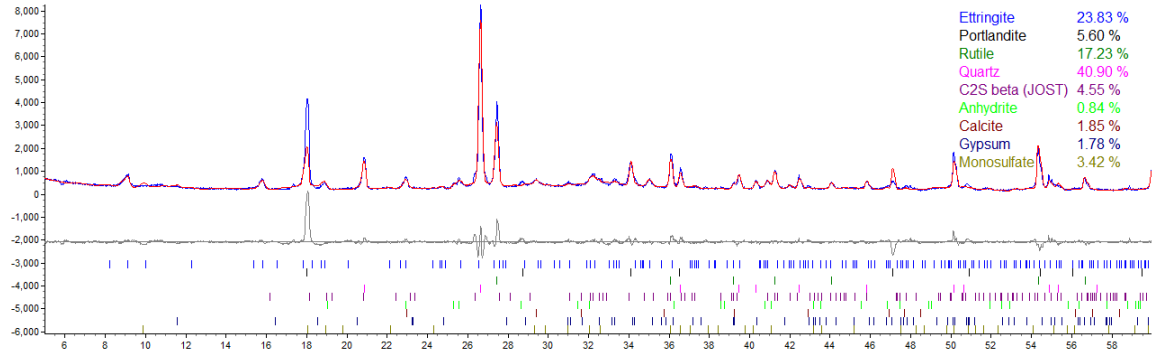

Figure A37. X-ray diffraction pattern and Rietveld refinement: C1-F3(35)-G(8).

C1-F3(35)-G(10A)

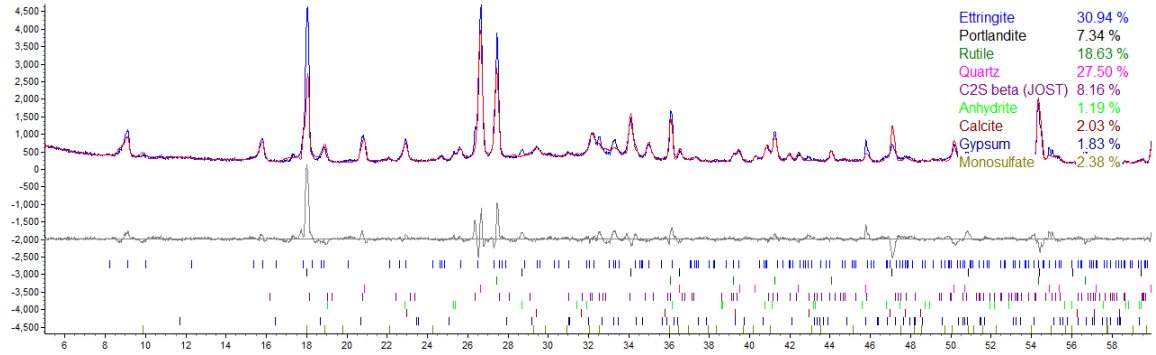

C1-F3(35)-G(10B)

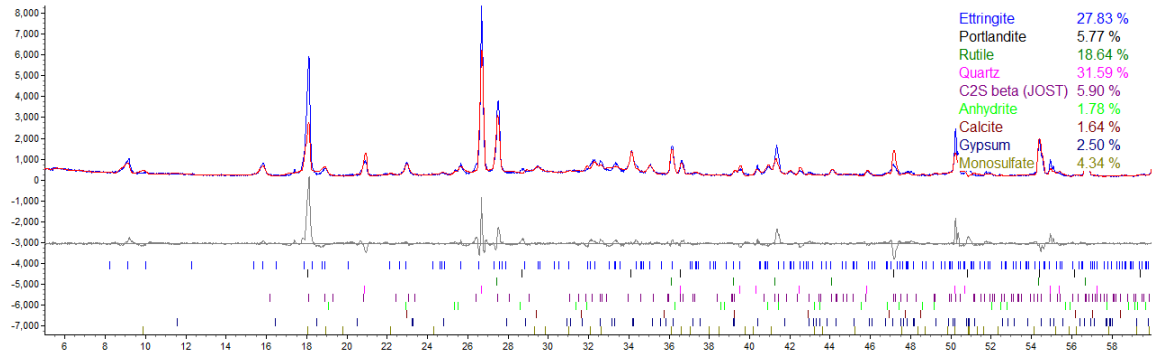

Figure A38. X-ray diffraction pattern and Rietveld refinement: C1-F3(35)-G(10).

C1-F3(35)-G(12A)

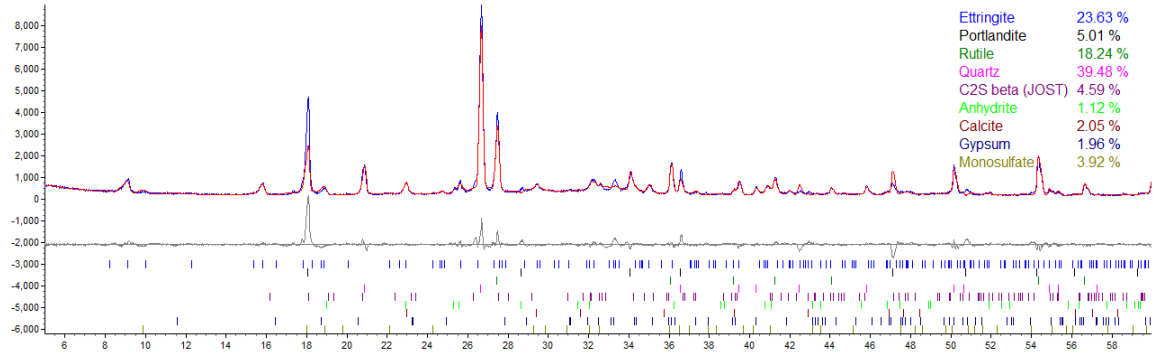

C1-F3(35)-G(12B)

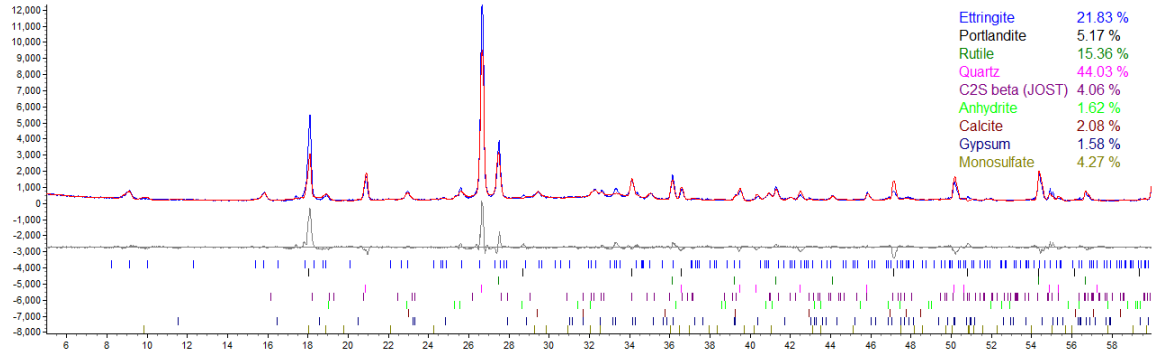

Figure A39. X-ray diffraction pattern and Rietveld refinement: C1-F3(35)-G(12).

C1-F3(35)-G(15A)

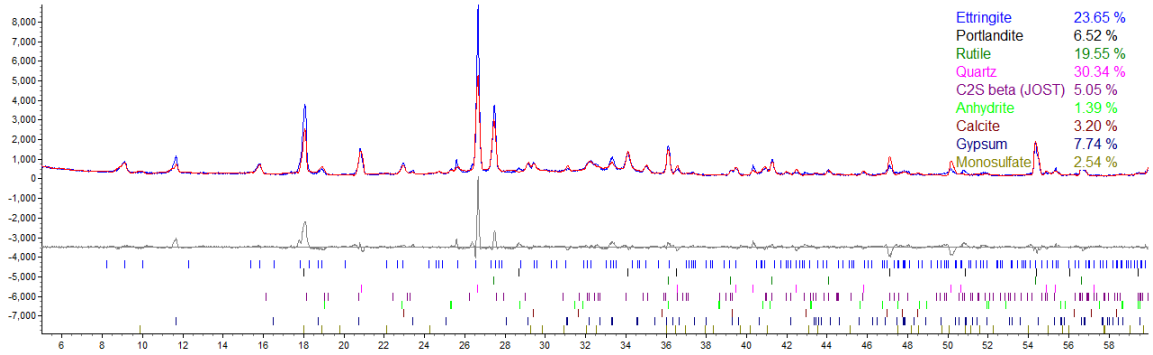

C1-F3(35)-G(15B)

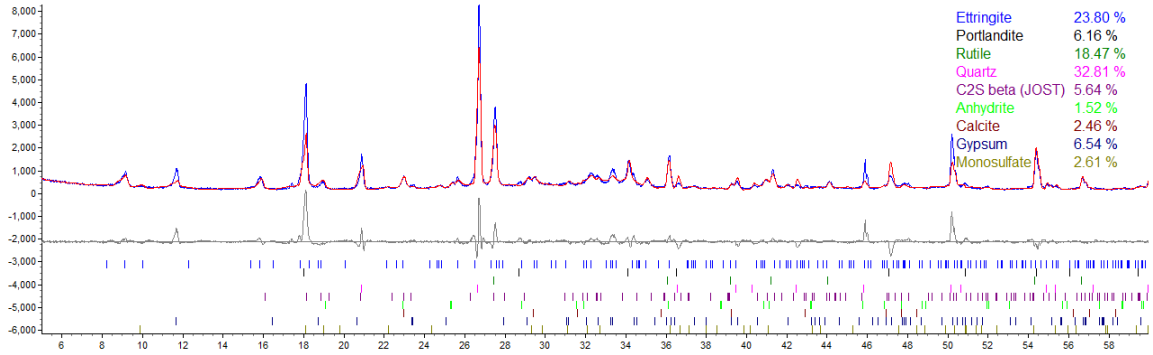

Figure A40. X-ray diffraction pattern and Rietveld refinement: C1-F3(35)-G(15).

28 Days C1-F3(35)-G(0A)

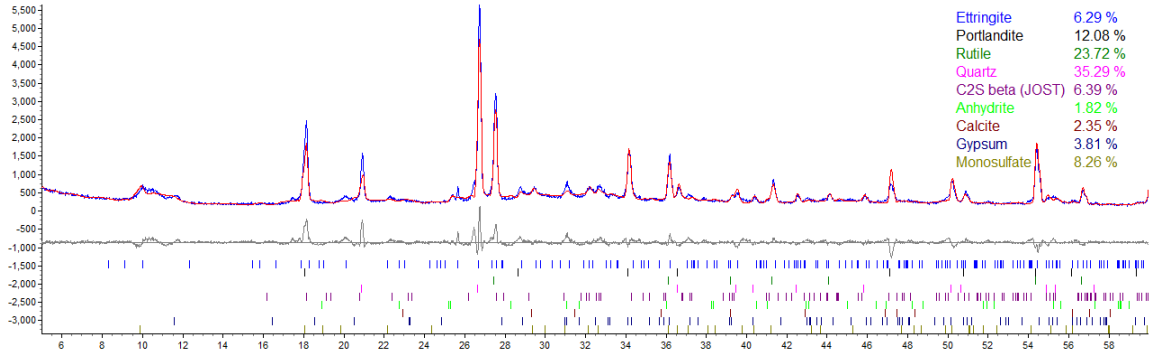

28 Days C1-F3(35)-G(0C)

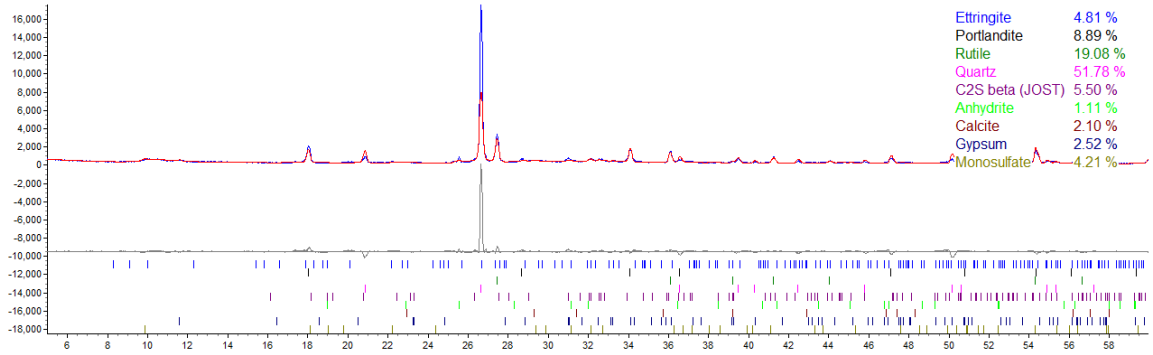

Figure A41. X-ray diffraction pattern and Rietveld refinement: C1-F3(35)-G(0) at 28 days.

28 Days C1-F3(35)-G(2A)

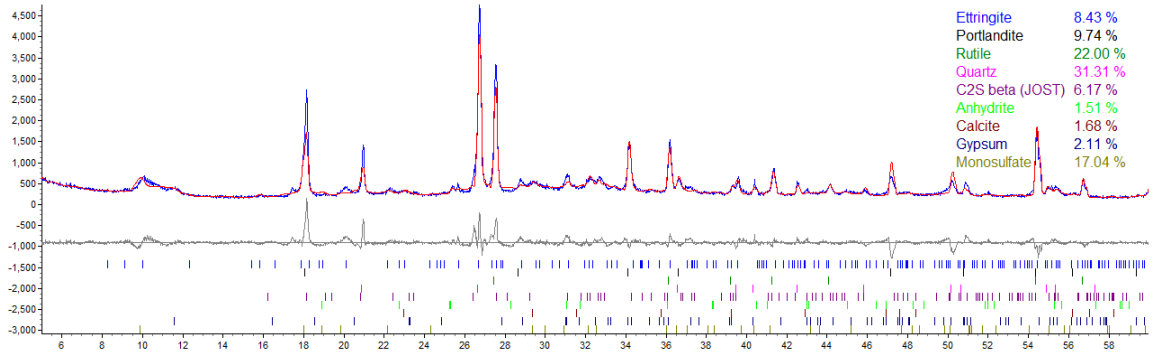

28 Days C1-F3(35)-G(2C)

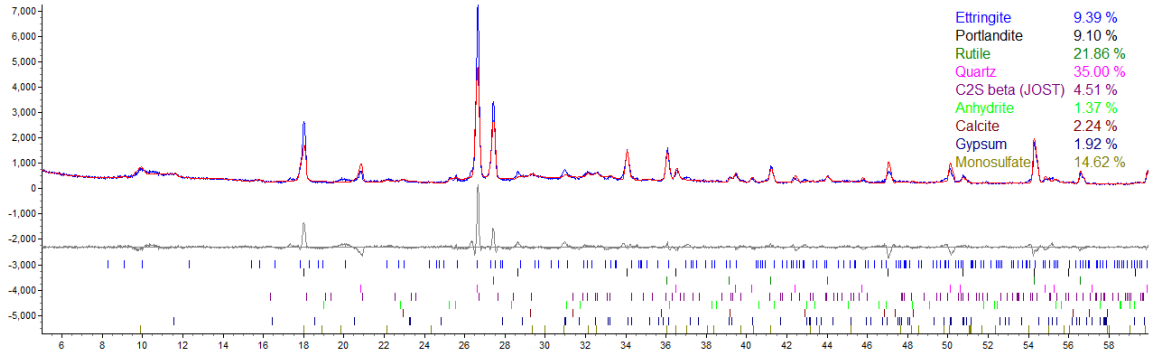

Figure A42. X-ray diffraction pattern and Rietveld refinement: C1-F3(35)-G(2) at 28 days.

28 Days C1-F3(35)-G(4A)

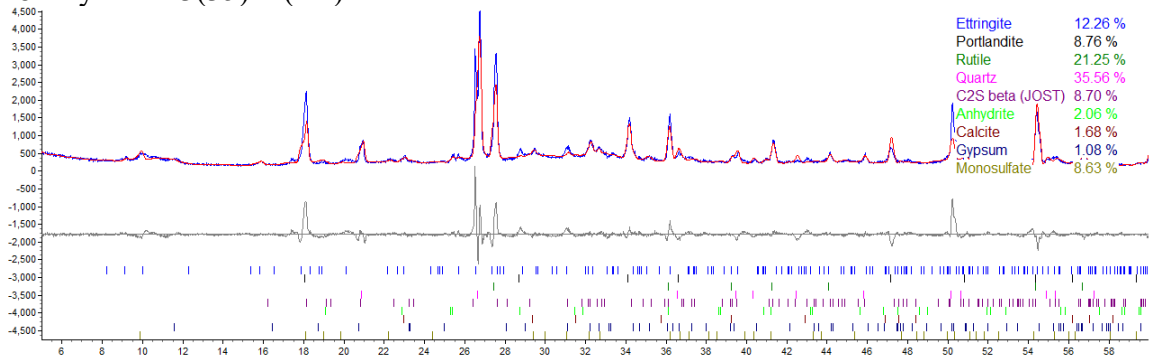

28 Days C1-F3(35)-G(4C)

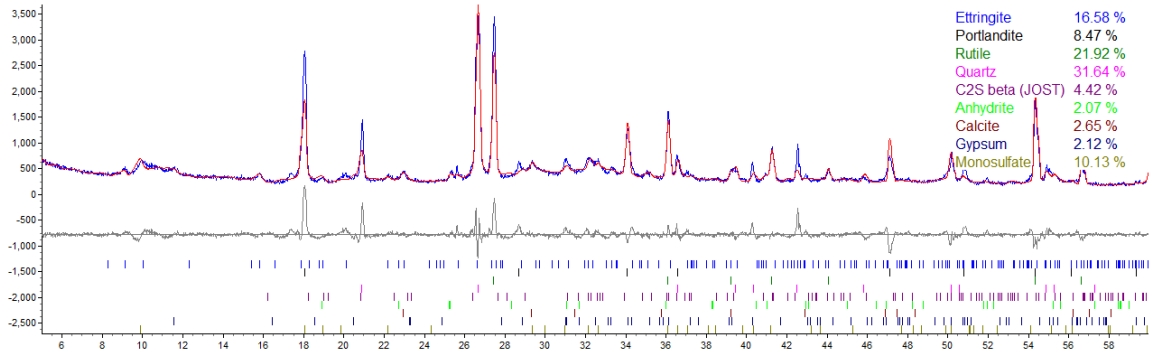

Figure A43. X-ray diffraction pattern and Rietveld refinement: C1-F3(35)-G(4) at 28 days.

28 Days C1-F3(35)-G(6A)

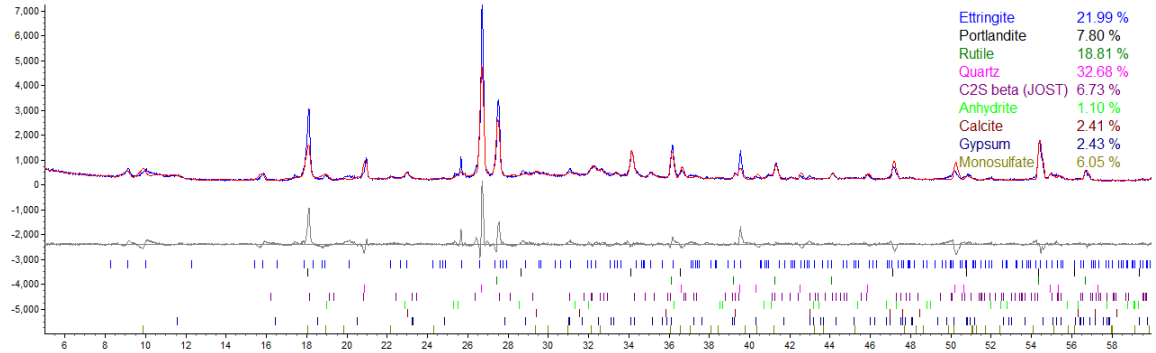

28 Days C1-F3(35)-G(6B)

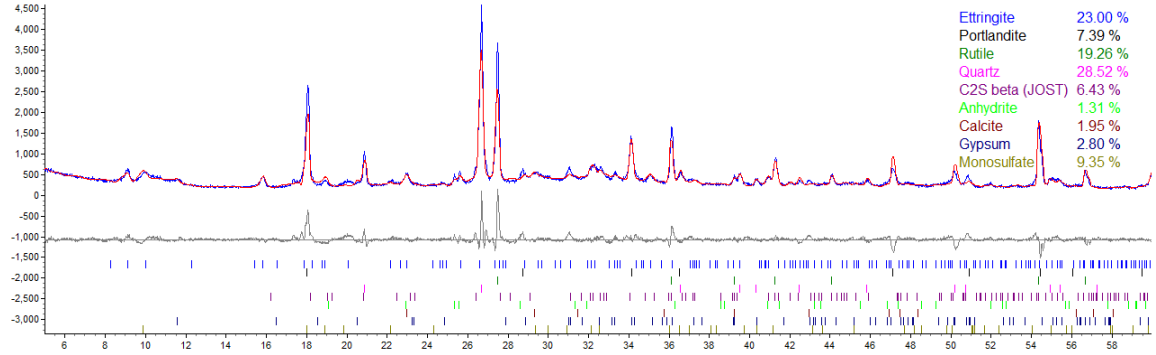

Figure A44. X-ray diffraction pattern and Rietveld refinement: C1-F3(35)-G(6) at 28 days.

28 Days C1-F3(35)-G(8B)

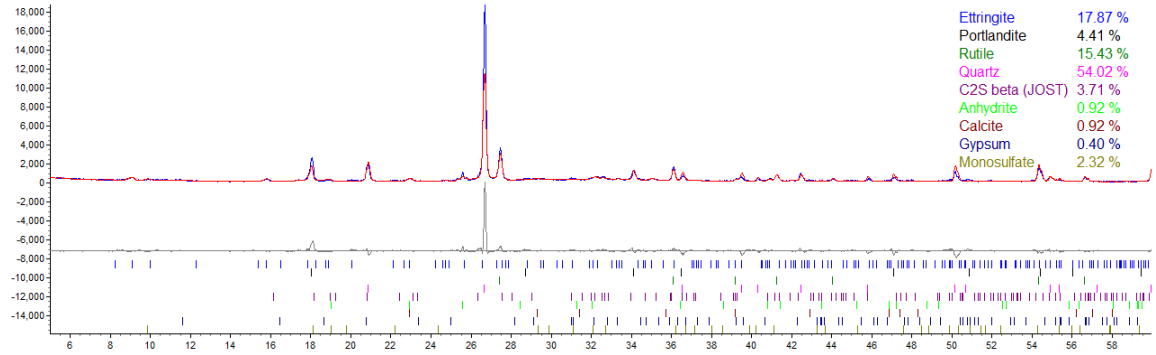

28 Days C1-F3(35)-G(8C)

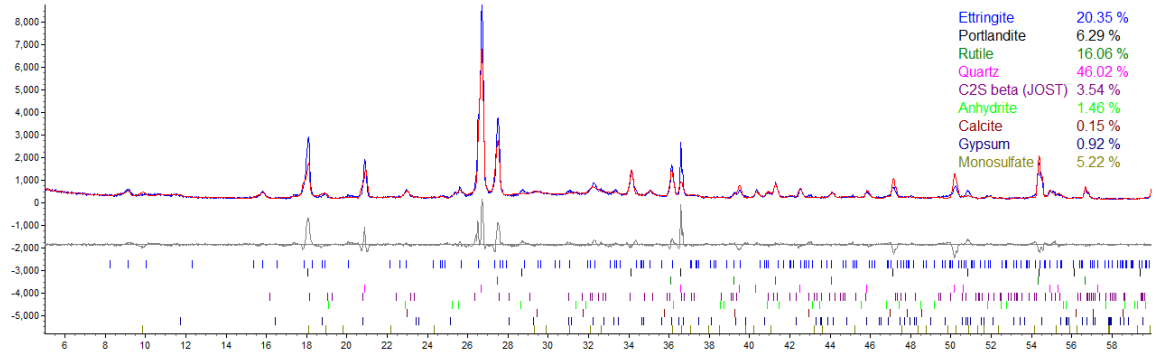

Figure A45. X-ray diffraction pattern and Rietveld refinement: C1-F3(35)-G(8) at 28 days.

28 Days C1-F3(35)-G(10A)

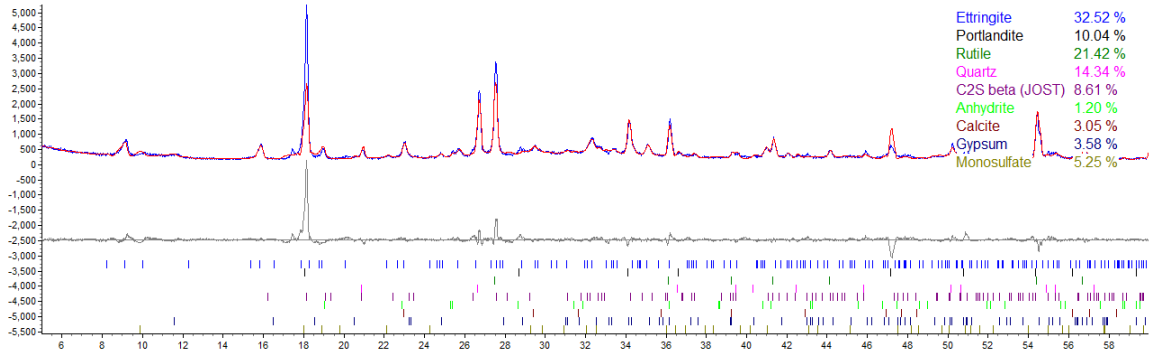

28 Days C1-F3(35)-G(10B)

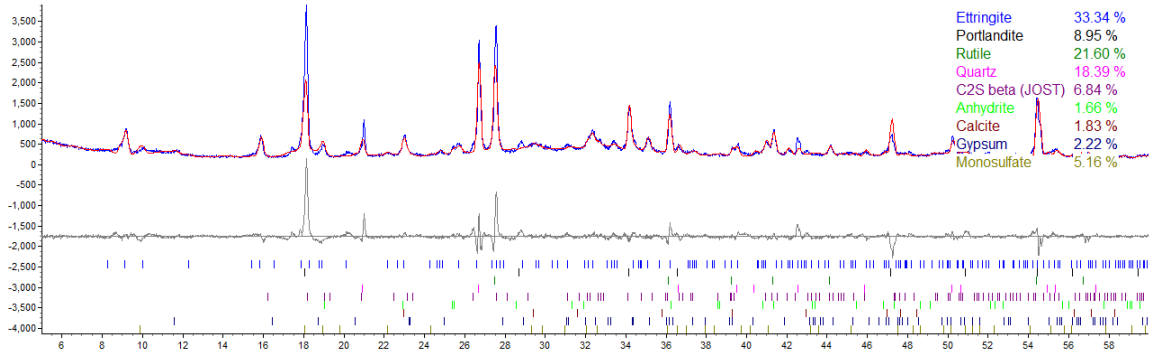

Figure A46. X-ray diffraction pattern and Rietveld refinement: C1-F3(35)-G(10) at 28 days.

28 Days C1-F3(35)-G(12A)

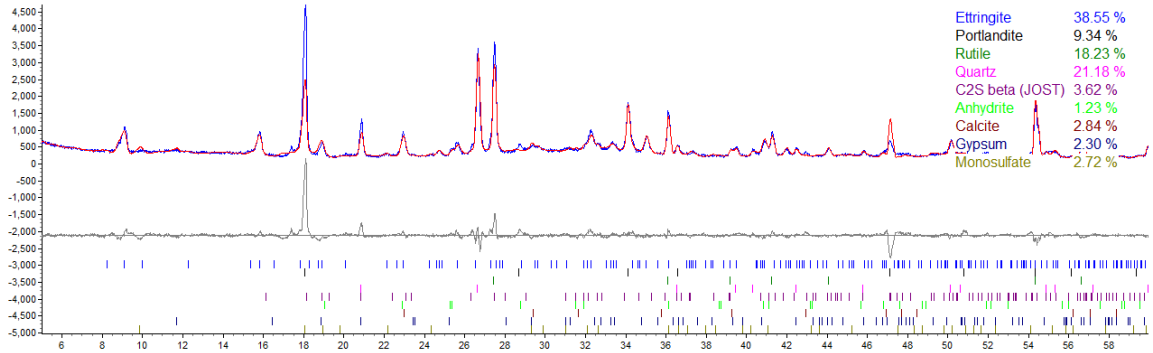

28 Days C1-F3(35)-G(12B)

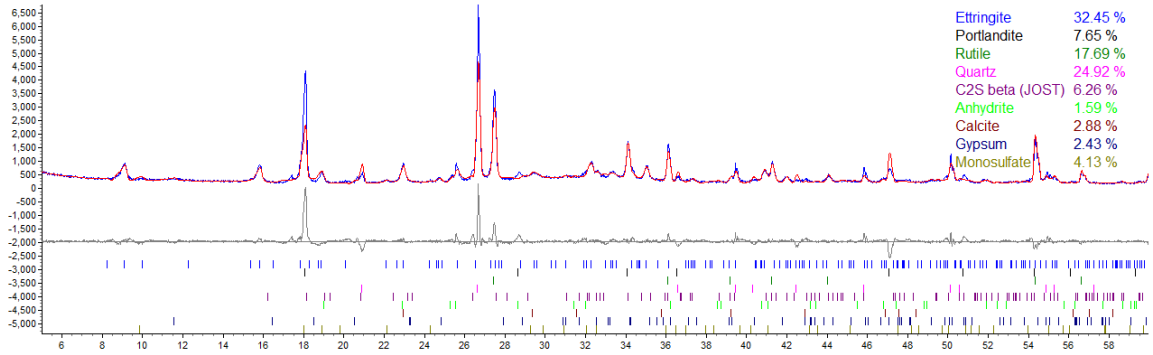

Figure A47. X-ray diffraction pattern and Rietveld refinement: C1-F3(35)-G(12) at 28 days.

28 Days C1-F3(35)-G(15A)

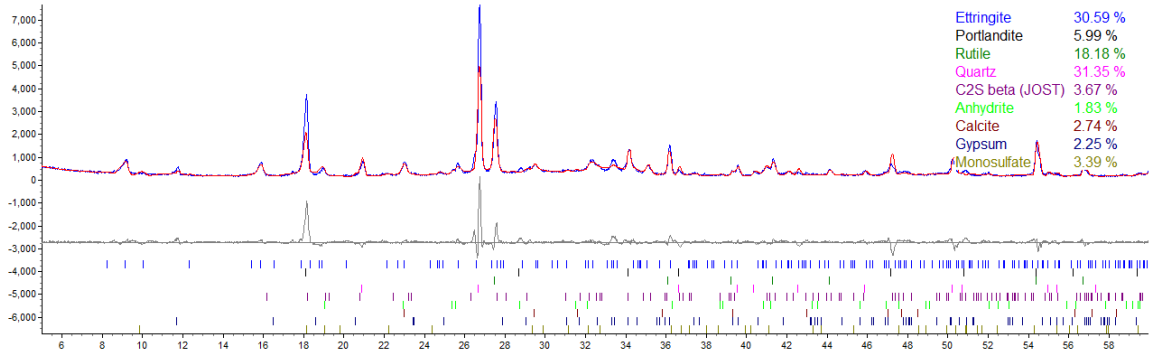

28 Days C1-F3(35)-G(15B)

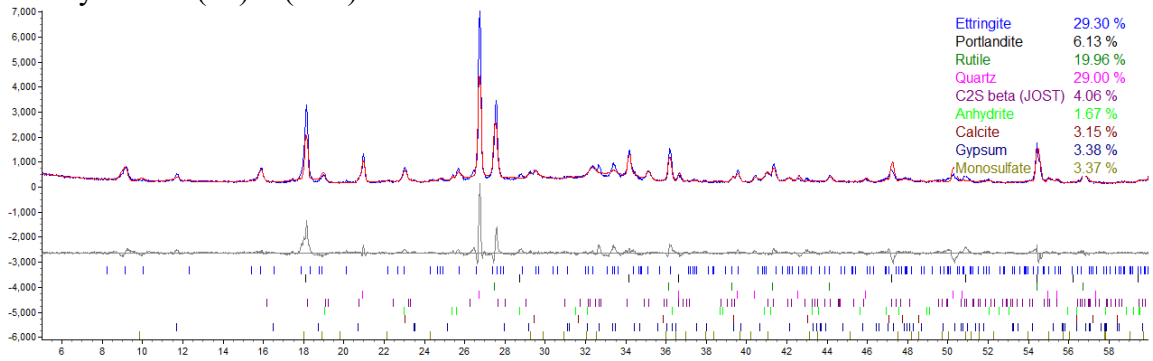

Figure A48. X-ray diffraction pattern and Rietveld refinement: C1-F3(35)-G(15) at 28 days.

C1-F1(20)-G(0A)

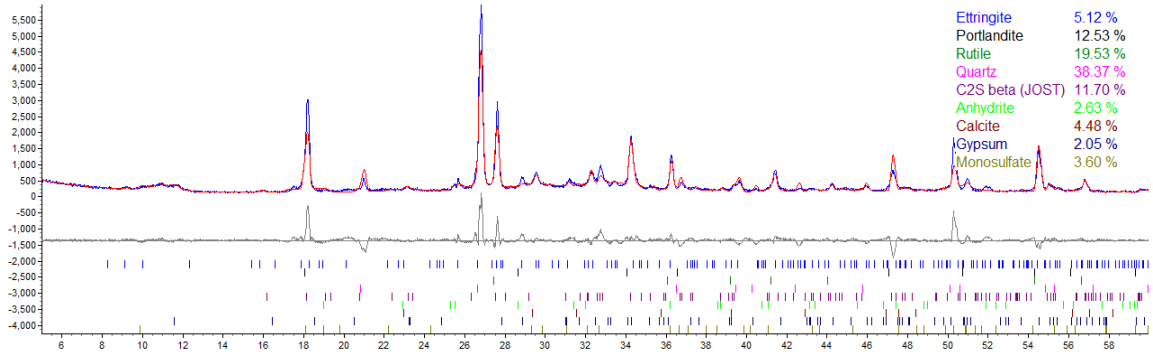

C1-F1(20)-G(0B)

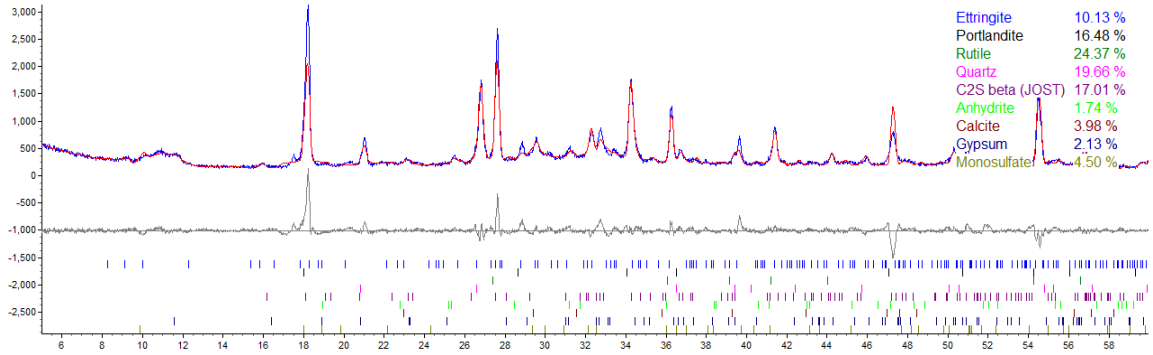

Figure A49. X-ray diffraction pattern and Rietveld refinement: C1-F1(20)-G(0).

C1-F1(20)-G(2B)

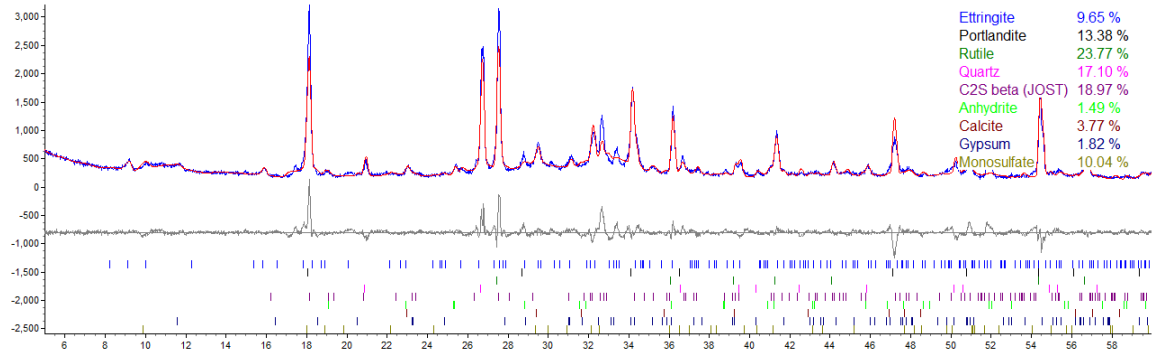

C1-F1(20)-G(2C)

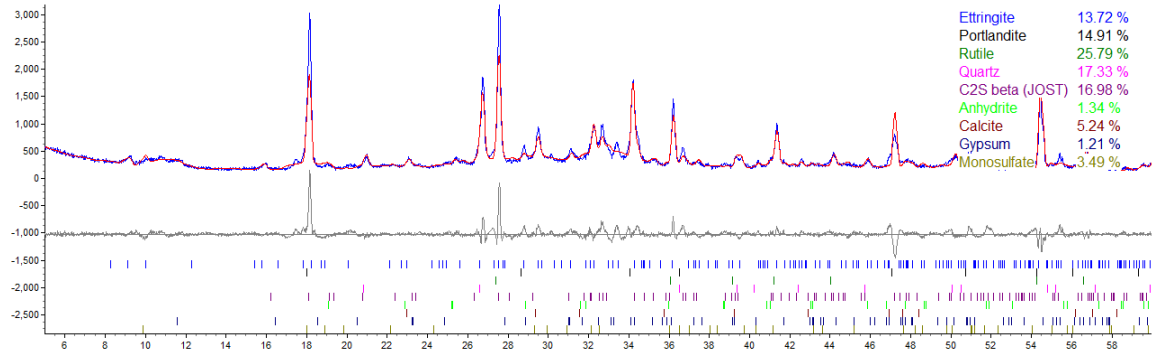

Figure A50. X-ray diffraction pattern and Rietveld refinement: C1-F1(20)-G(2).

C1-F1(20)-G(4A)

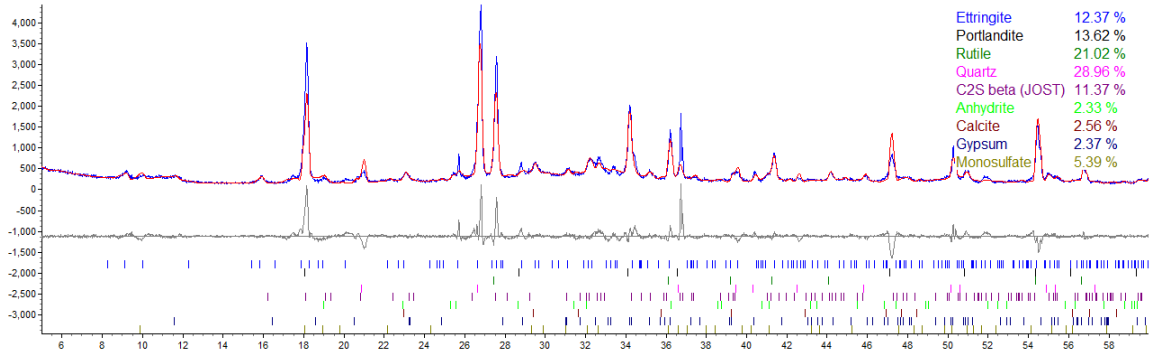

C1-F1(20)-G(4B)

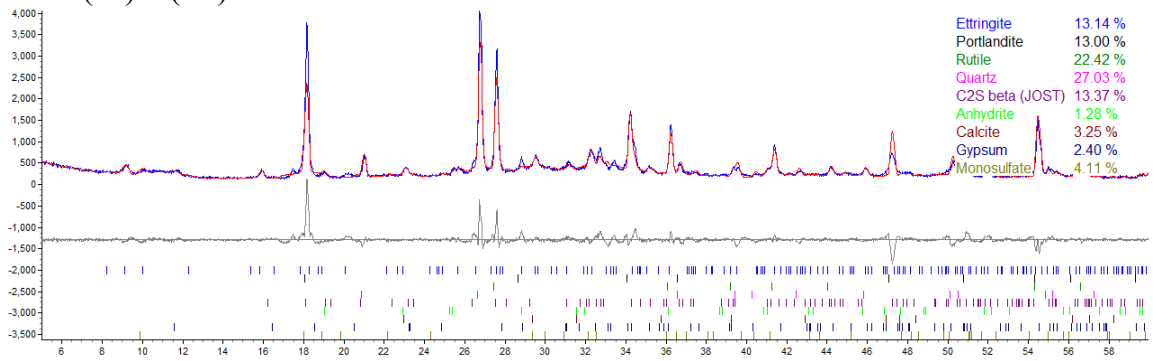

Figure A51. X-ray diffraction pattern and Rietveld refinement: C1-F1(20)-G(4).

C1-F1(20)-G(6A)

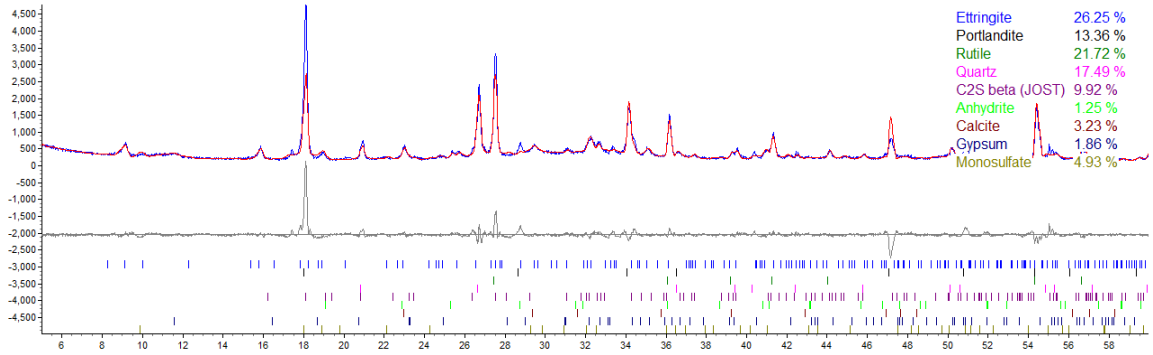

C1-F1(20)-G(6B)

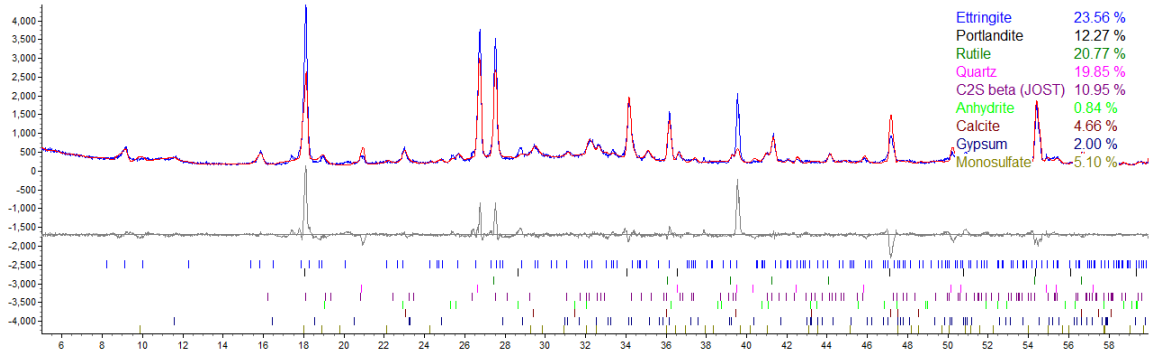

Figure A52. X-ray diffraction pattern and Rietveld refinement: C1-F1(20)-G(6).

C1-F1(20)-G(8A)

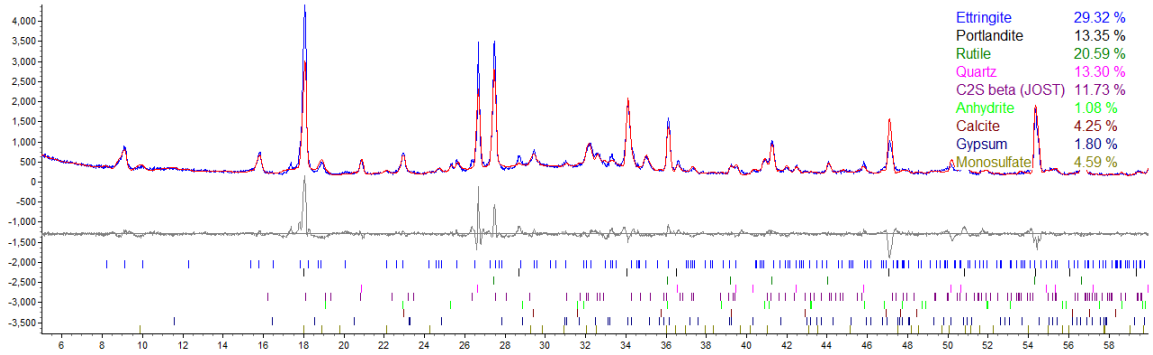

C1-F1(20)-G(8C)

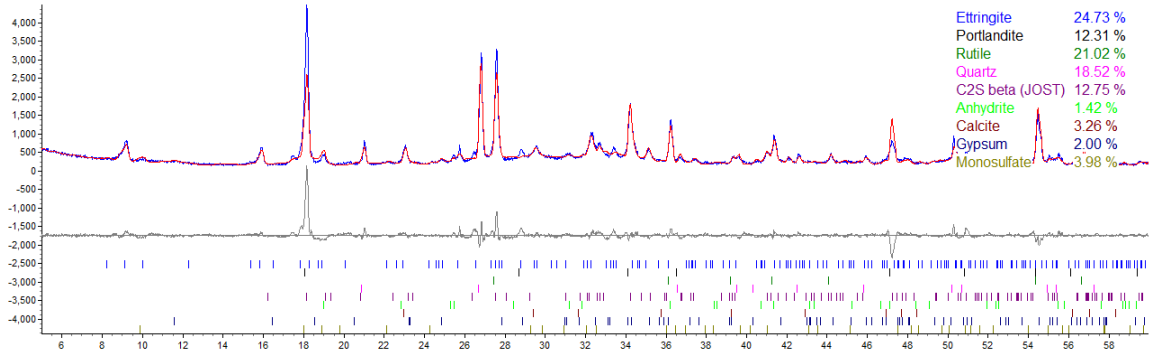

Figure A53. X-ray diffraction pattern and Rietveld refinement: C1-F1(20)-G(8).

C1-F1(20)-G(10A)

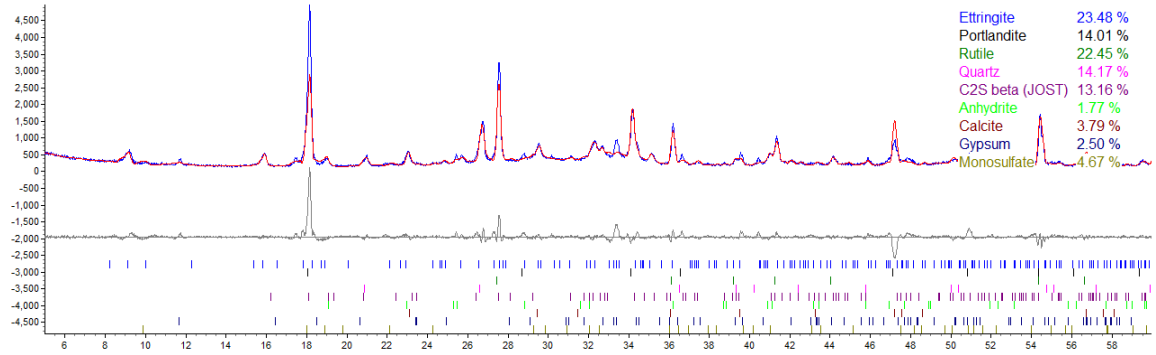

C1-F1(20)-G(10B)

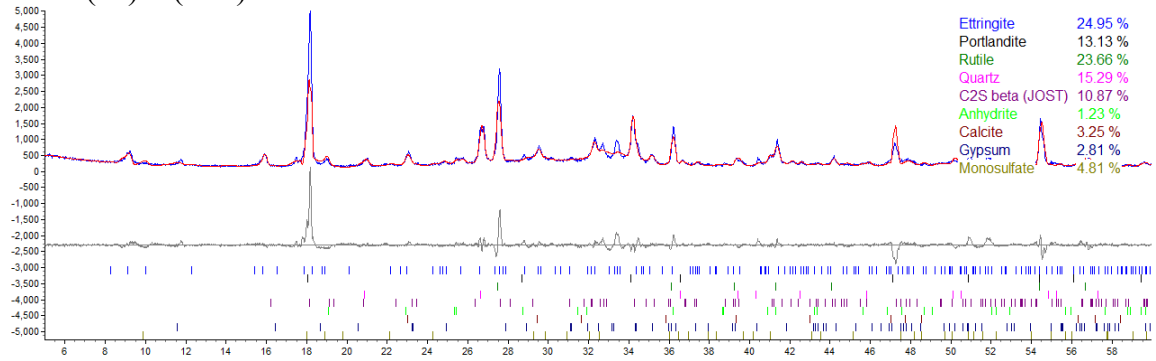

Figure A54. X-ray diffraction pattern and Rietveld refinement: C1-F1(20)-G(10).

C1-F1(20)-G(12A)

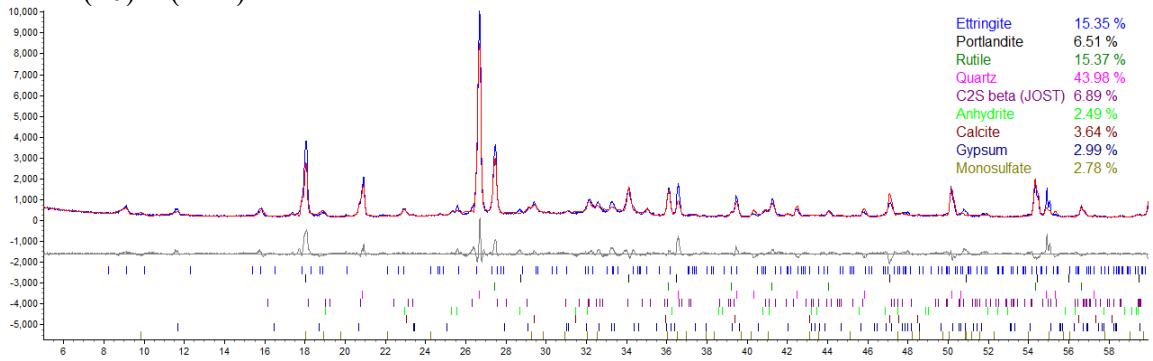

C1-F1(20)-G(12B)

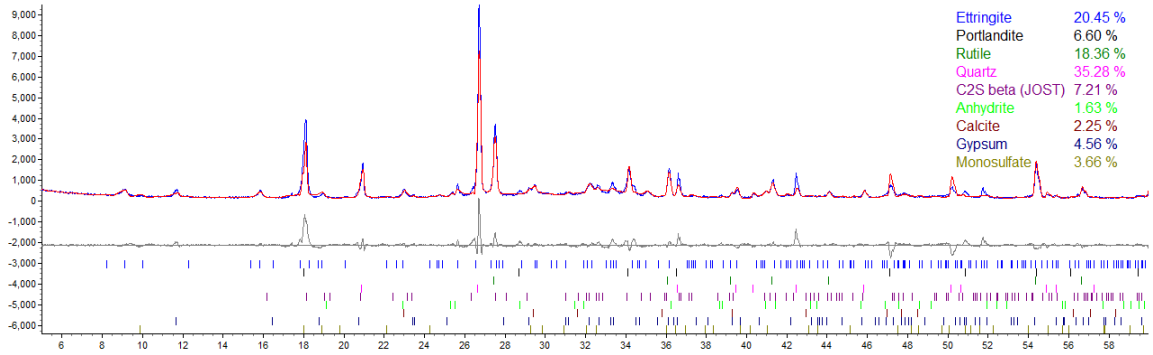

Figure A55. X-ray diffraction pattern and Rietveld refinement: C1-F1(20)-G(12).

C1-F1(20)-G(15A)

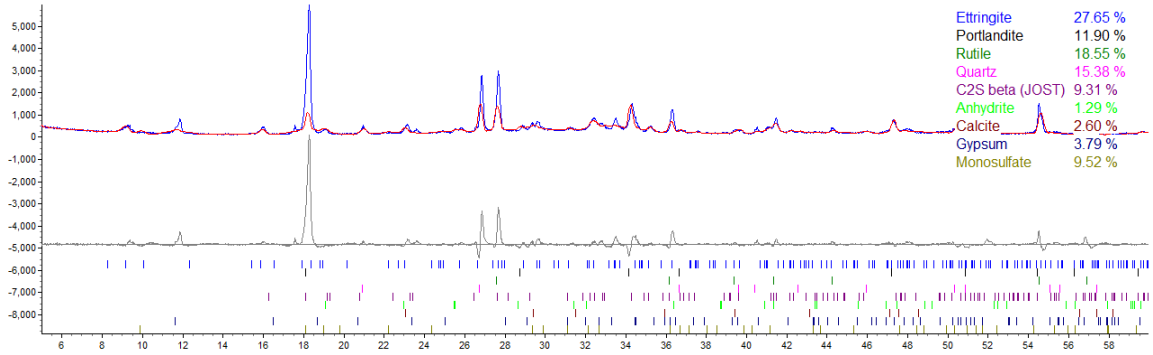

C1-F1(20)-G(15B)

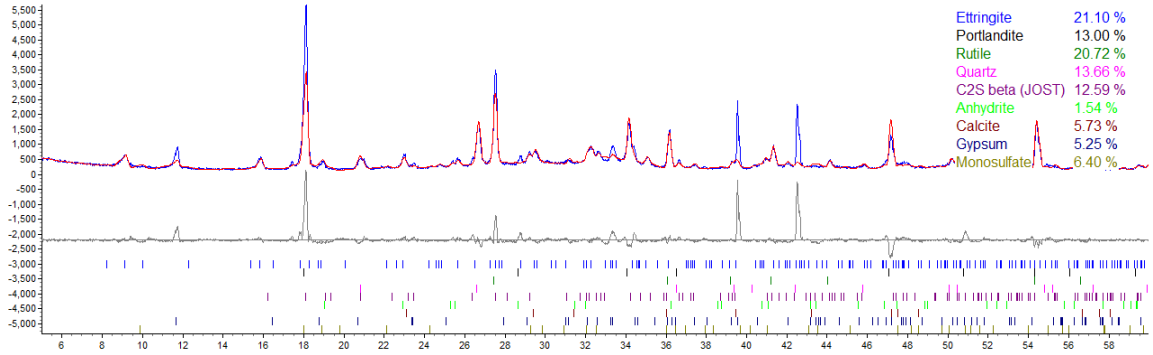

Figure A56. X-ray diffraction pattern and Rietveld refinement: C1-F1(20)-G(15).

28 Days C1-F1(20)-G(0A)

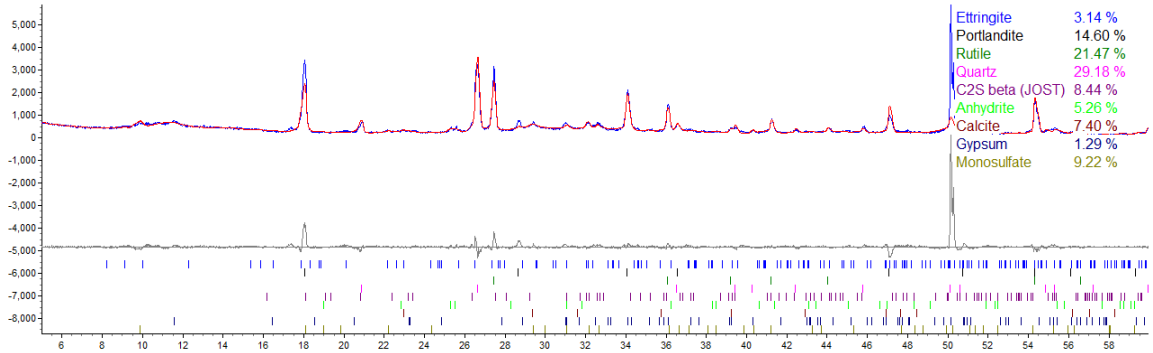

28 Days C1-F1(20)-G(0B)

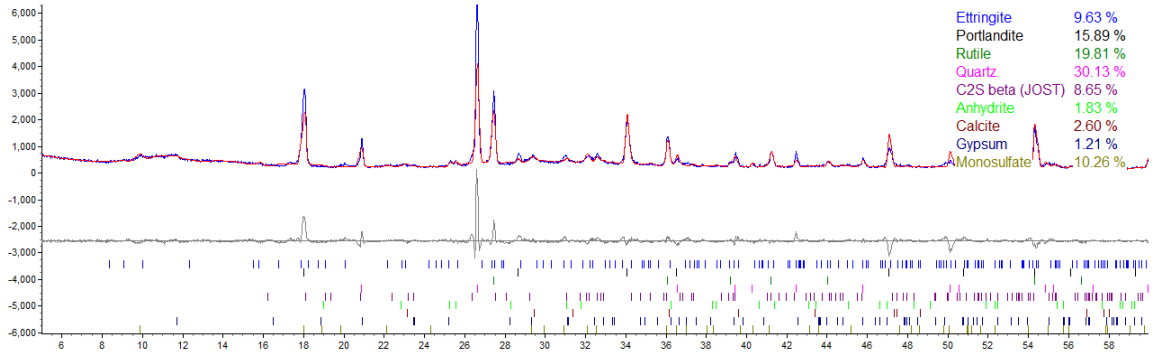

Figure A57. X-ray diffraction pattern and Rietveld refinement: C1-F1(20)-G(0) at 28 days.

28 Days C1-F1(20)-G(2A)

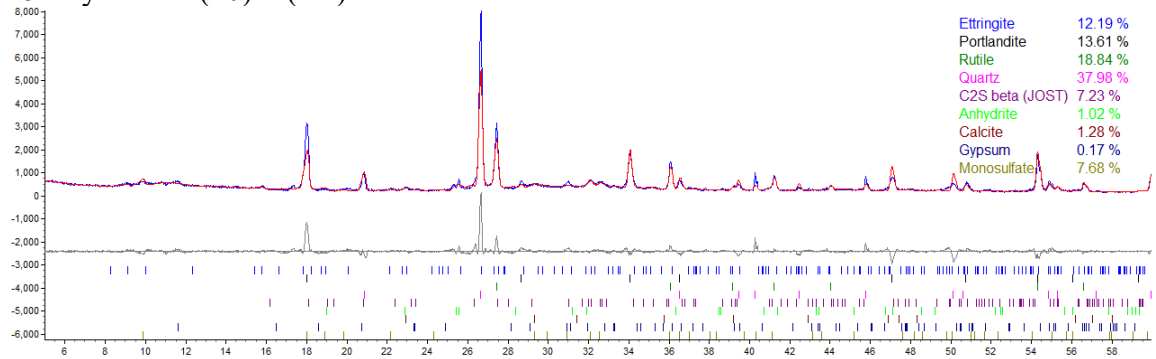

28 Days C1-F1(20)-G(2B)

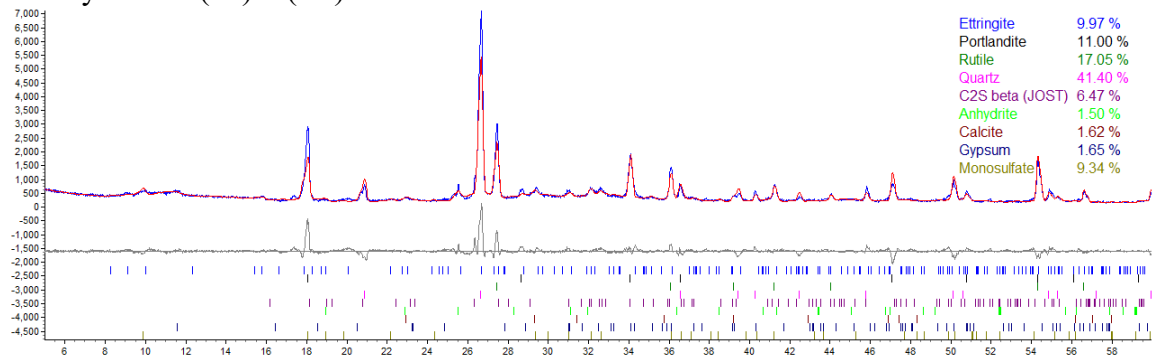

Figure A58. X-ray diffraction pattern and Rietveld refinement: C1-F1(20)-G(2) at 28 days.

28 Days C1-F1(20)-G(4A)

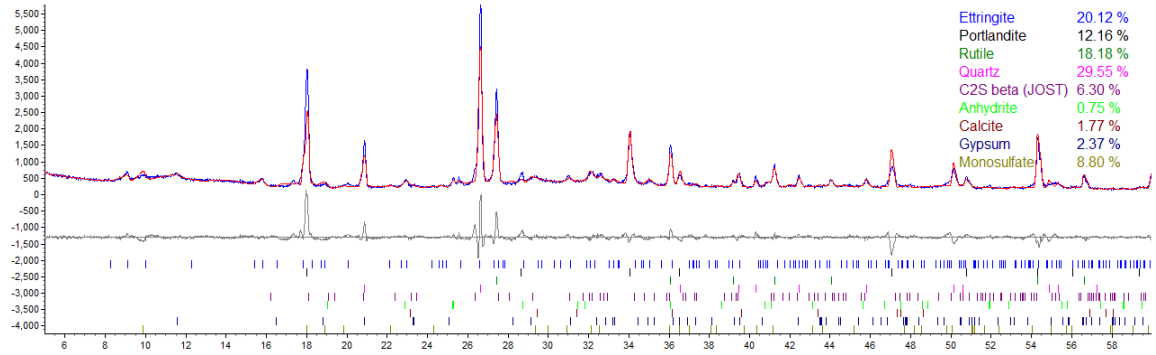

28 Days C1-F1(20)-G(4B)

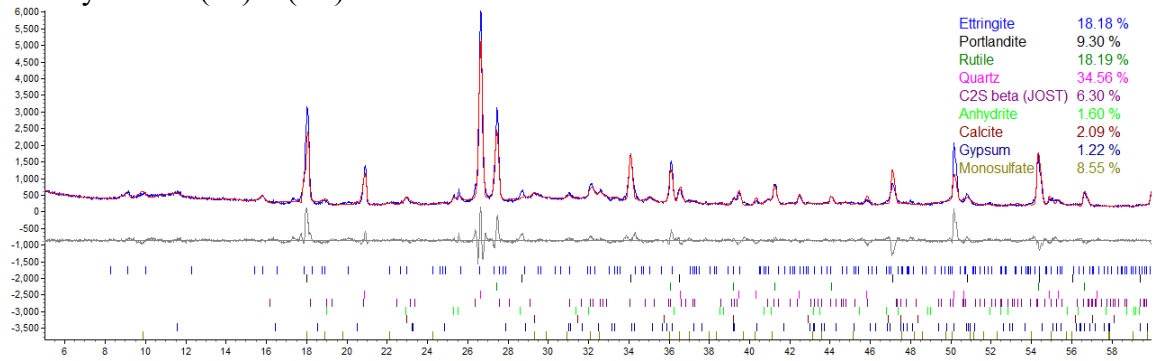

Figure A59. X-ray diffraction pattern and Rietveld refinement: C1-F1(20)-G(4) at 28 days.

28 Days C1-F1(20)-G(6A)

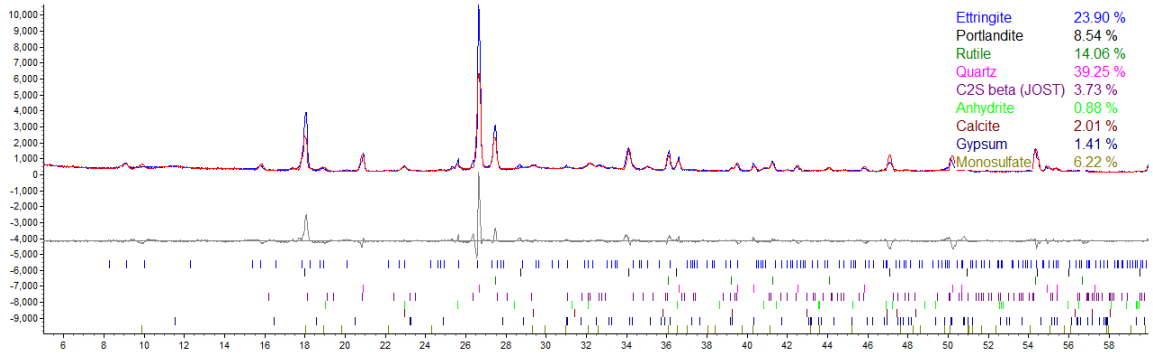

28 Days C1-F1(20)-G(6B)

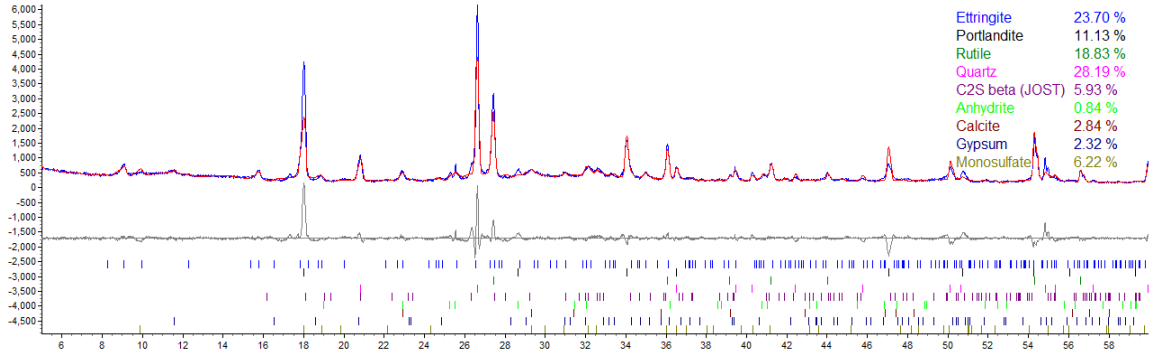

Figure A60. X-ray diffraction pattern and Rietveld refinement: C1-F1(20)-G(6) at 28 days.

28 Days C1-F1(20)-G(8B)

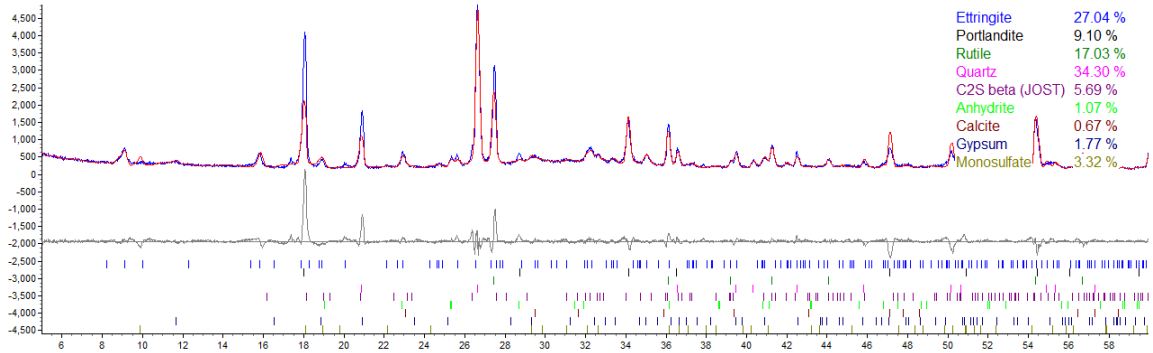

28 Days C1-F1(20)-G(8C)

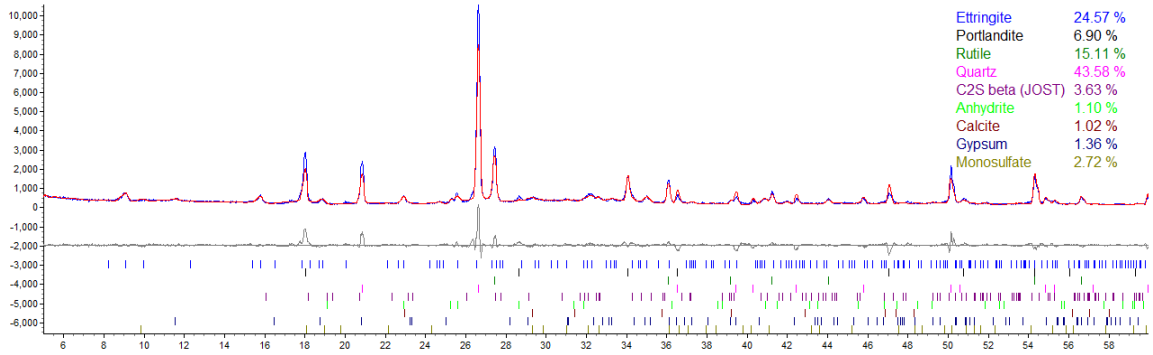

Figure A61. X-ray diffraction pattern and Rietveld refinement: C1-F1(20)-G(8) at 28 days.

28 Days C1-F1(20)-G(10A)

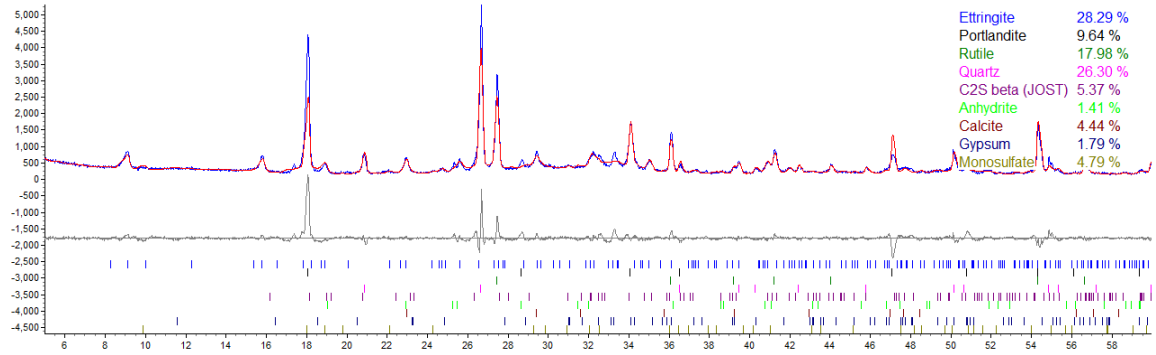

28 Days C1-F1(20)-G(10B)

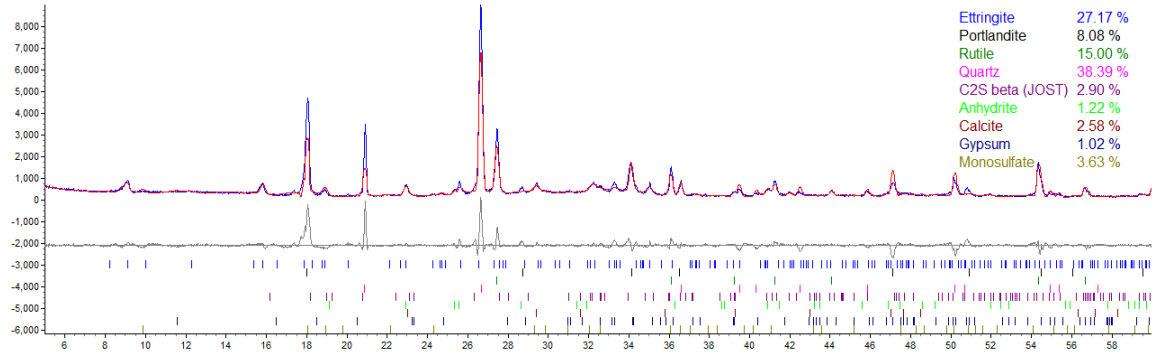

Figure A62. X-ray diffraction pattern and Rietveld refinement: C1-F1(20)-G(10) at 28 days.

28 Days C1-F1(20)-G(12A)

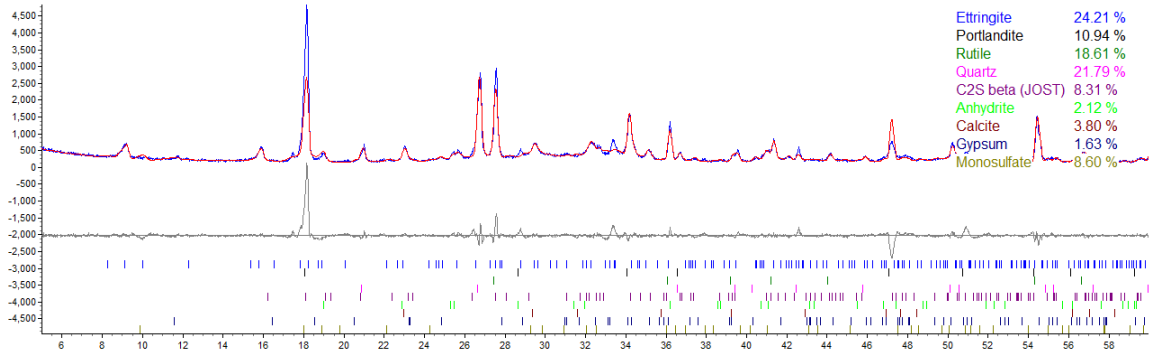

28 Days C1-F1(20)-G(12B)

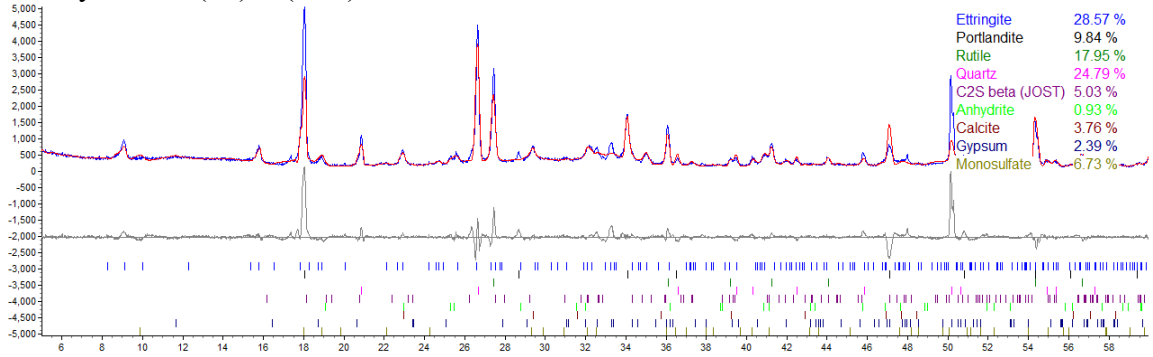

Figure A63. X-ray diffraction pattern and Rietveld refinement: C1-F1(20)-G(12) at 28 days.

28 Days C1-F1(20)-G(15A)

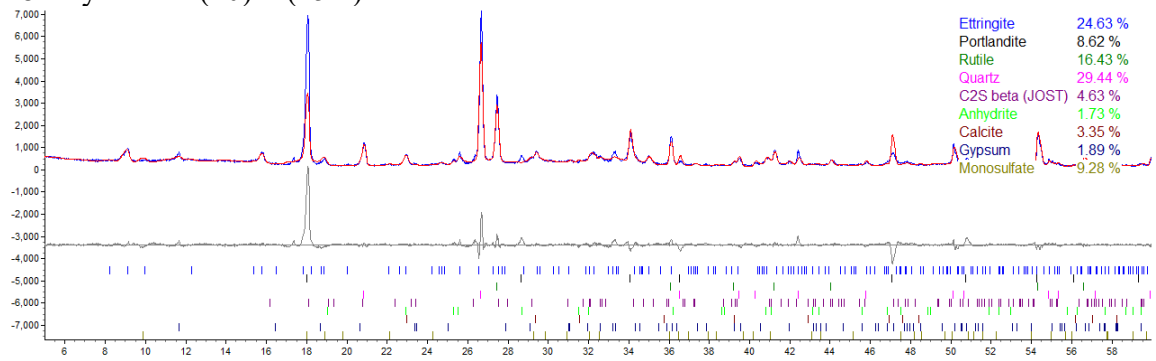

28 Days C1-F1(20)-G(15B)

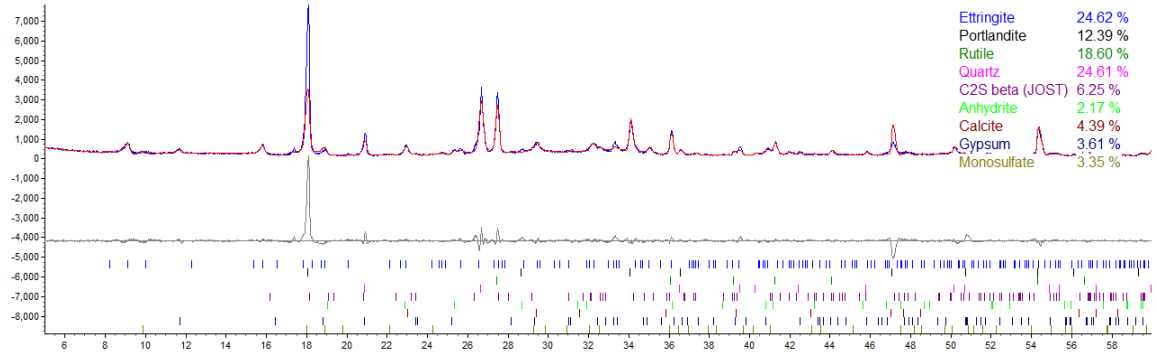

Figure A64. X-ray diffraction pattern and Rietveld refinement: C1-F1(20)-G(15) at 28 days.

C1-F2(20)-G(0A)

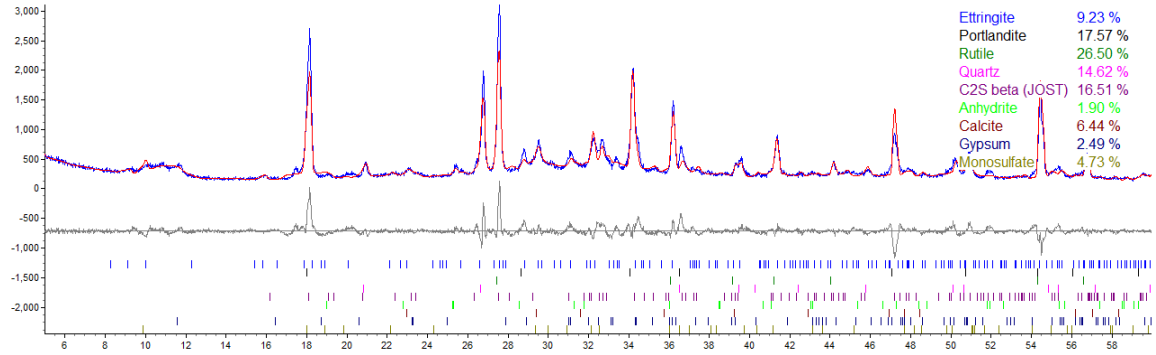

C1-F2(20)-G(0B)

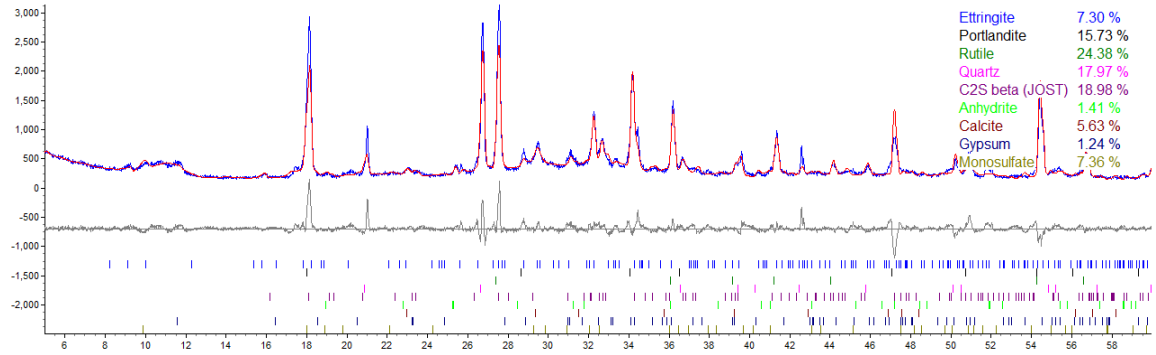

Figure A65. X-ray diffraction pattern and Rietveld refinement: C1-F2(20)-G(0).

C1-F2(20)-G(2A)

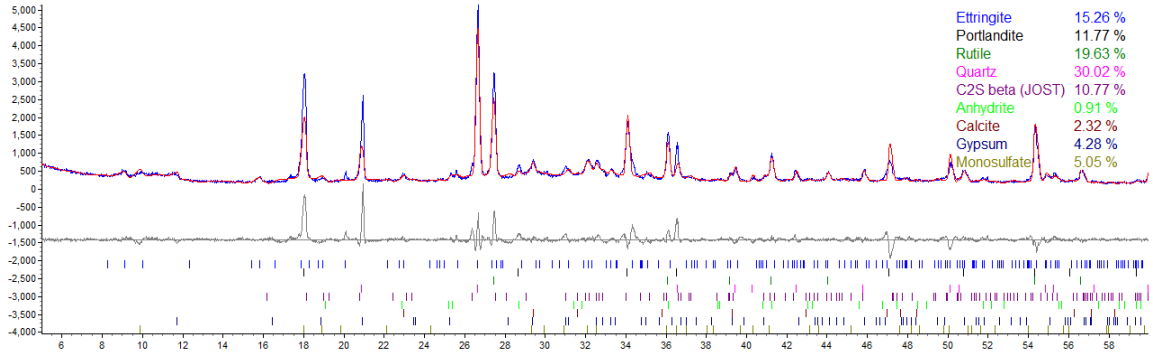

C1-F2(20)-G(2C)

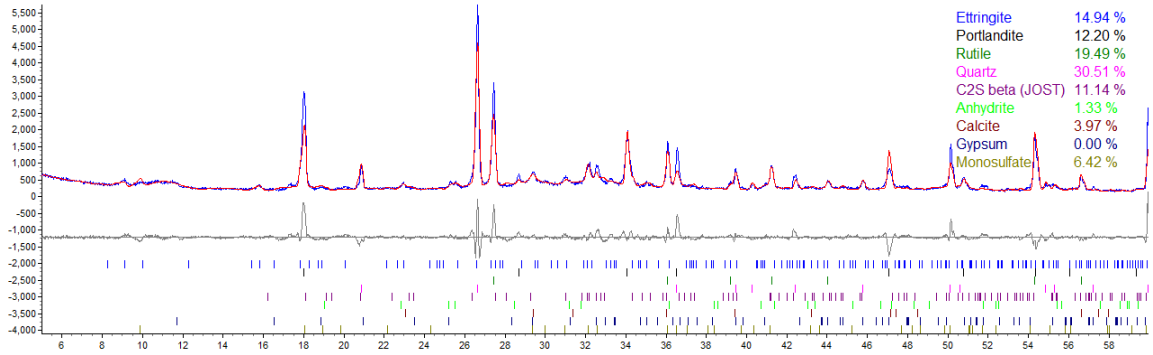

Figure A66. X-ray diffraction pattern and Rietveld refinement: C1-F2(20)-G(2).

C1-F2(20)-G(4A)

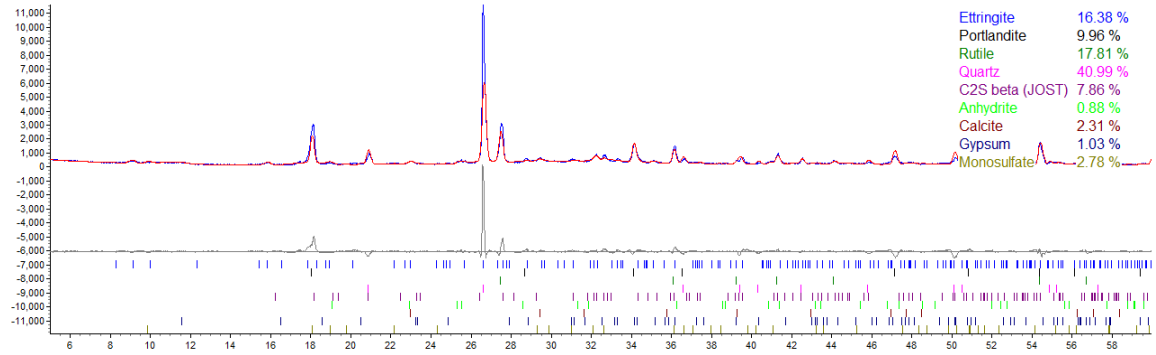

C1-F2(20)-G(4C)

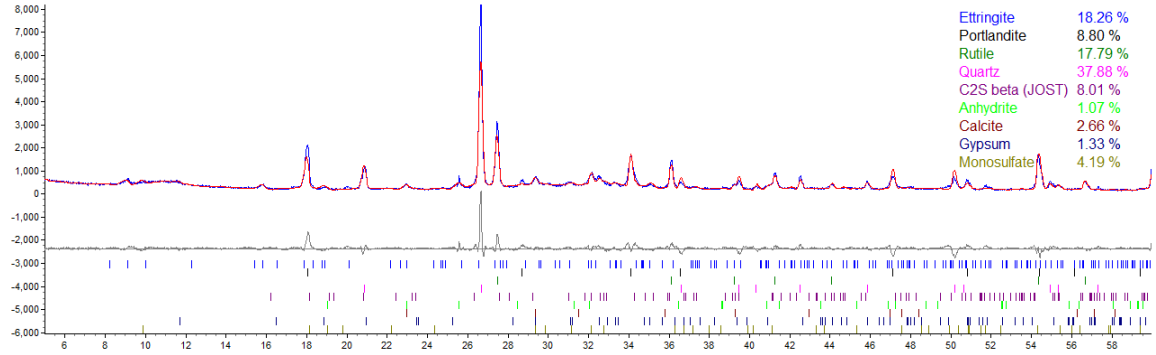

Figure A67. X-ray diffraction pattern and Rietveld refinement: C1-F2(20)-G(4).

C1-F2(20)-G(6A)

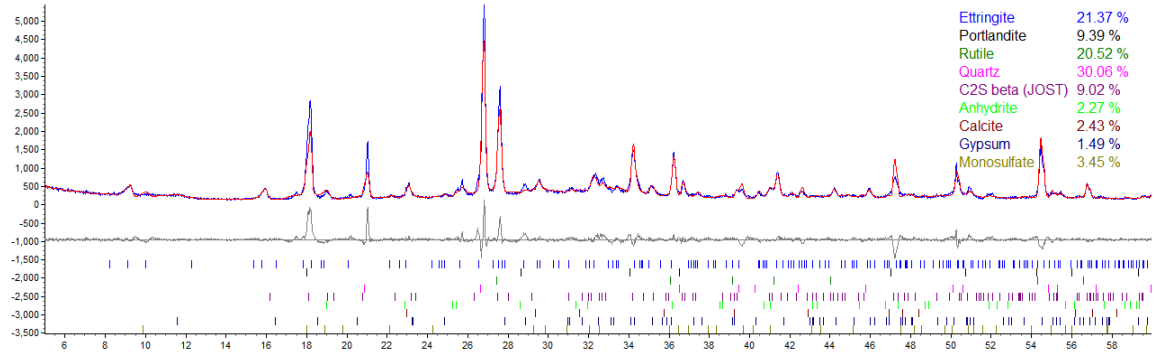

C1-F2(20)-G(6B)

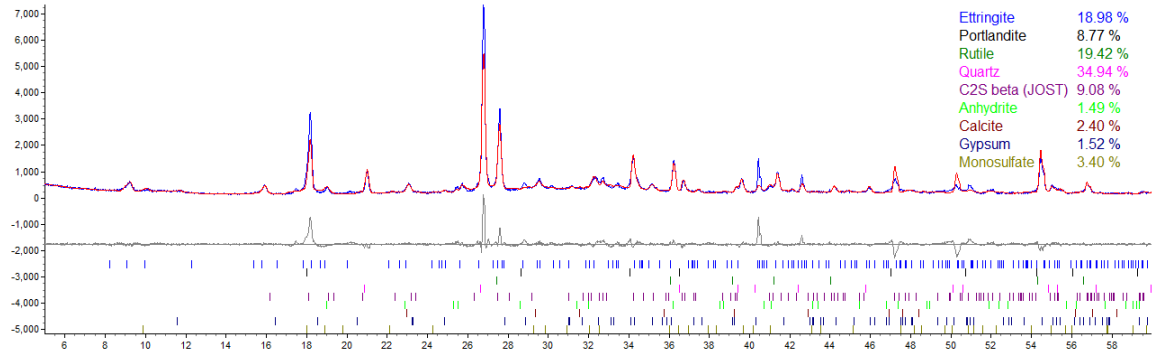

Figure A68. X-ray diffraction pattern and Rietveld refinement: C1-F2(20)-G(6).

C1-F2(20)-G(8A)

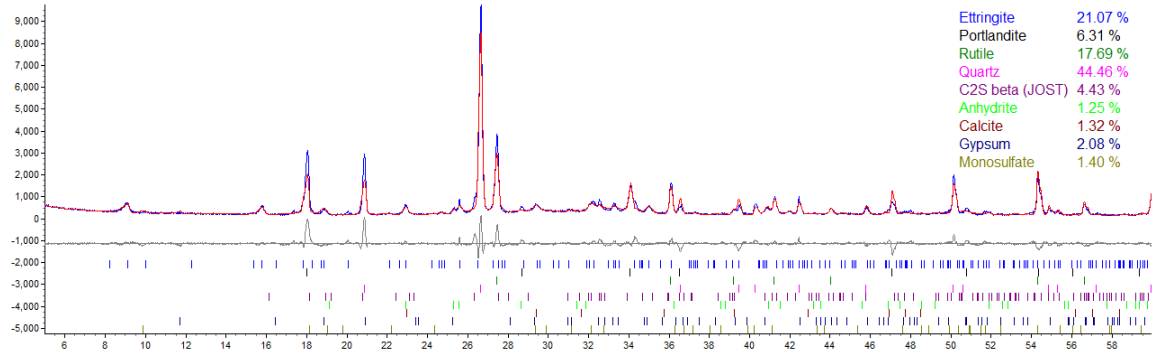

C1-F2(20)-G(8B)

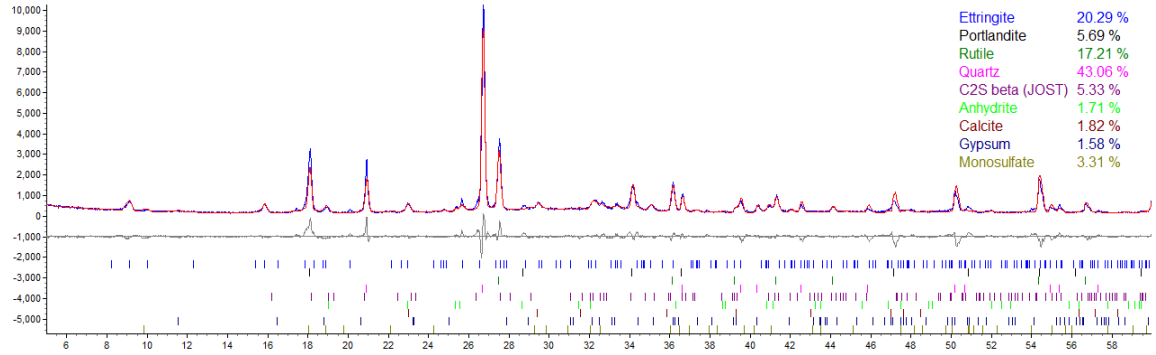

Figure A69. X-ray diffraction pattern and Rietveld refinement: C1-F2(20)-G(8).

C1-F2(20)-G(10A)

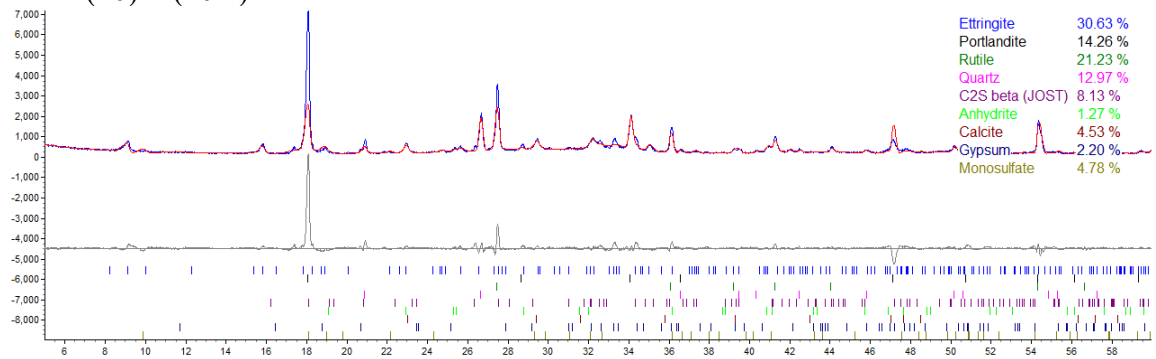

C1-F2(20)-G(10B)

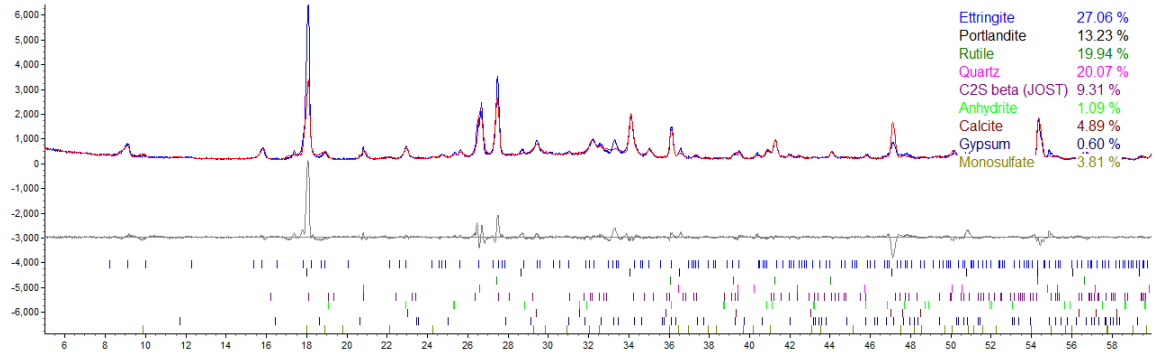

Figure A70. X-ray diffraction pattern and Rietveld refinement: C1-F2(20)-G(10).

C1-F2(20)-G(12A)

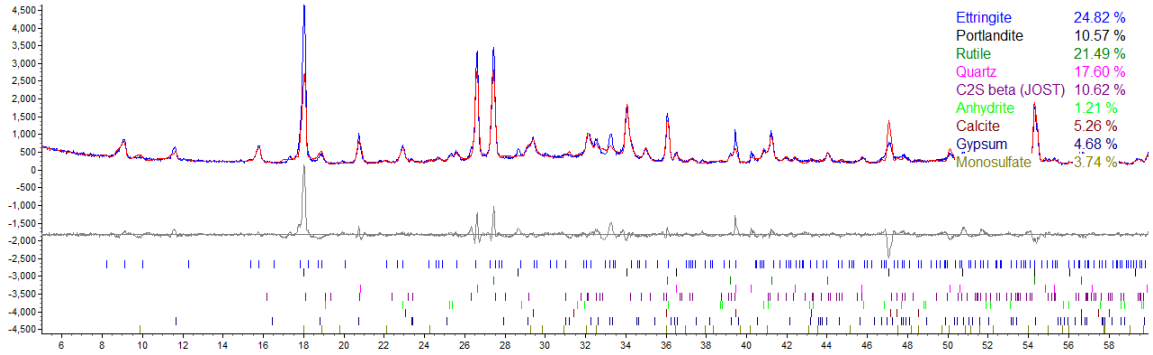

C1-F2(20)-G(12B)

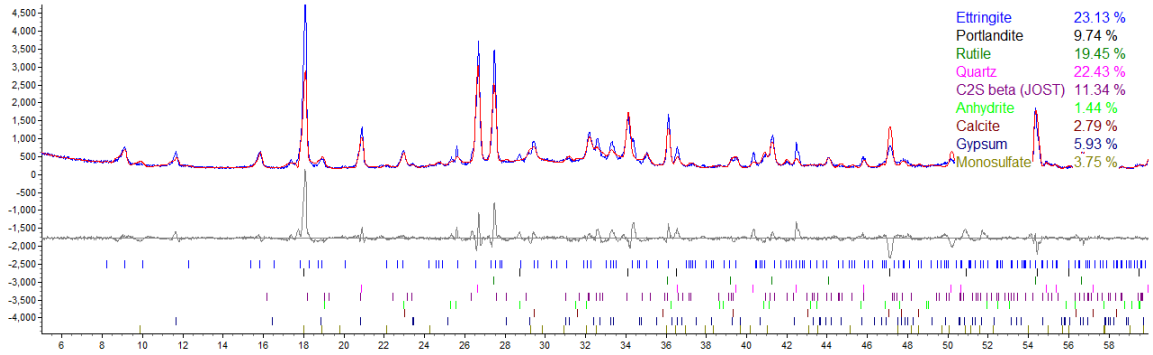

Figure A71. X-ray diffraction pattern and Rietveld refinement: C1-F2(20)-G(12).

C1-F2(20)-G(15B)

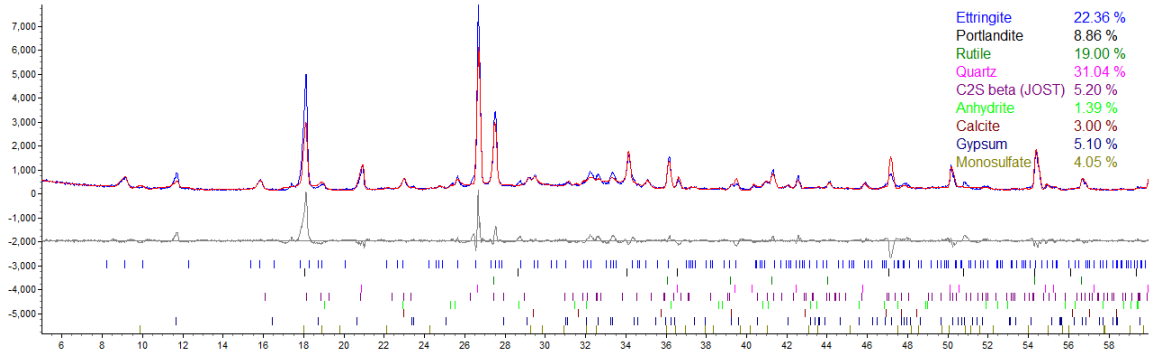

C1-F2(20)-G(15C)

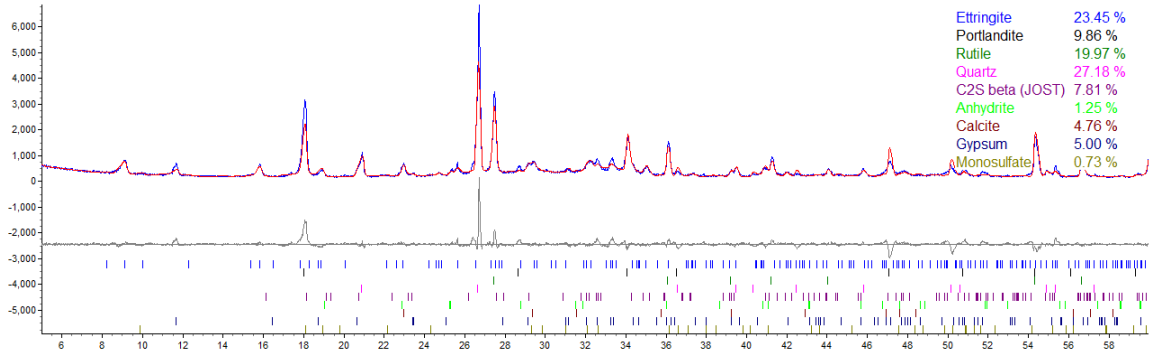

Figure A72. X-ray diffraction pattern and Rietveld refinement: C1-F2(20)-G(15).

28 Days C1-F2(20)-G(0A)

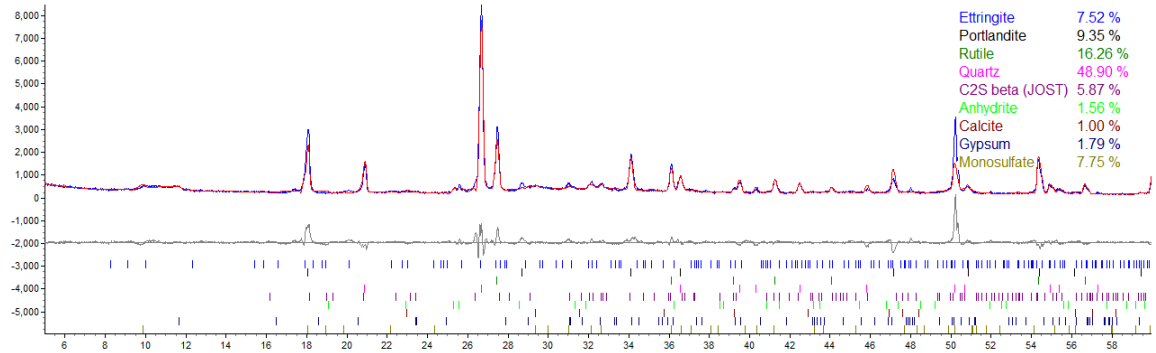

28 Days C1-F2(20)-G(0B)

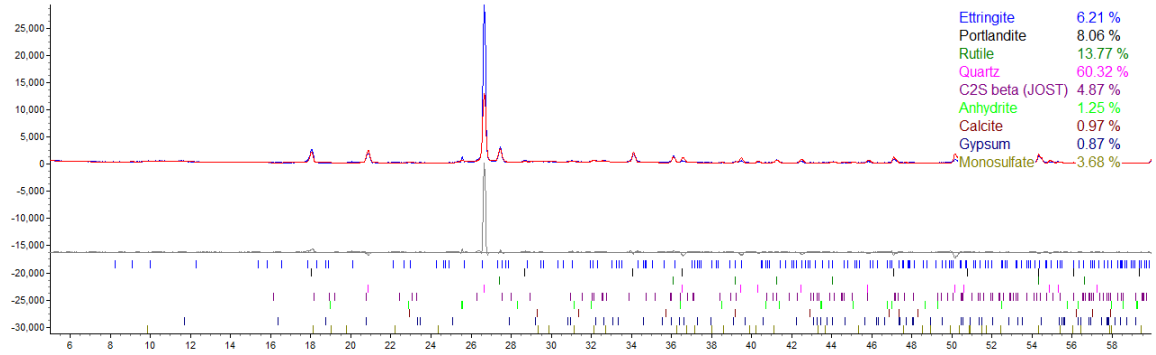

Figure A73. X-ray diffraction pattern and Rietveld refinement: C1-F2(20)-G(0) at 28 days.

28 Days C1-F2(20)-G(2A)

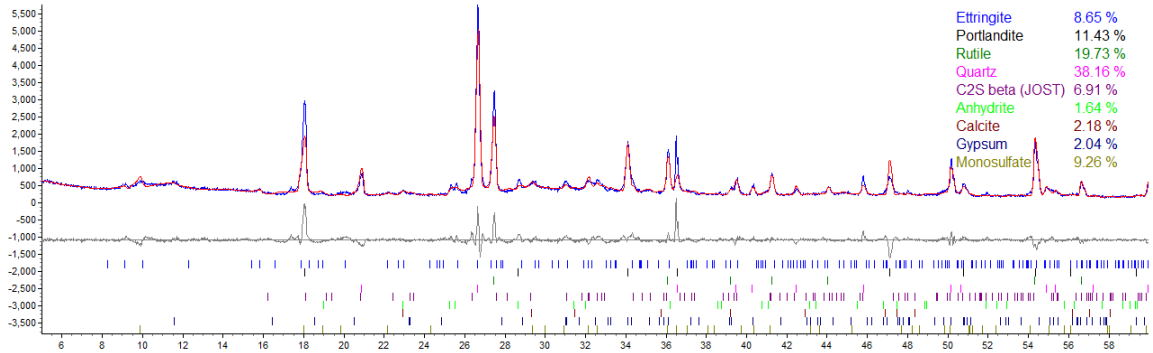

28 Days C1-F2(20)-G(2B)

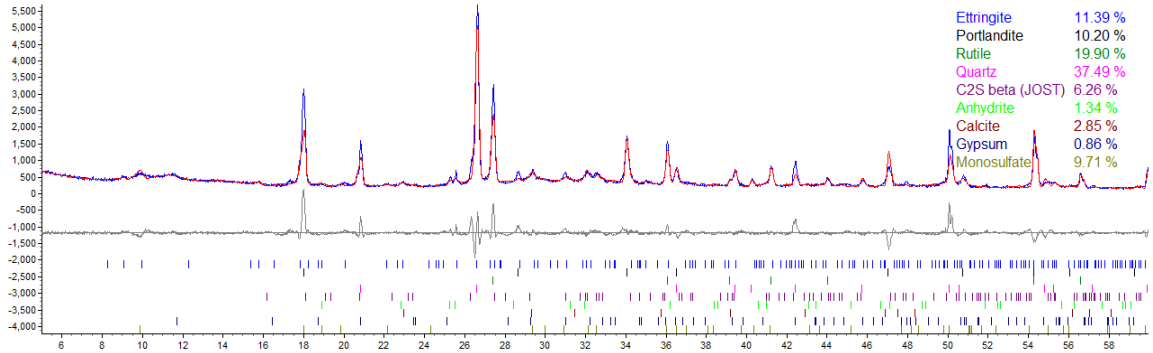

Figure A74. X-ray diffraction pattern and Rietveld refinement: C1-F2(20)-G(2) at 28 days.

28 Days C1-F2(20)-G(4B)

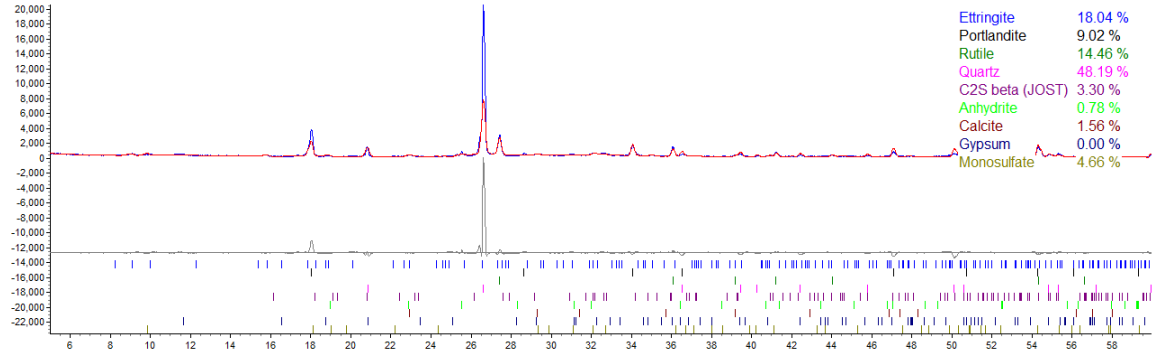

28 Days C1-F2(20)-G(4C)

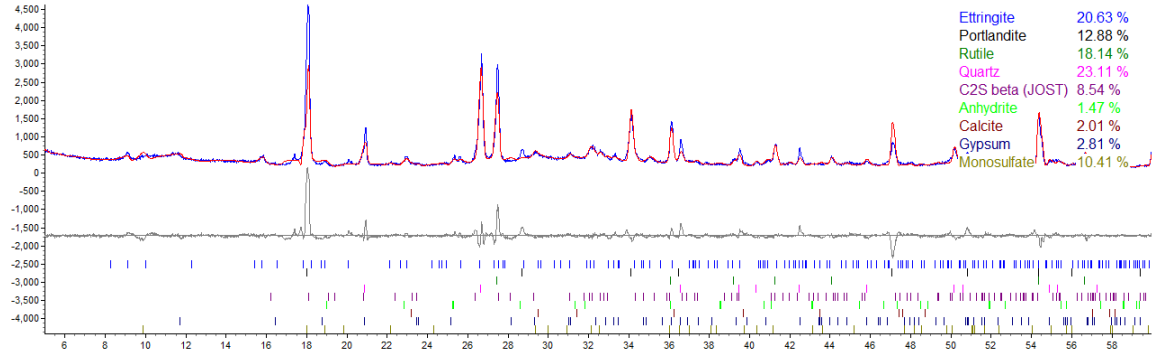

Figure A75. X-ray diffraction pattern and Rietveld refinement: C1-F2(20)-G(4) at 28 days.

28 Days C1-F2(20)-G(6A)

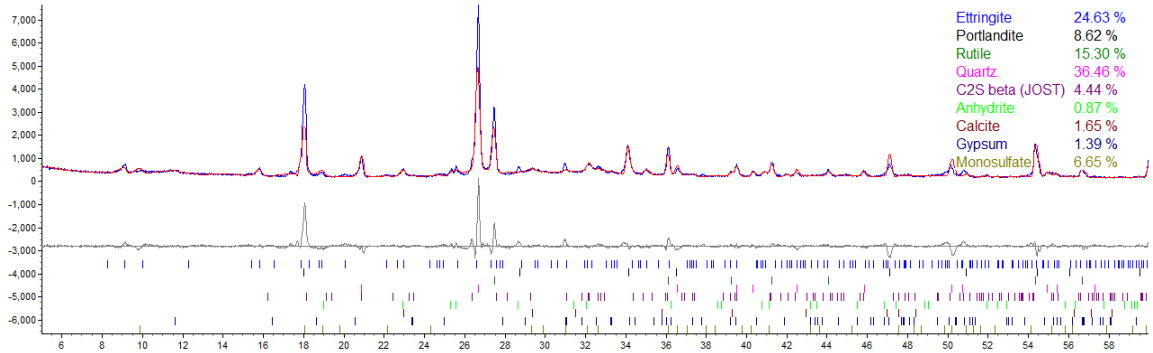

28 Days C1-F2(20)-G(6B)

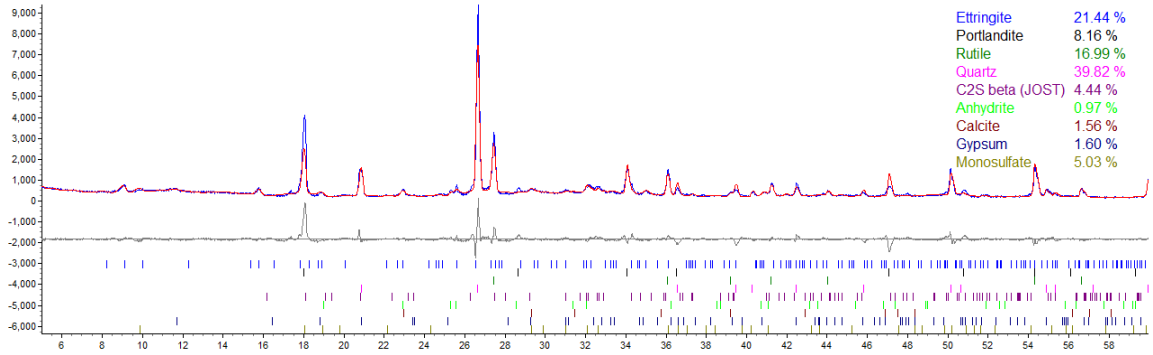

Figure A76. X-ray diffraction pattern and Rietveld refinement: C1-F2(20)-G(6) at 28 days.

28 Days C1-F2(20)-G(8B)

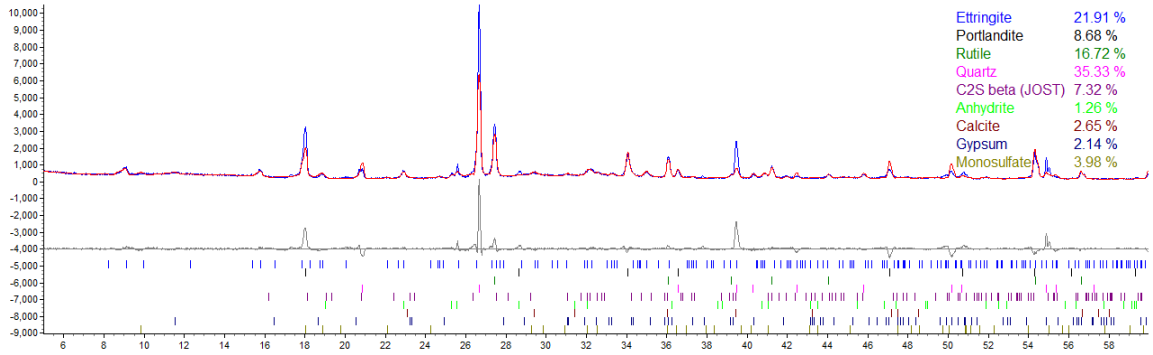

28 Days C1-F2(20)-G(8c)

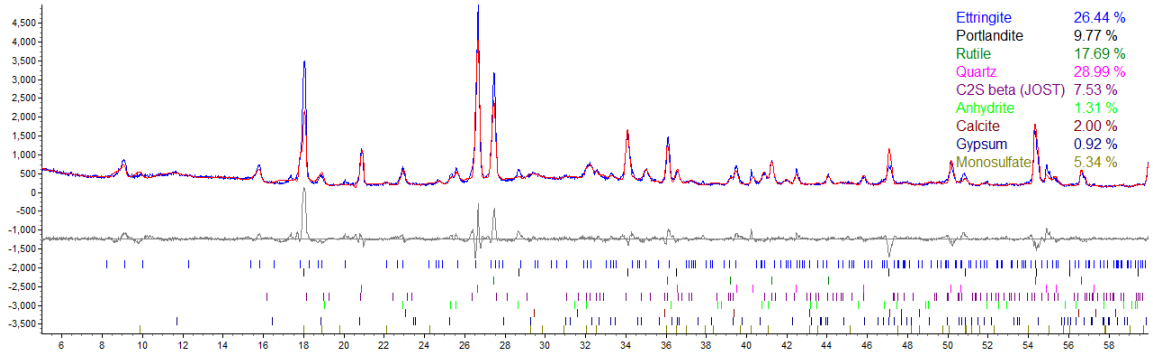

Figure A77. X-ray diffraction pattern and Rietveld refinement: C1-F2(20)-G(8) at 28 days.

28 Days C1-F2(20)-G(10A))

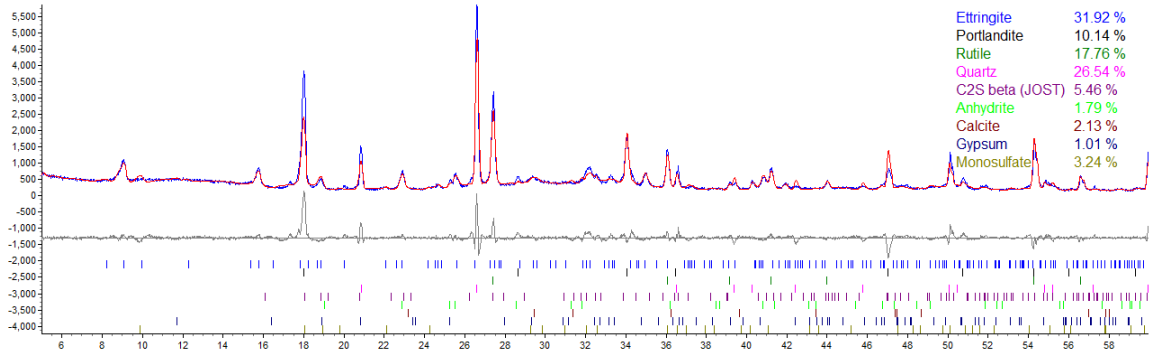

28 Days C1-F2(20)-G(10B)

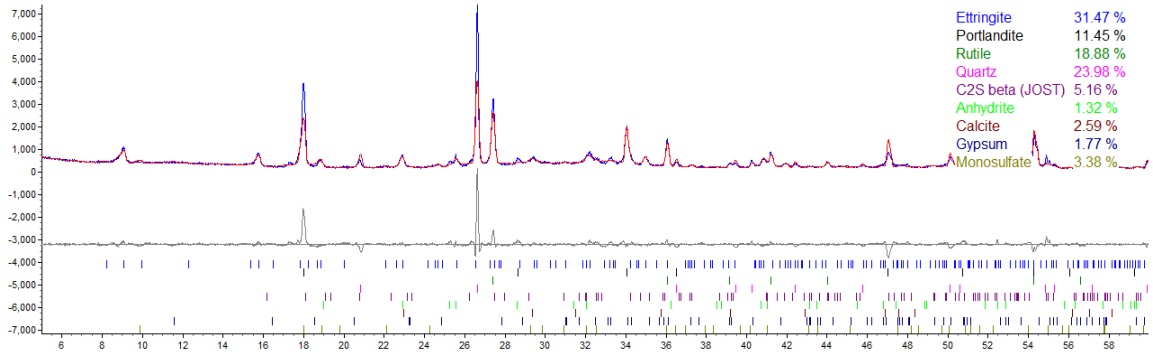

Figure A78. X-ray diffraction pattern and Rietveld refinement: C1-F2(20)-G(10) at 28 days.

28 Days C1-F2(20)-G(12A)

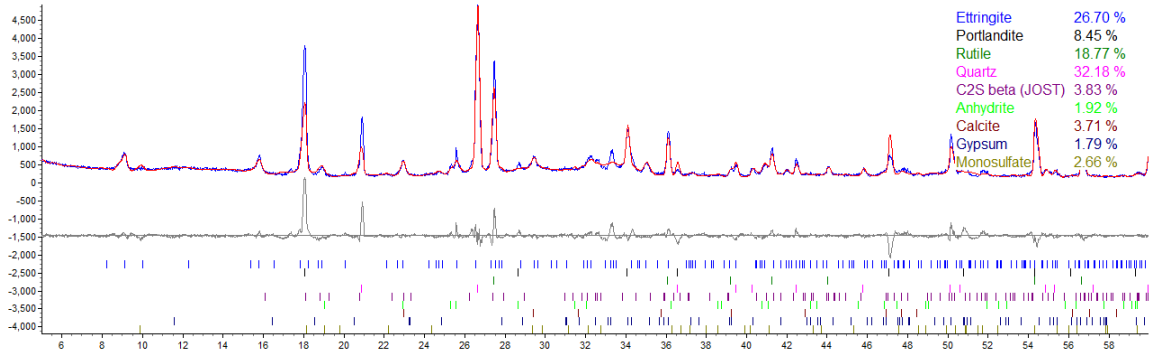

28 Days C1-F2(20)-G(12B)

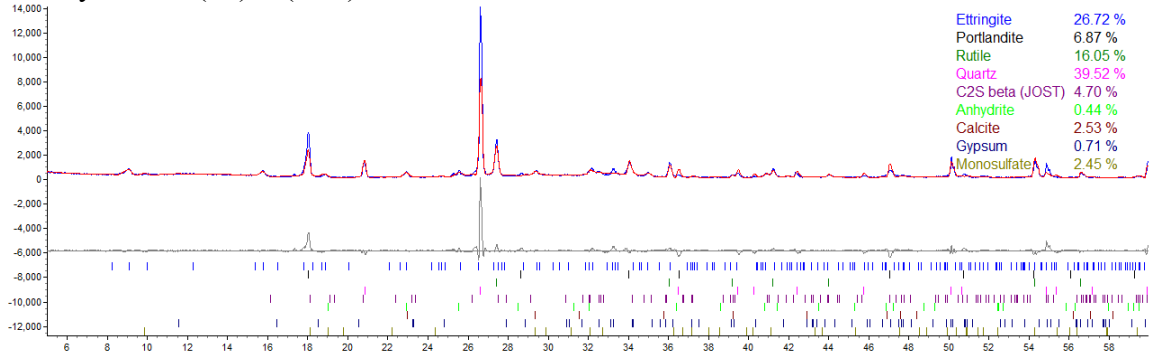

Figure A79. X-ray diffraction pattern and Rietveld refinement: C1-F2(20)-G(12) at 28 days.

28 Days C1-F2(20)-G(15A)

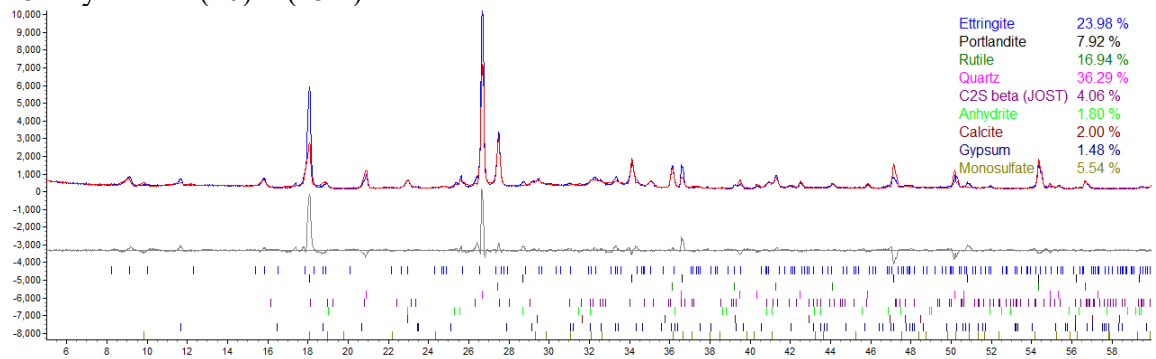

28 Days C1-F2(20)-G(15B)

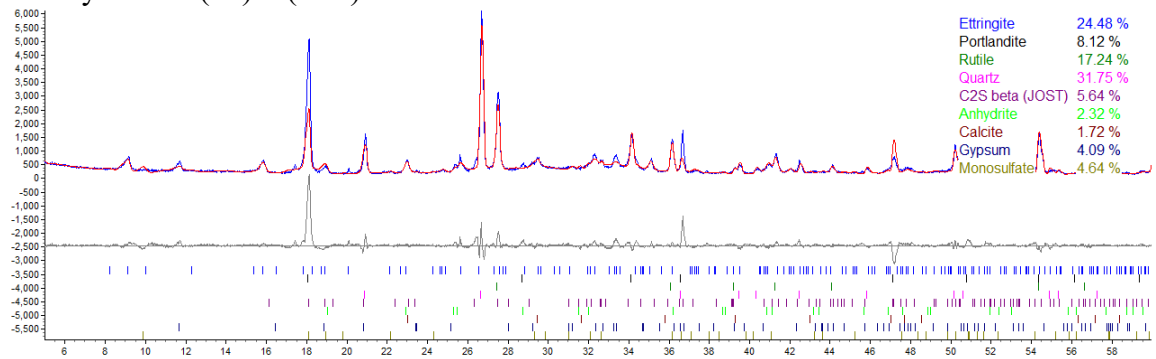

Figure A80. X-ray diffraction pattern and Rietveld refinement: C1-F2(20)-G(15) at 28 days.

C1-F3(20)-G(0A)

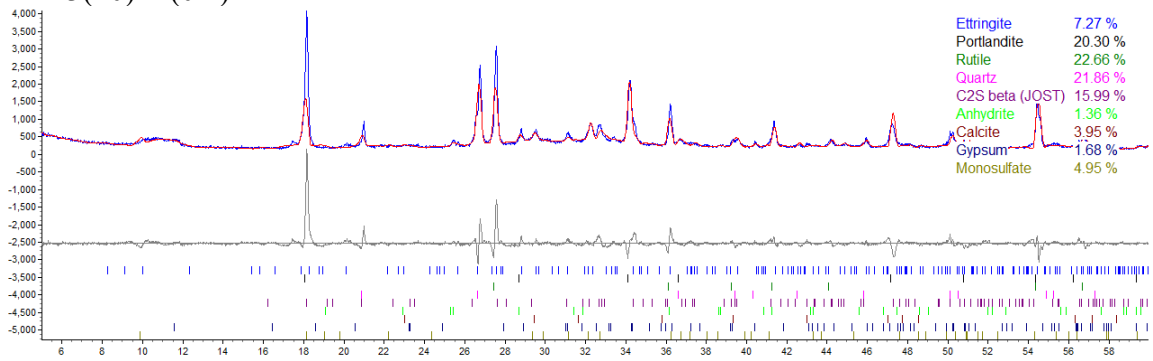

C1-F3(20)-G(0B)

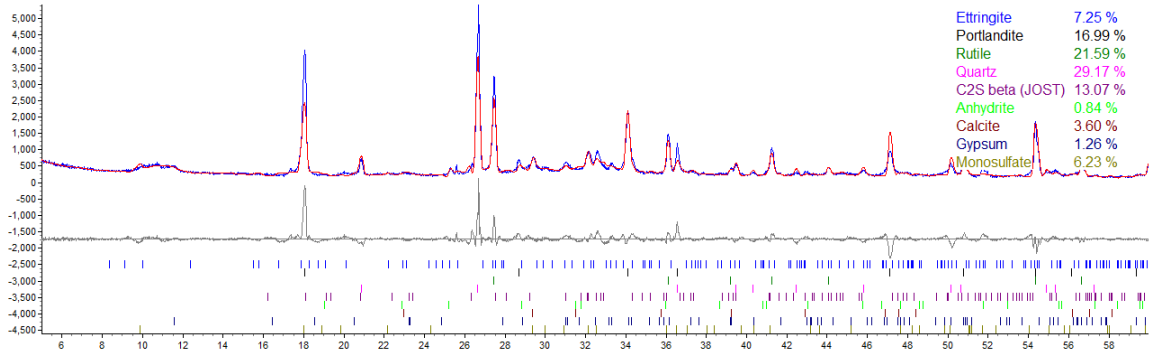

Figure A81. X-ray diffraction pattern and Rietveld refinement: C1-F3(20)-G(0).

C1-F3(20)-G(2A)

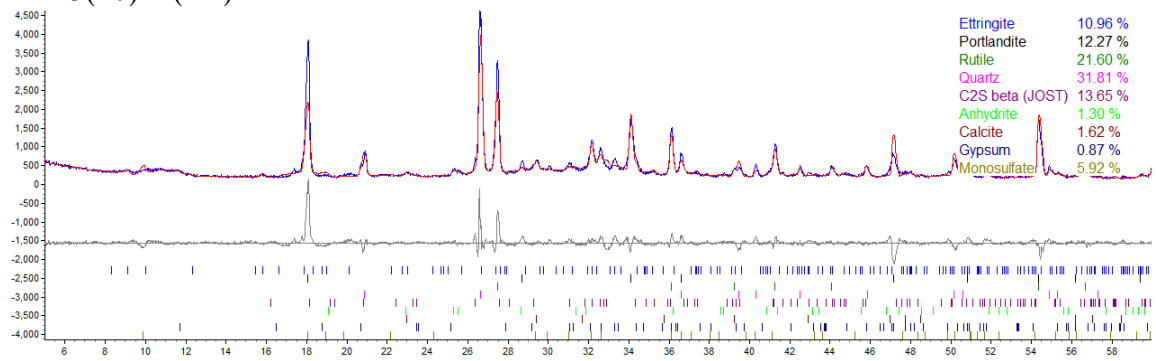

C1-F3(20)-G(2B)

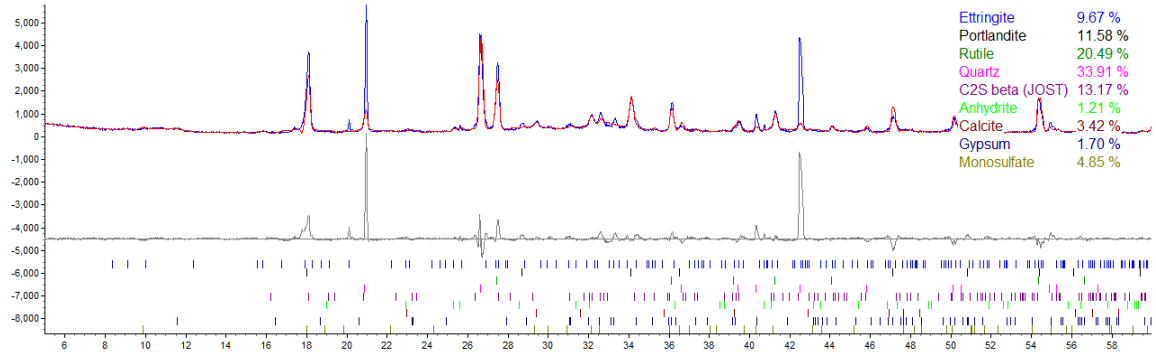

Figure A82. X-ray diffraction pattern and Rietveld refinement: C1-F3(20)-G(2).

C1-F3(20)-G(4A)

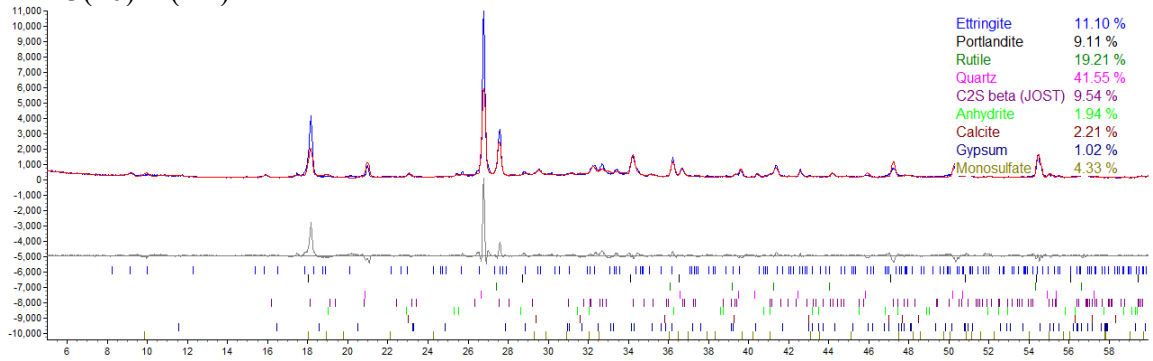

C1-F3(20)-G(4C)

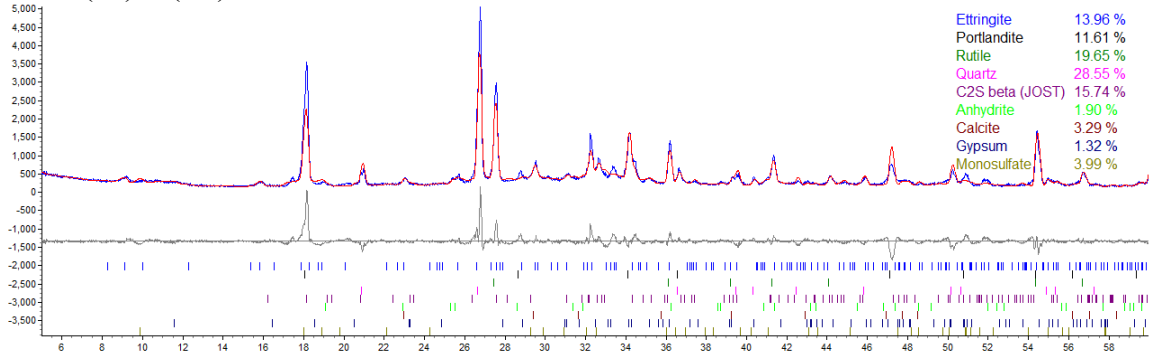

Figure A83. X-ray diffraction pattern and Rietveld refinement: C1-F3(20)-G(4).

C1-F3(20)-G(6A)

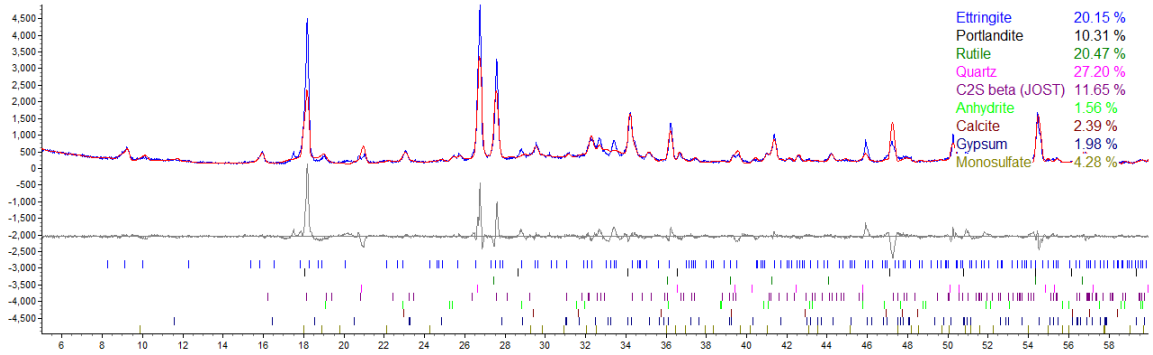

C1-F3(20)-G(6B)

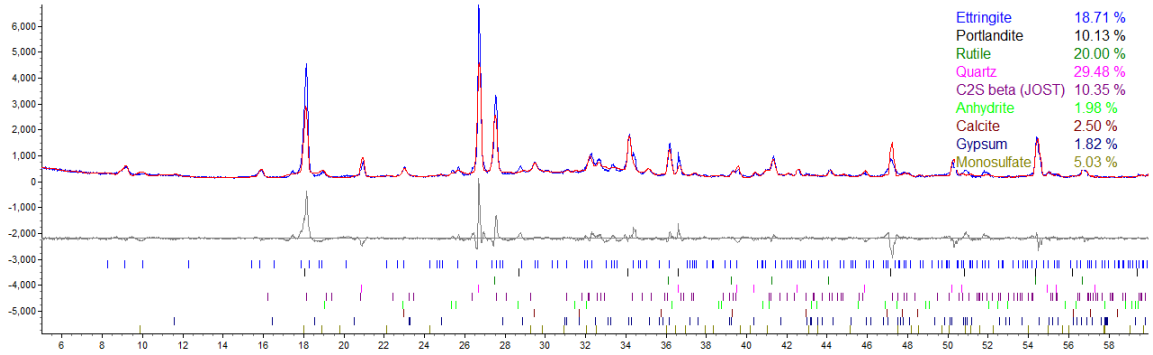

Figure A84. X-ray diffraction pattern and Rietveld refinement: C1-F3(20)-G(6).

C1-F3(20)-G(8B)

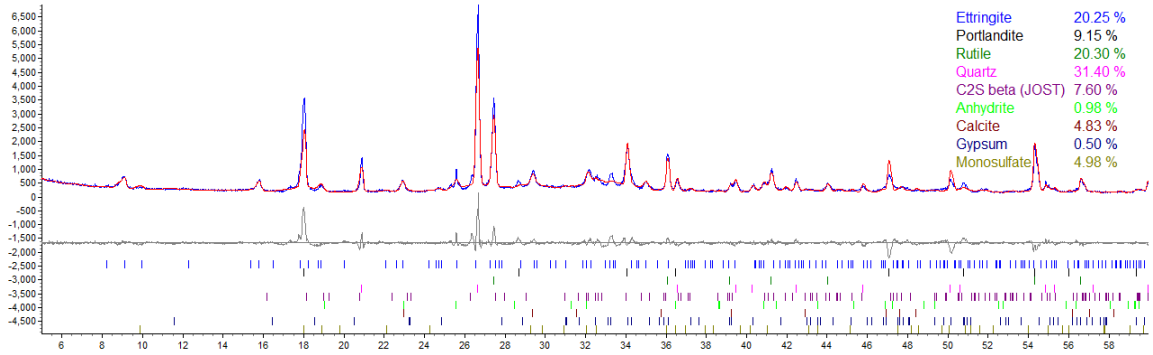

C1-F3(20)-G(8C)

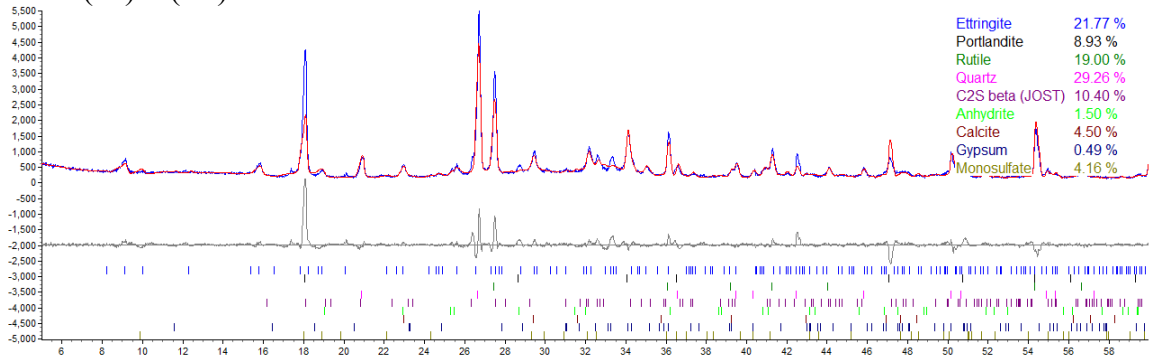

Figure A85. X-ray diffraction pattern and Rietveld refinement: C1-F3(20)-G(8).

C1-F3(20)-G(10A)

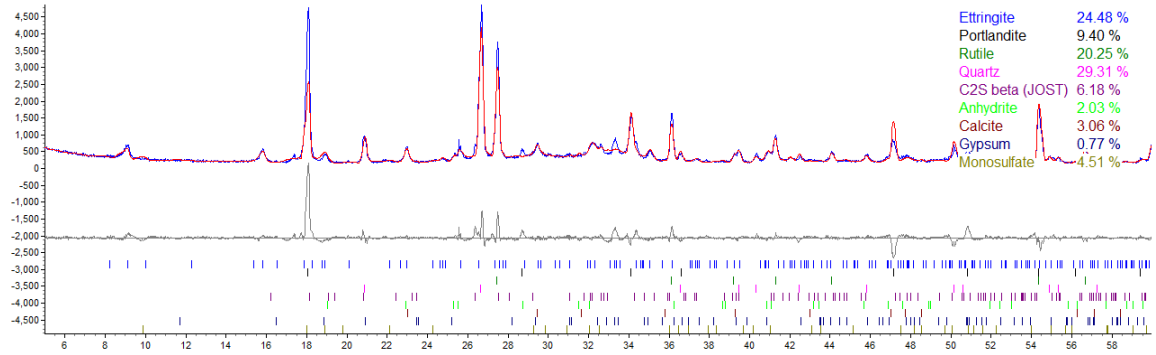

C1-F3(20)-G(10B)

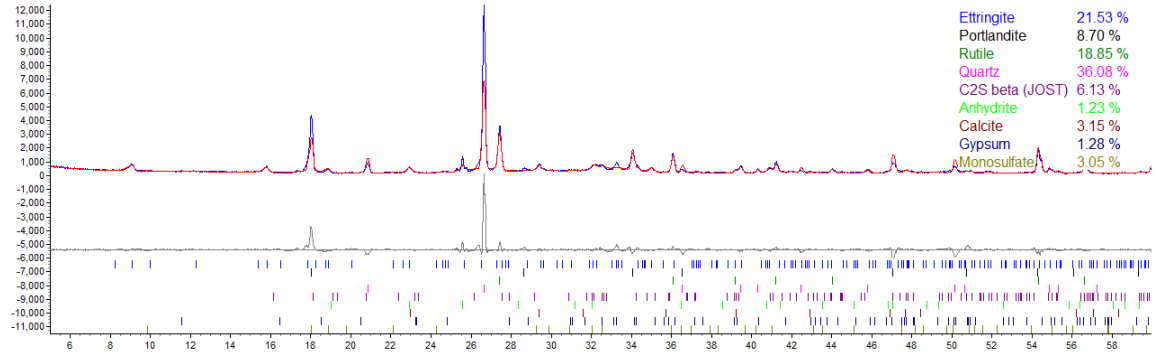

Figure A86. X-ray diffraction pattern and Rietveld refinement: C1-F3(20)-G(10).

C1-F3(20)-G(12A)

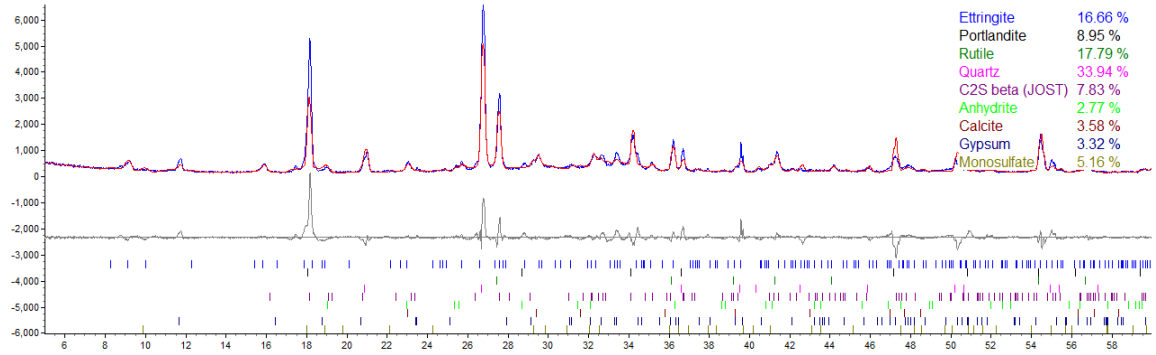

C1-F3(20)-G(12B)

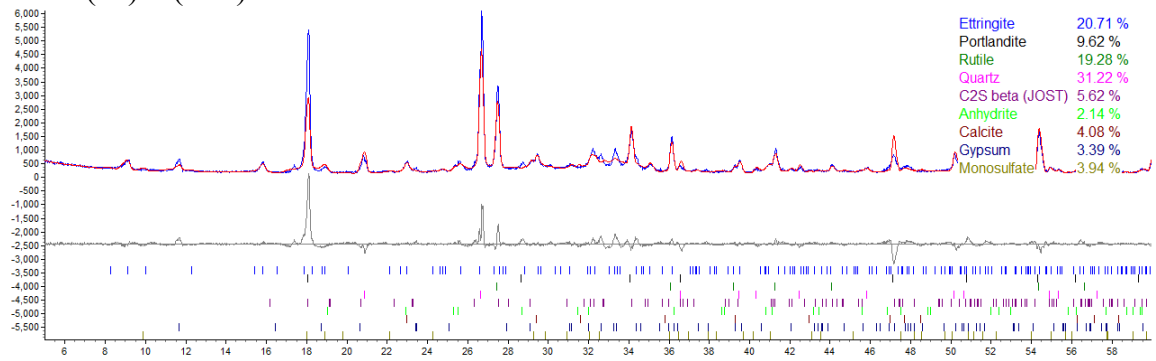

Figure A87. X-ray diffraction pattern and Rietveld refinement: C1-F3(20)-G(12).

C1-F3(20)-G(15A)

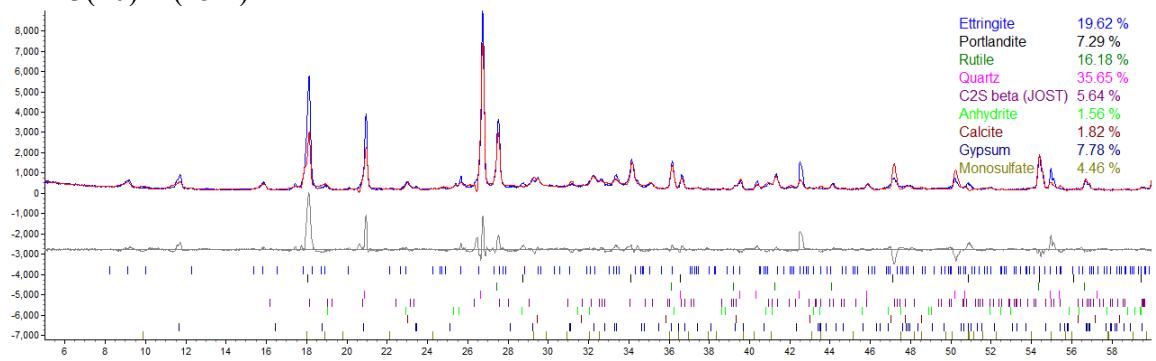

C1-F3(20)-G(15B)

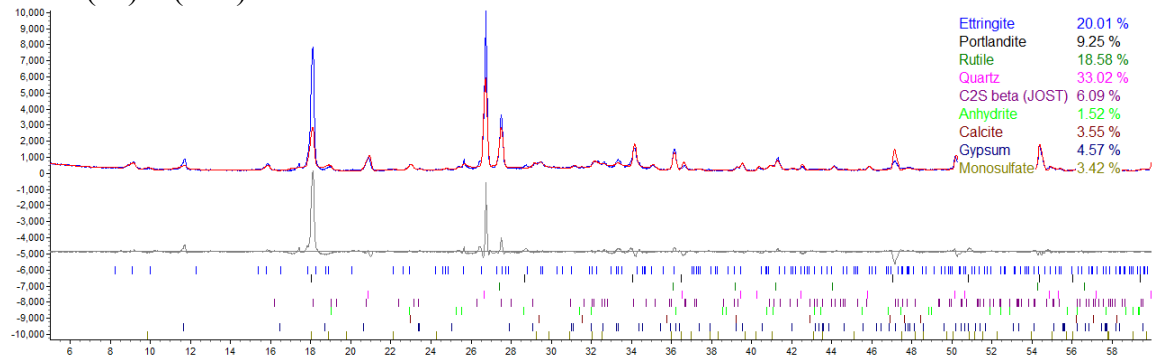

Figure A88. X-ray diffraction pattern and Rietveld refinement: C1-F3(20)-G(15).

28 Days C1-F3(20)-G(0A)

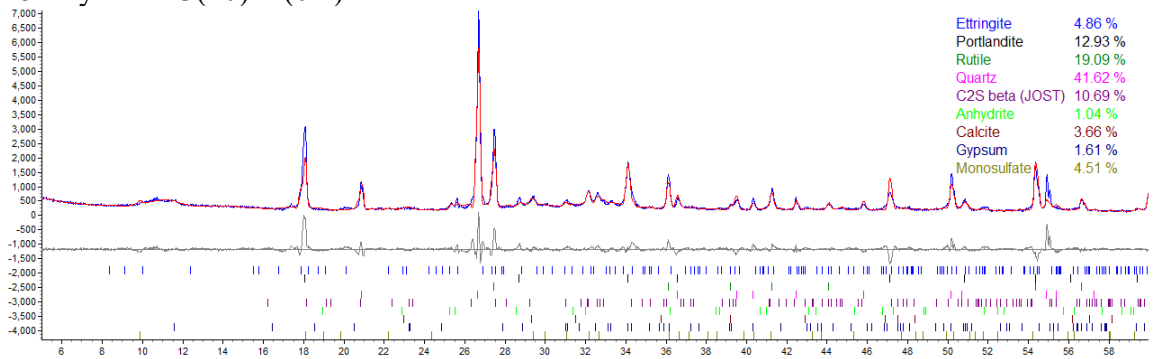

28 Days C1-F3(20)-G(0B)

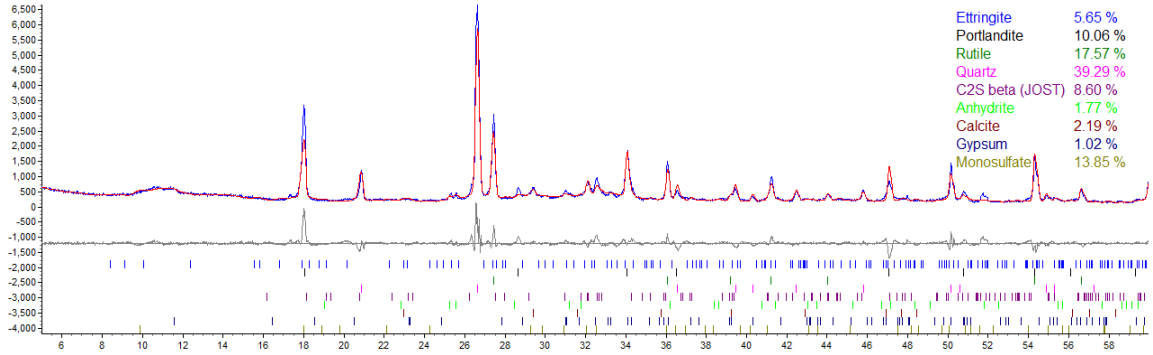

Figure A89. X-ray diffraction pattern and Rietveld refinement: C1-F3(20)-G(0) at 28 days.

28 Days C1-F3(20)-G(2A)

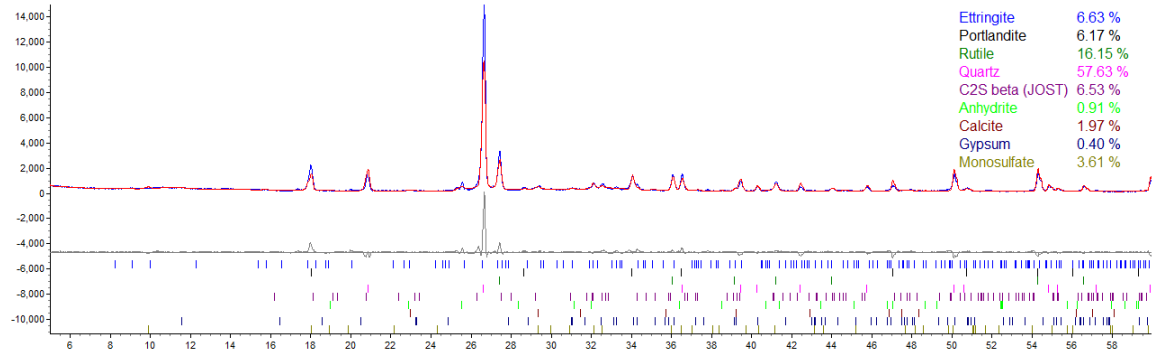

28 Days C1-F3(20)-G(2B)

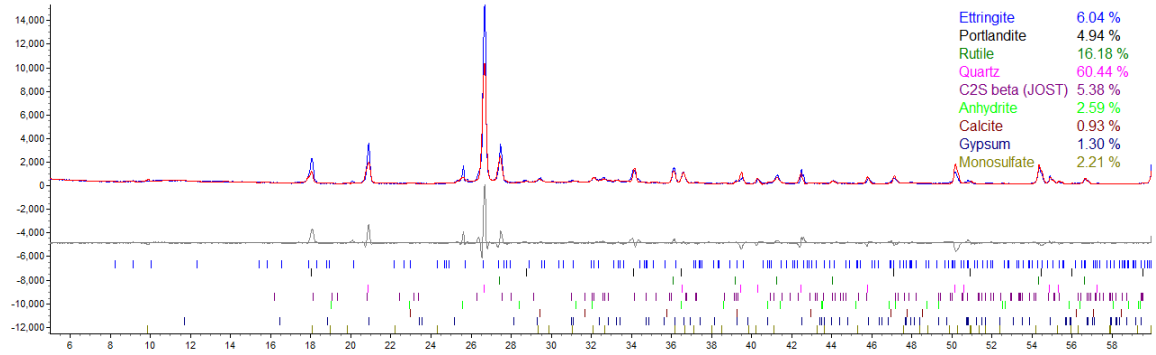

Figure A90. X-ray diffraction pattern and Rietveld refinement: C1-F3(20)-G(2) at 28 days.

28 Days C1-F3(20)-G(4A)

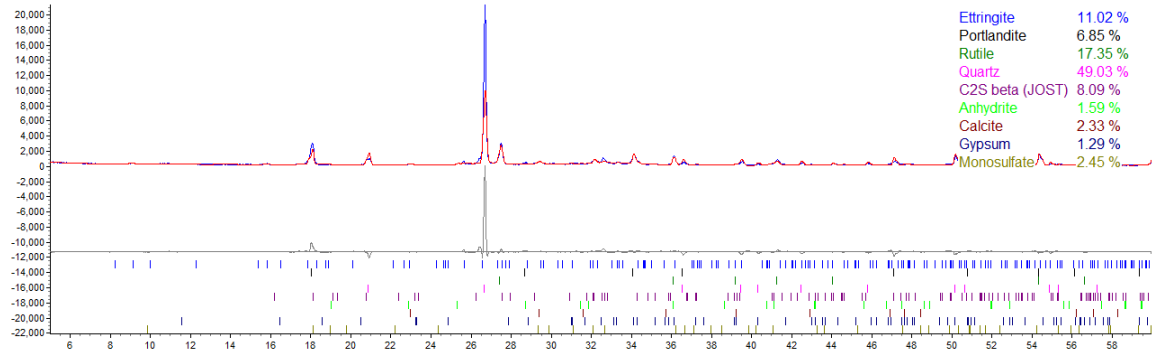

28 Days C1-F3(20)-G(4B)

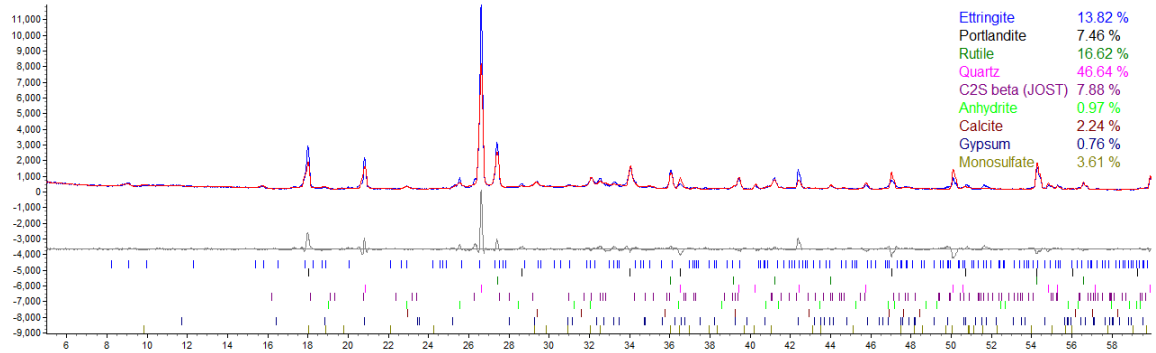

Figure A91. X-ray diffraction pattern and Rietveld refinement: C1-F3(20)-G(4) at 28 days.

28 Days C1-F3(20)-G(6A)

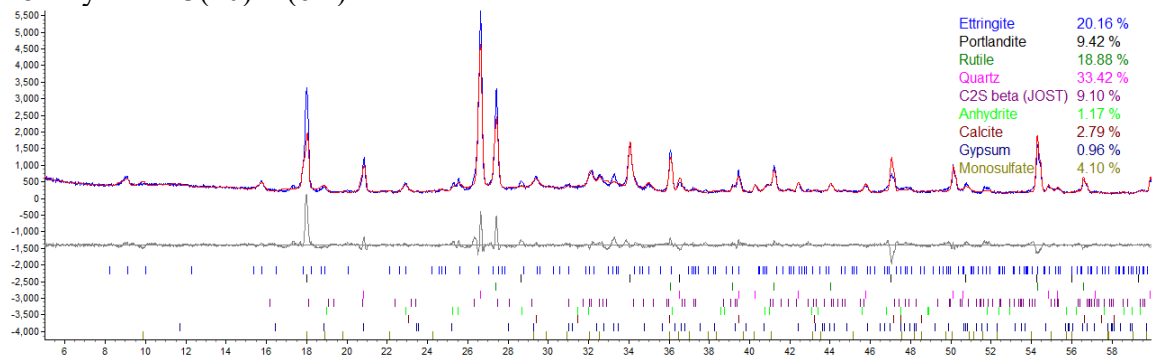

28 Days C1-F3(20)-G(6B)

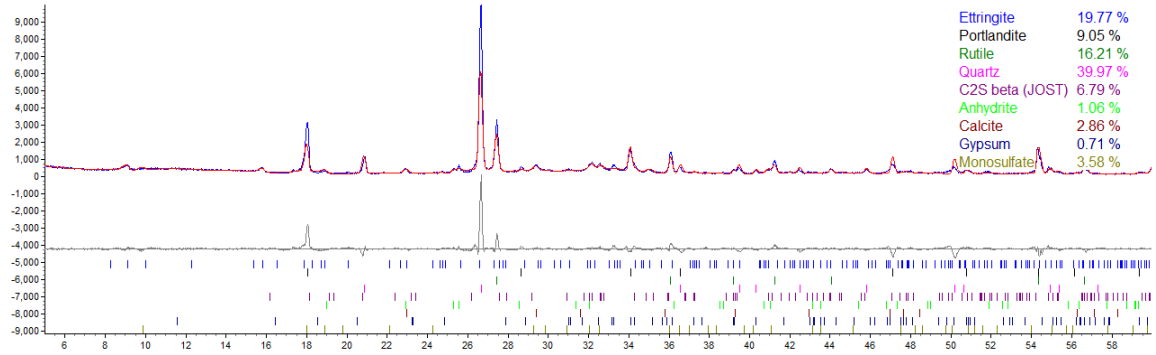

Figure A92. X-ray diffraction pattern and Rietveld refinement: C1-F3(20)-G(6) at 28 days.

28 Days C1-F3(20)-G(8A)

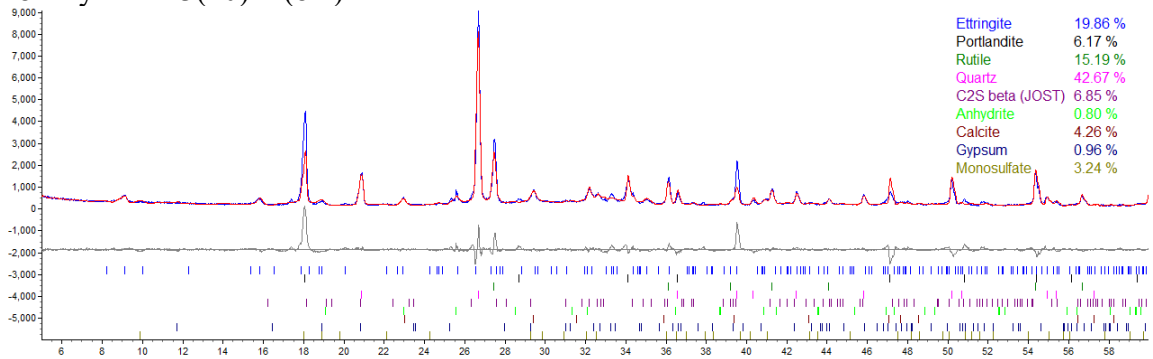

28 Days C1-F3(20)-G(8B)

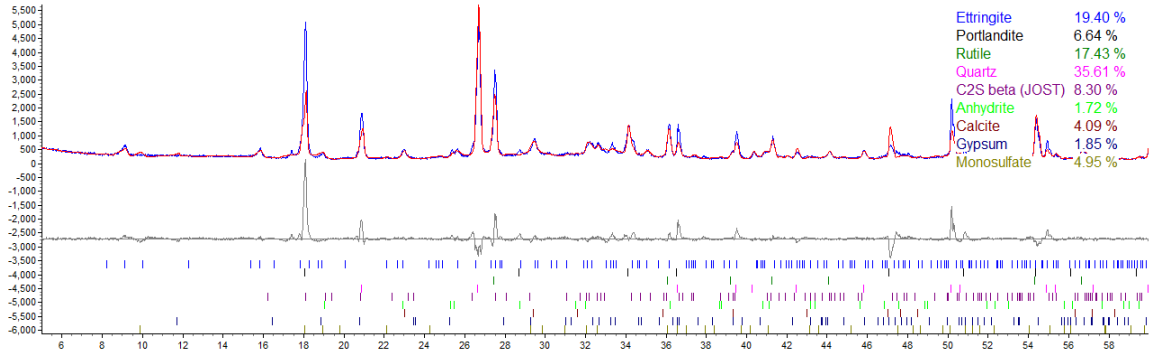

Figure A93. X-ray diffraction pattern and Rietveld refinement: C1-F3(20)-G(8) at 28 days.

28 Days C1-F3(20)-G(10A)

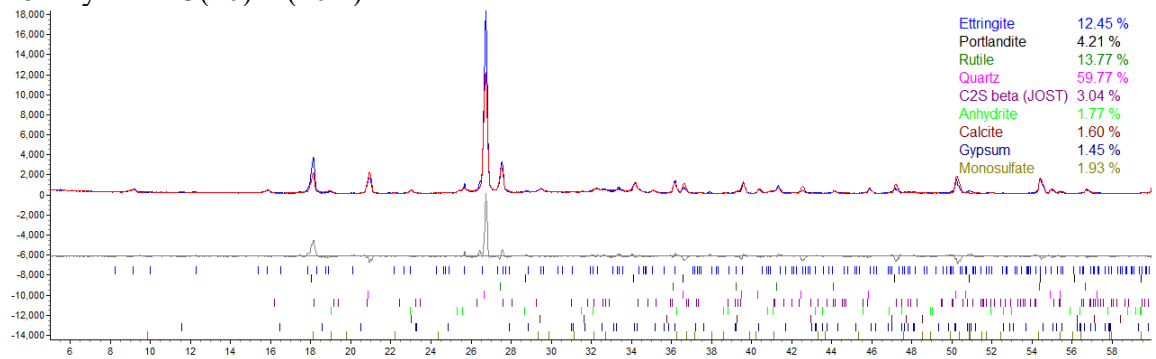

28 Days C1-F3(20)-G(10B)

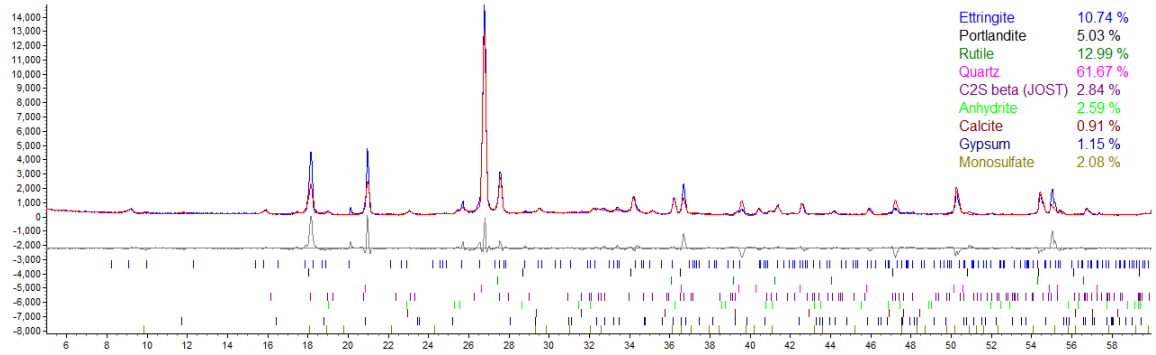

Figure A94 X-ray diffraction pattern and Rietveld refinement: C1-F3(20)-G(10) at 28 days.

28 Days C1-F3(20)-G(12A)

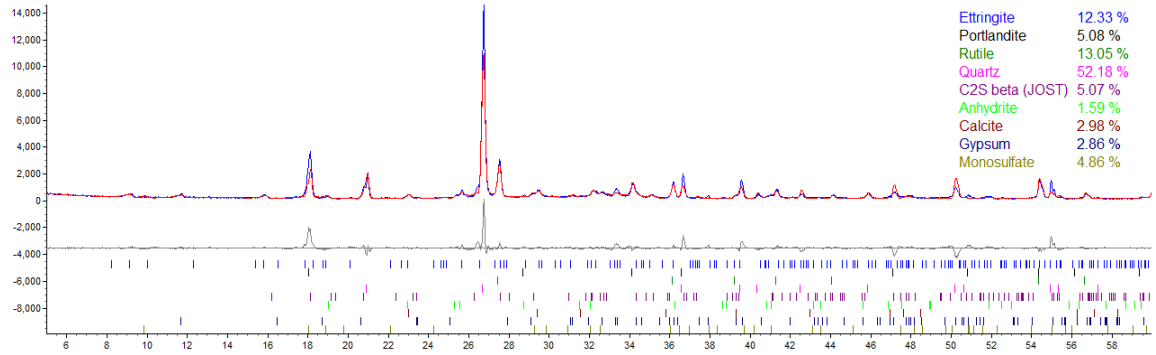

28 Days C1-F3(20)-G(12B)

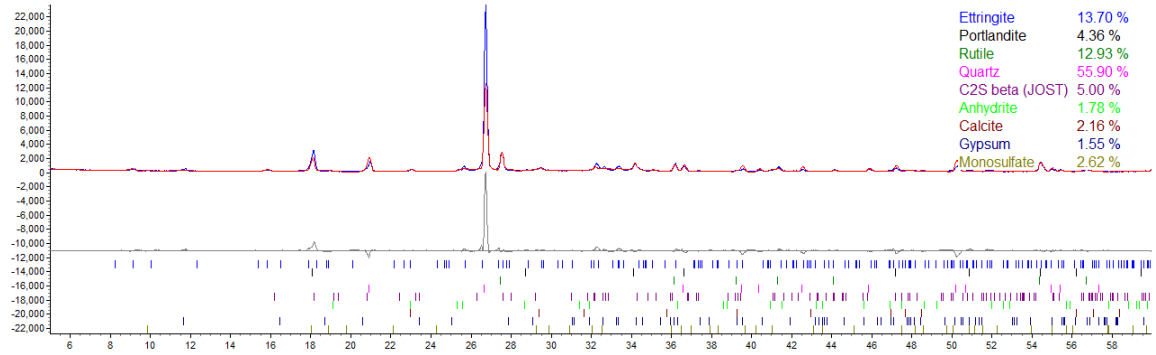

Figure A95 X-ray diffraction pattern and Rietveld refinement: C1-F3(20)-G(12) at 28 days.

28 Days C1-F3(20)-G(15A)

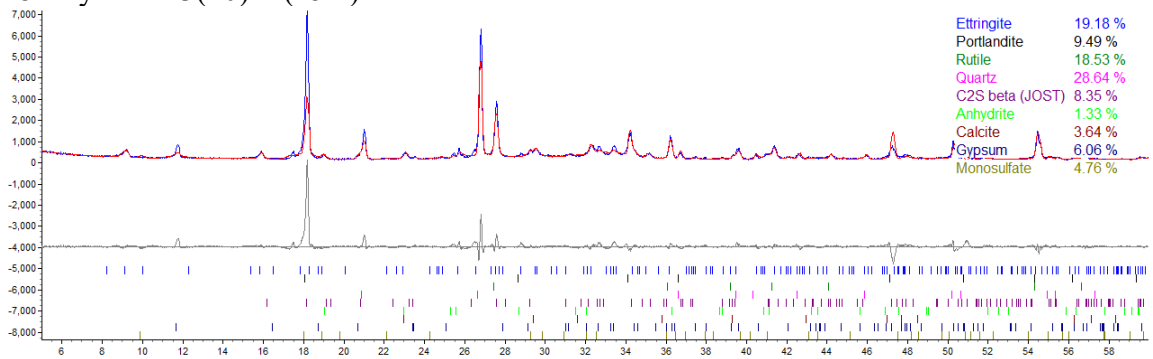

28 Days C1-F3(20)-G(15B)

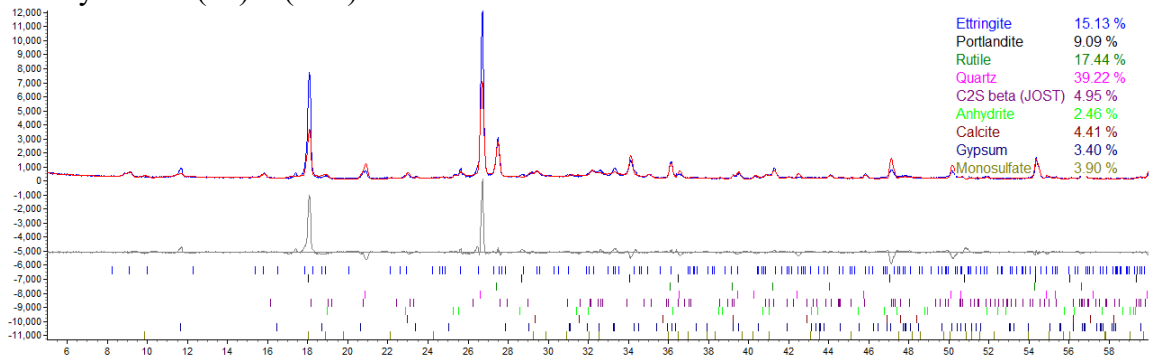

Figure A96 X-ray diffraction pattern and Rietveld refinement: C1-F3(20)-G(15) at 28 days.

C2-F1(35)-G(0A)

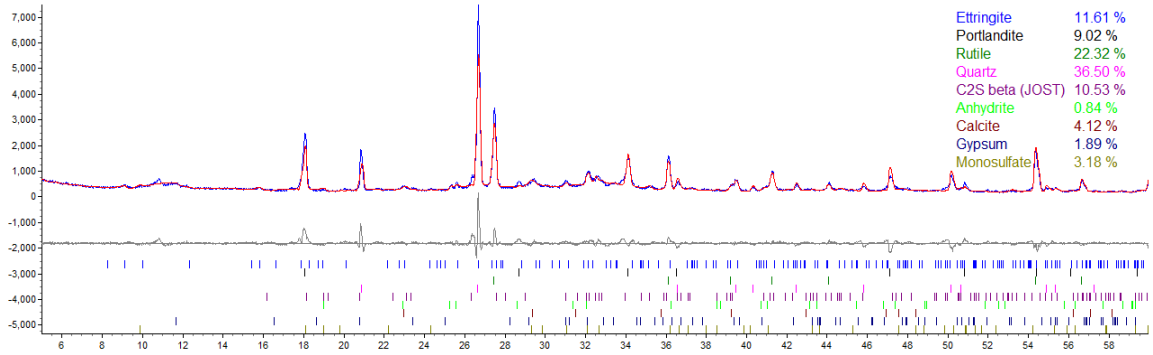

C2-F1(35)-G(0B)

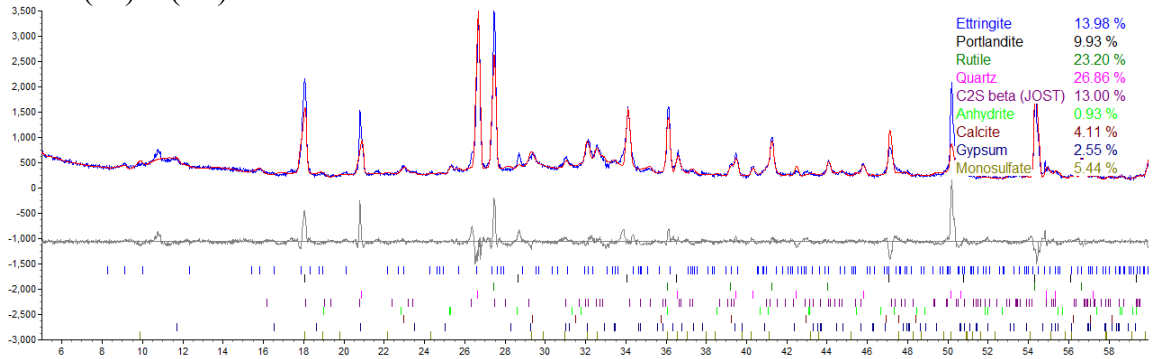

Figure A97 X-ray diffraction pattern and Rietveld refinement: C2-F1(35)-G(0).

C2-F1(35)-G(2A)

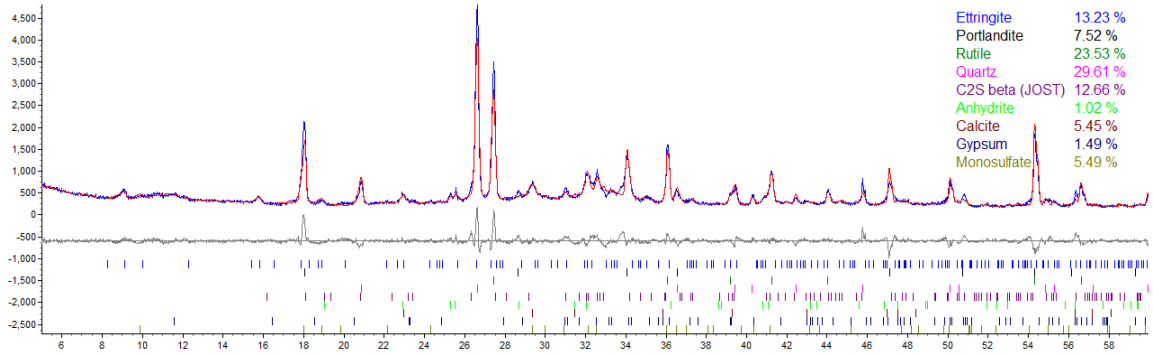

C2-F1(35)-G(2B)

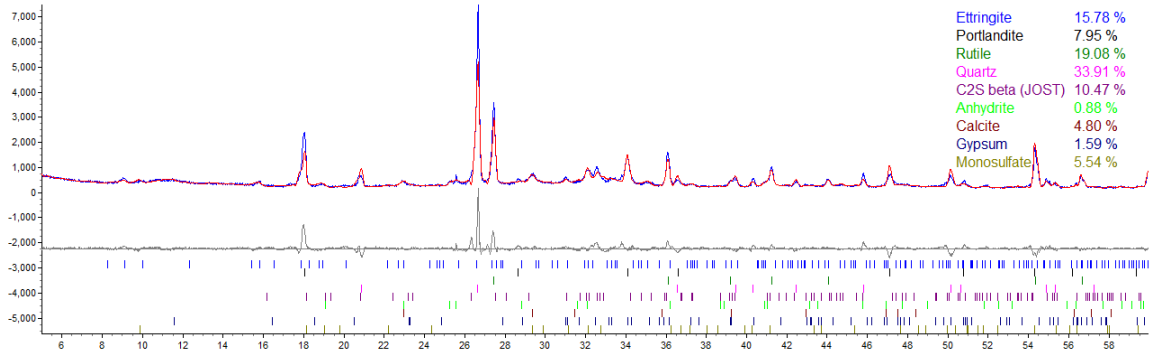

Figure A98 X-ray diffraction pattern and Rietveld refinement: C2-F1(35)-G(2).

C2-F1(35)-G(4A)

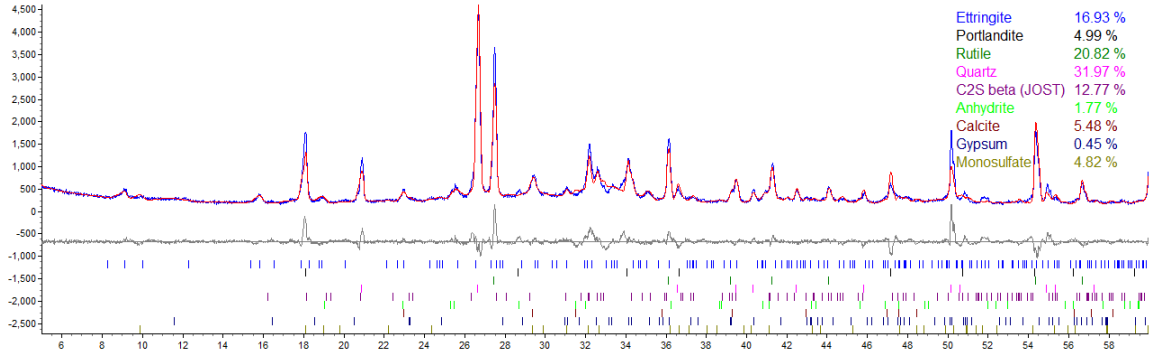

C2-F1(35)-G(4B)

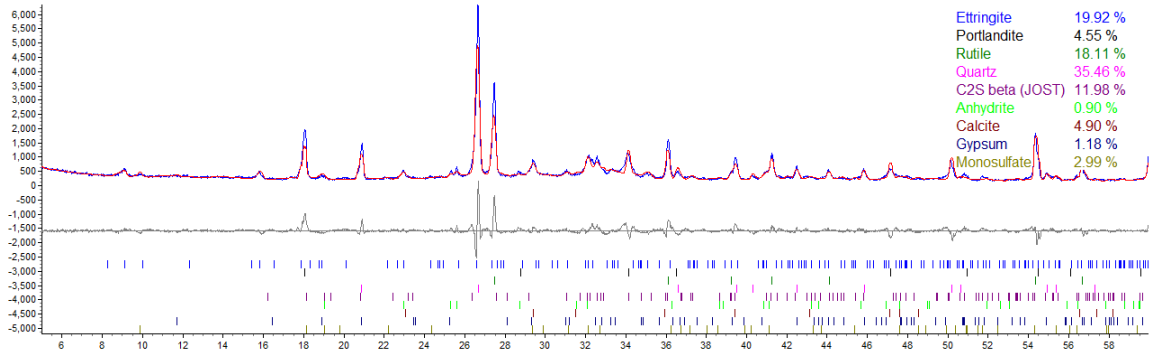

Figure A99 X-ray diffraction pattern and Rietveld refinement: C2-F1(35)-G(4).

C2-F1(35)-G(6A)

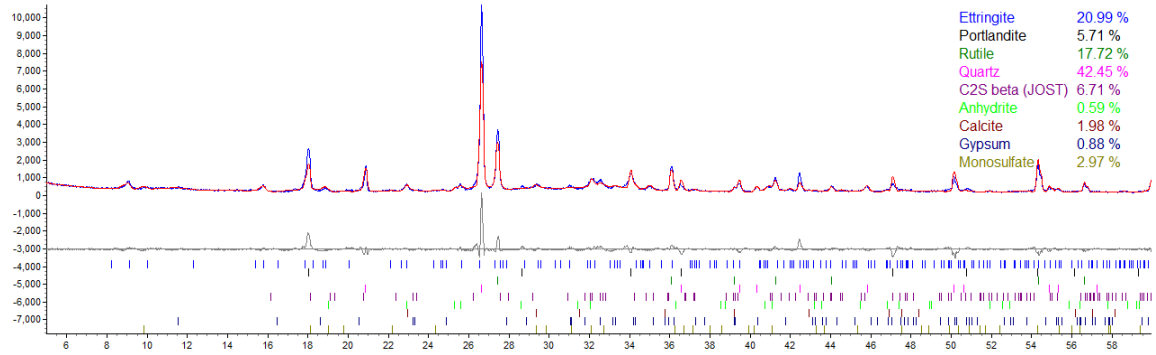

C2-F1(35)-G(6B)

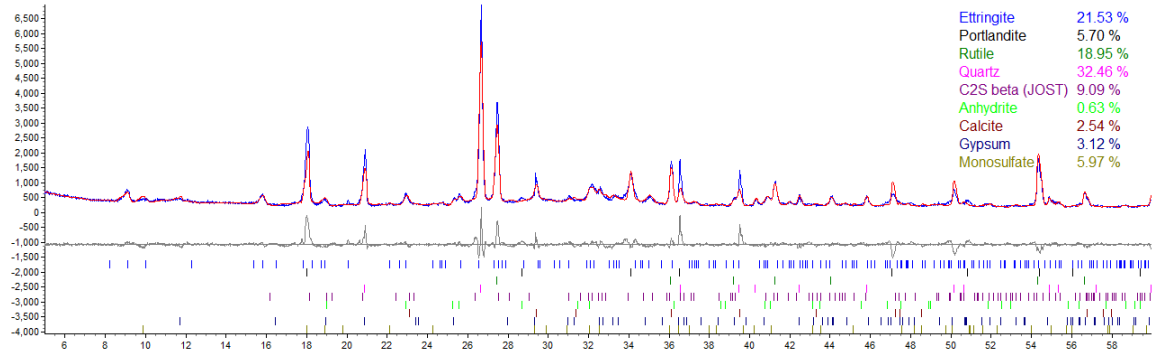

Figure A100 X-ray diffraction pattern and Rietveld refinement: C2-F1(35)-G(6).

C2-F1(35)-G(8A)

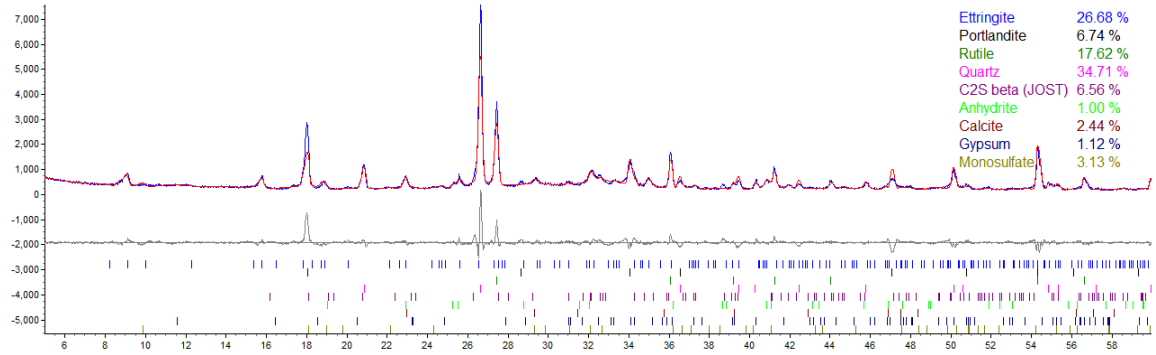

C2-F1(35)-G(8B)

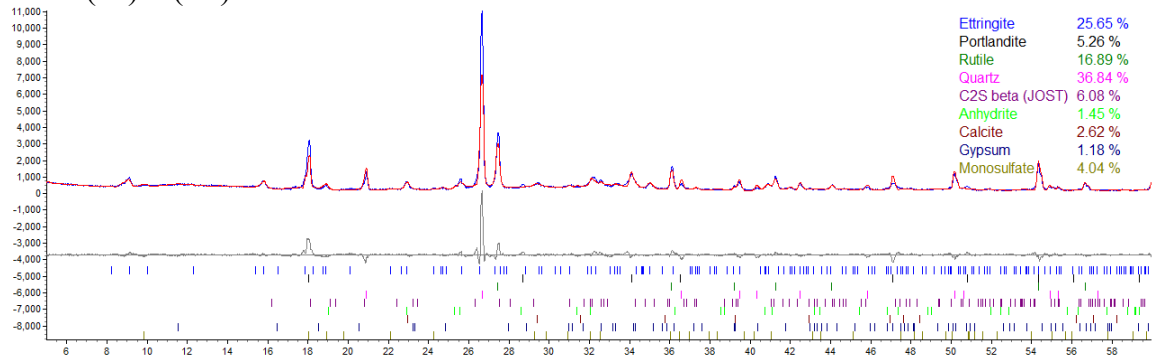

Figure A101 X-ray diffraction pattern and Rietveld refinement: C2-F1(35)-G(8).

C2-F1(35)-G(10B)

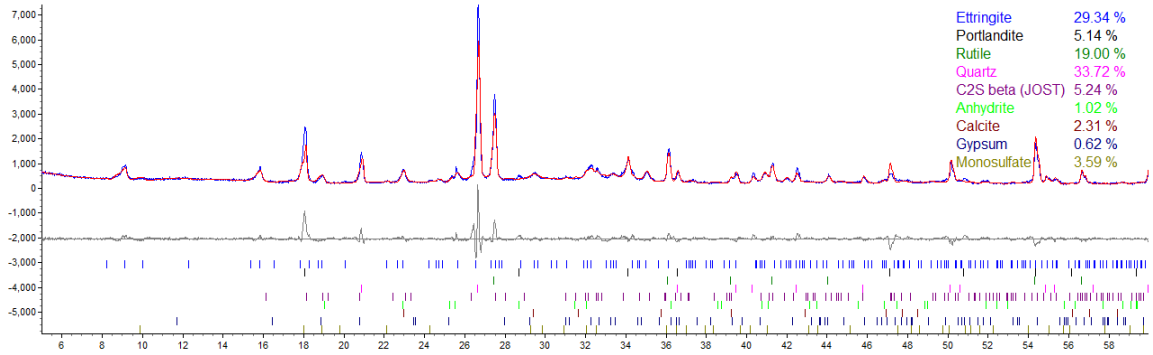

C2-F1(35)-G(10C)

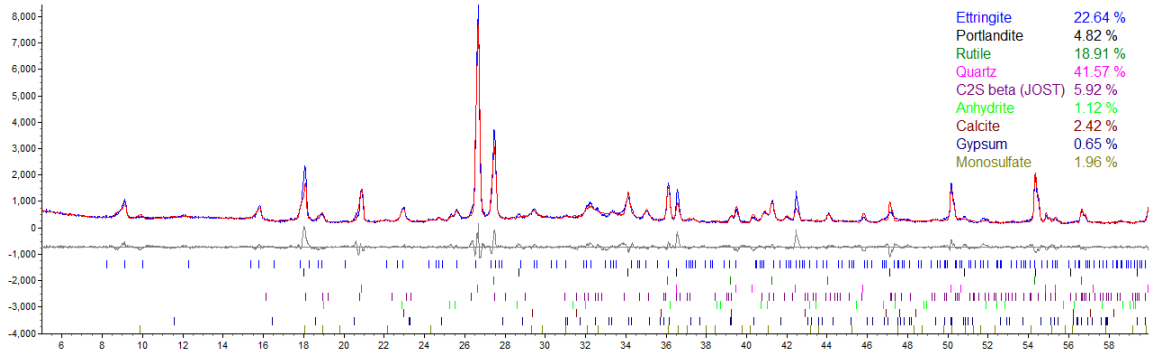

Figure A102 X-ray diffraction pattern and Rietveld refinement: C2-F1(35)-G(10).

C2-F1(35)-G(12A)

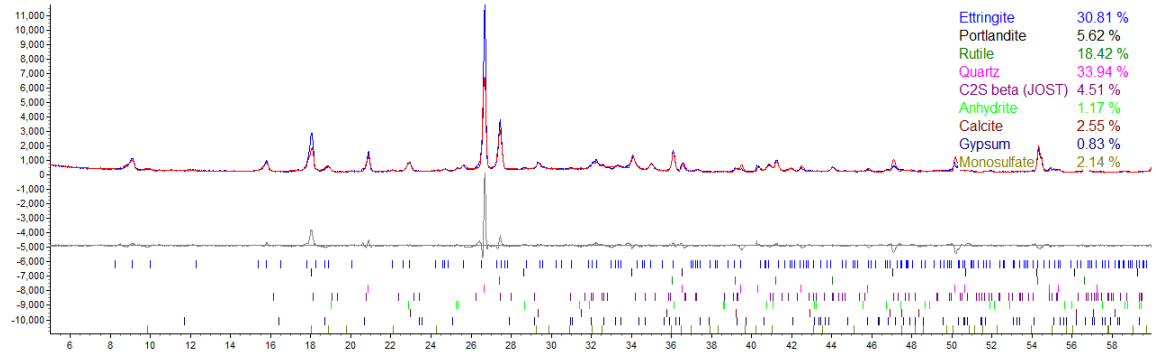

C2-F1(35)-G(12B)

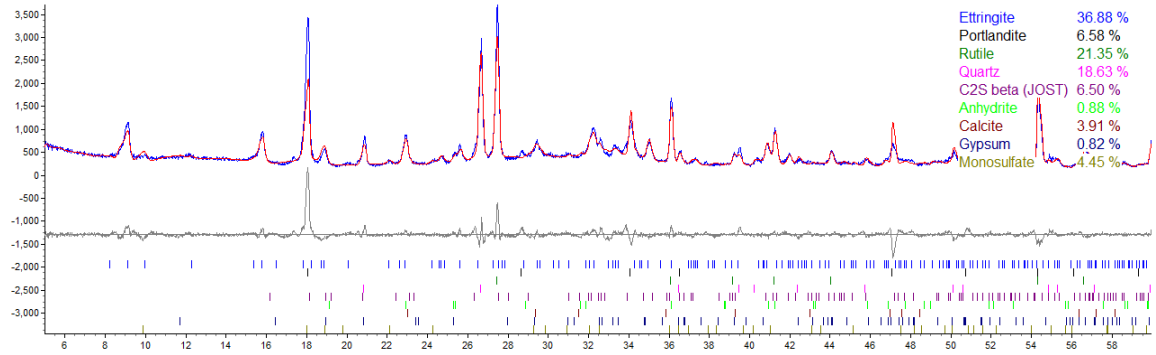

Figure A103 X-ray diffraction pattern and Rietveld refinement: C2-F1(35)-G(12).

C2-F1(35)-G(15A)

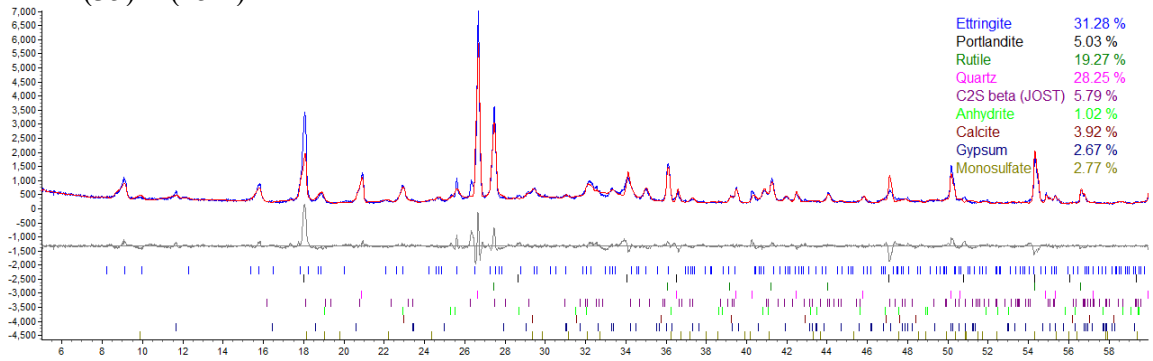

C2-F1(35)-G(15B)

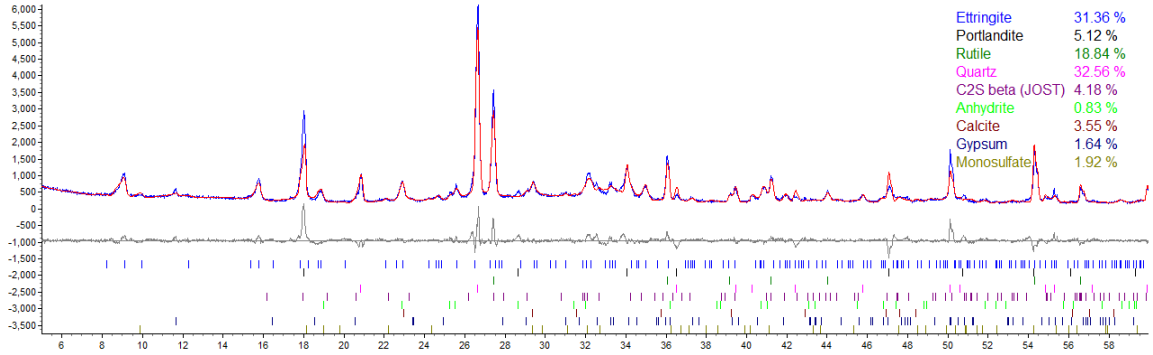

Figure A104 X-ray diffraction pattern and Rietveld refinement: C2-F1(35)-G(15).

28 Days C2-F1(35)-G(0A)

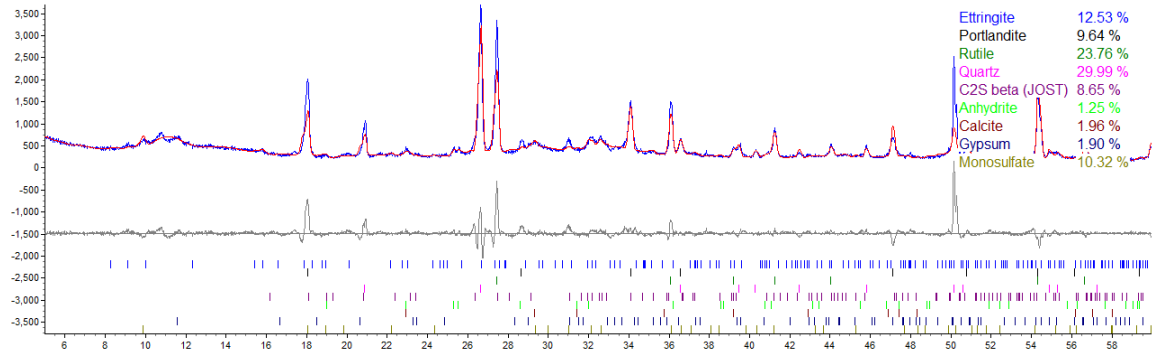

28 Days C2-F1(35)-G(0B)

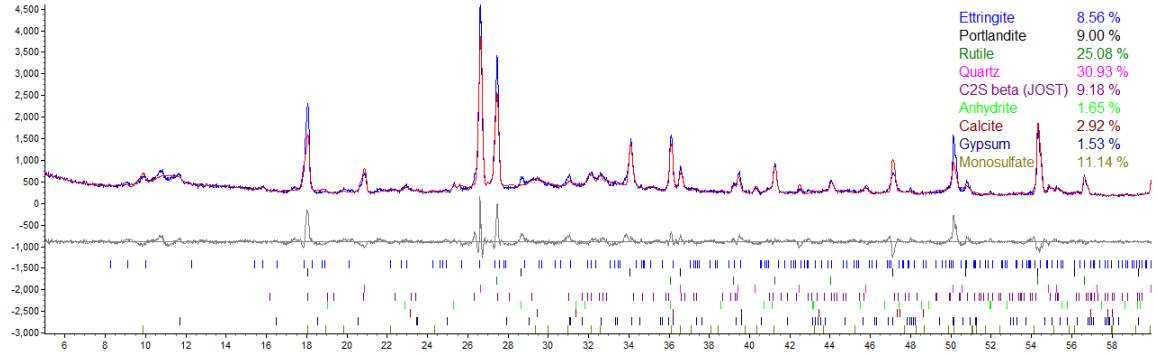

Figure A105 X-ray diffraction pattern and Rietveld refinement: C2-F1(35)-G(0) at 28 days.

28 Days C2-F1(35)-G(2A)

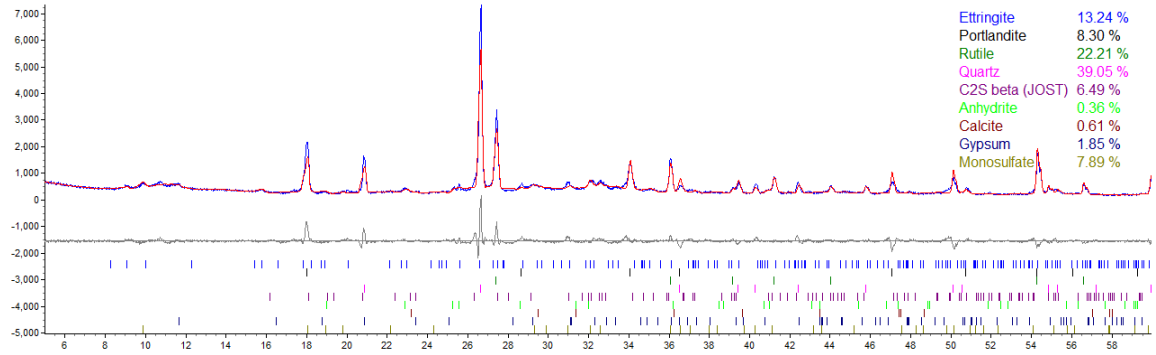

28 Days C2-F1(35)-G(2B)

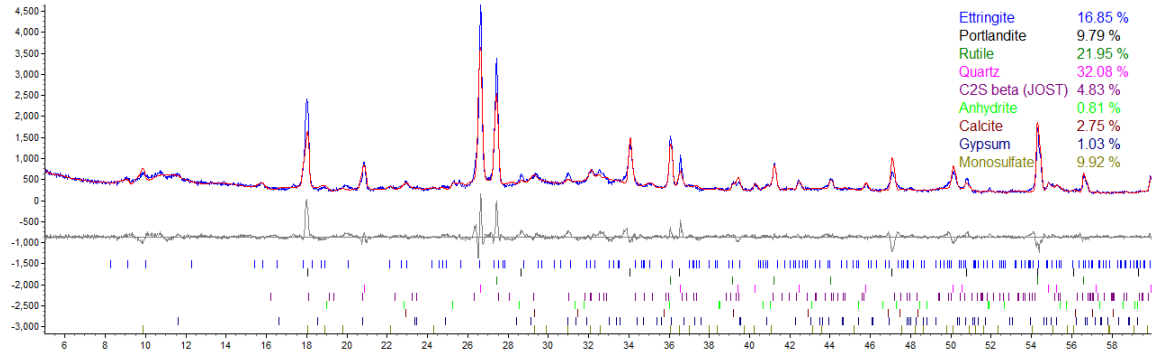

Figure A106 X-ray diffraction pattern and Rietveld refinement: C2-F1(35)-G(2) at 28 days.

28 Days C2-F1(35)-G(4A)

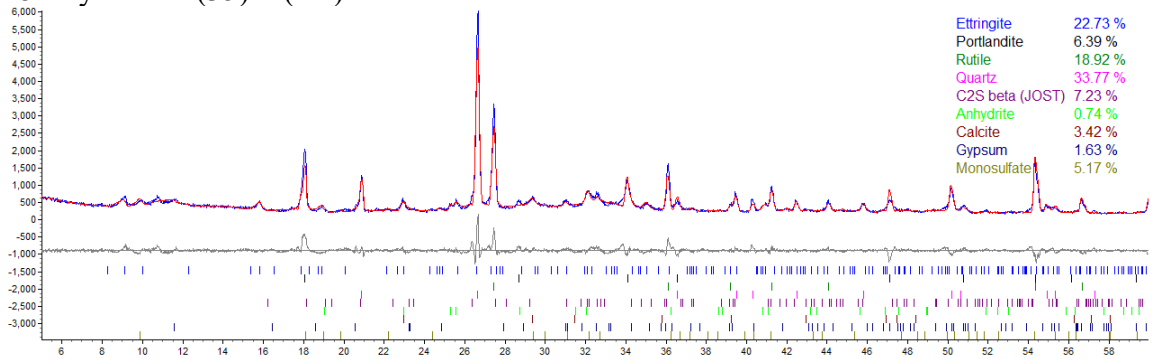

28 Days C2-F1(35)-G(4B)

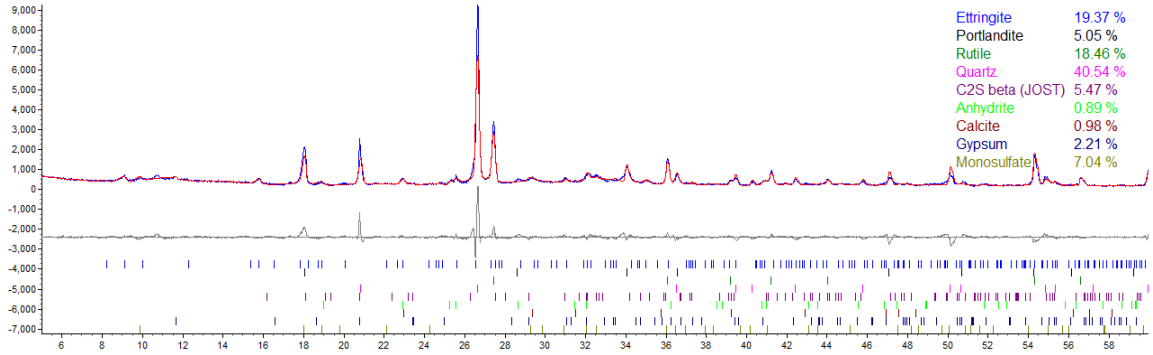

Figure A107 X-ray diffraction pattern and Rietveld refinement: C2-F1(35)-G(4) at 28 days.

28 Days C2-F1(35)-G(6A)

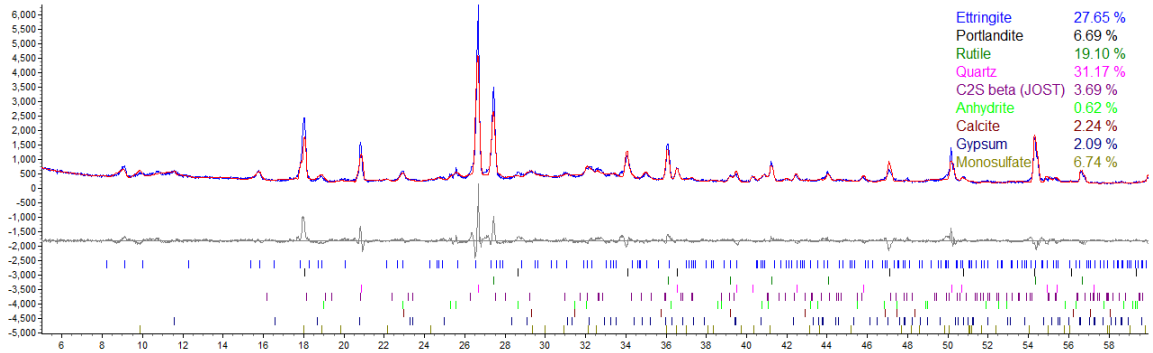

28 Days C2-F1(35)-G(6C)

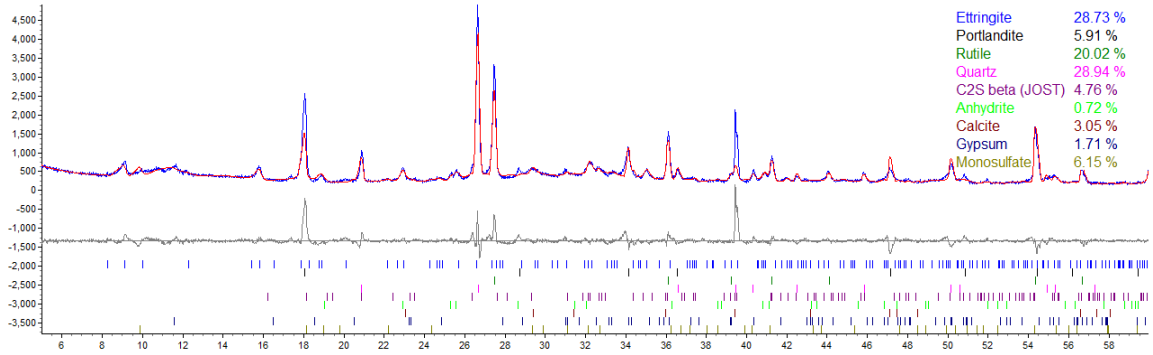

Figure A108 X-ray diffraction pattern and Rietveld refinement: C2-F1(35)-G(6) at 28 days.

28 Days C2-F1(35)-G(8A)

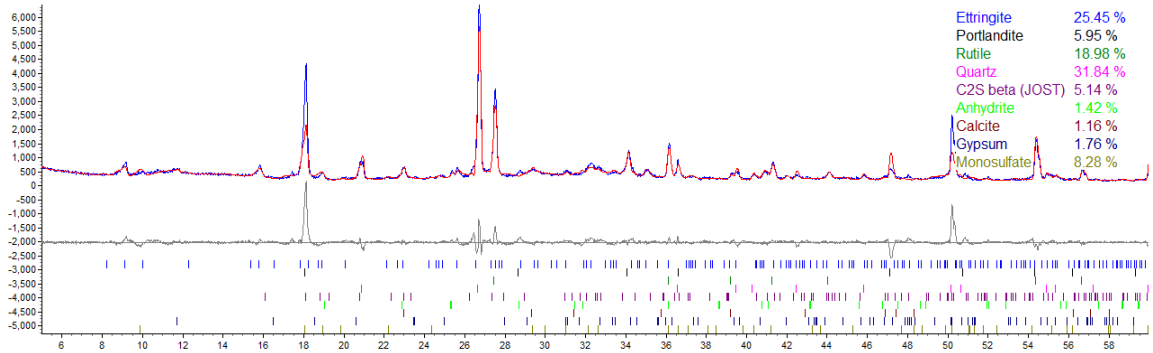

28 Days C2-F1(35)-G(8B)

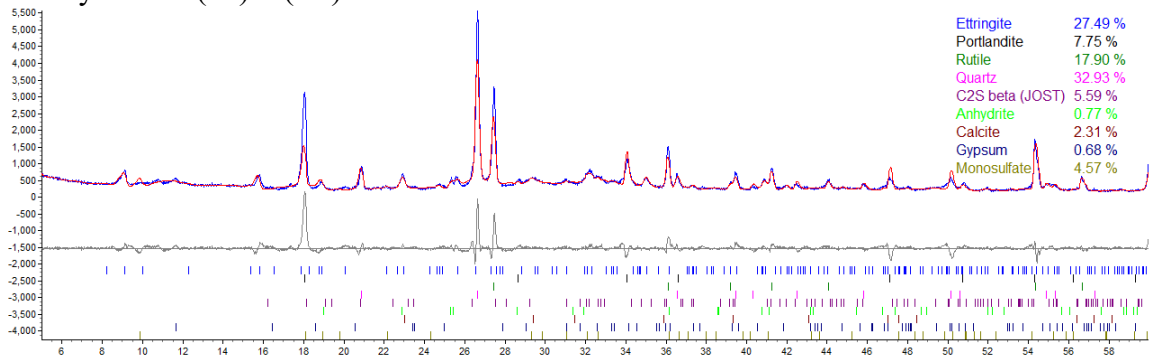

Figure A109 X-ray diffraction pattern and Rietveld refinement: C2-F1(35)-G(8) at 28 days.

28 Days C2-F1(35)-G(10B)

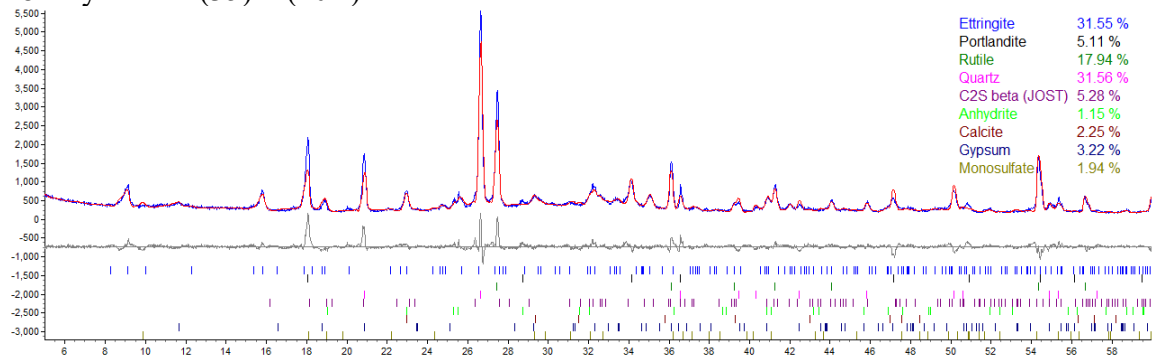

28 Days C2-F1(35)-G(10C)

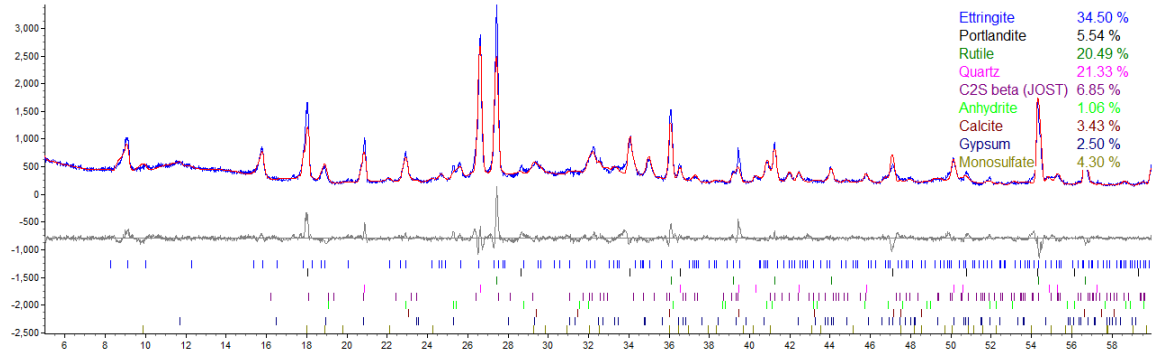

Figure A110 X-ray diffraction pattern and Rietveld refinement: C2-F1(35)-G(10) at 28 days.

28 Days C2-F1(35)-G(12A)

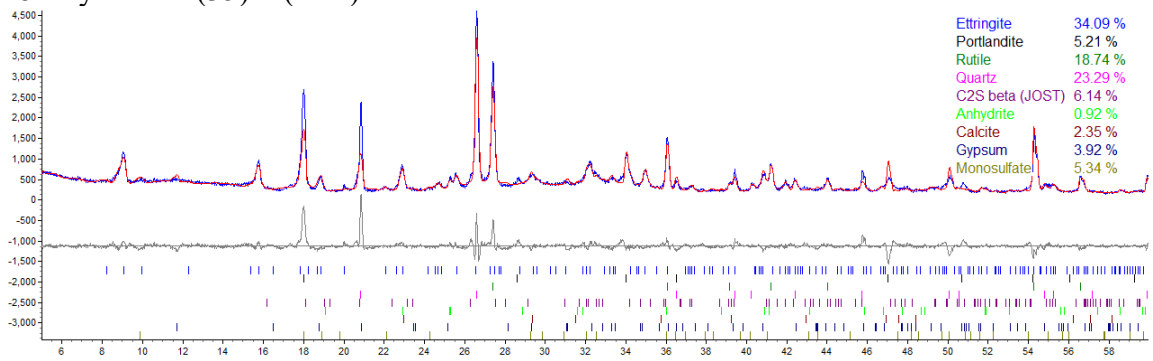

28 Days C2-F1(35)-G(12B)

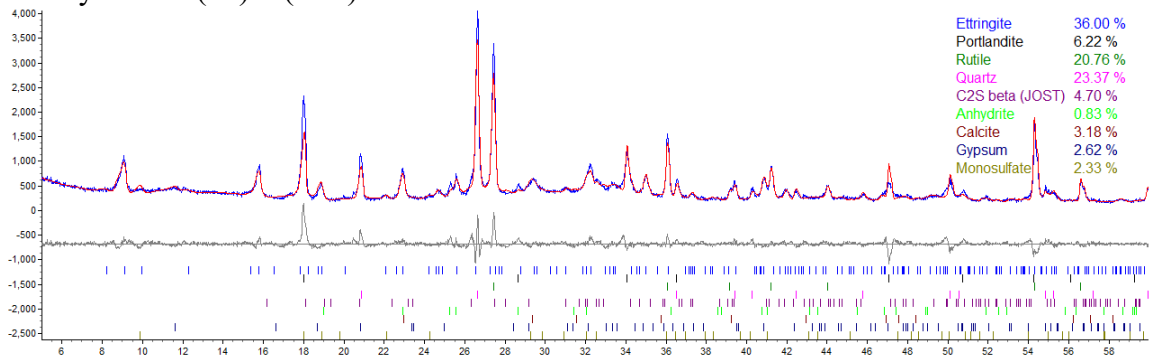

Figure A111 X-ray diffraction pattern and Rietveld refinement: C2-F1(35)-G(12) at 28 days.

28 Days C2-F1(35)-G(15A)

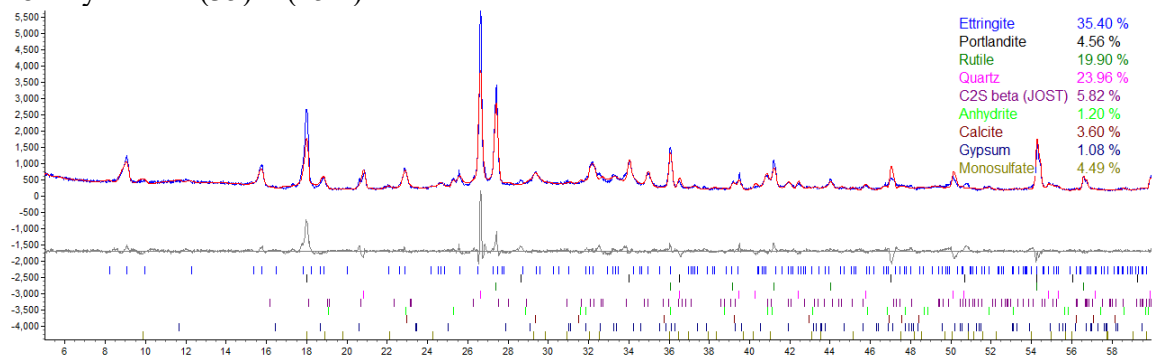

28 Days C2-F1(35)-G(15B)))))

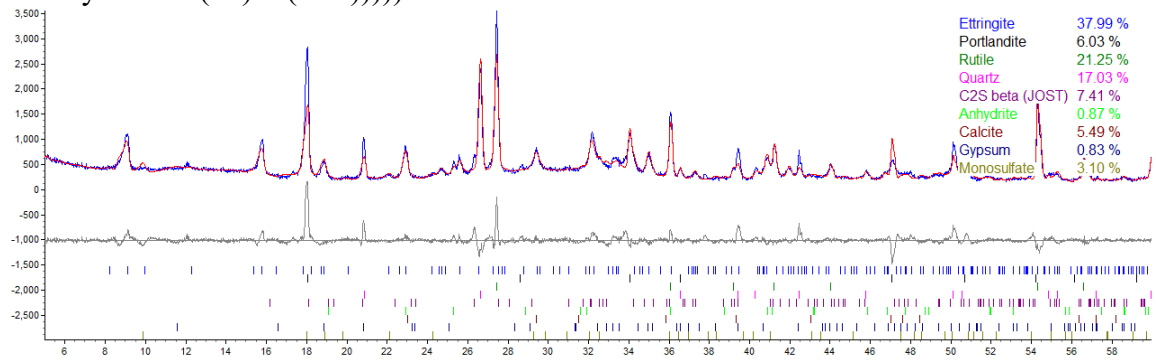

Figure A112 X-ray diffraction pattern and Rietveld refinement: C2-F1(35)-G(15) at 28 days.

C2-F2(35)-G(0A)

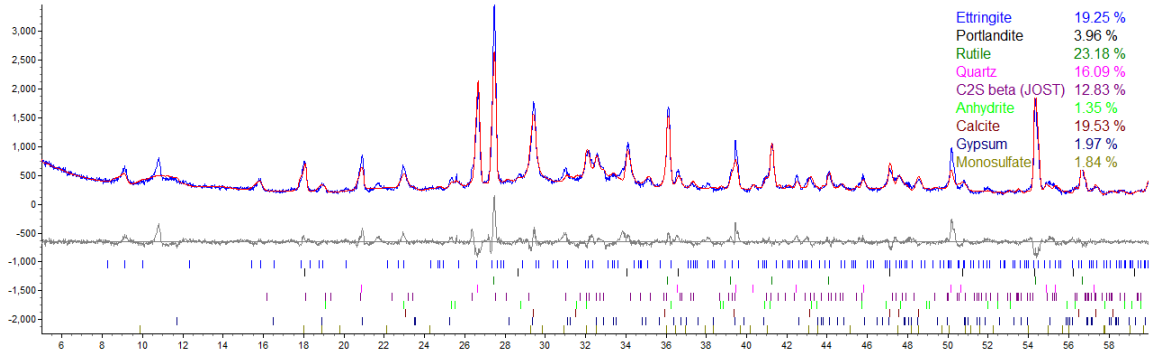

C2-F2(35)-G(0B)

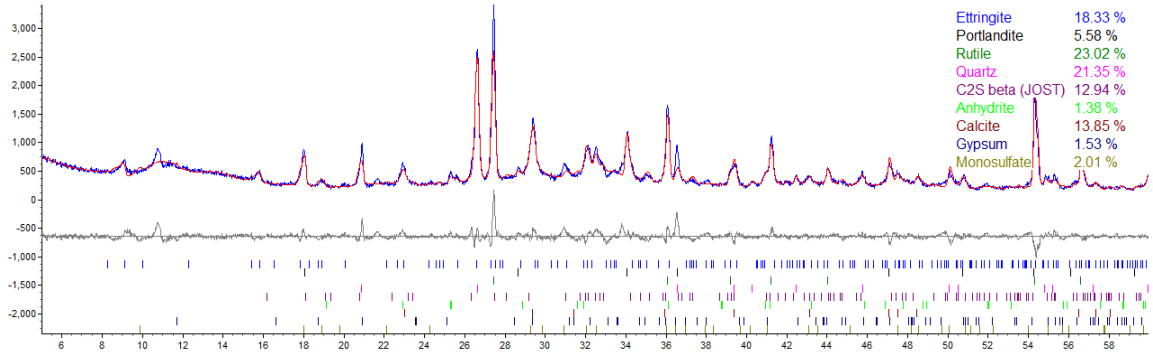

Figure A113 X-ray diffraction pattern and Rietveld refinement: C2-F2(35)-G(0).

C2-F2(35)-G(2A)

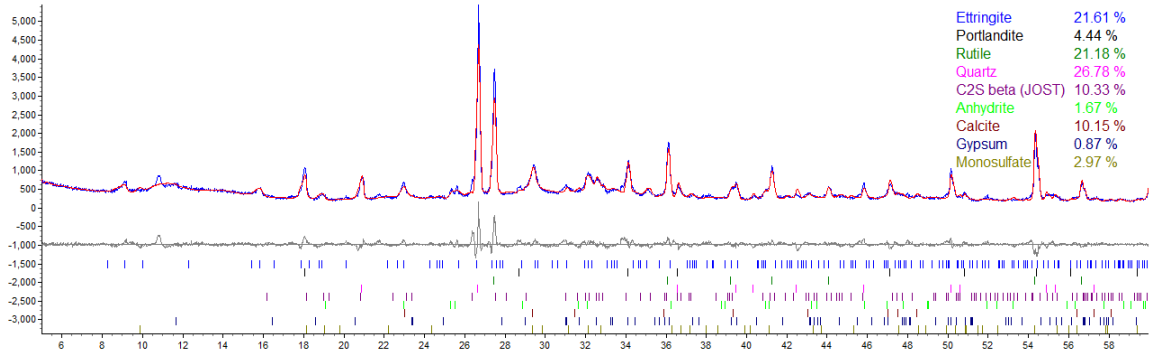

C2-F2(35)-G(2B)

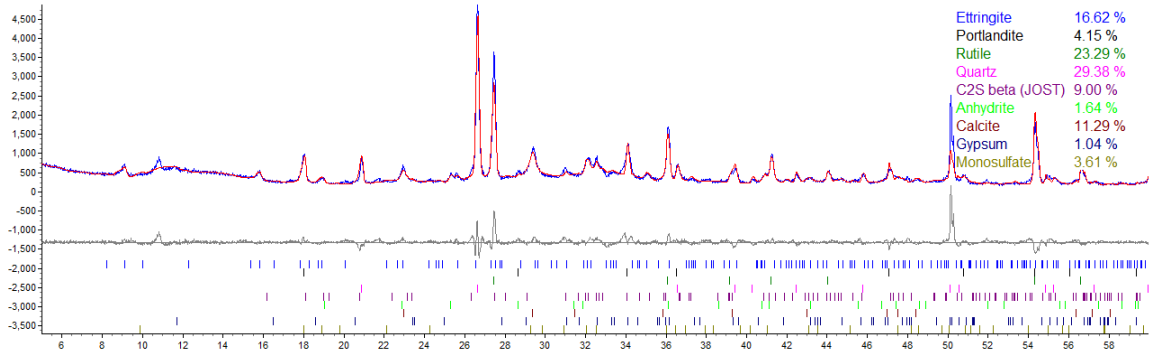

Figure A114 X-ray diffraction pattern and Rietveld refinement: C2-F2(35)-G(2).

C2-F2(35)-G(4A)

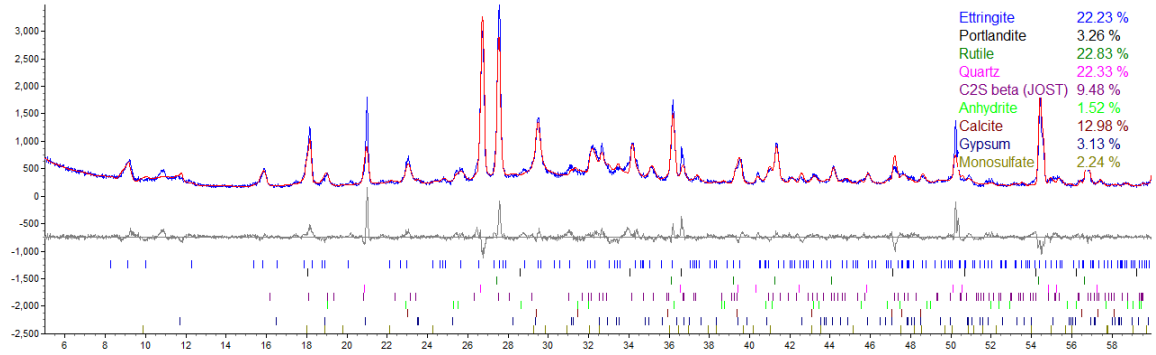

C2-F2(35)-G(4B)

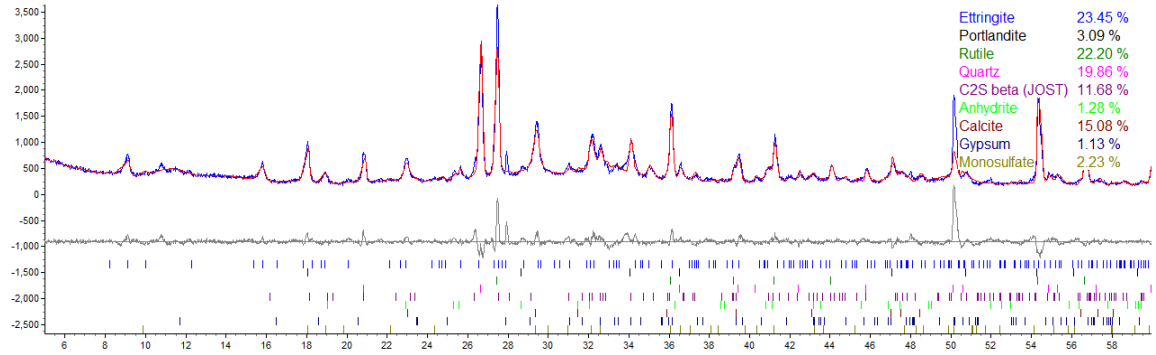

Figure A115 X-ray diffraction pattern and Rietveld refinement: C2-F2(35)-G(4).

C2-F2(35)-G(6A)

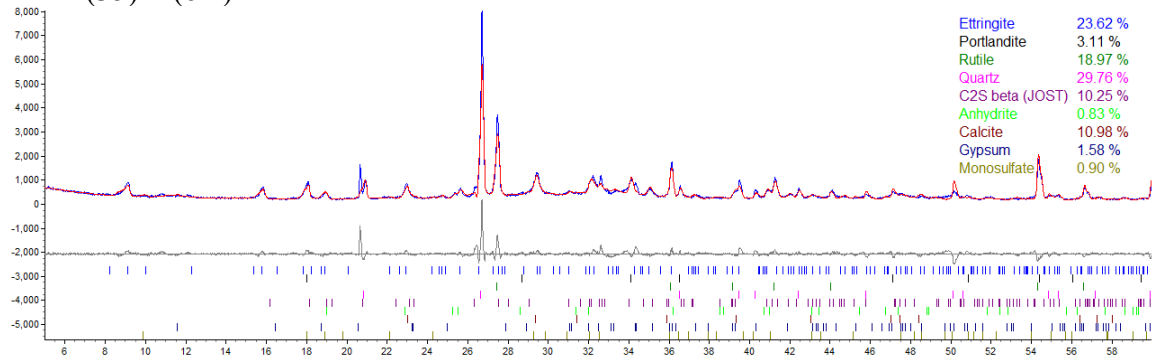

C2-F2(35)-G(6B)

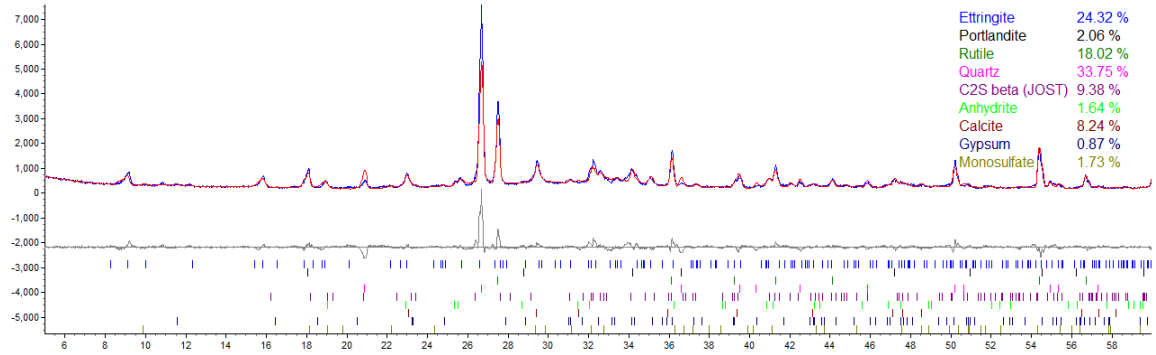

Figure A116 X-ray diffraction pattern and Rietveld refinement: C2-F2(35)-G(6).

C2-F2(35)-G(8A)

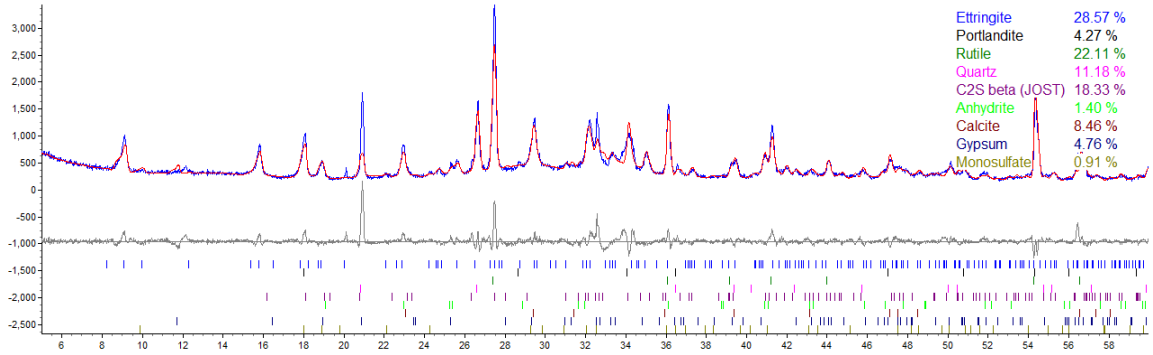

C2-F2(35)-G(8B)

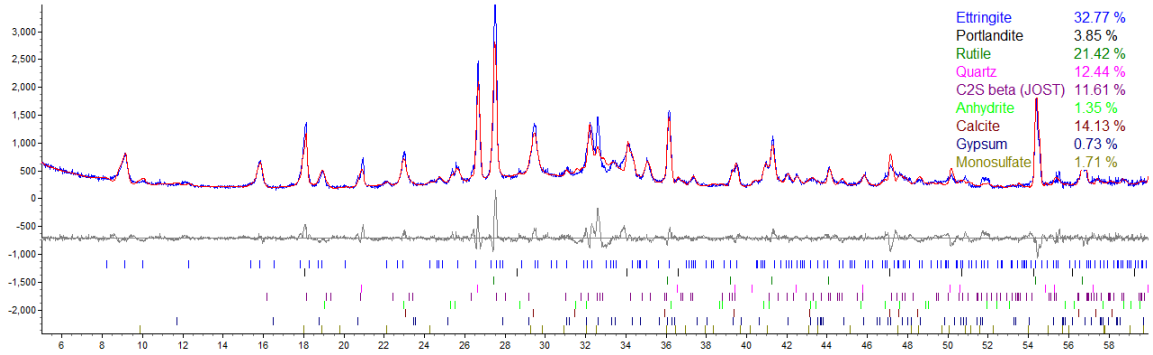

Figure A117 X-ray diffraction pattern and Rietveld refinement: C2-F2(35)-G(8).

C2-F2(35)-G(10A)

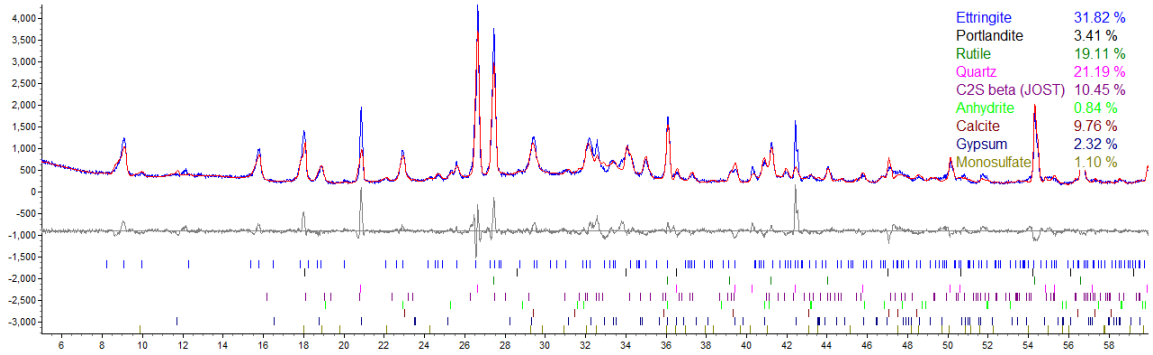

C2-F2(35)-G(10B)

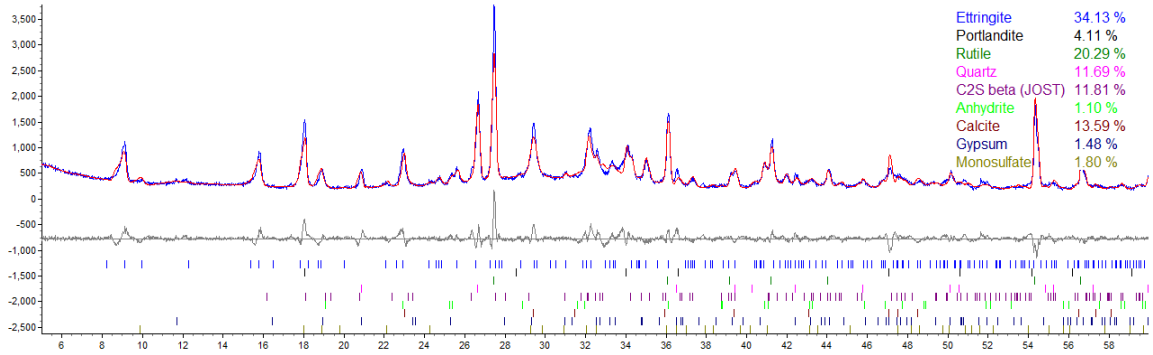

Figure A118 X-ray diffraction pattern and Rietveld refinement: C2-F2(35)-G(10).

C2-F2(35)-G(12A)

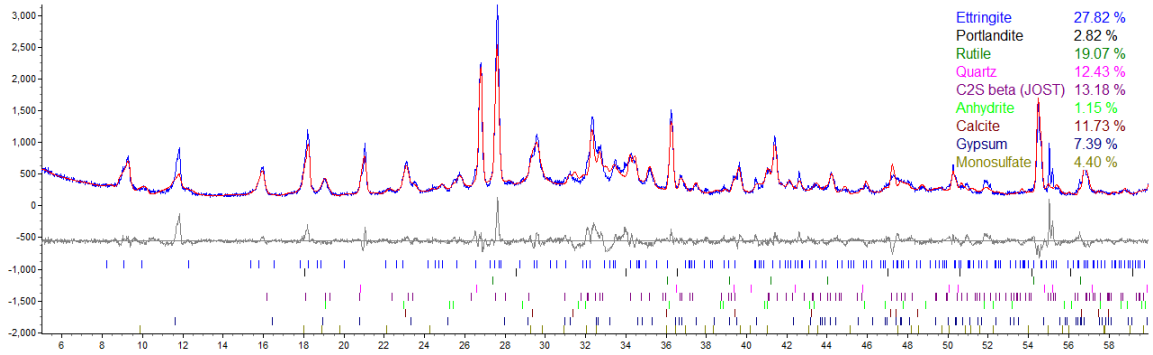

C2-F2(35)-G(12B)

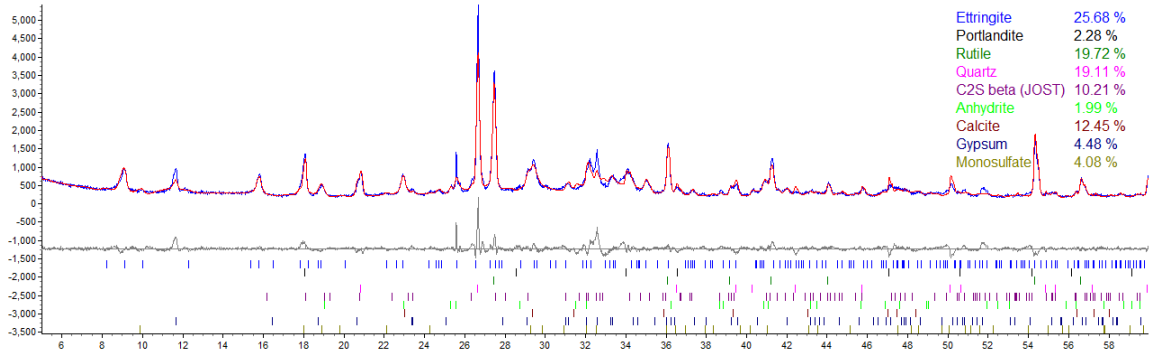

Figure A119 X-ray diffraction pattern and Rietveld refinement: C2-F2(35)-G(12).

C2-F2(35)-G(15C)

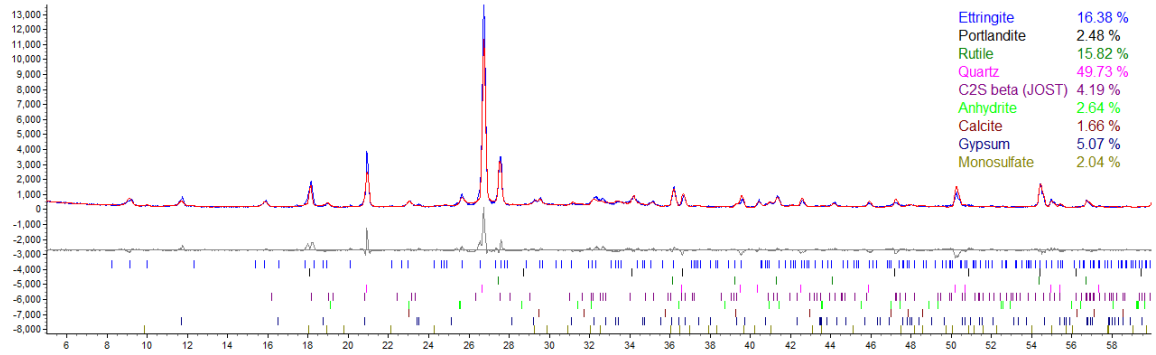

C2-F2(35)-G(15D)

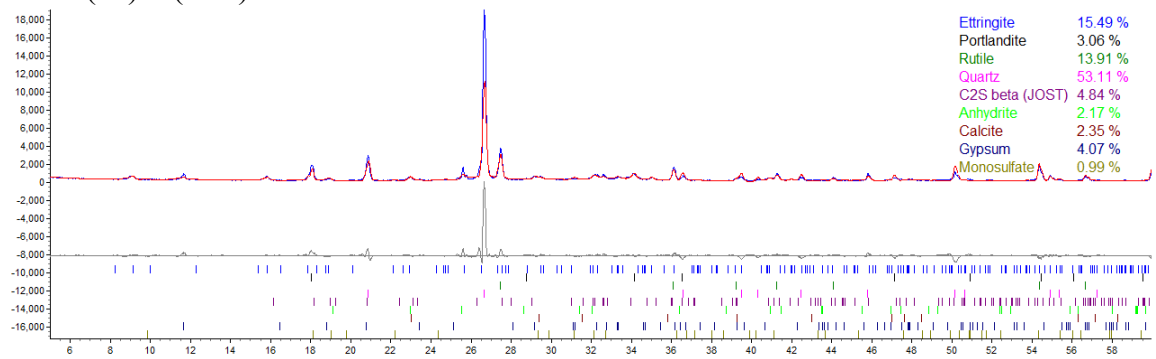

Figure A120 X-ray diffraction pattern and Rietveld refinement: C2-F2(35)-G(15).

28 DaysC2-F2(35)-G(0A)

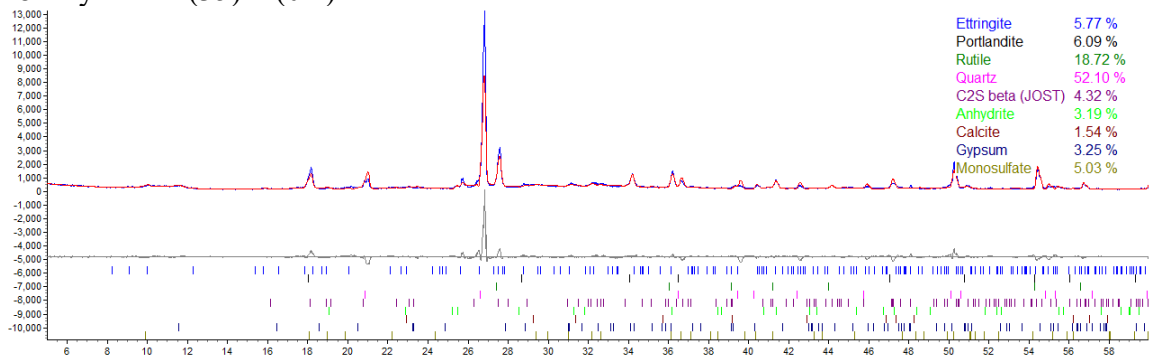

28 DaysC2-F2(35)-G(0B)

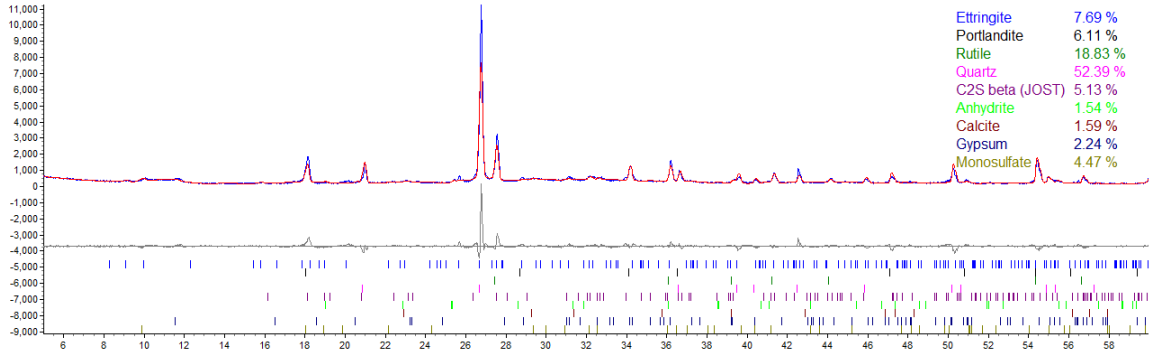

Figure A121 X-ray diffraction pattern and Rietveld refinement: C2-F2(35)-G(0) at 28 days.

28 DaysC2-F2(35)-G(2A)

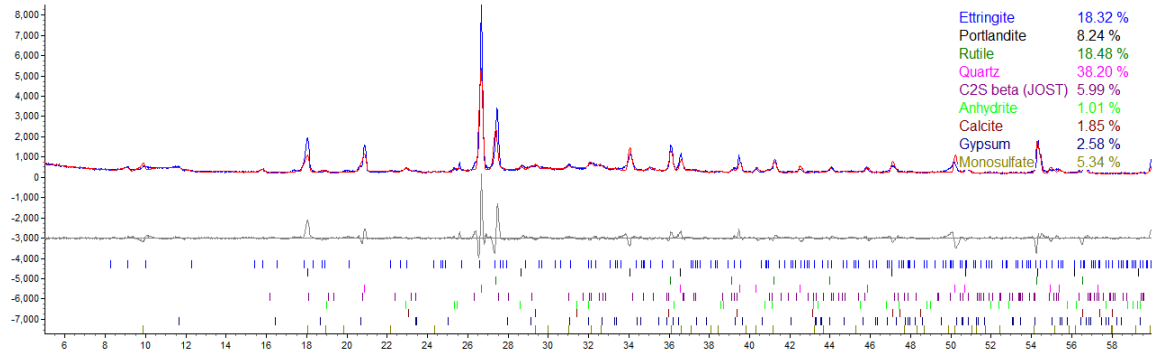

28 DaysC2-F2(35)-G(2B)

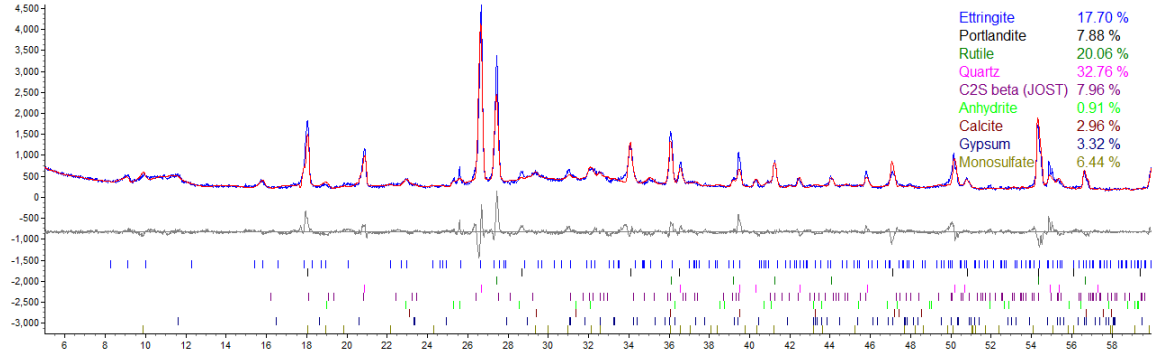

Figure A122 X-ray diffraction pattern and Rietveld refinement: C2-F2(35)-G(2) at 28 days.

28 DaysC2-F2(35)-G(4A)

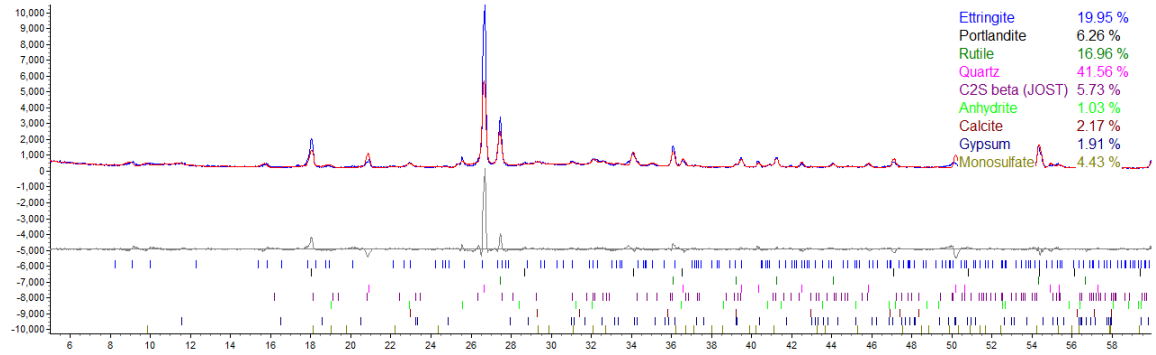

28 DaysC2-F2(35)-G(4B)

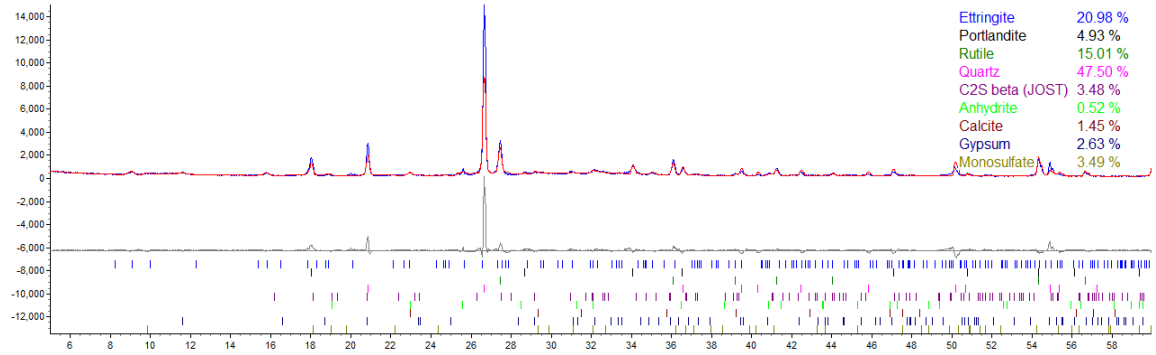

Figure A123 X-ray diffraction pattern and Rietveld refinement: C2-F2(35)-G(4) at 28 days.

28 DaysC2-F2(35)-G(6A)

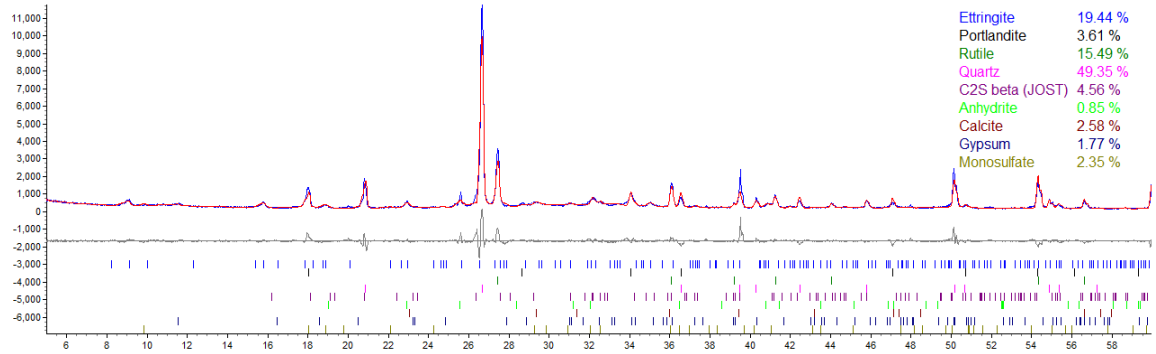

28 DaysC2-F2(35)-G(6B)

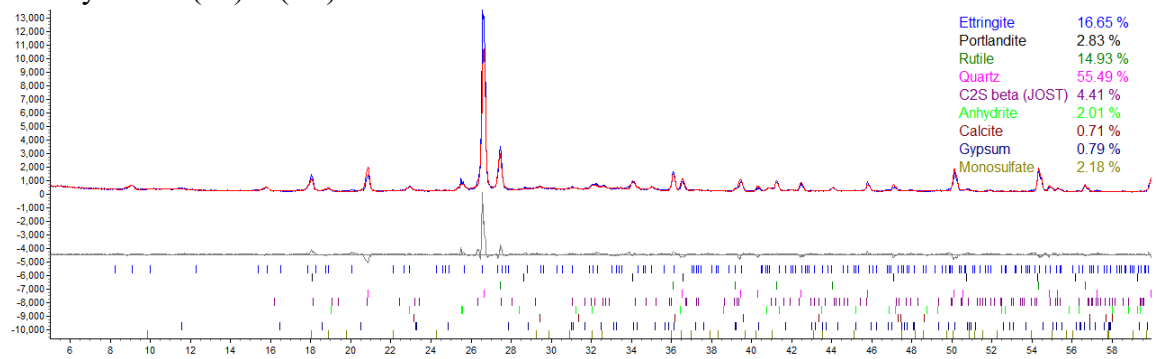

Figure A124 X-ray diffraction pattern and Rietveld refinement: C2-F2(35)-G(6) at 28 days.

28 DaysC2-F2(35)-G(8A)

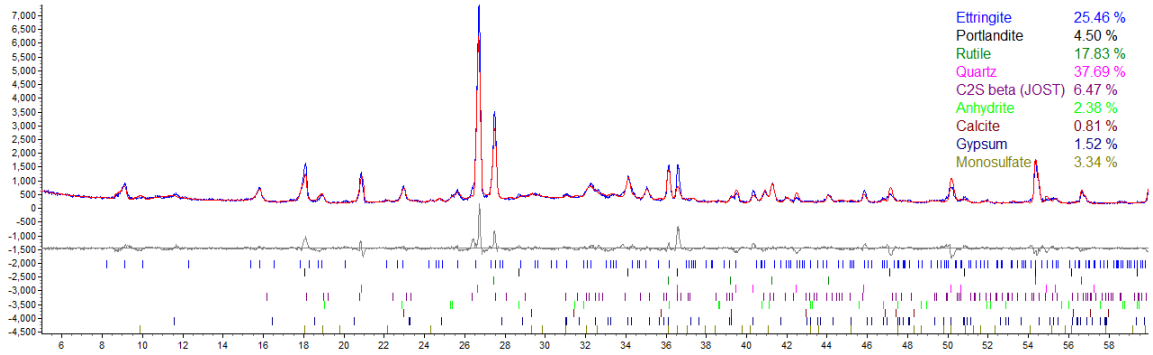

28 DaysC2-F2(35)-G(8B)

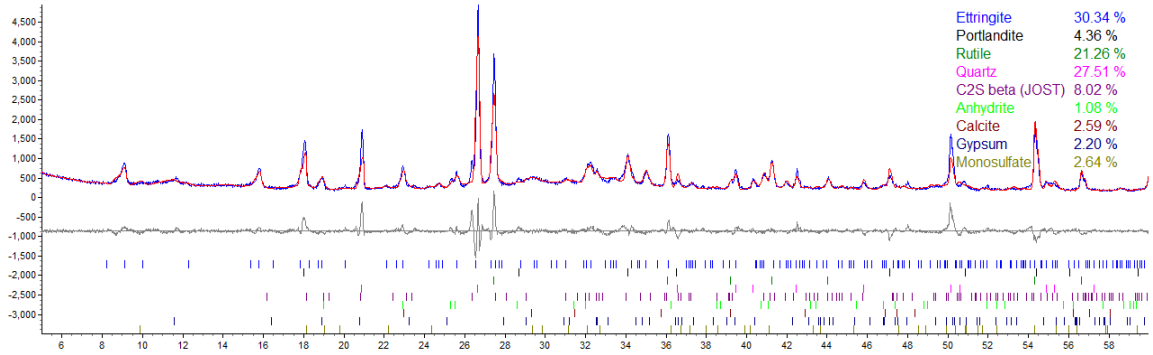

Figure A125 X-ray diffraction pattern and Rietveld refinement: C2-F2(35)-G(8) at 28 days.

28 DaysC2-F2(35)-G(10A)

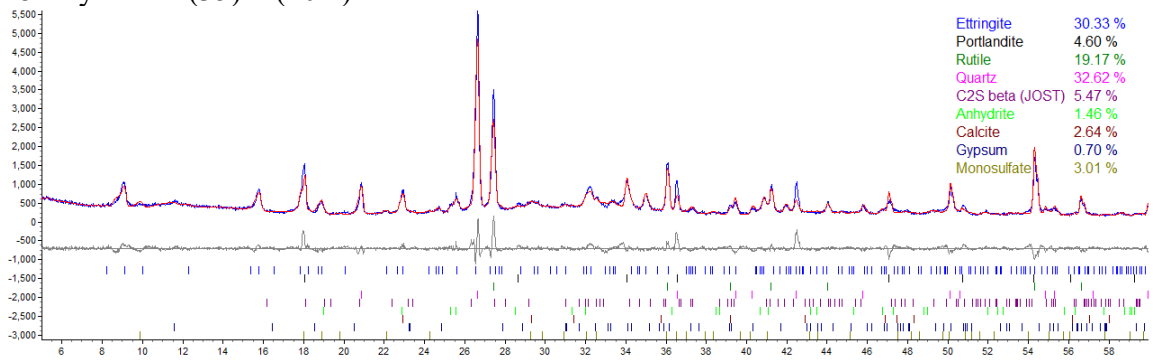

28 DaysC2-F2(35)-G(10B)

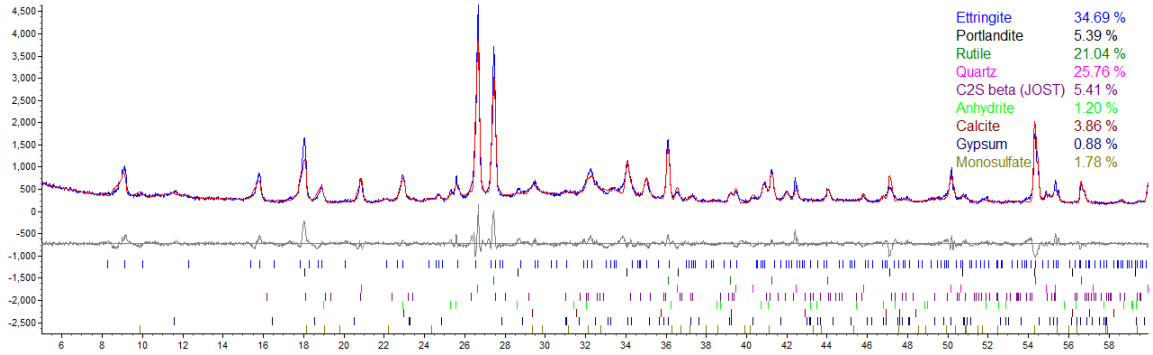

Figure A126 X-ray diffraction pattern and Rietveld refinement: C2-F2(35)-G(10) at 28 days.

28 DaysC2-F2(35)-G(12A)

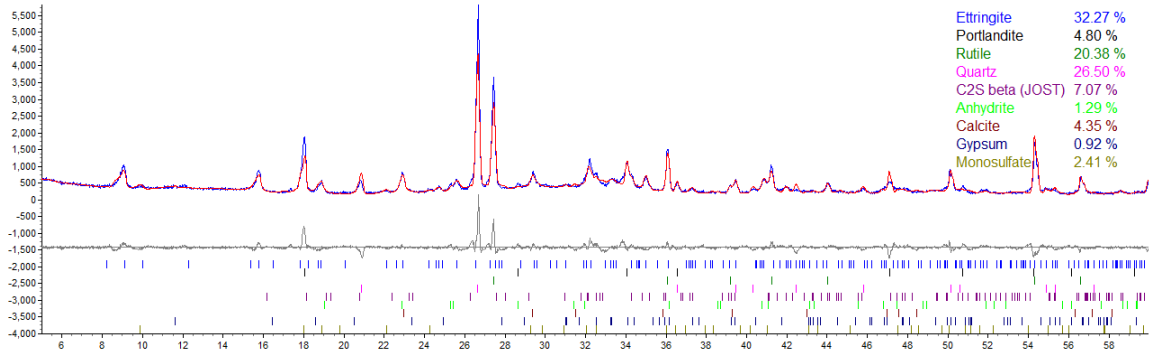

28 DaysC2-F2(35)-G(12B)

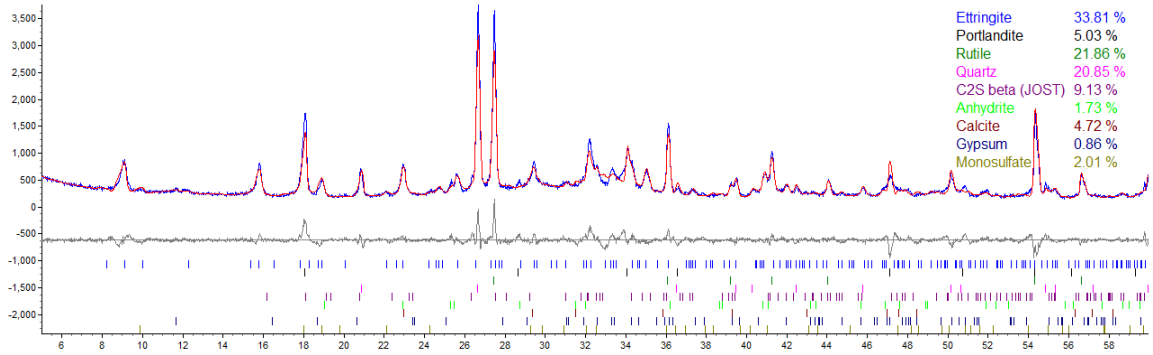

Figure A127 X-ray diffraction pattern and Rietveld refinement: C2-F2(35)-G(12) at 28 days.

28 DaysC2-F2(35)-G(15A)

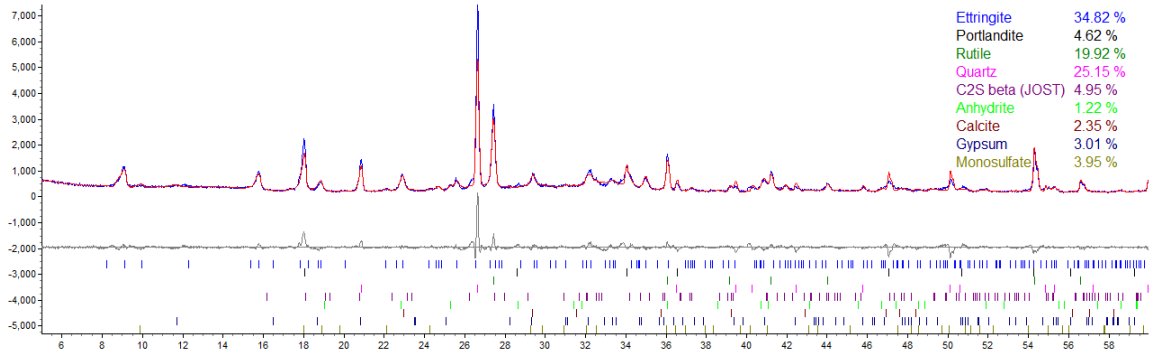

28 DaysC2-F2(35)-G(15B)

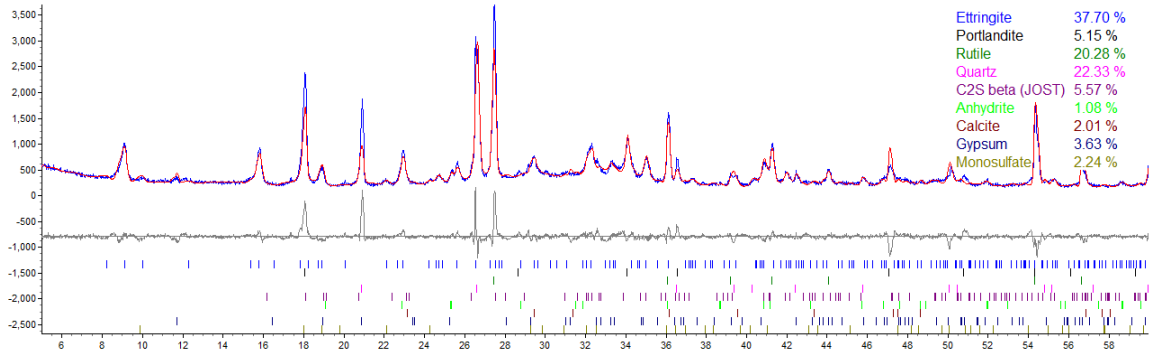

Figure A128 X-ray diffraction pattern and Rietveld refinement: C2-F2(35)-G(15) at 28 days.

C2-F3(35)-G(0A)

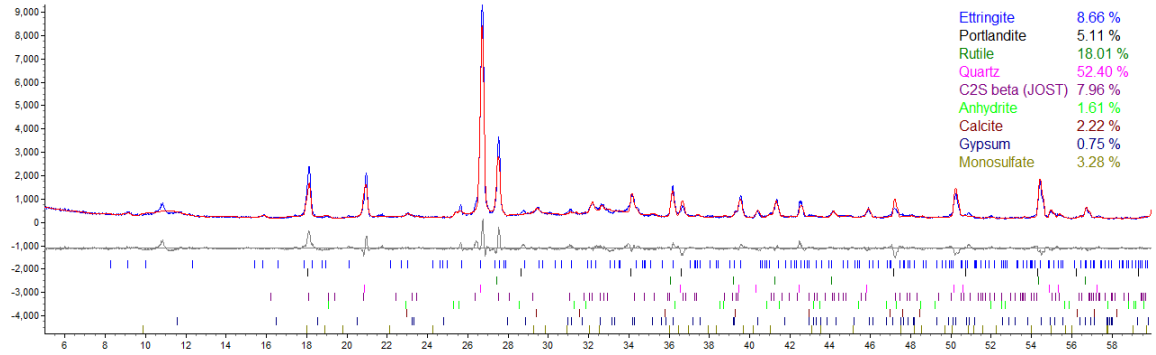

C2-F3(35)-G(0B)

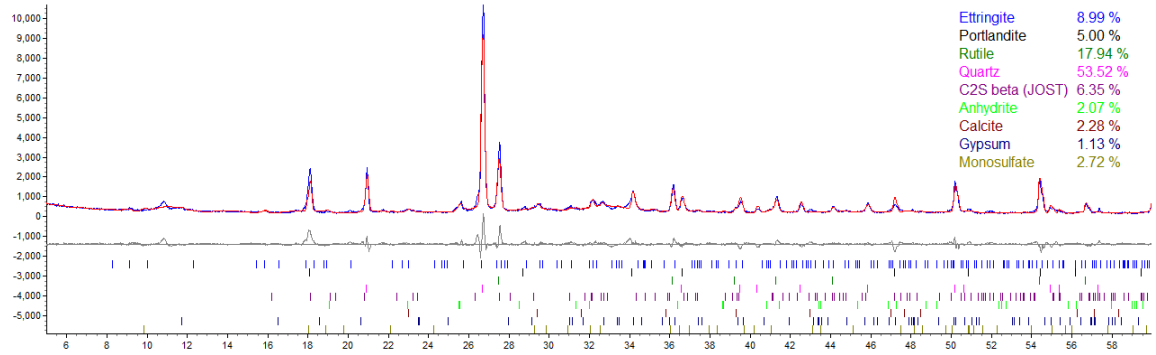

Figure A129 X-ray diffraction pattern and Rietveld refinement: C2-F3(35)-G(0).

C2-F3(35)-G(2B)

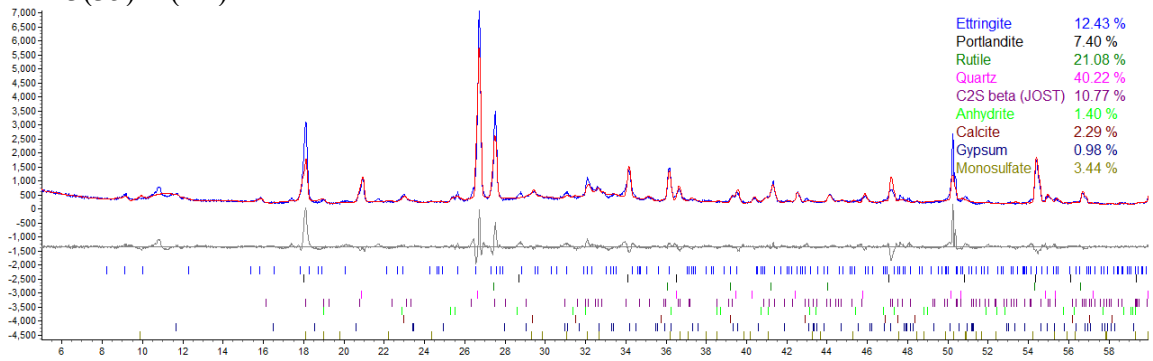

C2-F3(35)-G(2D)

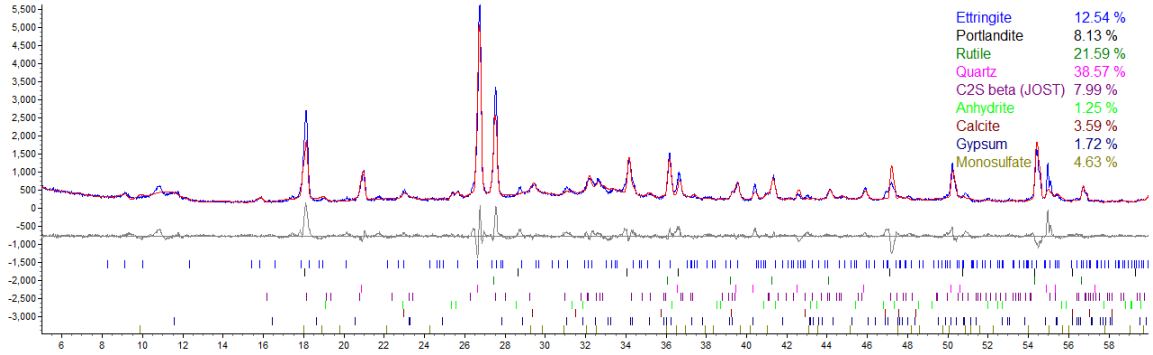

Figure A130 X-ray diffraction pattern and Rietveld refinement: C2-F3(35)-G(2).

C2-F3(35)-G(4B)

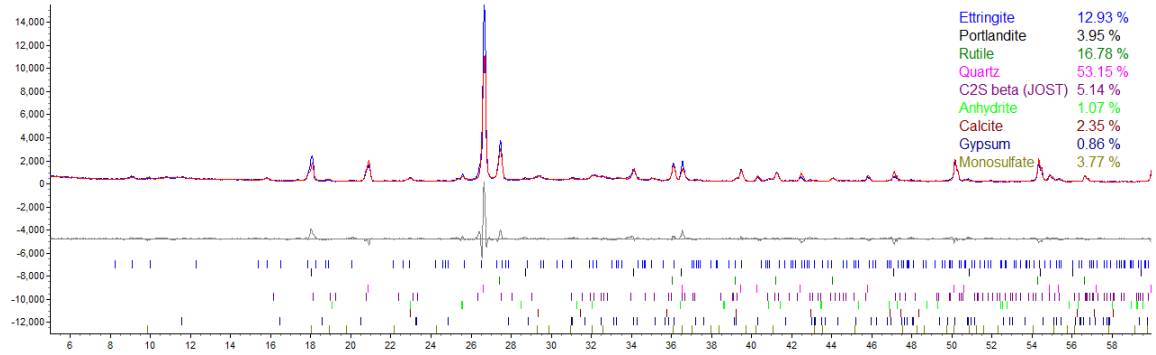

C2-F3(35)-G(4C)

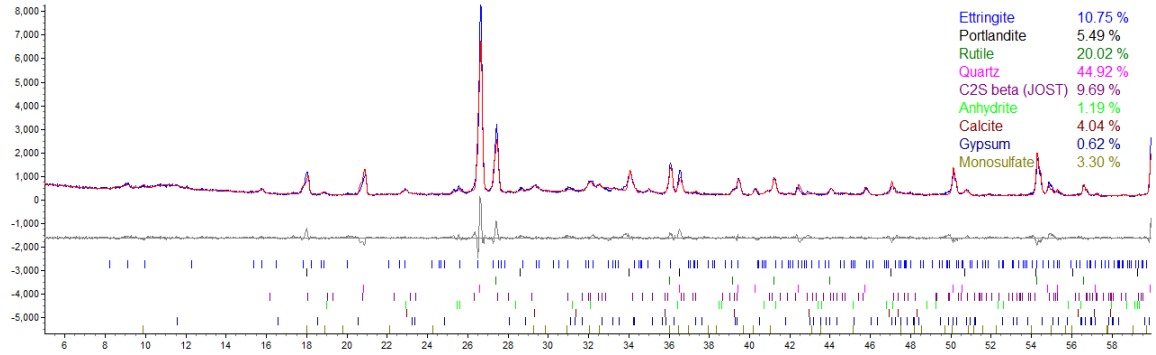

Figure A131 X-ray diffraction pattern and Rietveld refinement: C2-F3(35)-G(4).

C2-F3(35)-G(6B)

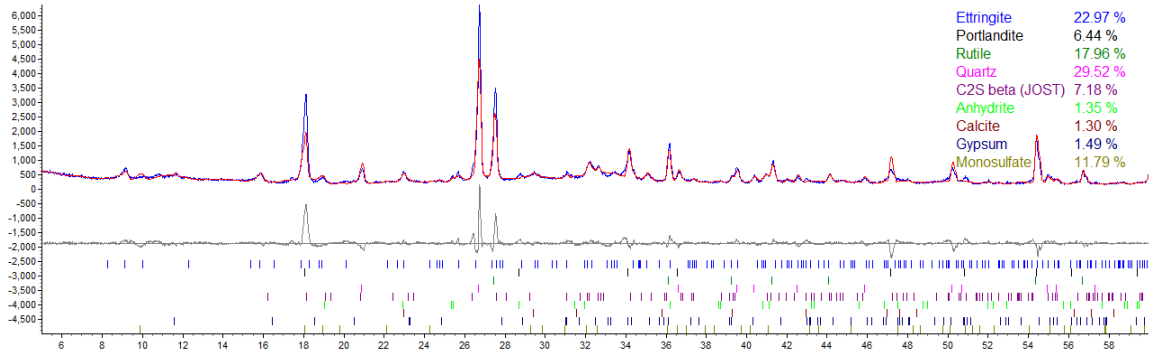

C2-F3(35)-G(6C)

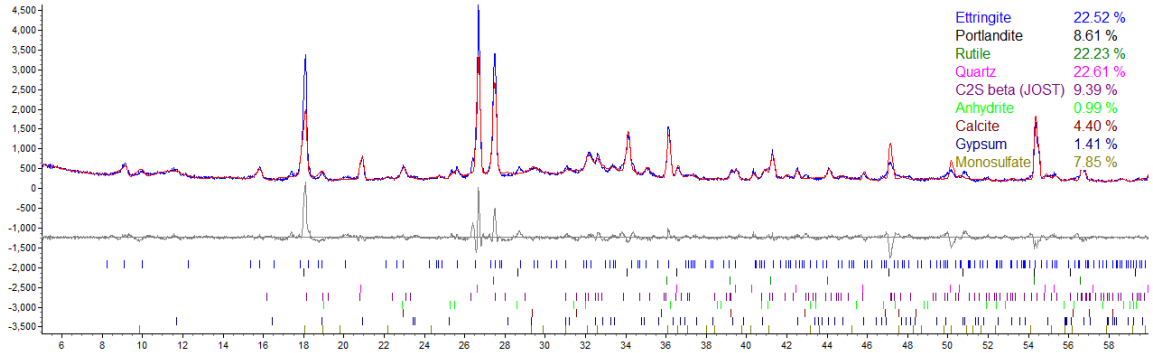

Figure A132 X-ray diffraction pattern and Rietveld refinement: C2-F3(35)-G(6).

C2-F3(35)-G(8A)

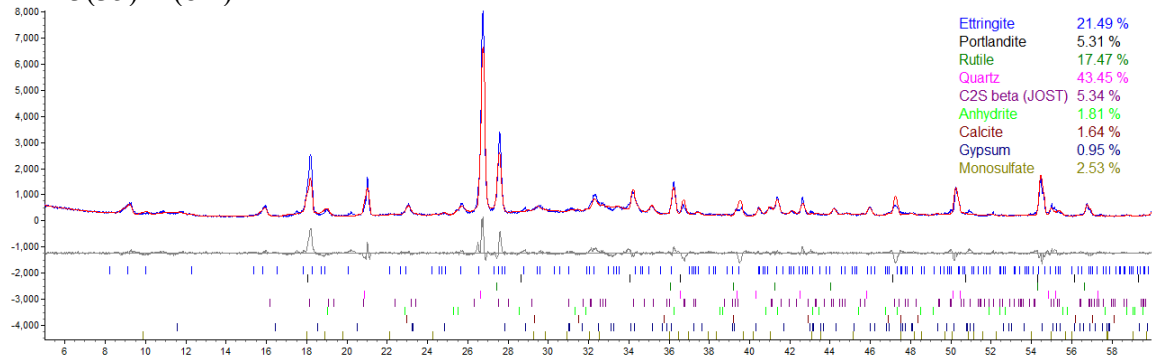

C2-F3(35)-G(8B)

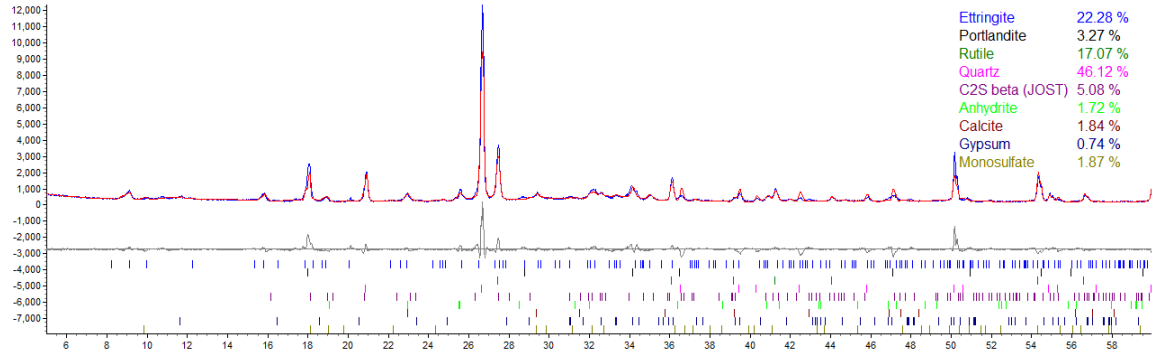

Figure A133 X-ray diffraction pattern and Rietveld refinement: C2-F3(35)-G(8).

C2-F3(35)-G(10A)

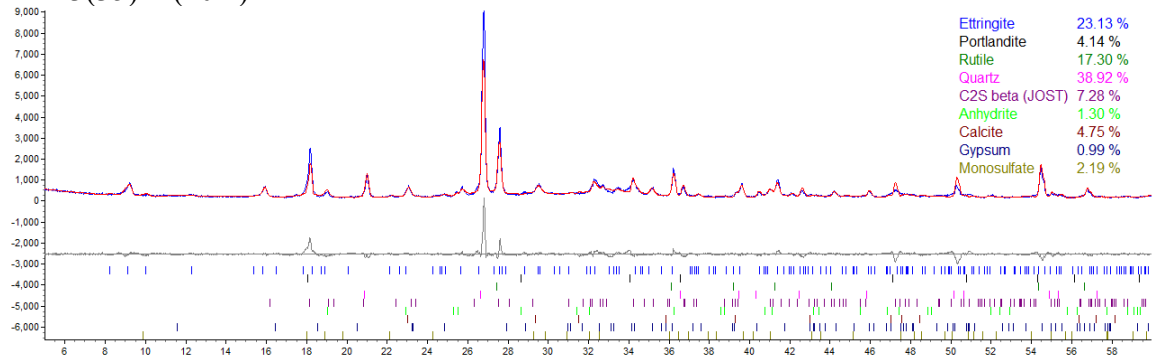

C2-F3(35)-G(10B)

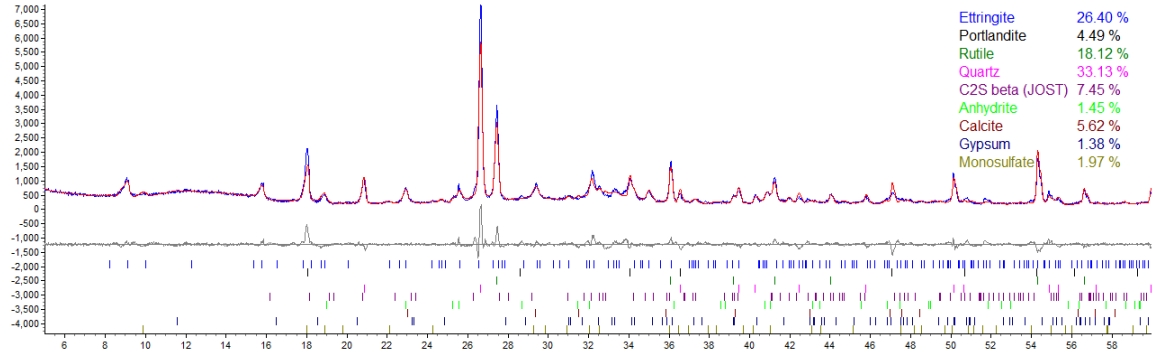

Figure A134 X-ray diffraction pattern and Rietveld refinement: C2-F3(35)-G(10).

C2-F3(35)-G(12A)

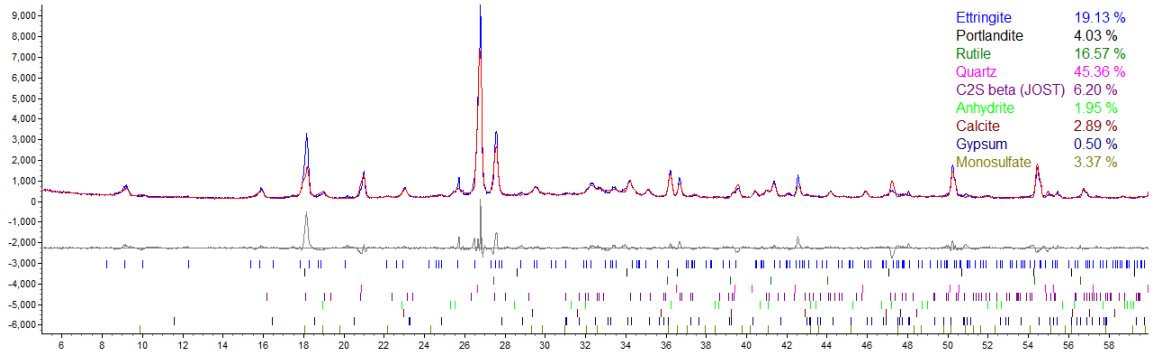

C2-F3(35)-G(12B)

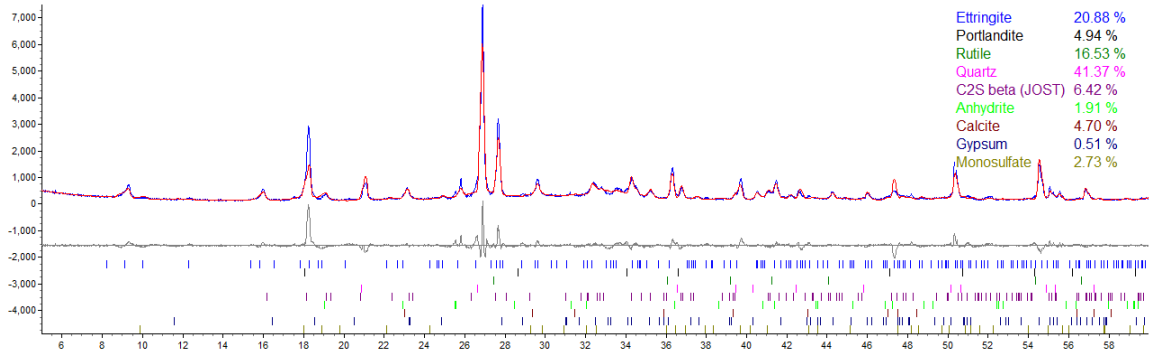

Figure A135 X-ray diffraction pattern and Rietveld refinement: C2-F3(35)-G(12).

C2-F3(35)-G(15A)

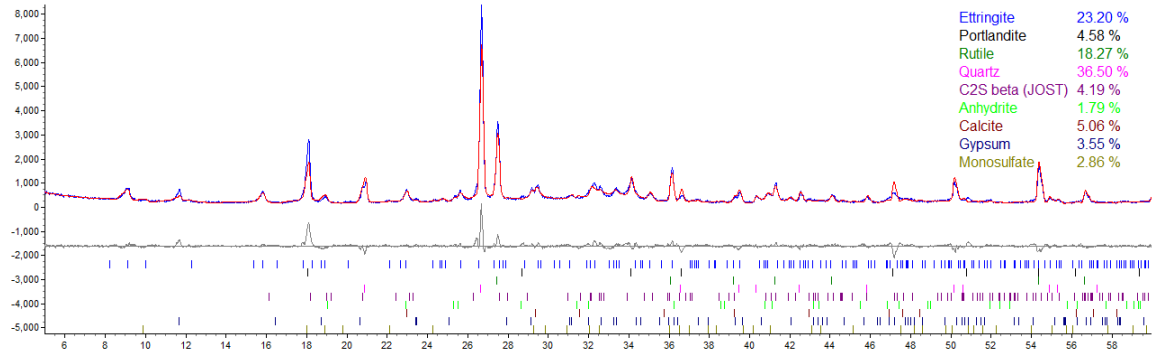

C2-F3(35)-G(15B)

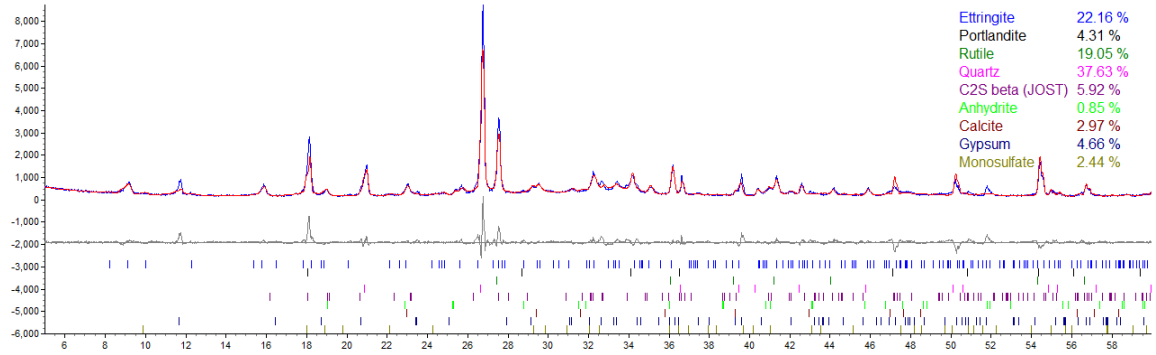

Figure A136 X-ray diffraction pattern and Rietveld refinement: C2-F3(35)-G(15).

28 Days C2-F3(35)-G(0A)

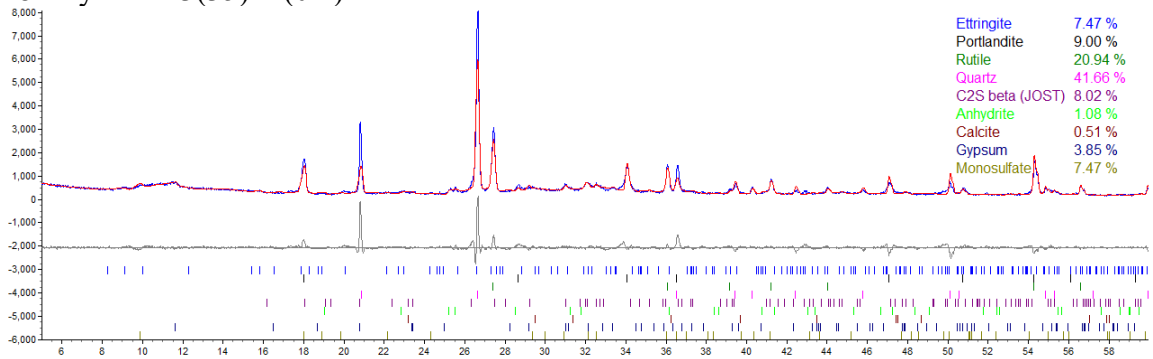

28 Days C2-F3(35)-G(0B)

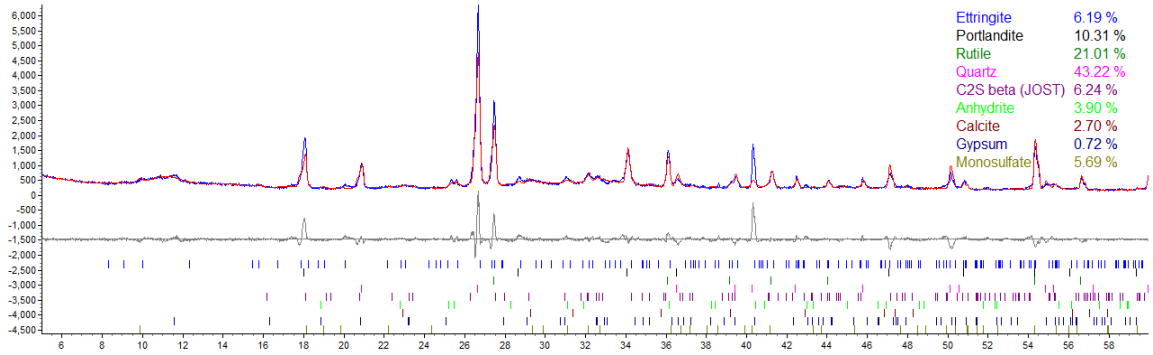

Figure A137 X-ray diffraction pattern and Rietveld refinement: C2-F3(35)-G(0) at 28 days.

28 Days C2-F3(35)-G(2A)

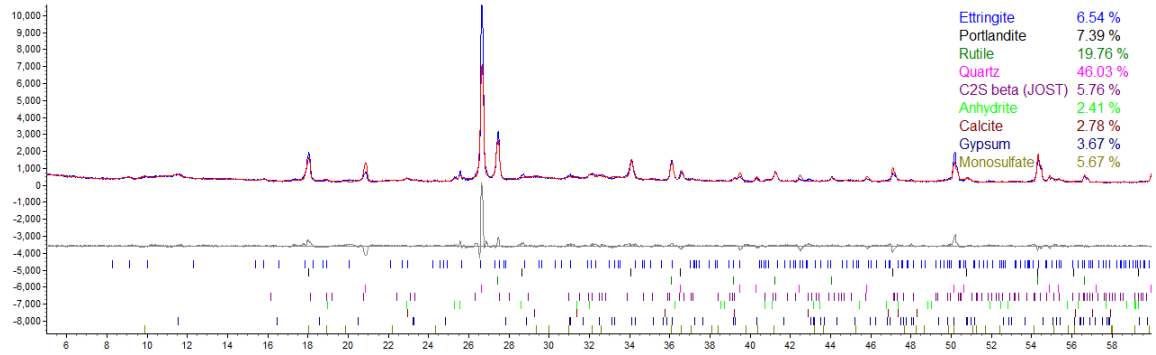

28 Days C2-F3(35)-G(2C)

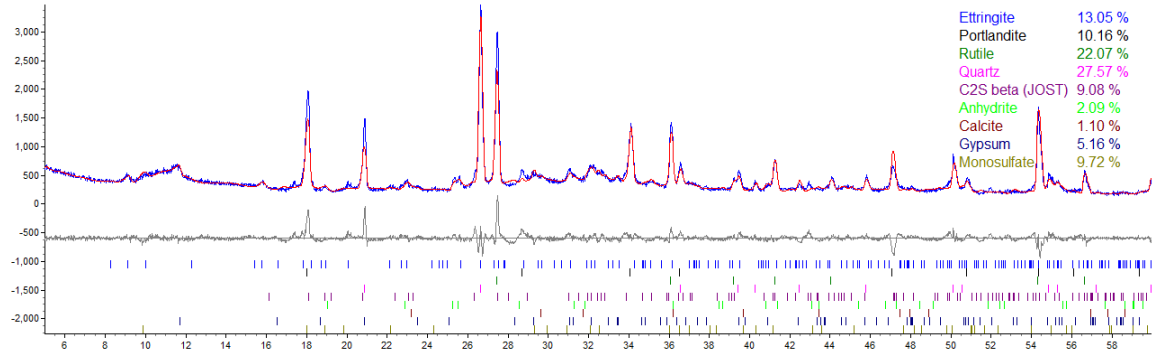

Figure A138 X-ray diffraction pattern and Rietveld refinement: C2-F3(35)-G(2) at 28 days.

28 Days C2-F3(35)-G(4A)

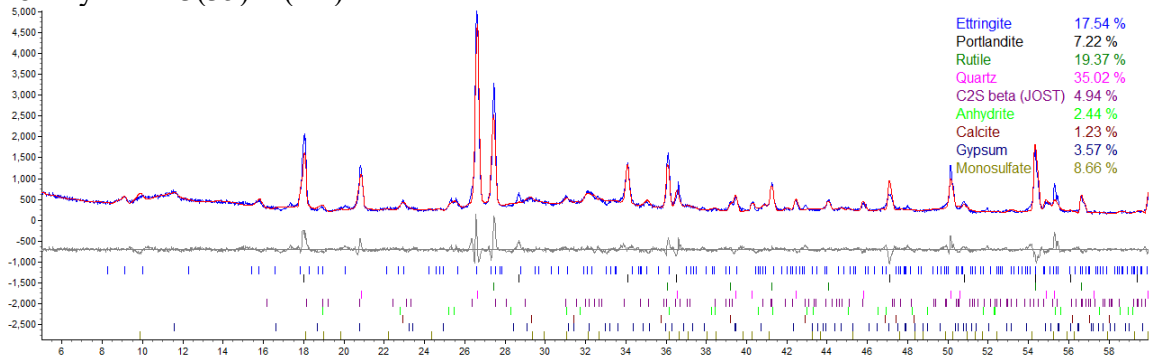

28 Days C2-F3(35)-G(4B)

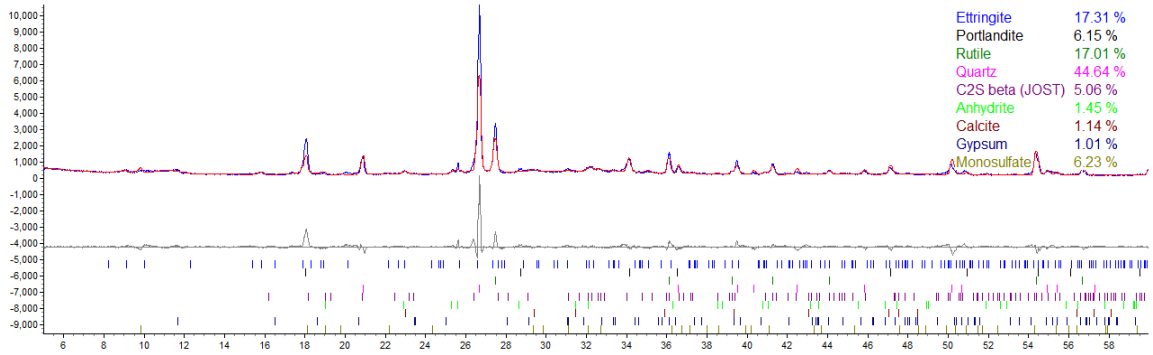

Figure A139 X-ray diffraction pattern and Rietveld refinement: C2-F3(35)-G(4) at 28 days.

28 Days C2-F3(35)-G(6B)

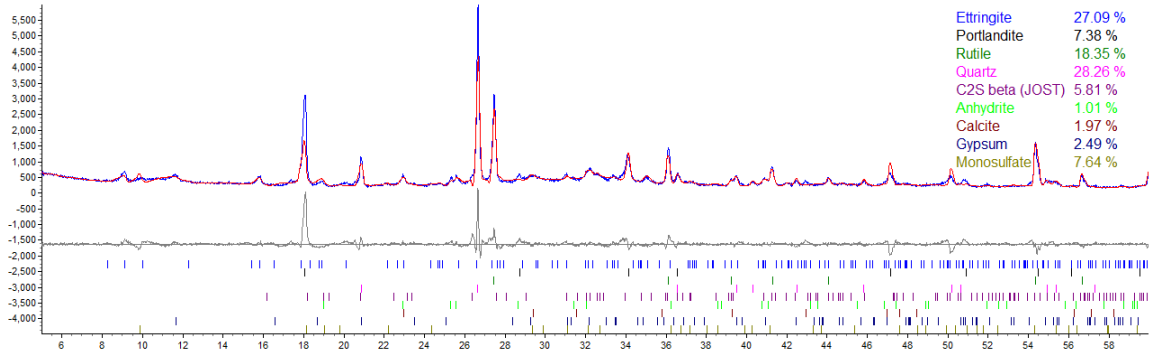

28 Days C2-F3(35)-G(6C)

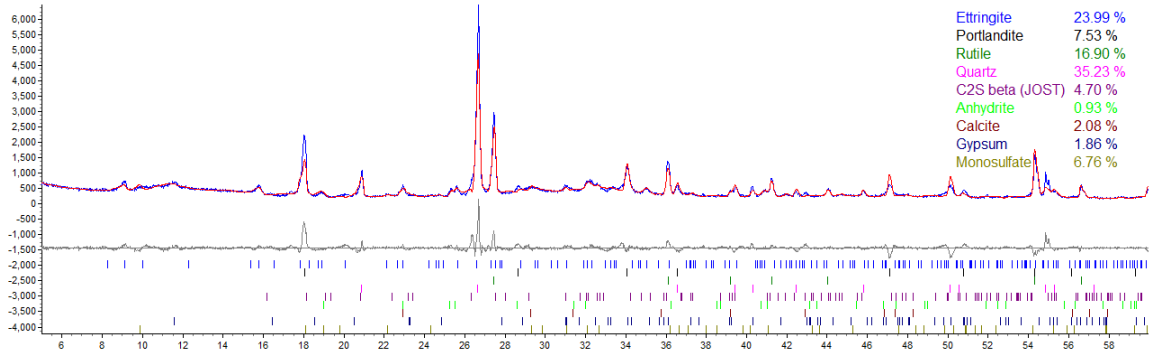

Figure A140 X-ray diffraction pattern and Rietveld refinement: C2-F3(35)-G(6) at 28 days.

28 Days C2-F3(35)-G(8A)

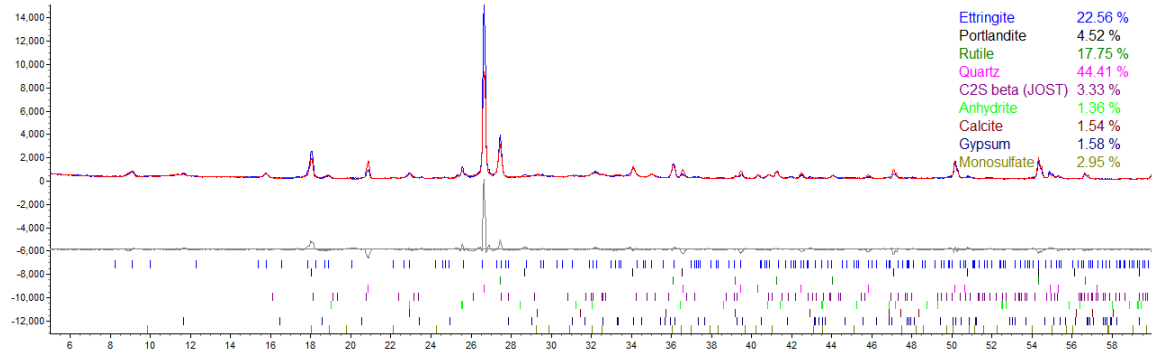

28 Days C2-F3(35)-G(8C)

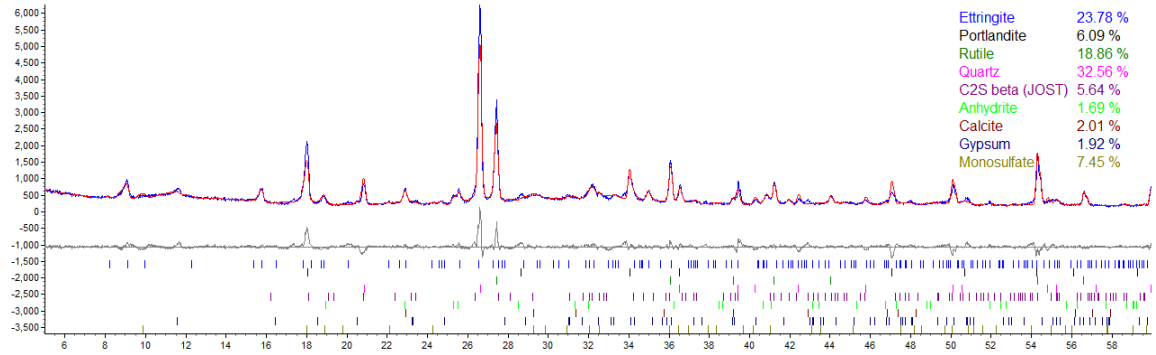

Figure A141 X-ray diffraction pattern and Rietveld refinement: C2-F3(35)-G(8) at 28 days.

28 Days C2-F3(35)-G(10A)

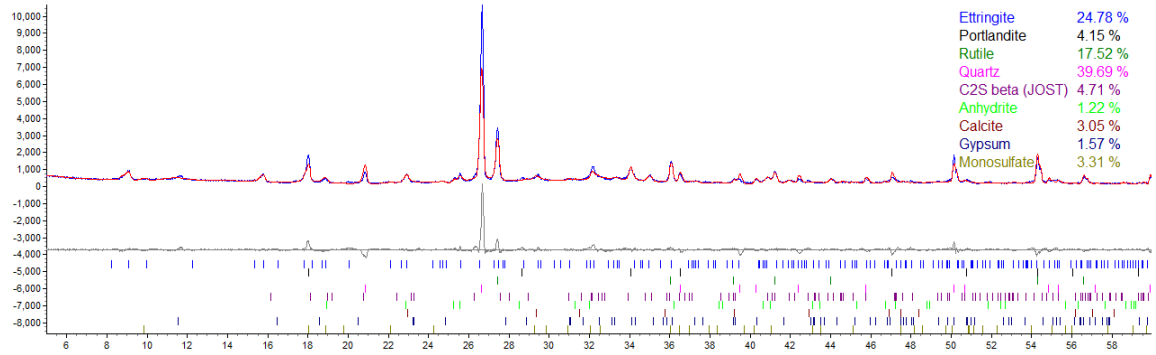

28 Days C2-F3(35)-G(10B)

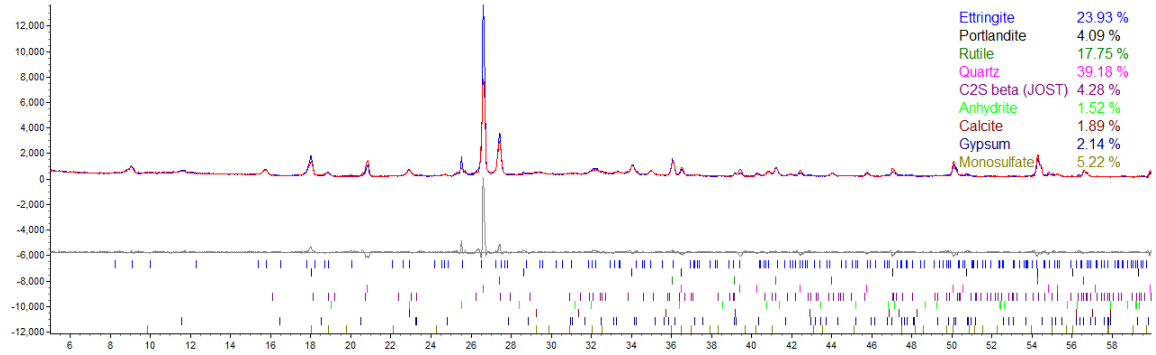

Figure A142 X-ray diffraction pattern and Rietveld refinement: C2-F3(35)-G(10) at 28 days.

28 Days C2-F3(35)-G(12A)

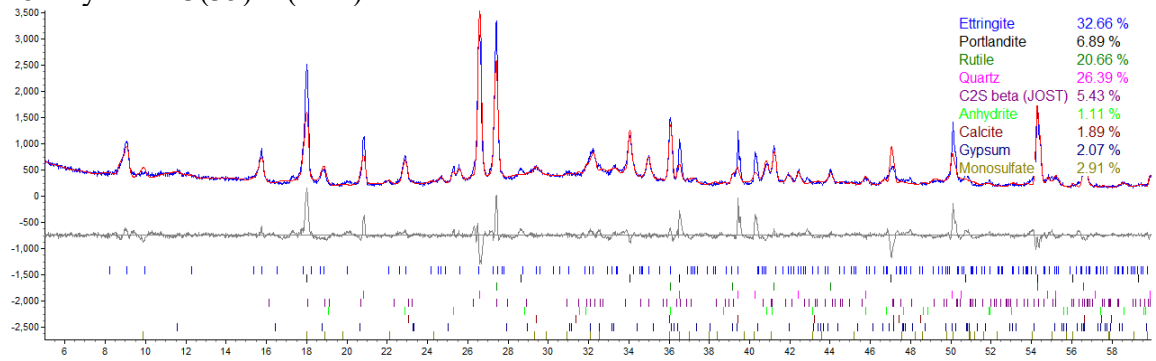

28 Days C2-F3(35)-G(12B)

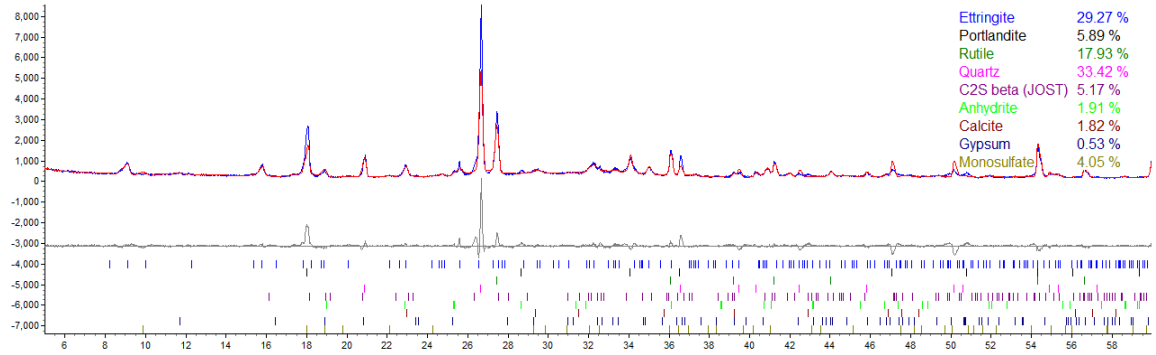

Figure A143 X-ray diffraction pattern and Rietveld refinement: C2-F3(35)-G(12) at 28 days.

28 Days C2-F3(35)-G(15A)

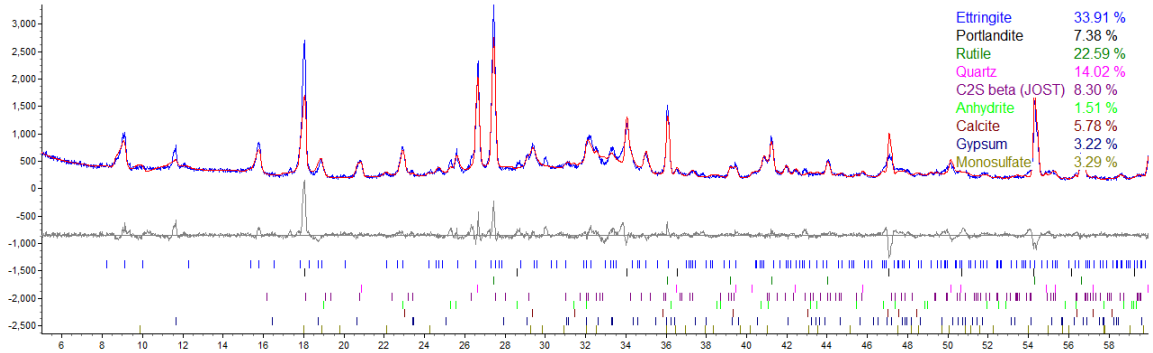

28 Days C2-F3(35)-G(15B)

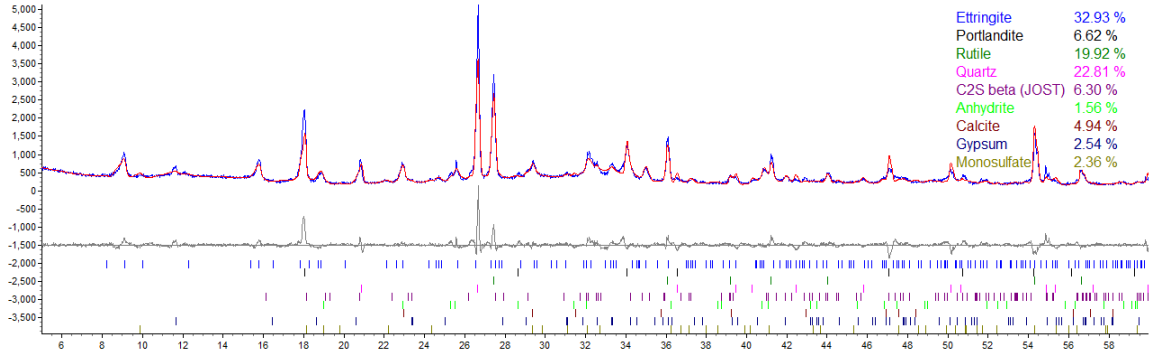

Figure A144 X-ray diffraction pattern and Rietveld refinement: C2-F3(35)-G(15) at 28 days.

C2-F1(20)-G(0A)

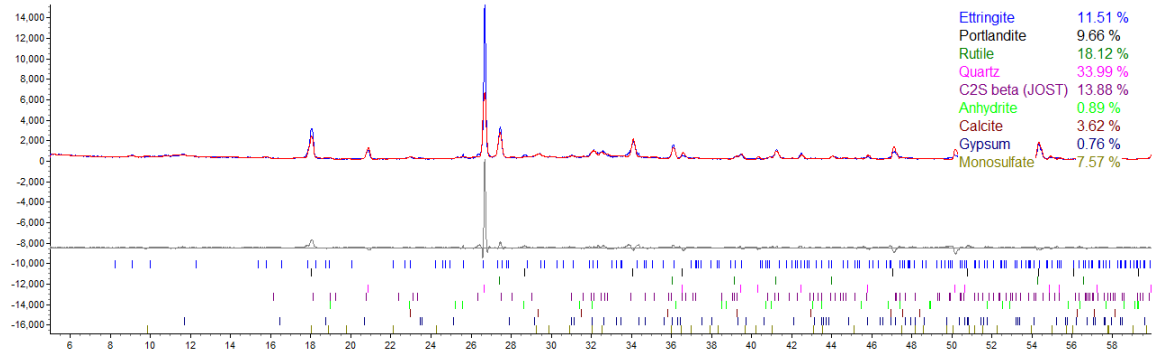

C2-F1(20)-G(0C)

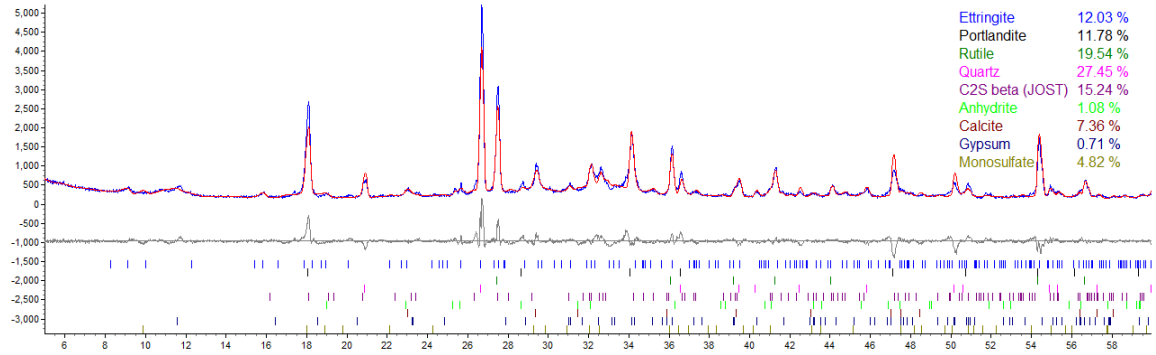

Figure A145 X-ray diffraction pattern and Rietveld refinement: C2-F1(20)-G(0).

C2-F1(20)-G(2A)

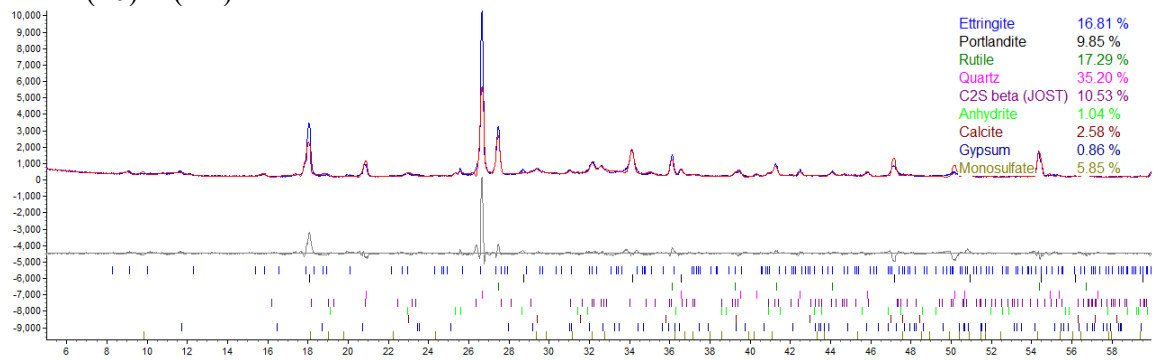

C2-F1(20)-G(2B)

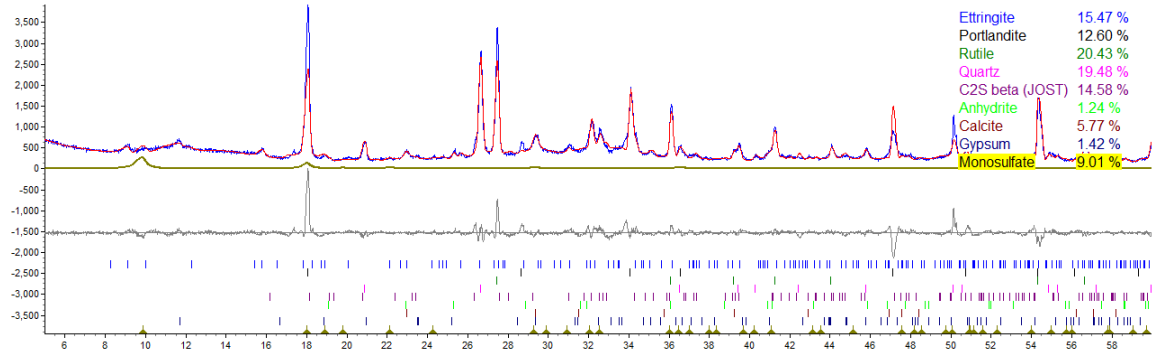

Figure A146 X-ray diffraction pattern and Rietveld refinement: C2-F1(20)-G(2).

C2-F1(20)-G(4A)

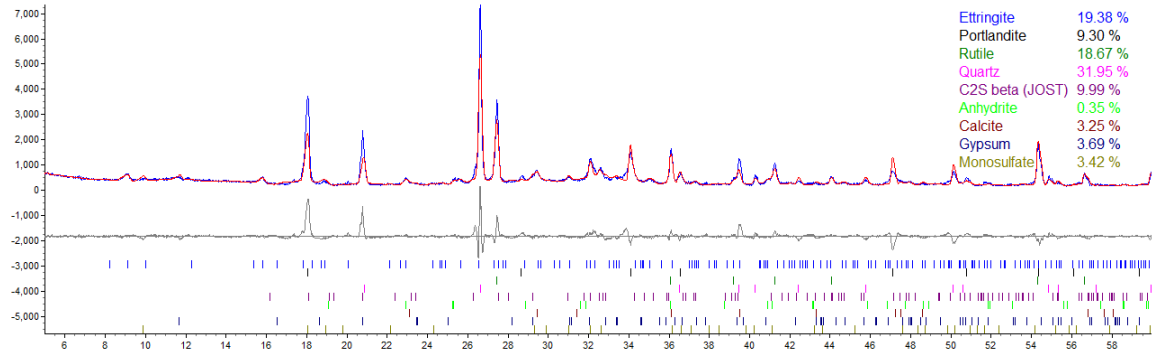

C2-F1(20)-G(4B)

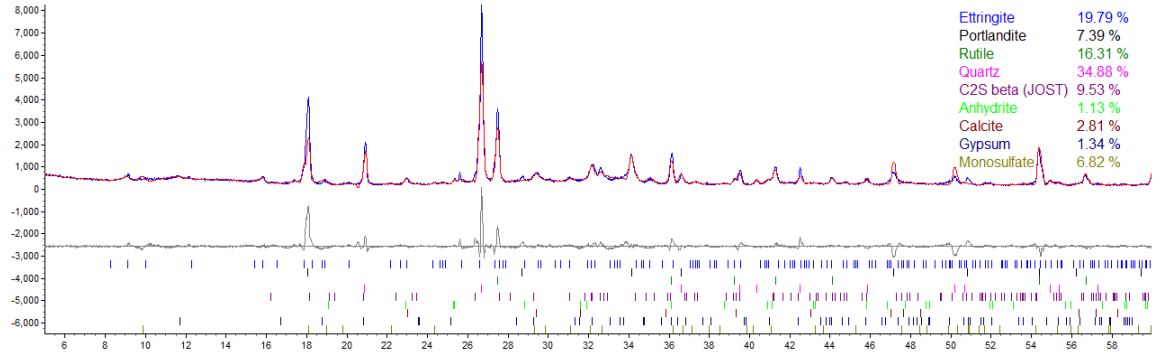

Figure A147 X-ray diffraction pattern and Rietveld refinement: C2-F1(20)-G(4).

C2-F1(20)-G(6A)

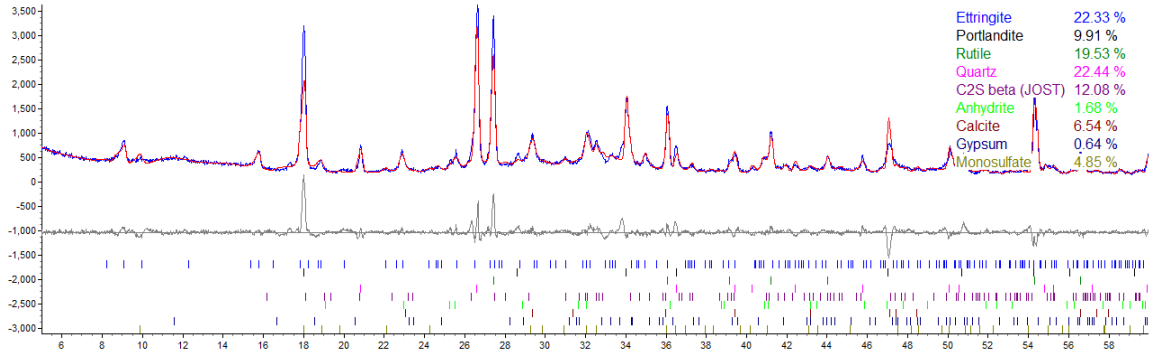

C2-F1(20)-G(6B)

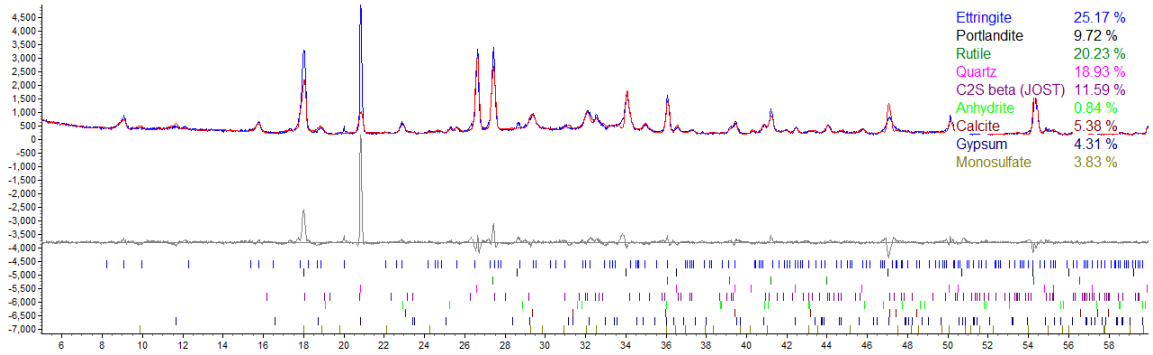

Figure A148 X-ray diffraction pattern and Rietveld refinement: C2-F1(20)-G(6).

C2-F1(20)-G(8A)

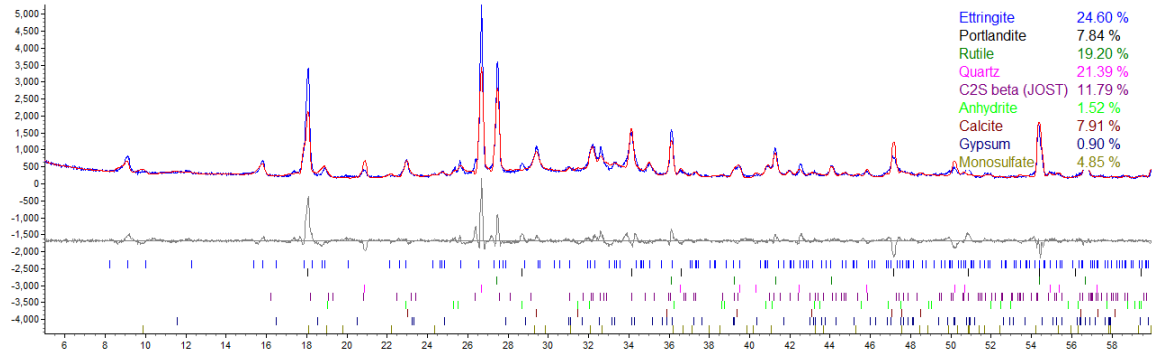

C2-F1(20)-G(8B)

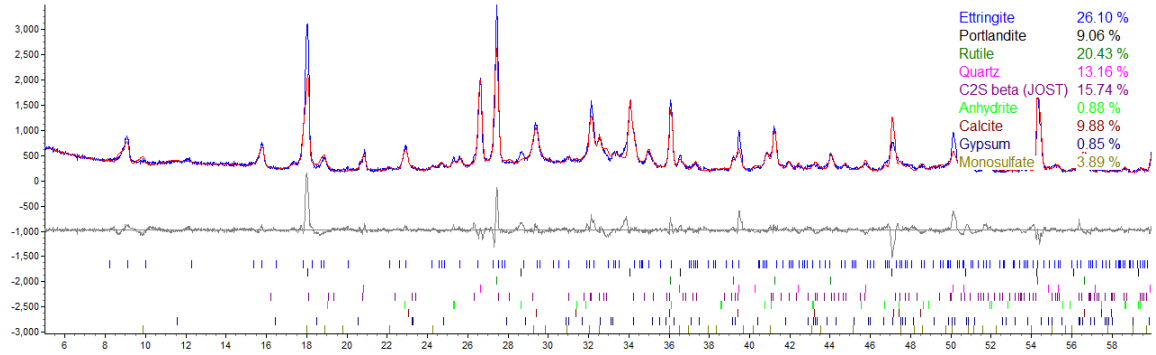

Figure A149 X-ray diffraction pattern and Rietveld refinement: C2-F1(20)-G(8).

C2-F1(20)-G(10A)

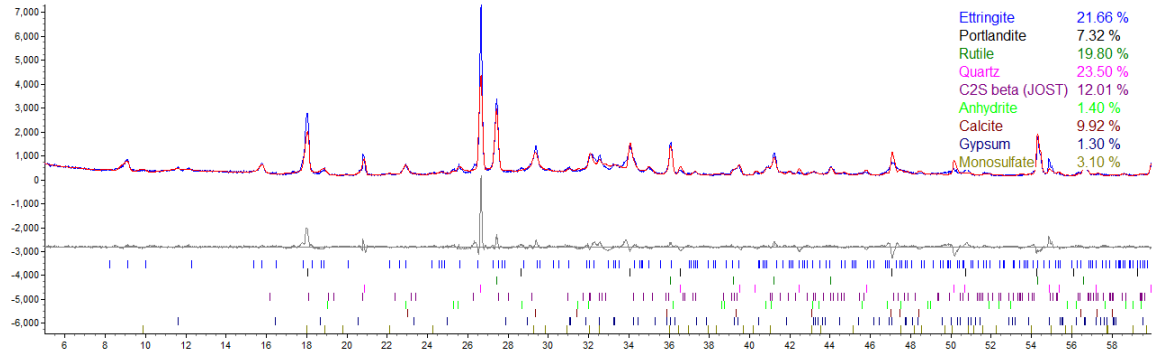

C2-F1(20)-G(10B)

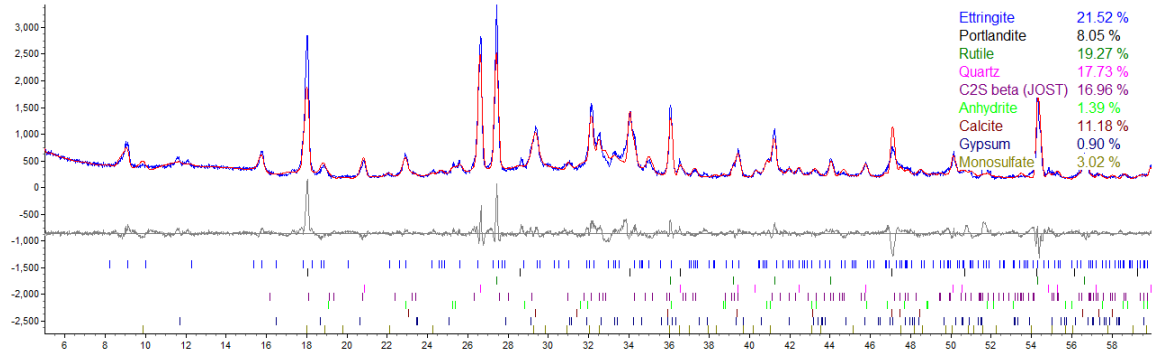

Figure A150 X-ray diffraction pattern and Rietveld refinement: C2-F1(20)-G(10).

C2-F1(20)-G(12A)

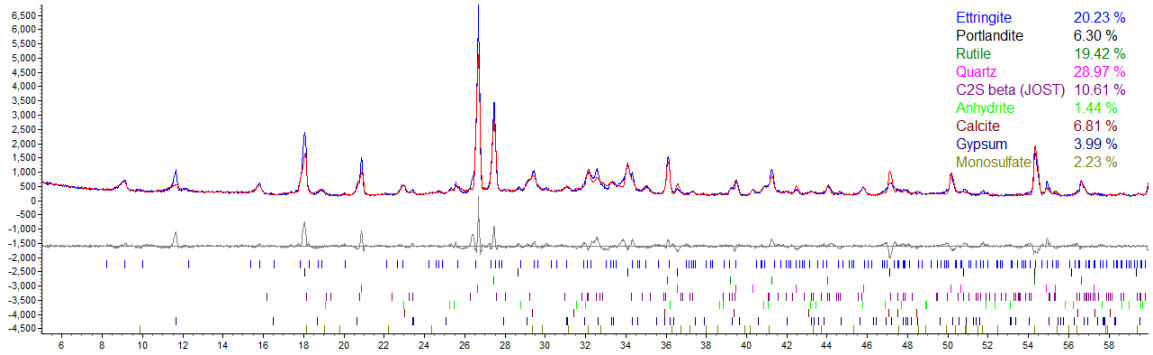

C2-F1(20)-G(12C)

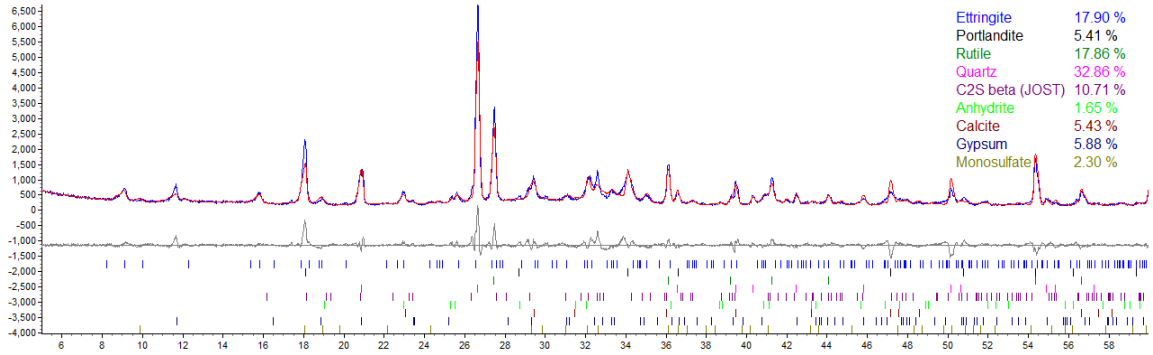

Figure A151 X-ray diffraction pattern and Rietveld refinement: C2-F1(20)-G(12).

C2-F1(20)-G(15A)

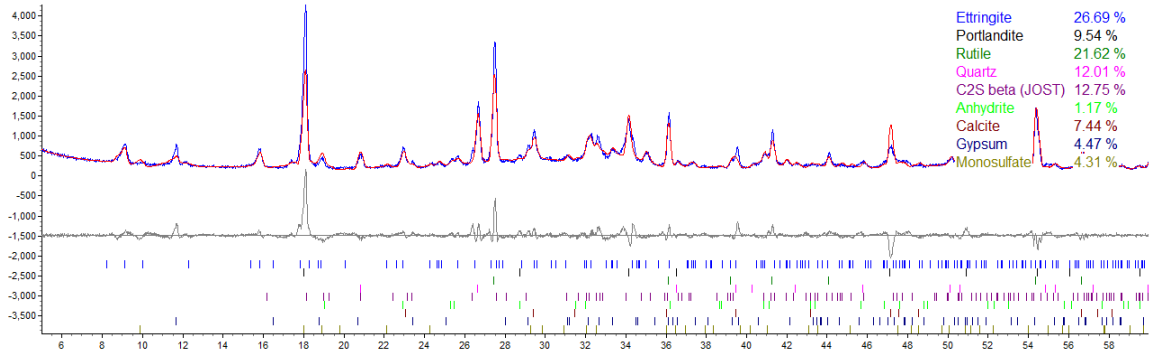

C2-F1(20)-G(15B)

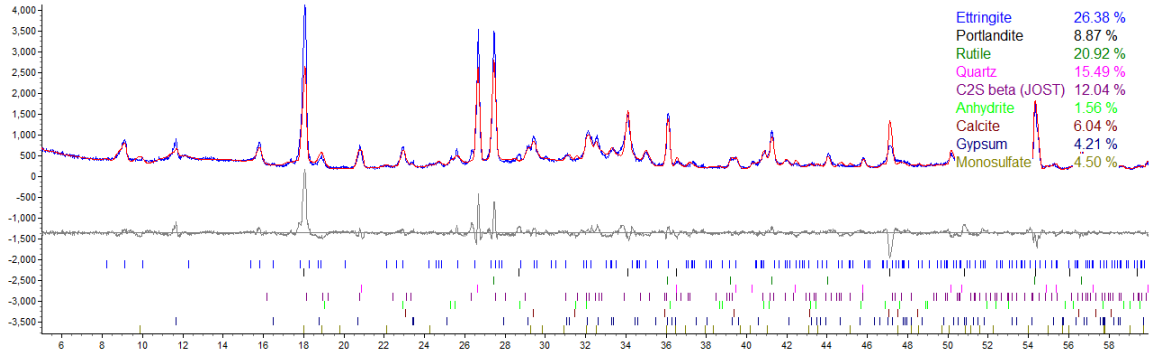

Figure A152 X-ray diffraction pattern and Rietveld refinement: C2-F1(20)-G(15).

28 Days C2-F1(20)-G(0A)

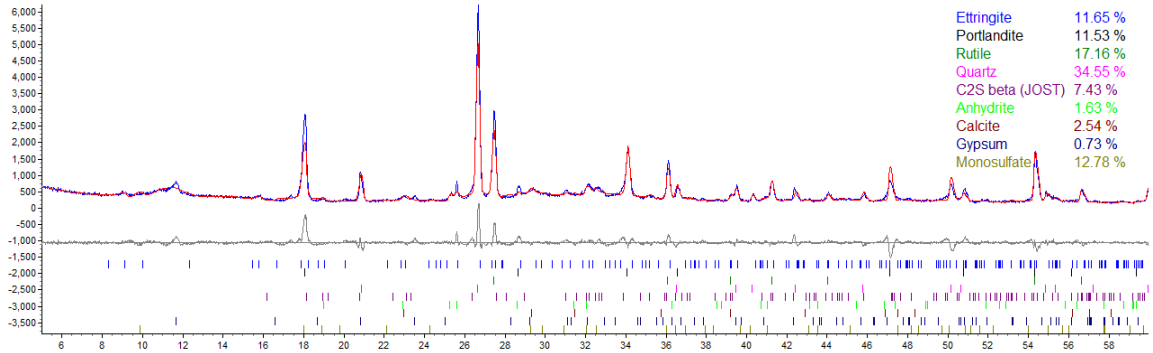

28 Days C2-F1(20)-G(0B)

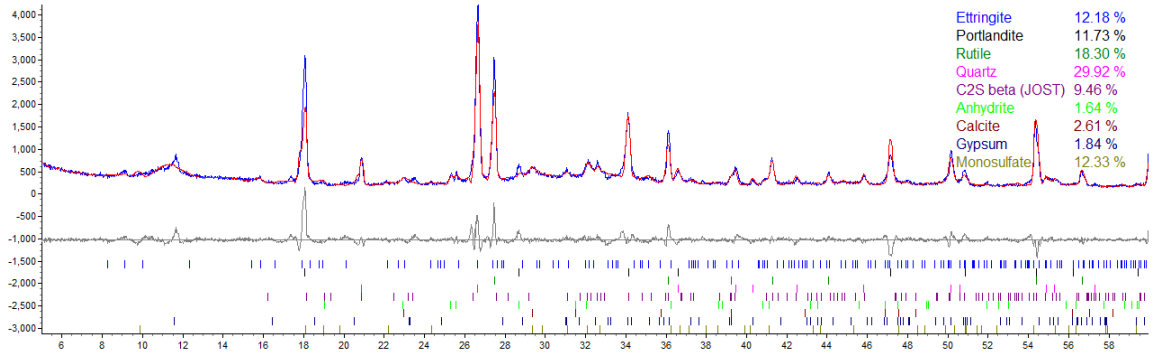

Figure A153 X-ray diffraction pattern and Rietveld refinement: C2-F1(20)-G(0) at 28 days.

28 Days C2-F1(20)-G(2A)

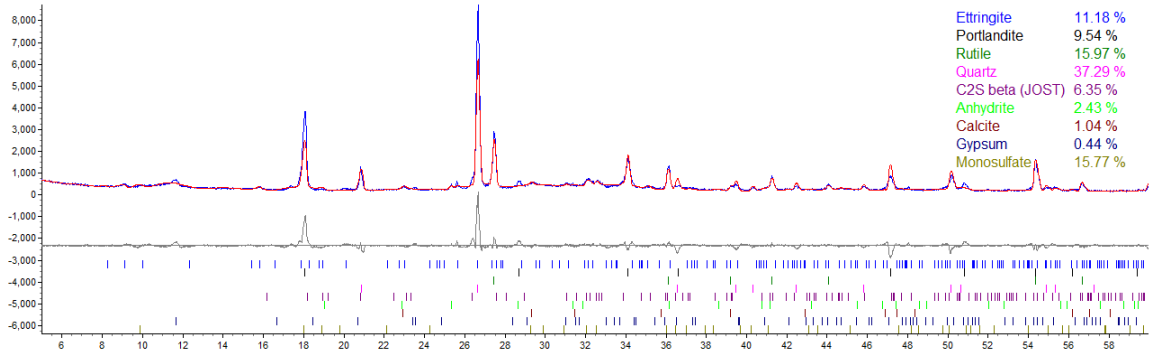

28 Days C2-F1(20)-G(2B)

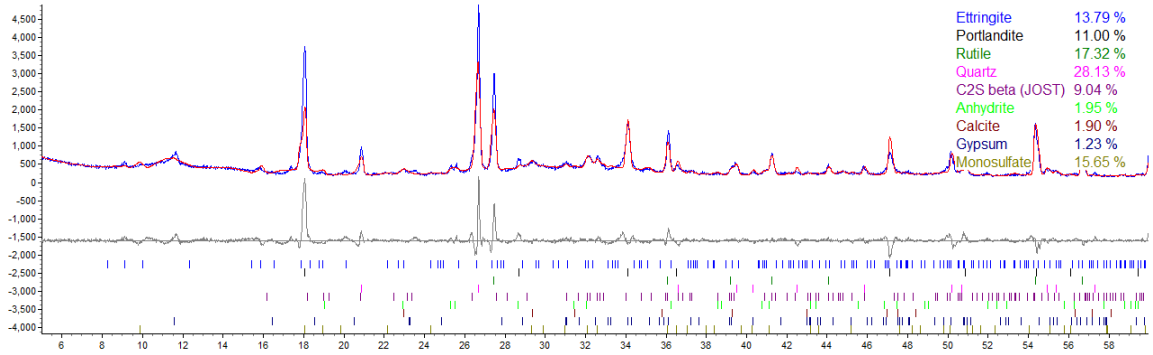

Figure A154 X-ray diffraction pattern and Rietveld refinement: C2-F1(20)-G(2) at 28 days.

28 Days C2-F1(20)-G(4B)

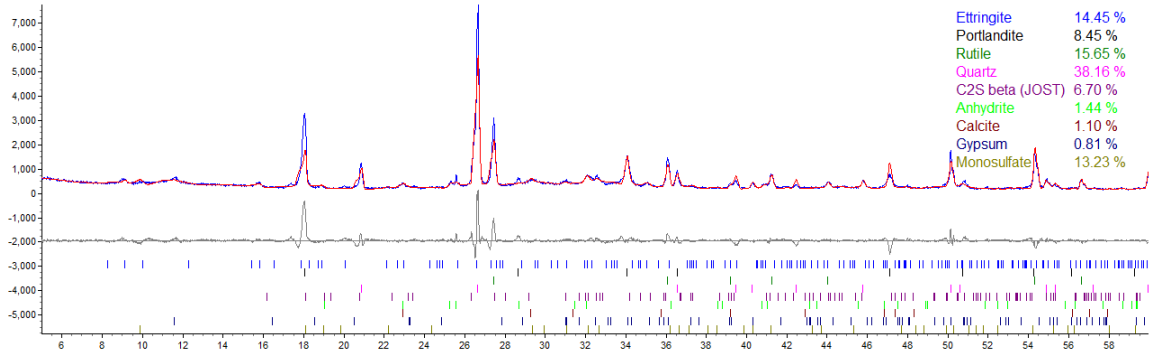

28 Days C2-F1(20)-G(4C

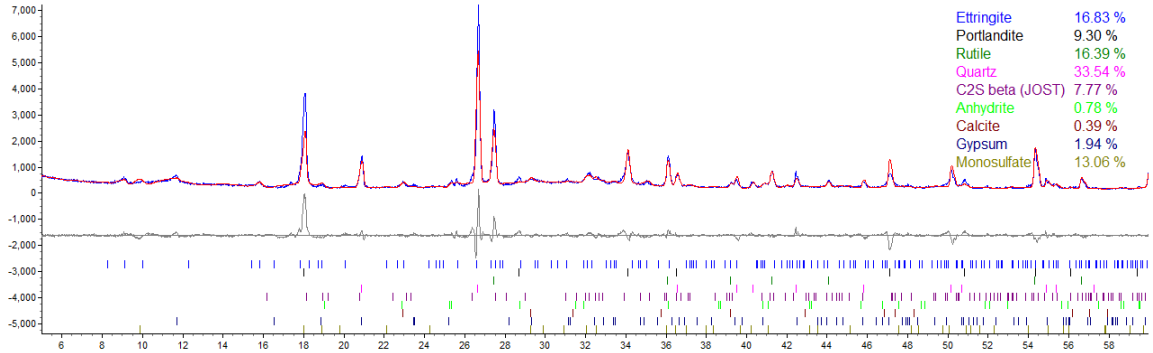

Figure A155 X-ray diffraction pattern and Rietveld refinement: C2-F1(20)-G(4) at 28 days.

28 Days C2-F1(20)-G(6A)

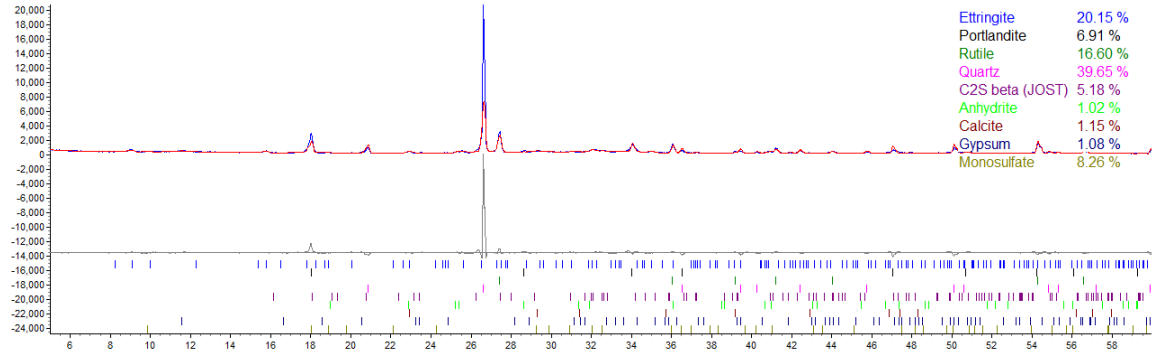

28 Days C2-F1(20)-G(6B)

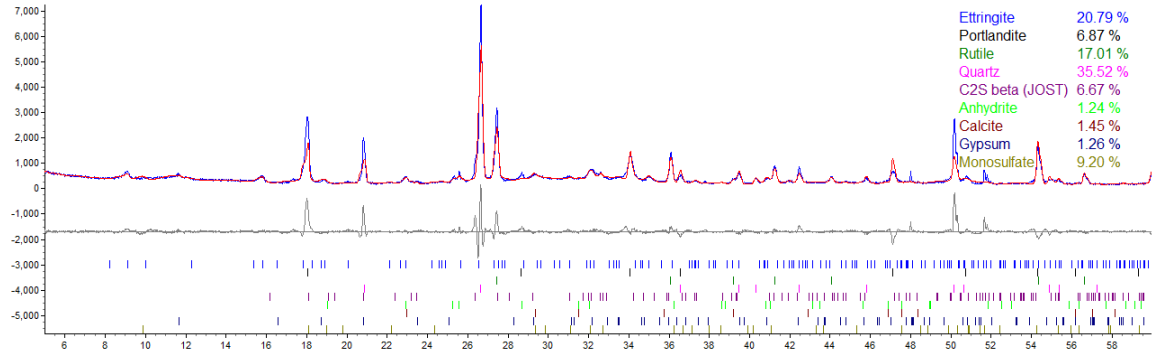

Figure A156 X-ray diffraction pattern and Rietveld refinement: C2-F1(20)-G(6) at 28 days.

28 Days C2-F1(20)-G(8A)

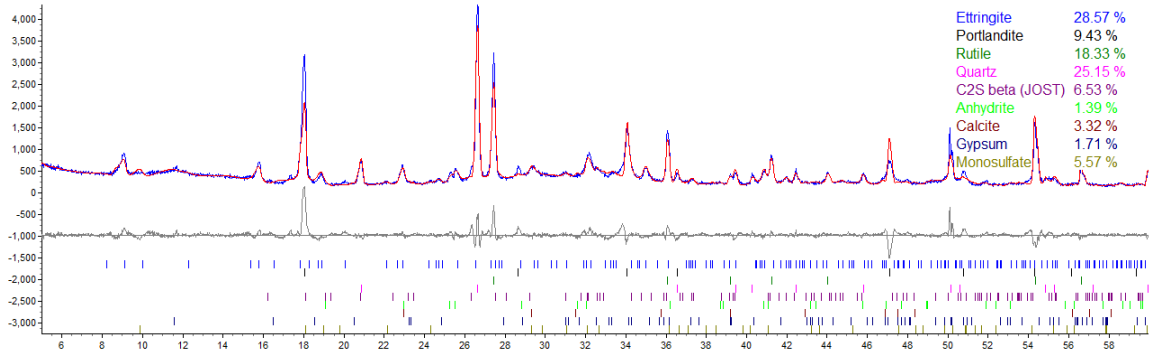

28 Days C2-F1(20)-G(8B)

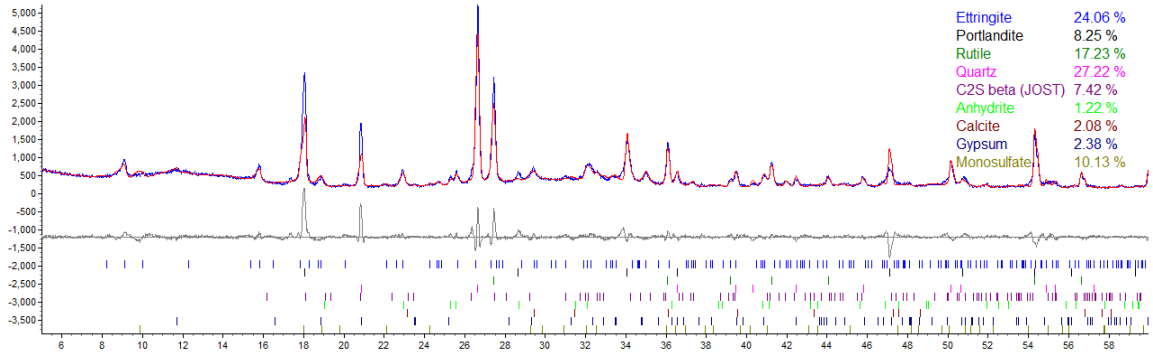

Figure A157 X-ray diffraction pattern and Rietveld refinement: C2-F1(20)-G(8) at 28 days.

28 Days C2-F1(20)-G(10A)

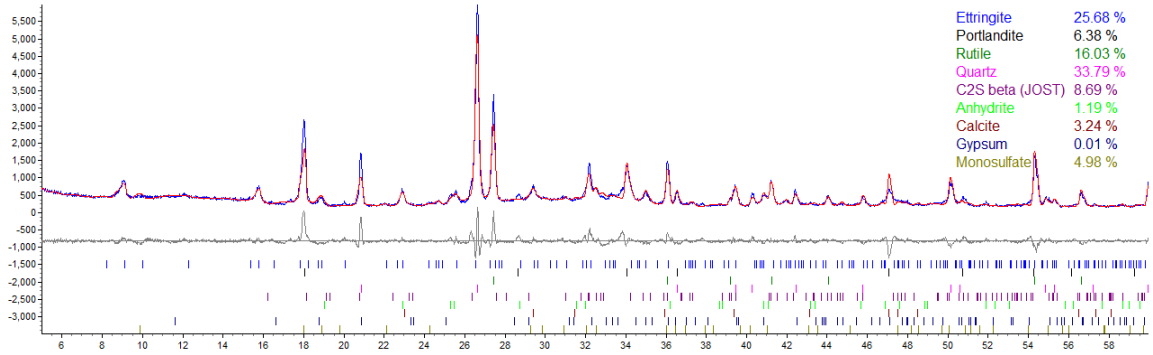

28 Days C2-F1(20)-G(10B)

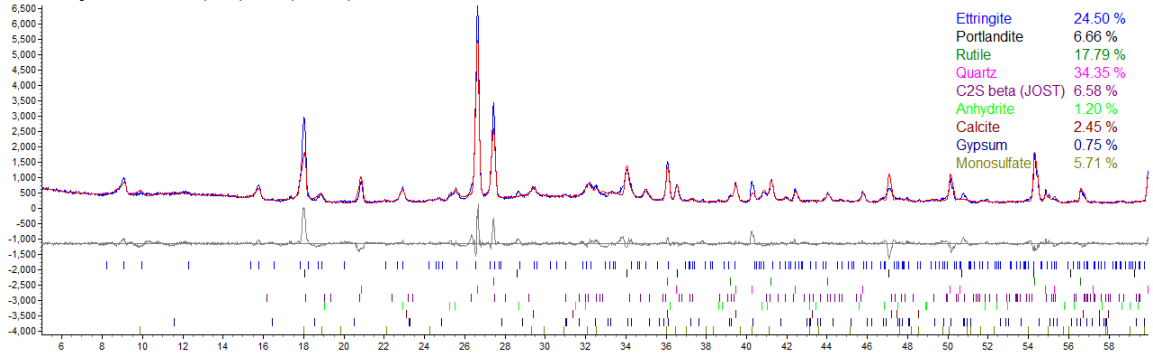

Figure A158 X-ray diffraction pattern and Rietveld refinement: C2-F1(20)-G(10) at 28 days.

28 Days C2-F1(20)-G(12A))))

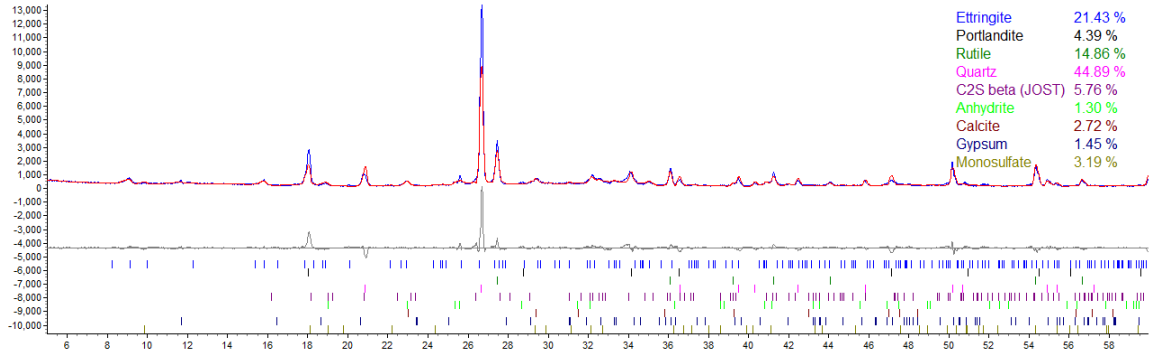

28 Days C2-F1(20)-G(12B)

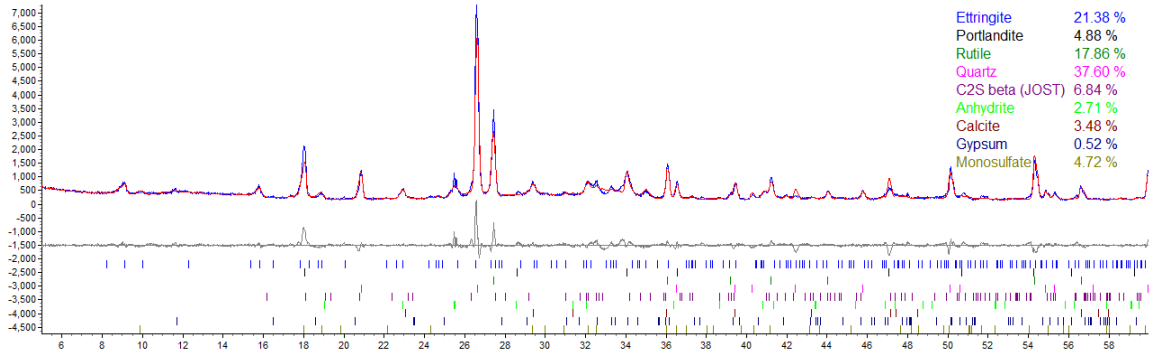

Figure A159 X-ray diffraction pattern and Rietveld refinement: C2-F1(20)-G(12) at 28 days.

28 Days C2-F1(20)-G(15A)

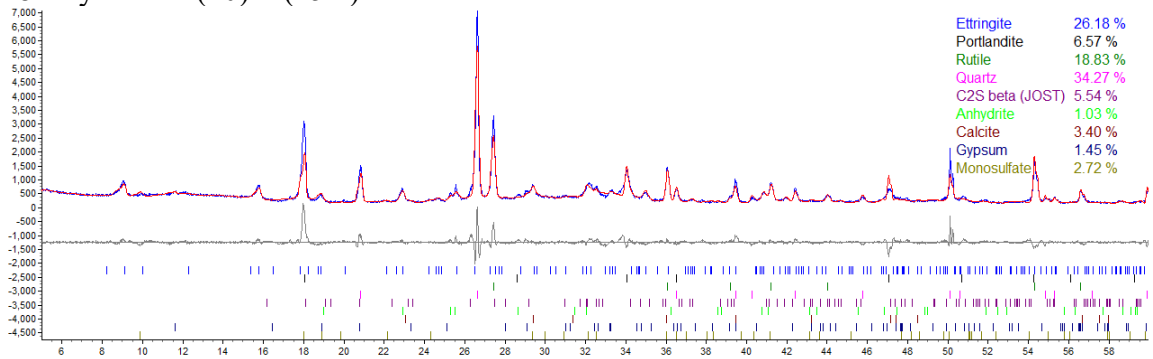

28 Days C2-F1(20)-G(15B)

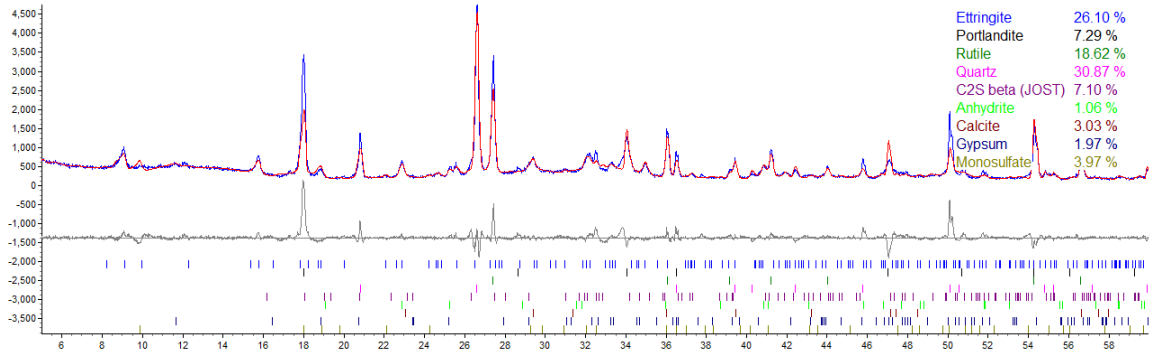

Figure A160 X-ray diffraction pattern and Rietveld refinement: C2-F1(20)-G(15) at 28 days.

C2-F2(20)-G(0A)

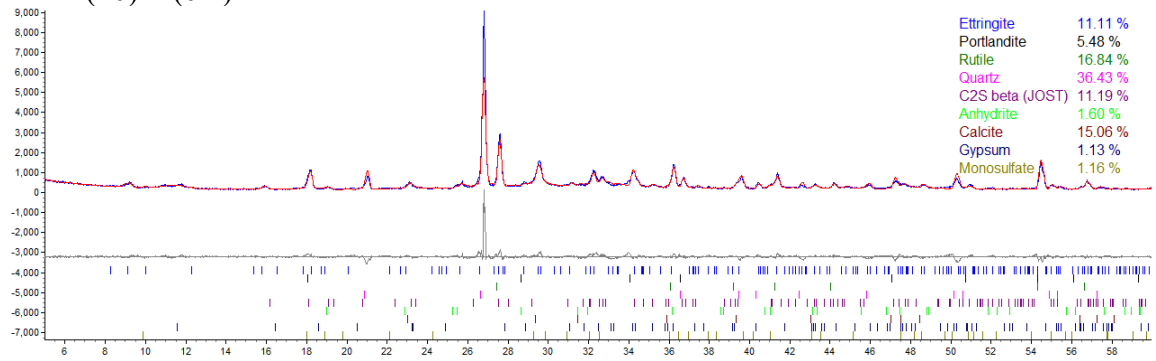

C2-F2(20)-G(0B)

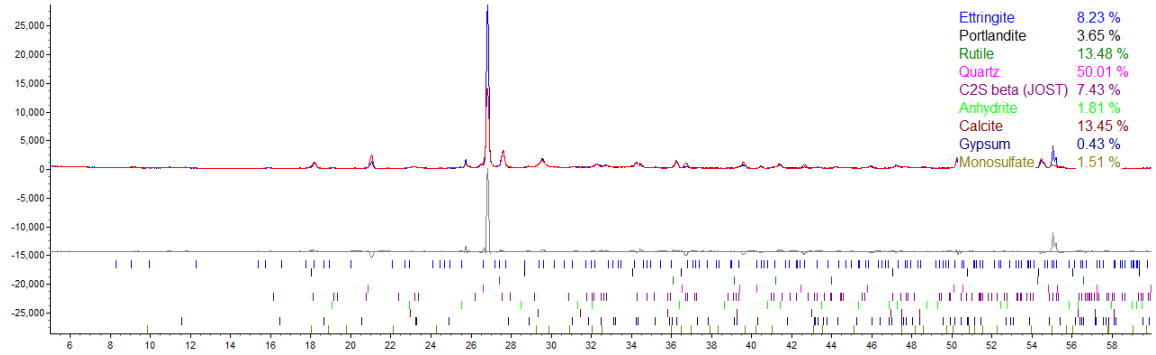

Figure A161 X-ray diffraction pattern and Rietveld refinement: C2-F2(20)-G(0).

C2-F2(20)-G(2A)

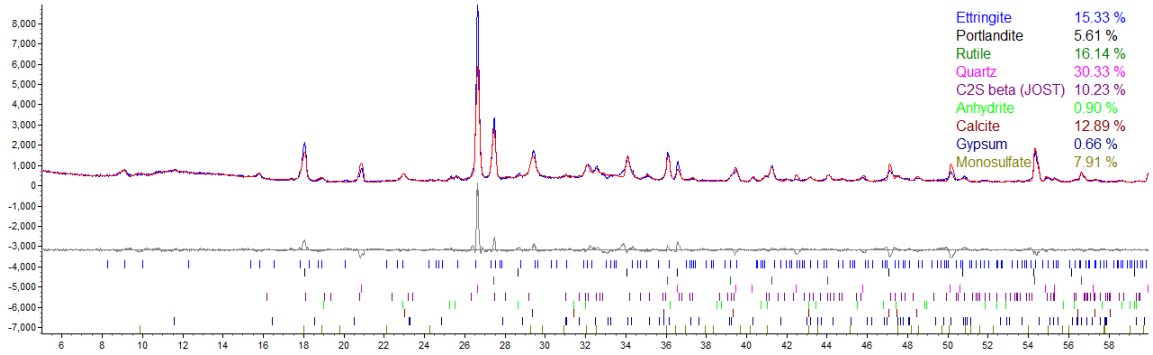

C2-F2(20)-G(2C)

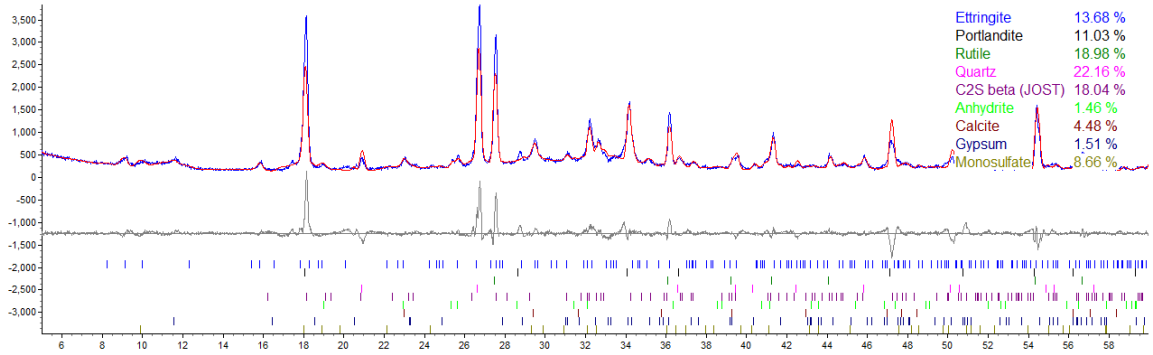

Figure A162 X-ray diffraction pattern and Rietveld refinement: C2-F2(20)-G(2).

C2-F2(20)-G(4A)

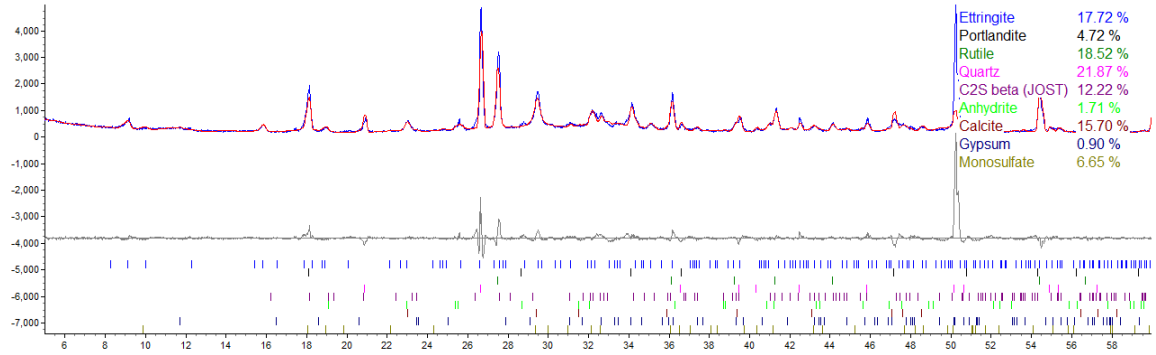

C2-F2(20)-G(4B)

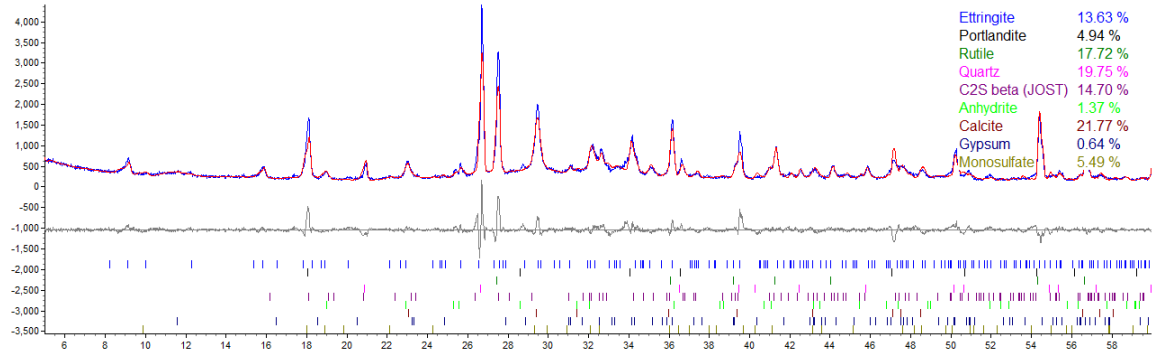

Figure A163 X-ray diffraction pattern and Rietveld refinement: C2-F2(20)-G(4).

C2-F2(20)-G(6A)

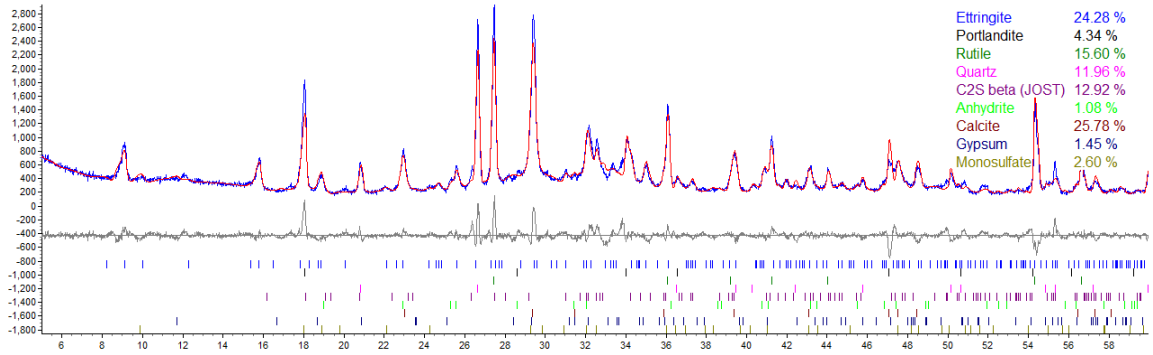

C2-F2(20)-G(6B)

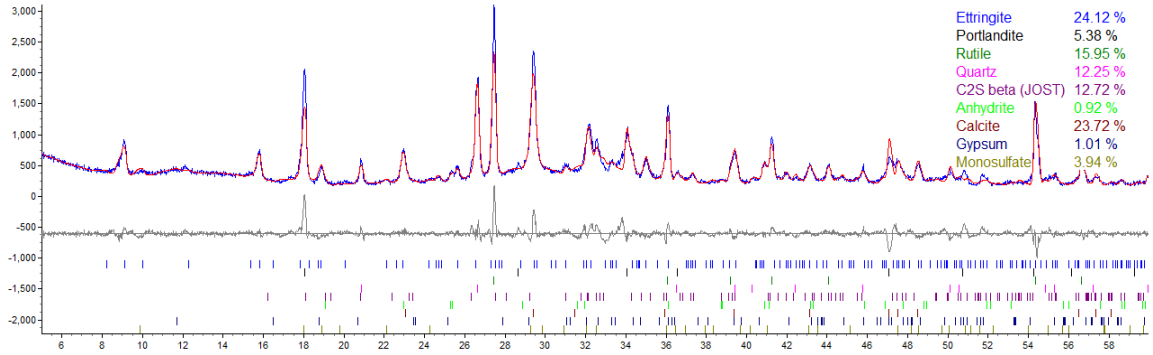

Figure A164 X-ray diffraction pattern and Rietveld refinement: C2-F2(20)-G(6).

C2-F2(20)-G(8A)

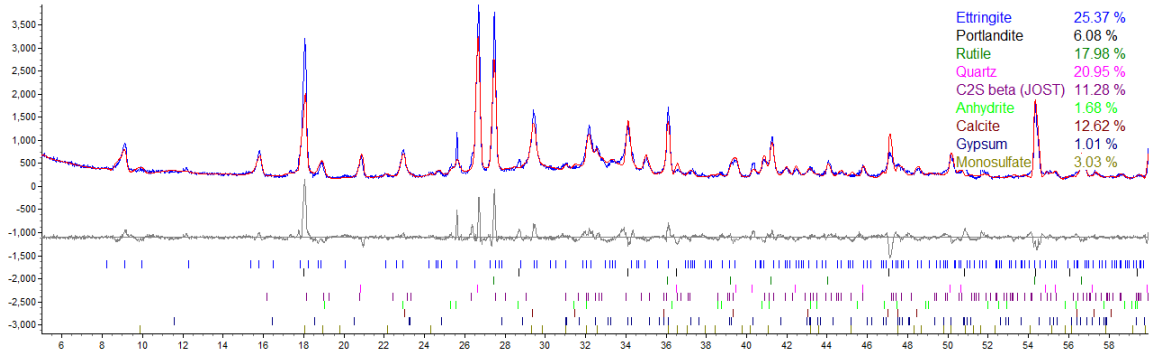

C2-F2(20)-G(8B)

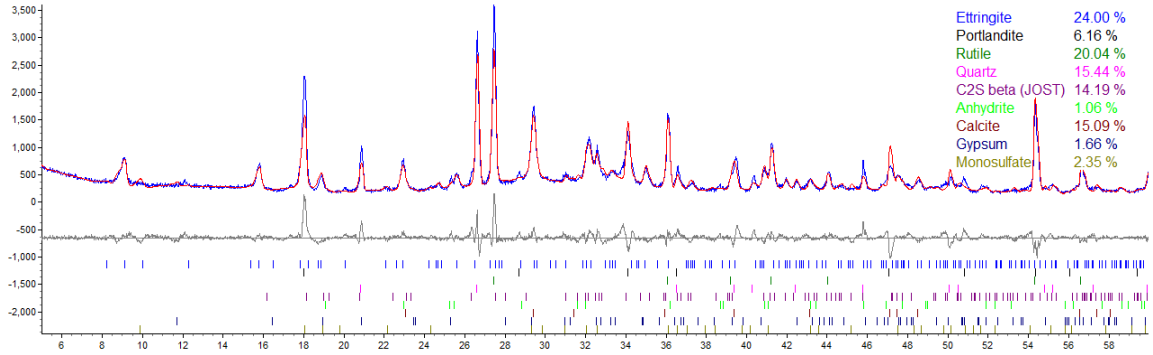

Figure A165 X-ray diffraction pattern and Rietveld refinement: C2-F2(20)-G(8).

C2-F2(20)-G(10A)

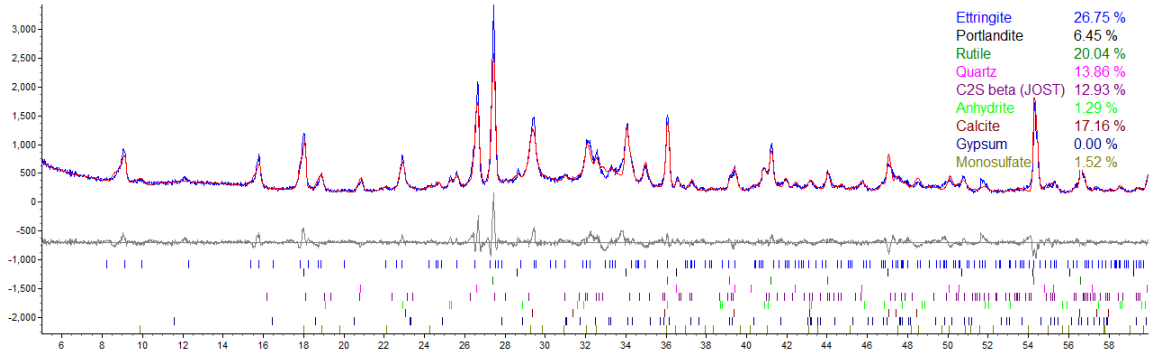

C2-F2(20)-G(10B)

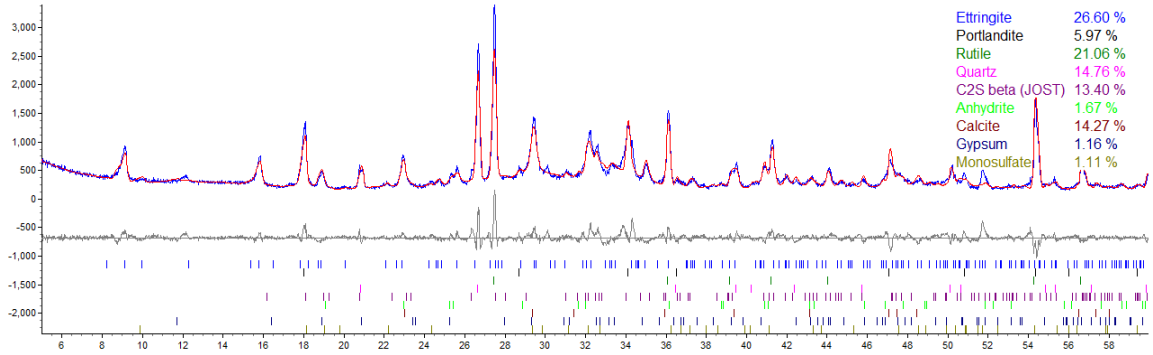

Figure A166 X-ray diffraction pattern and Rietveld refinement: C2-F2(20)-G(10).

C2-F2(20)-G(12A)

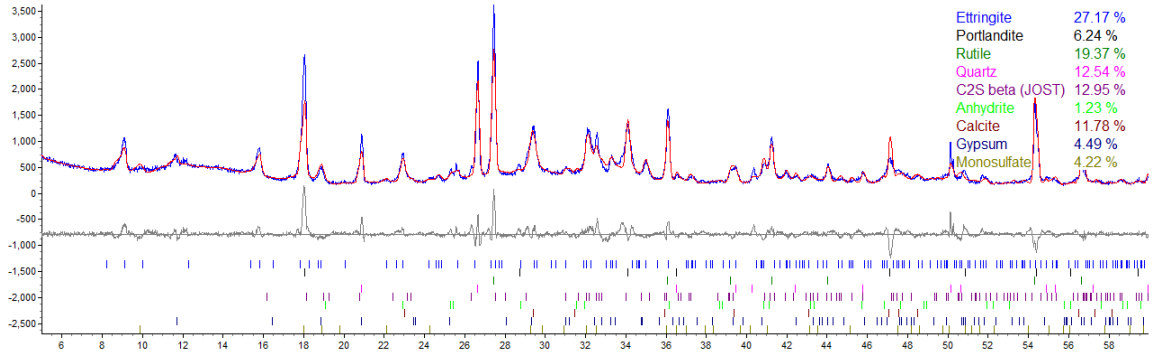

C2-F2(20)-G(12B)

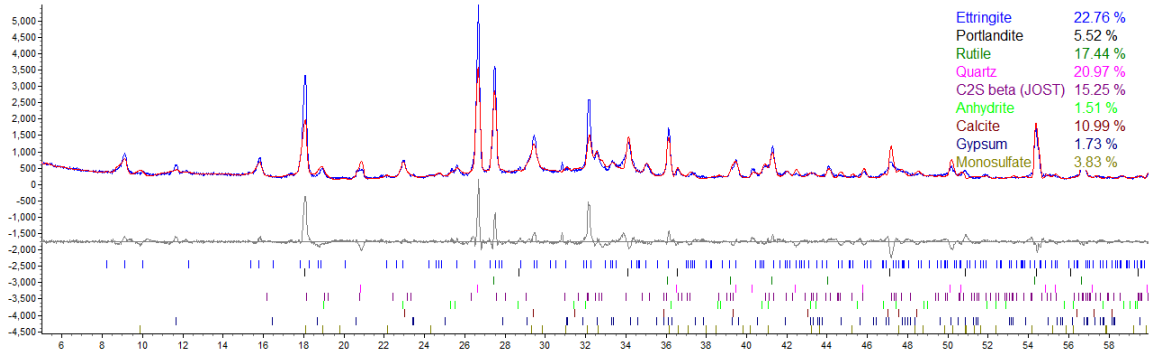

Figure A167 X-ray diffraction pattern and Rietveld refinement: C2-F2(20)-G(12).

C2-F2(20)-G(15A)

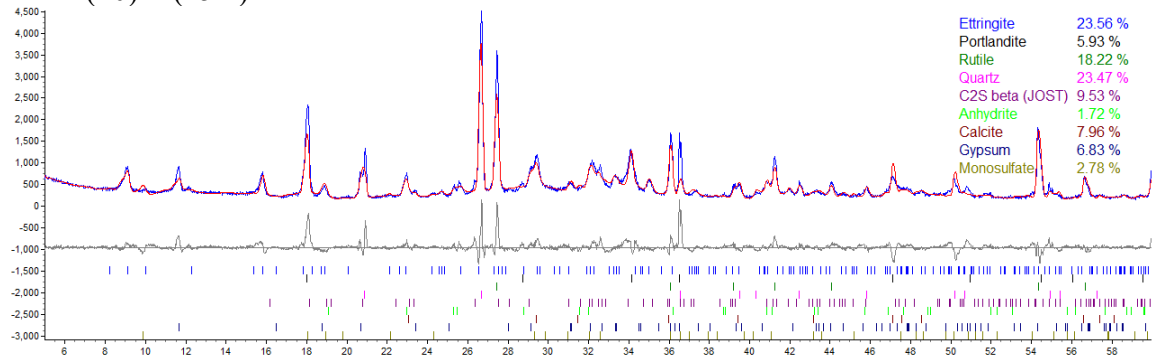

C2-F2(20)-G(15B)

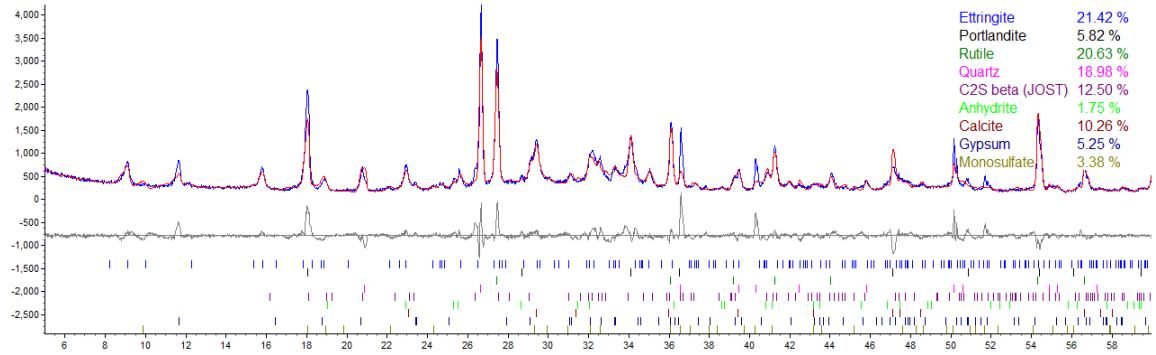

Figure A168 X-ray diffraction pattern and Rietveld refinement: C2-F2(20)-G(15).

28 Days C2-F2(20)-G(0A)

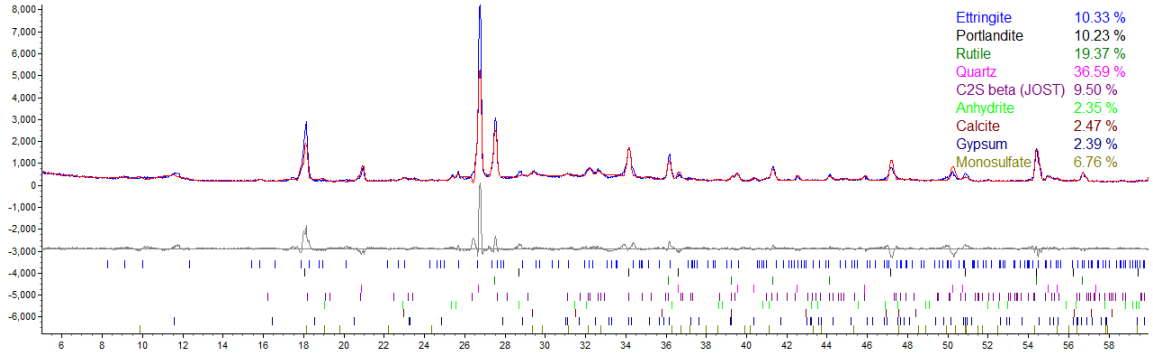

28 Days C2-F2(20)-G(0C)

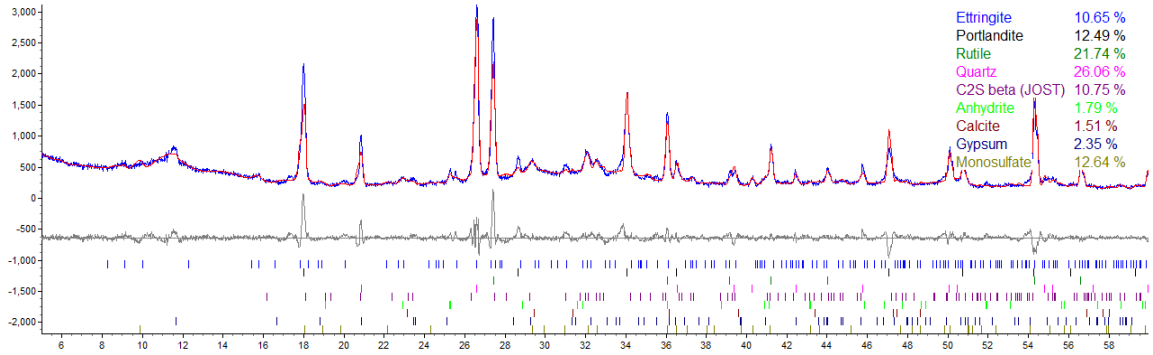

Figure A169 X-ray diffraction pattern and Rietveld refinement: C2-F2(20)-G(0) at 28 days.

28 Days C2-F2(20)-G(2A)

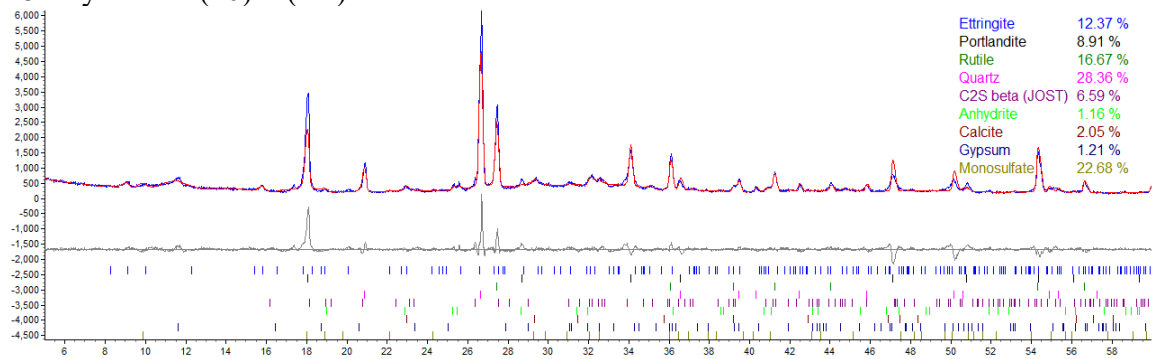

28 Days C2-F2(20)-G(2C)

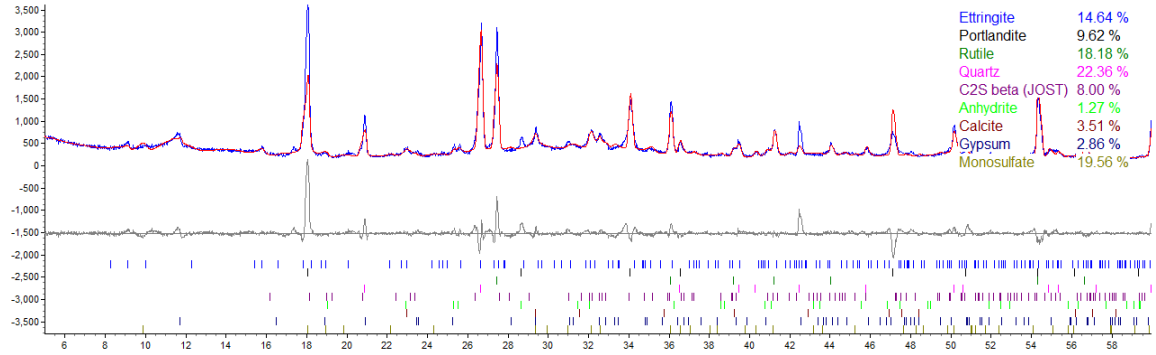

Figure A170 X-ray diffraction pattern and Rietveld refinement: C2-F2(20)-G(2) at 28 days.

28 Days C2-F2(20)-G(4A)

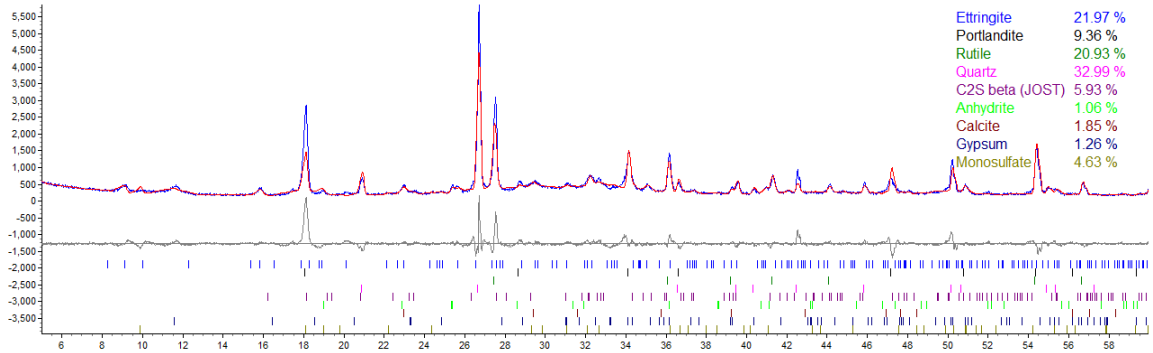

28 Days C2-F2(20)-G(4B)

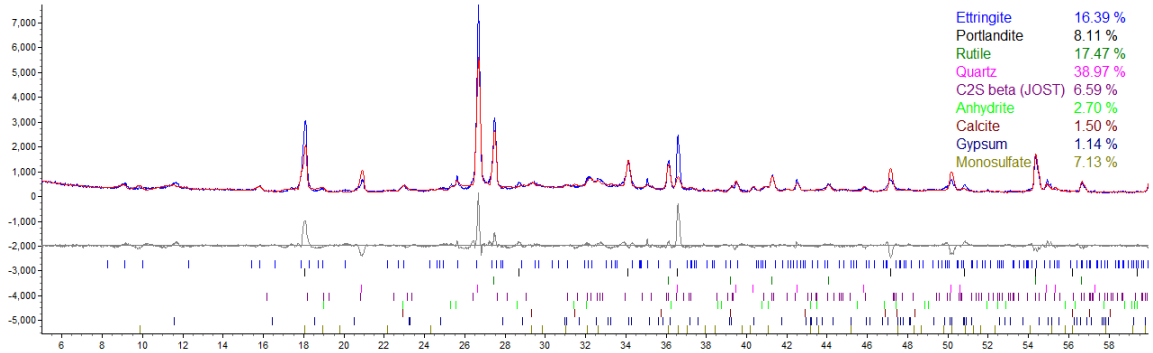

Figure A171 X-ray diffraction pattern and Rietveld refinement: C2-F2(20)-G(4) at 28 days.

28 Days C2-F2(20)-G(6A)

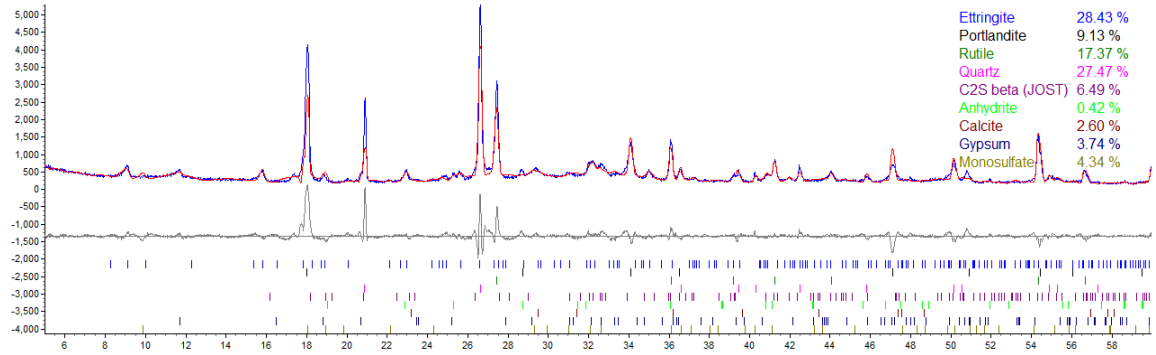

28 Days C2-F2(20)-G(6B)

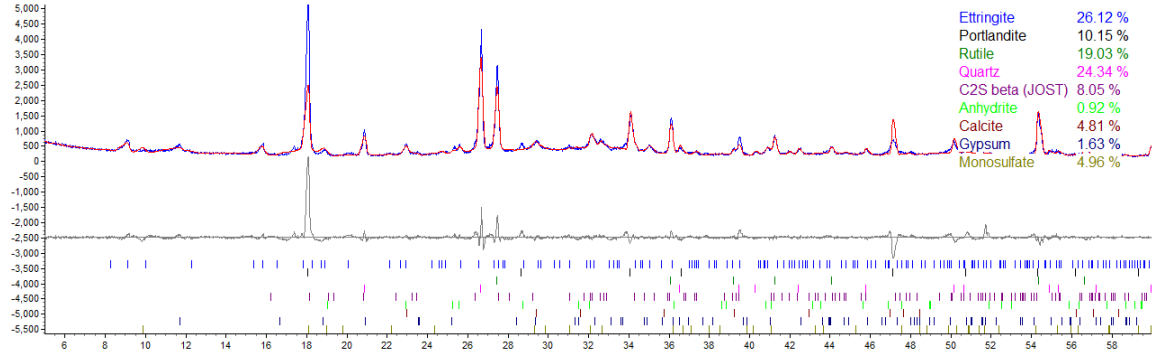

Figure A172 X-ray diffraction pattern and Rietveld refinement: C2-F2(20)-G(6) at 28 days.

28 Days C2-F2(20)-G(8A)

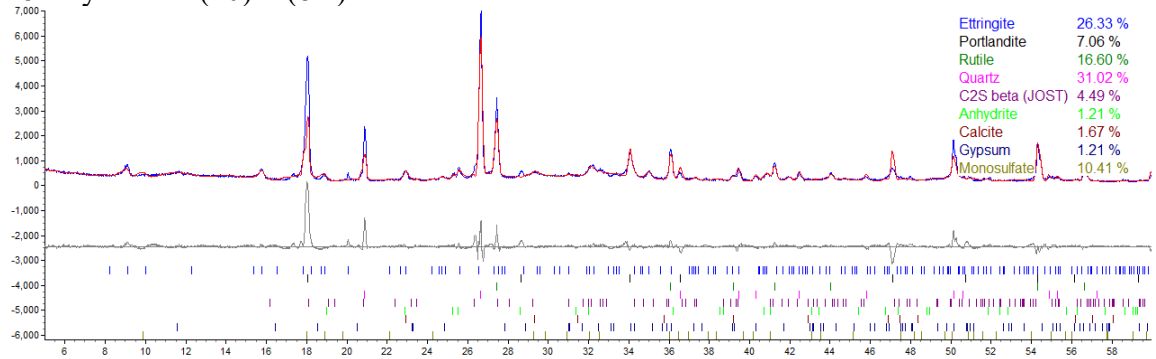

28 Days C2-F2(20)-G(8C)

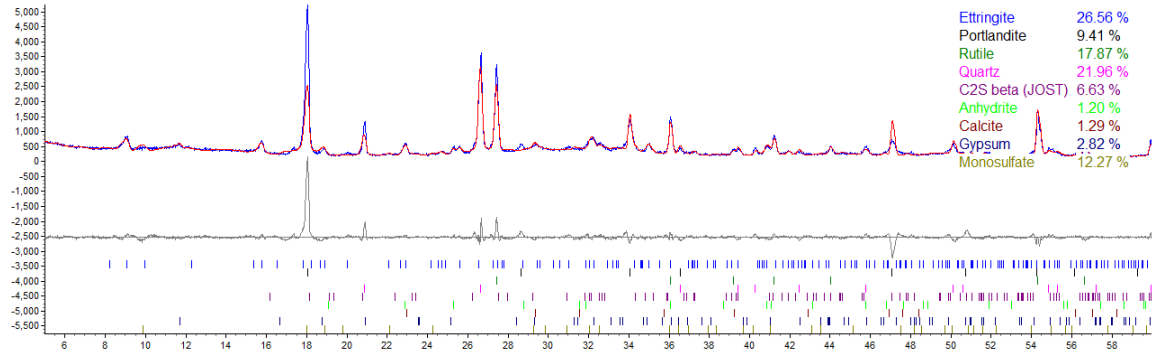

Figure A173 X-ray diffraction pattern and Rietveld refinement: C2-F2(20)-G(8) at 28 days.

28 Days C2-F2(20)-G(10A)

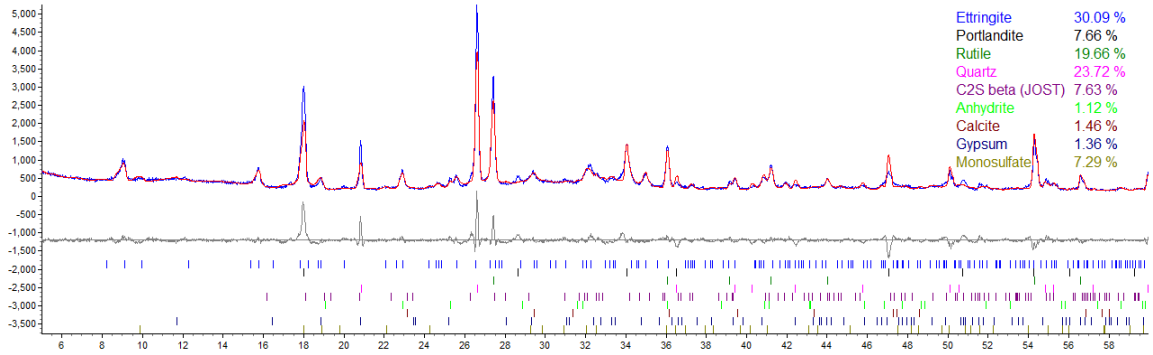

28 Days C2-F2(20)-G(10B)

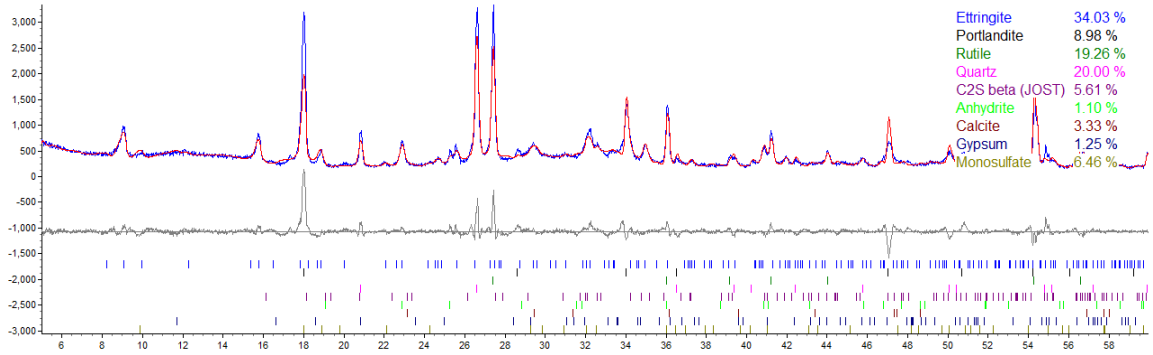

Figure A174 X-ray diffraction pattern and Rietveld refinement: C2-F2(20)-G(10) at 28 days.

28 Days C2-F2(20)-G(12A)

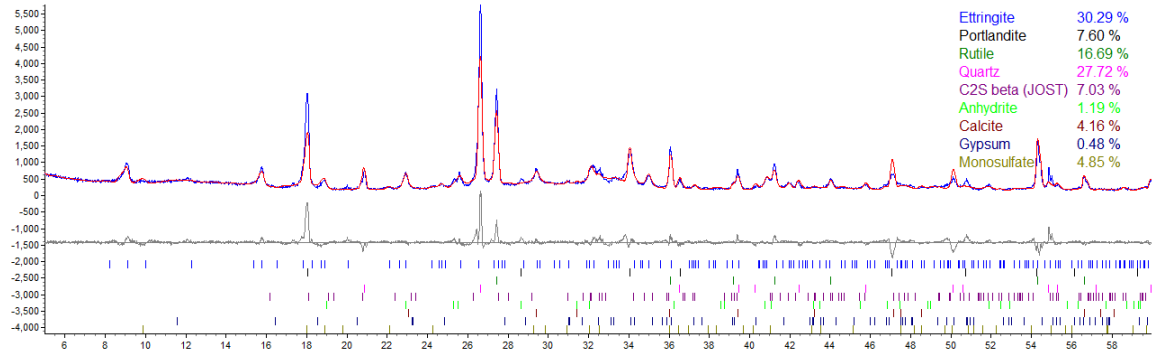

28 Days C2-F2(20)-G(12B)

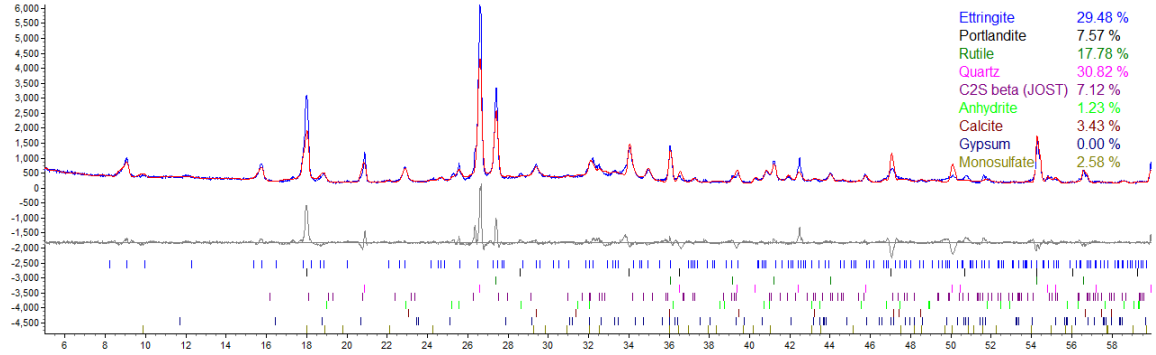

Figure A175 X-ray diffraction pattern and Rietveld refinement: C2-F2(20)-G(12) at 28 days.

28 Days C2-F2(20)-G(15A)

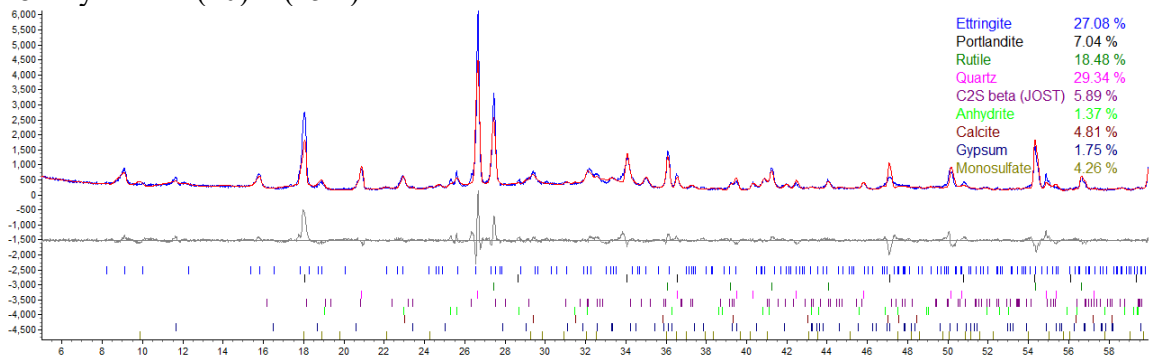

28 Days C2-F2(20)-G(15B)

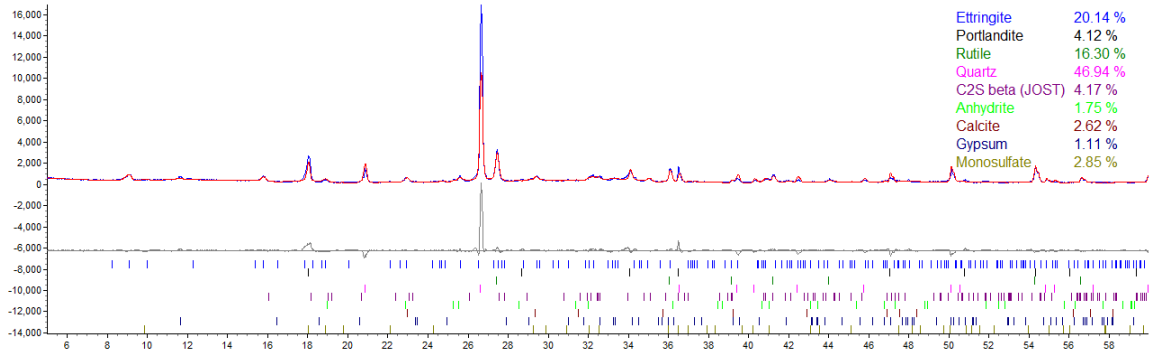

Figure A176 X-ray diffraction pattern and Rietveld refinement: C2-F2(20)-G(15) at 28 days.

C2-F3(20)-G(0A)

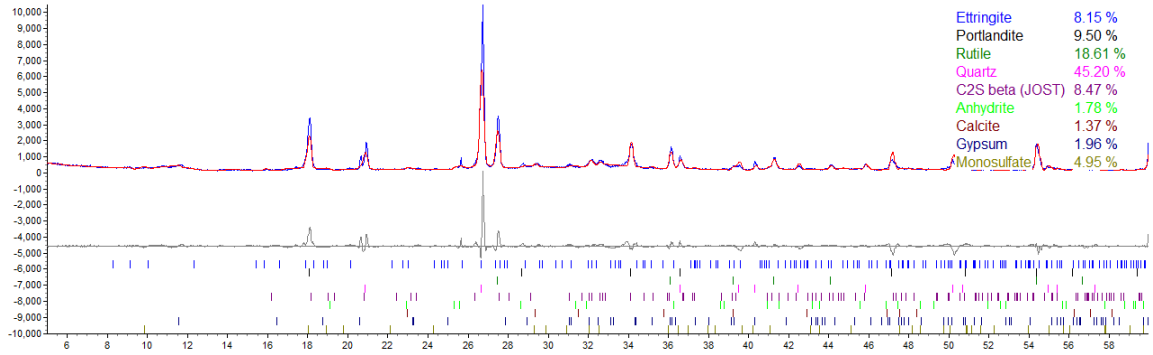

C2-F3(20)-G(0B)

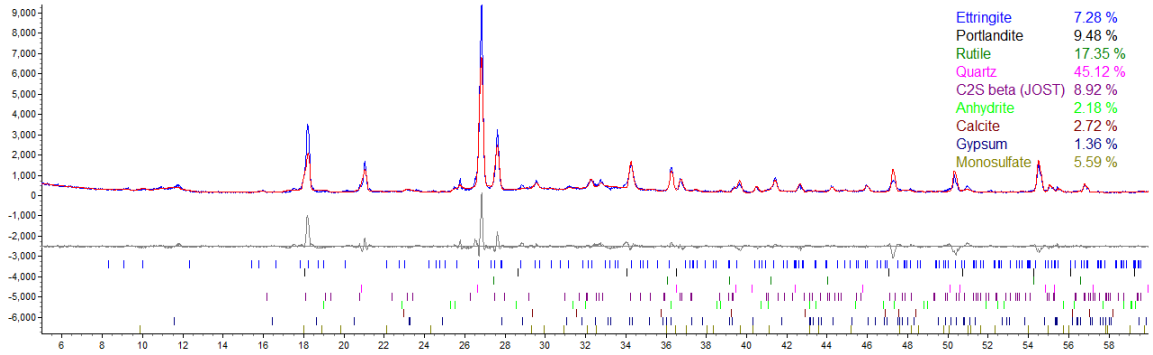

Figure A177 X-ray diffraction pattern and Rietveld refinement: C2-F3(20)-G(0).

C2-F3(20)-G(2A)

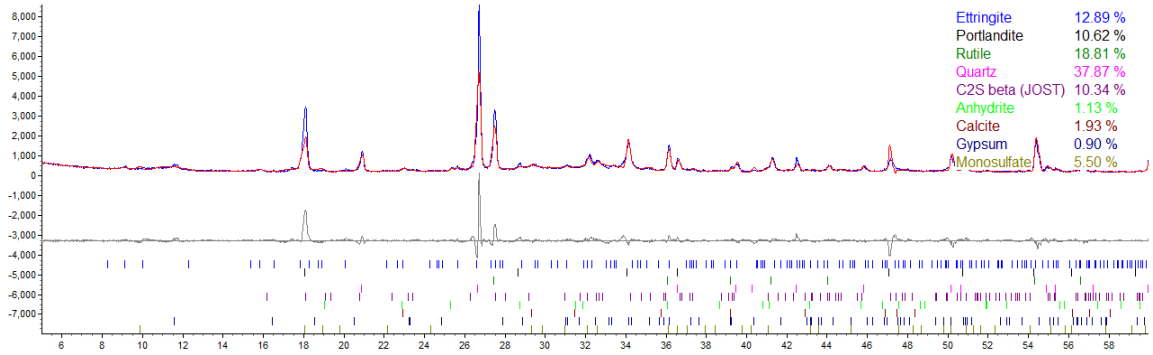

C2-F3(20)-G(2B)

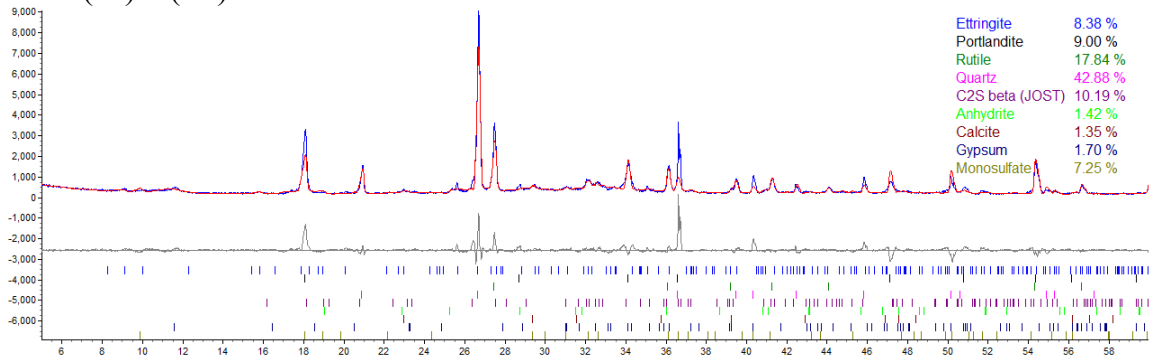

Figure A178 X-ray diffraction pattern and Rietveld refinement: C2-F3(20)-G(2).

C2-F3(20)-G(4A)

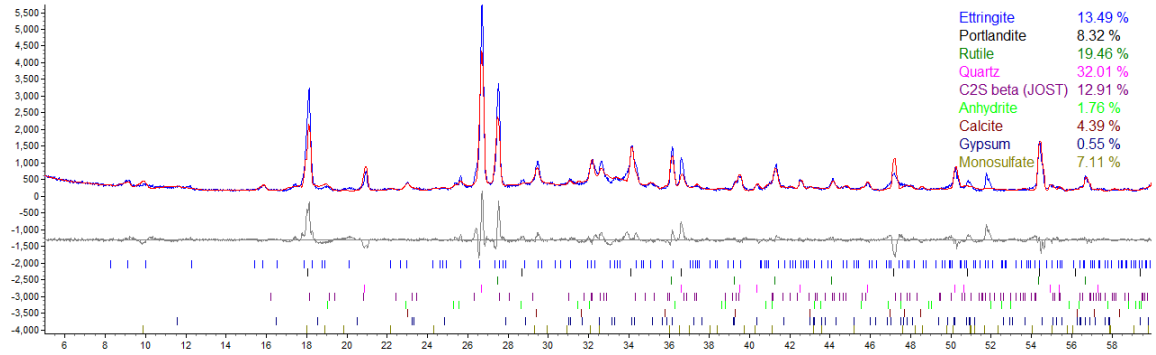

C2-F3(20)-G(4B)

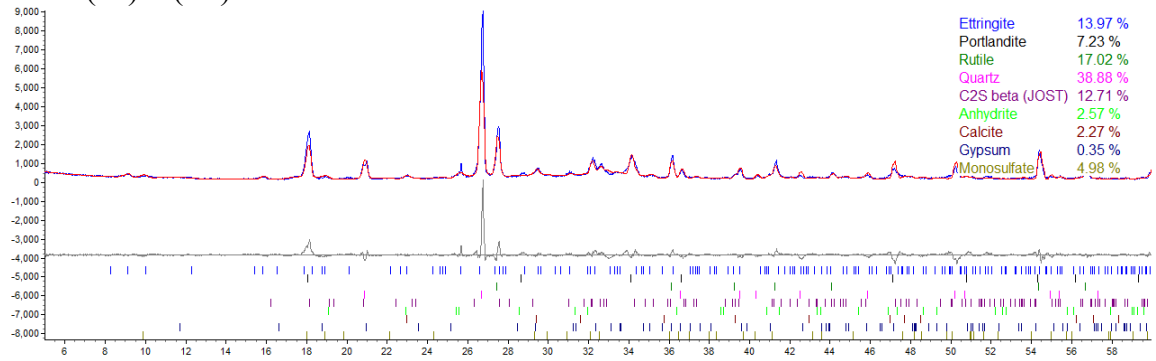

Figure A179 X-ray diffraction pattern and Rietveld refinement: C2-F3(20)-G(4).

C2-F3(20)-G(6A)

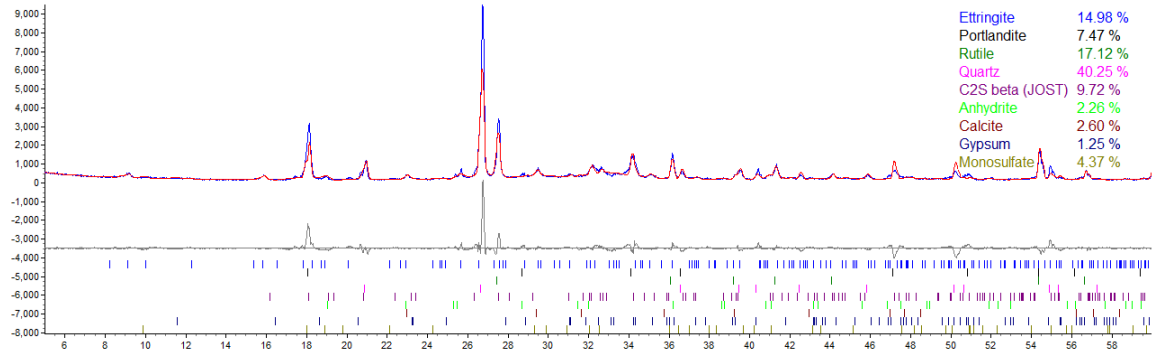

C2-F3(20)-G(6B)

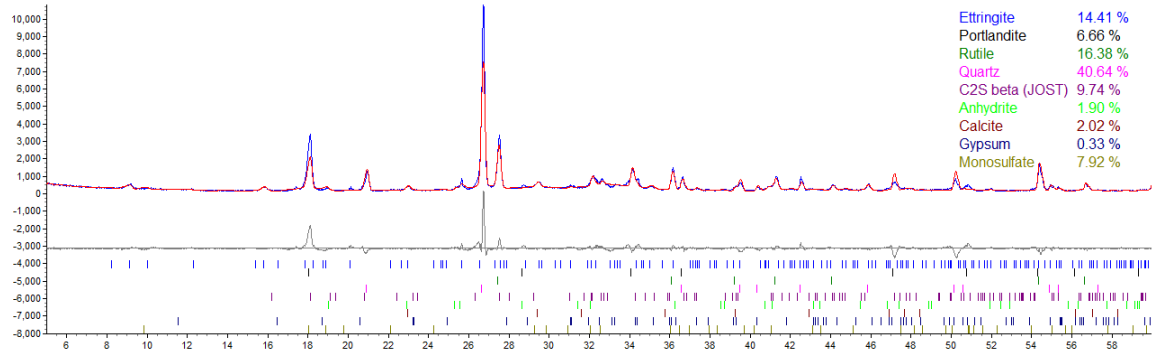

Figure A180 X-ray diffraction pattern and Rietveld refinement: C2-F3(20)-G(6).

C2-F3(20)-G(8A)

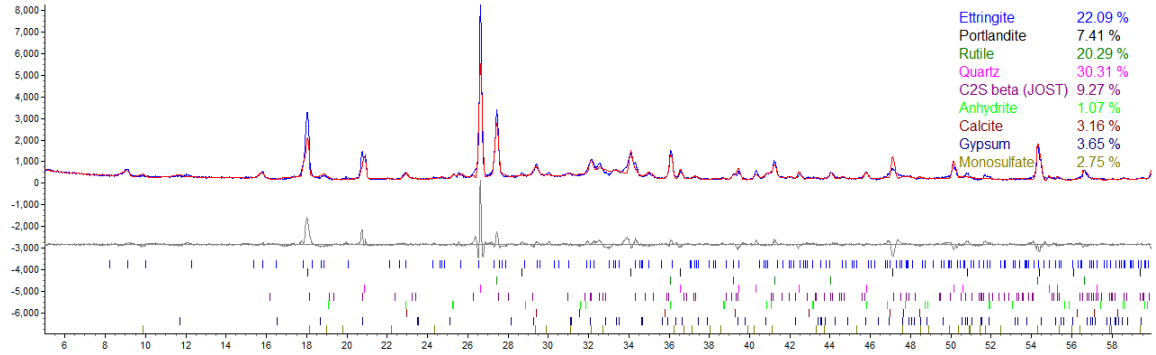

C2-F3(20)-G(8B)

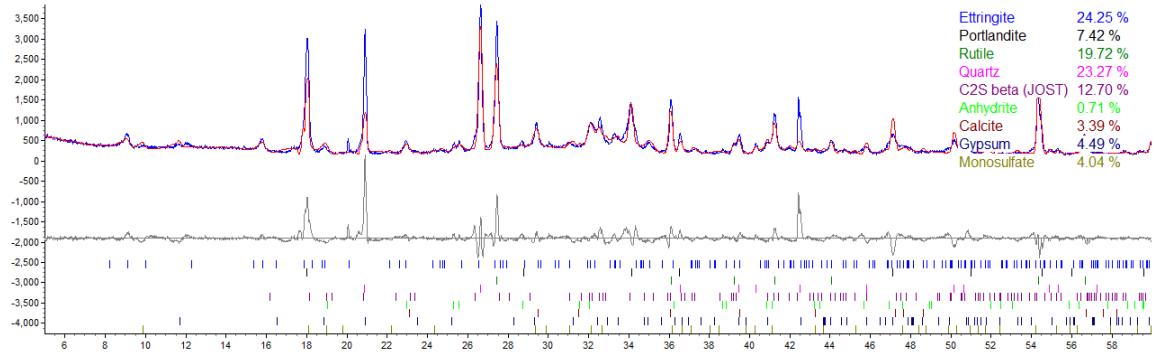

Figure A181 X-ray diffraction pattern and Rietveld refinement: C2-F3(20)-G(8).

C2-F3(20)-G(10A)

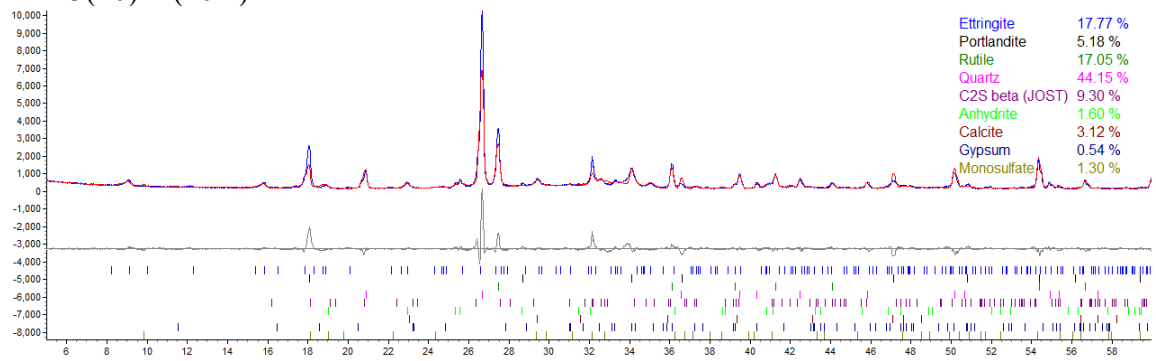

C2-F3(20)-G(10B)

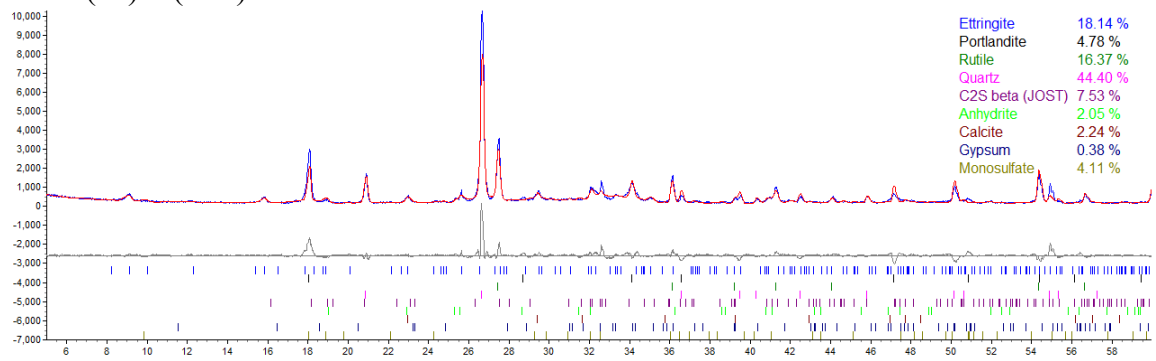

Figure A182 X-ray diffraction pattern and Rietveld refinement: C2-F3(20)-G(10).

C2-F3(20)-G(12A)

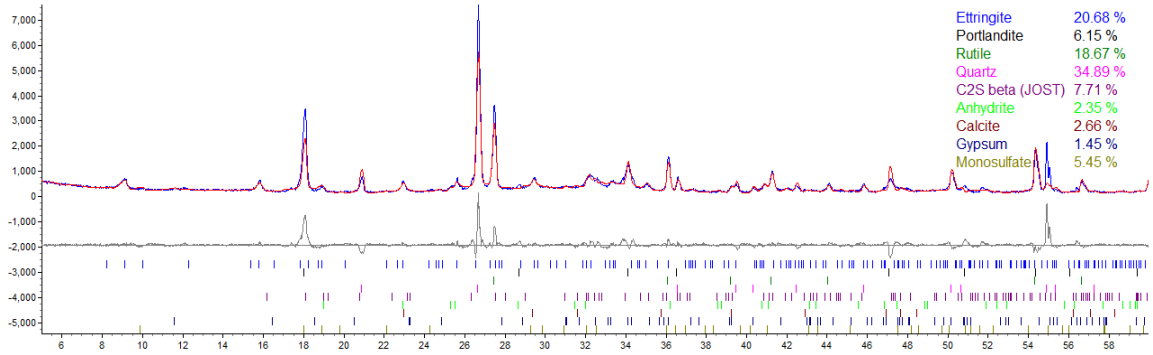

C2-F3(20)-G(12B)

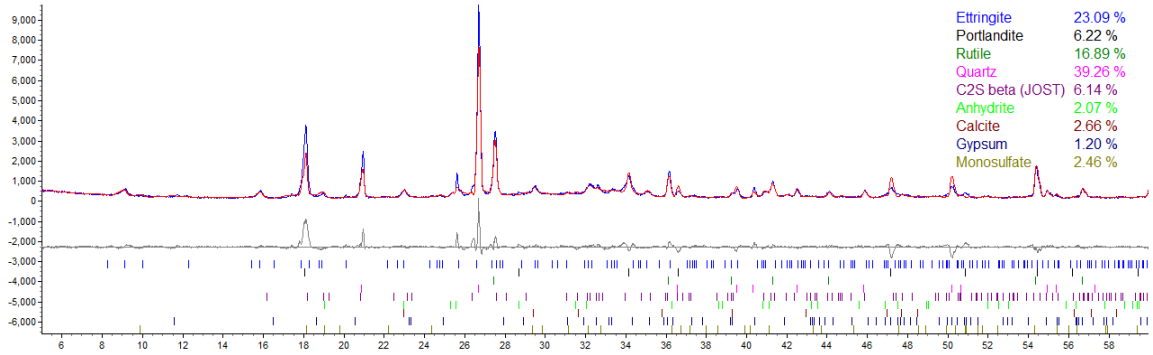

Figure A183 X-ray diffraction pattern and Rietveld refinement: C2-F3(20)-G(12).

C2-F3(20)-G(15A)

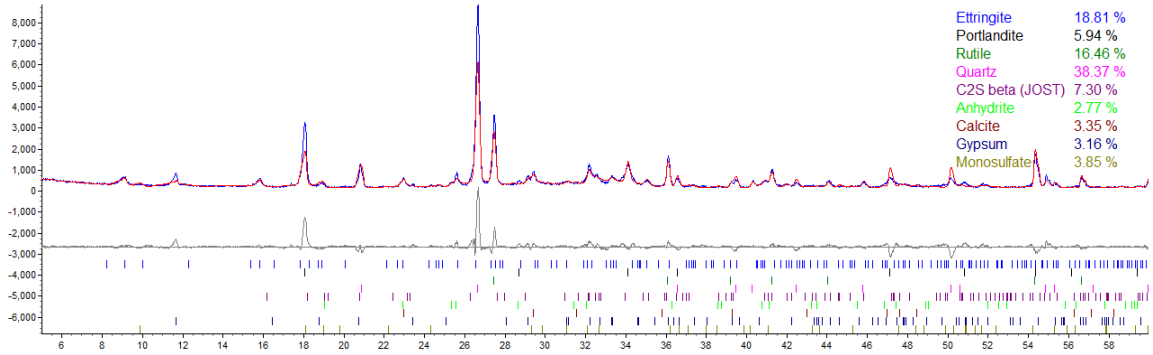

C2-F3(20)-G(15B)

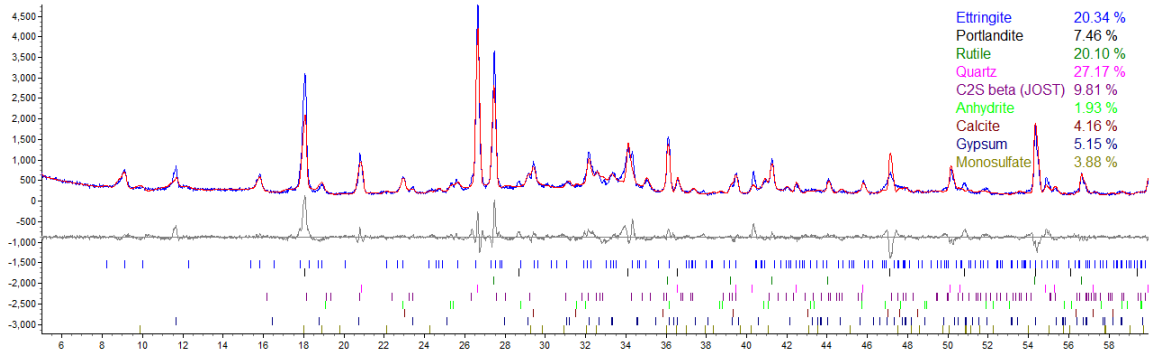

Figure A184 X-ray diffraction pattern and Rietveld refinement: C2-F3(20)-G(15).

28 Days C2-F3(20)-G(0B)

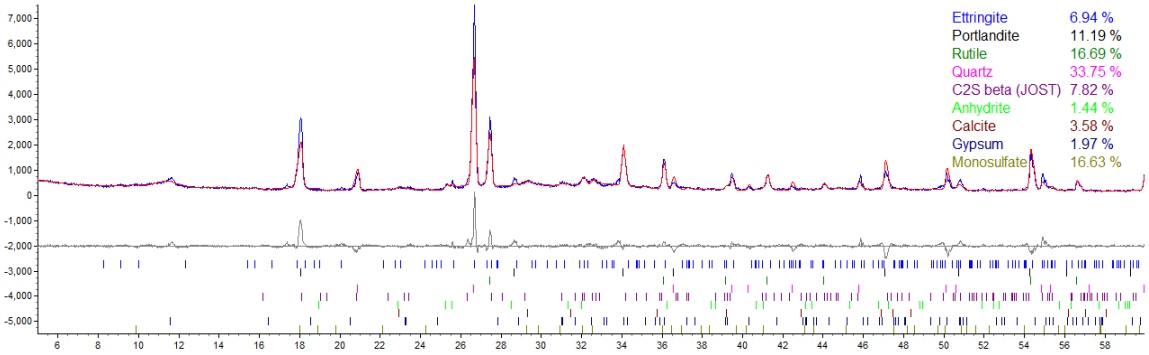

28 Days C2-F3(20)-G(0C)

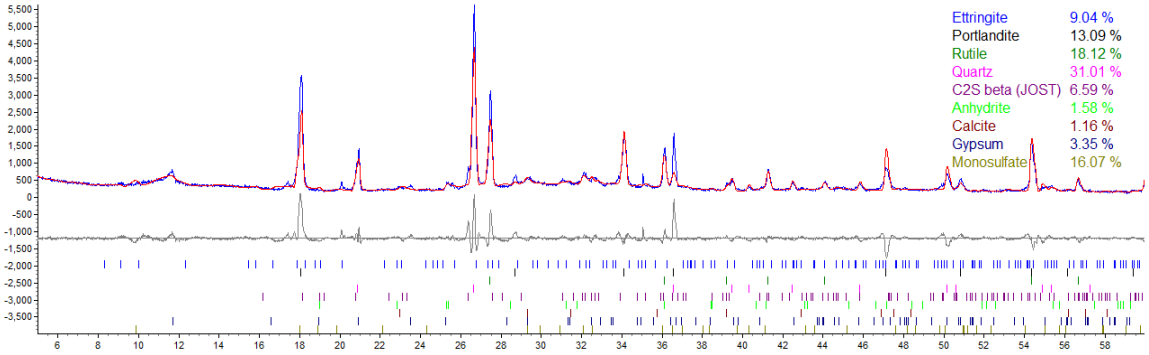

Figure A185 X-ray diffraction pattern and Rietveld refinement: C2-F3(20)-G(0) at 28 days.

28 Days C2-F3(20)-G(2B)

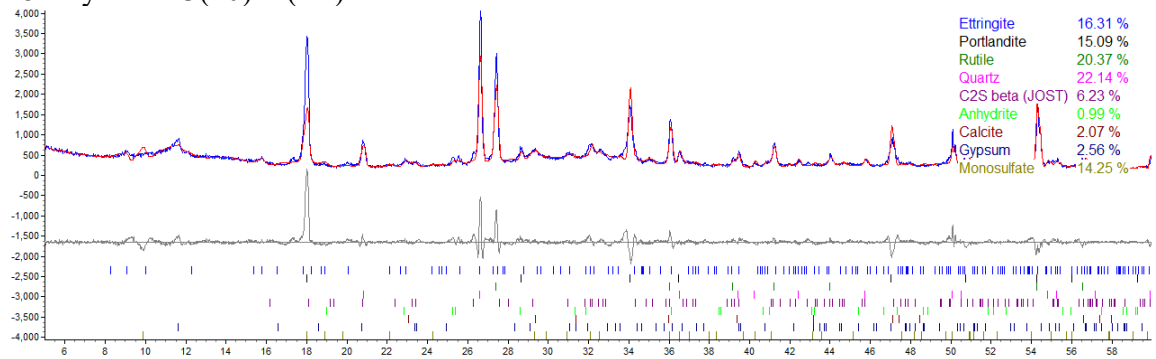

28 Days C2-F3(20)-G(2C)

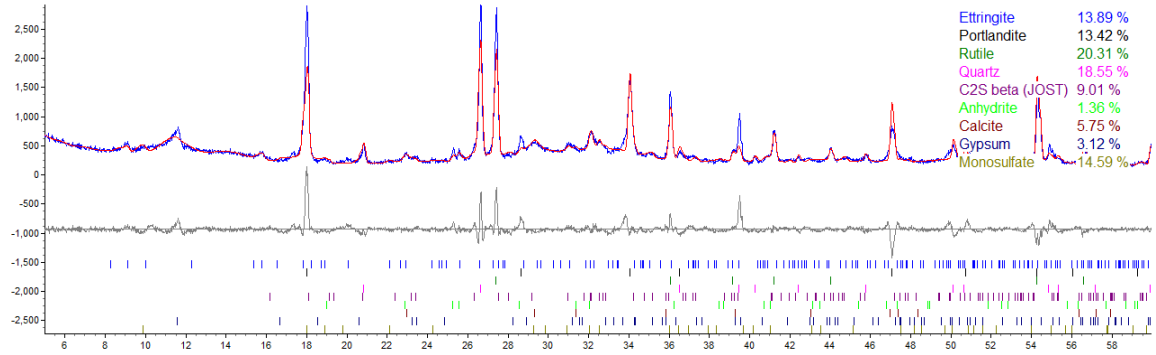

Figure A186 X-ray diffraction pattern and Rietveld refinement: C2-F3(20)-G(2) at 28 days.

28 Days C2-F3(20)-G(4A)

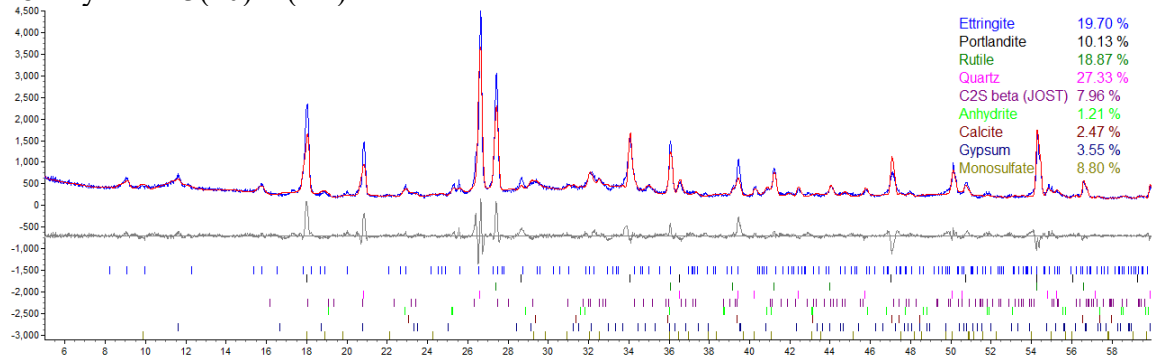

28 Days C2-F3(20)-G(4B)

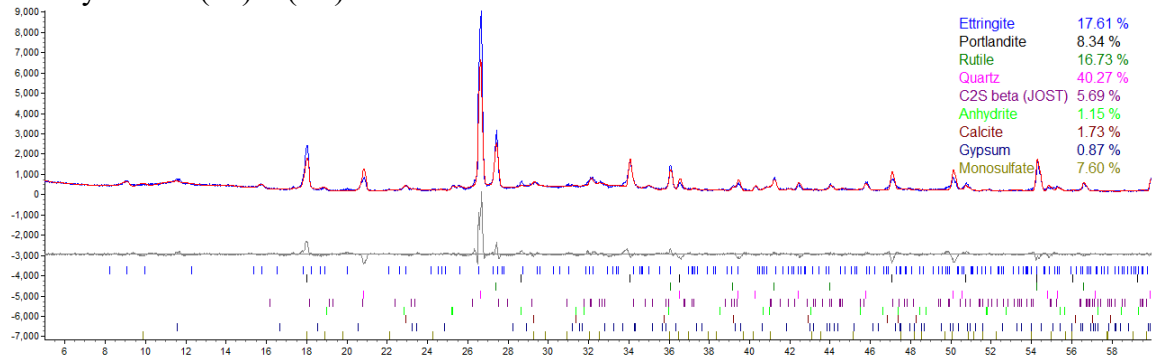

Figure A187 X-ray diffraction pattern and Rietveld refinement: C2-F3(20)-G(4) at 28 days.

28 Days C2-F3(20)-G(6A)

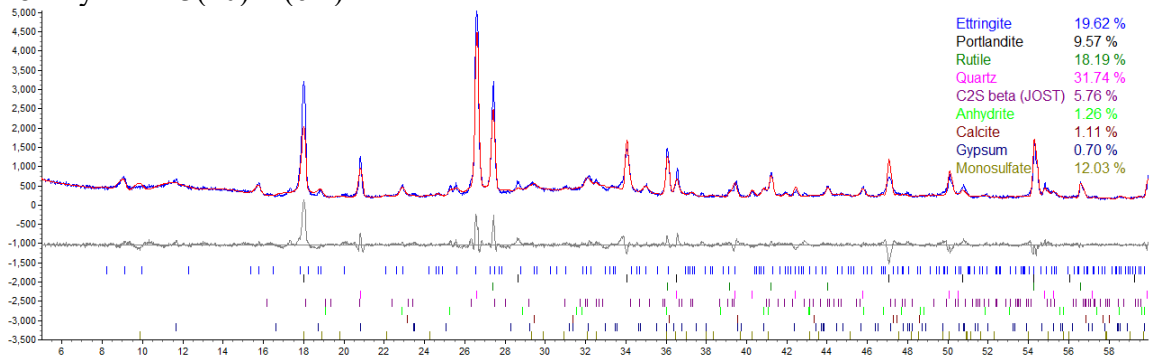

28 Days C2-F3(20)-G(6B)))))))

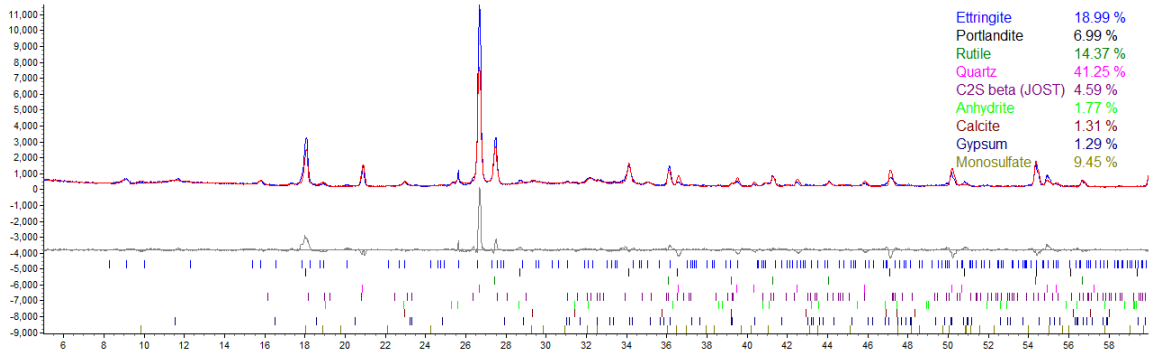

Figure A188 X-ray diffraction pattern and Rietveld refinement: C2-F3(20)-G(6) at 28 days.

28 Days C2-F3(20)-G(8A)

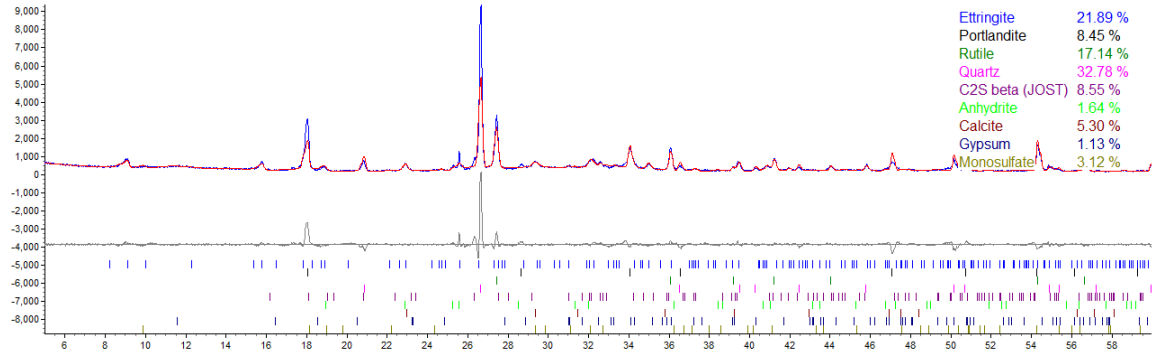

28 Days C2-F3(20)-G(8B)

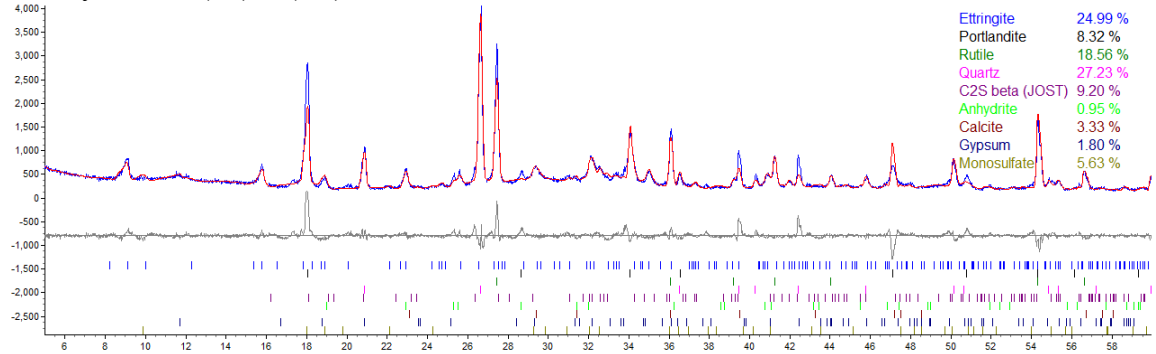

Figure A189 X-ray diffraction pattern and Rietveld refinement: C2-F3(20)-G(8) at 28 days.

28 Days C2-F3(20)-G(10A)

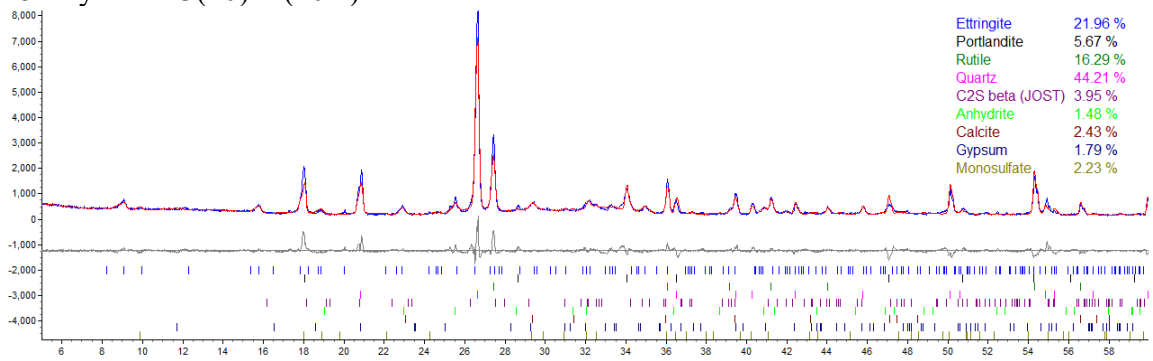

28 Days C2-F3(20)-G(10B)

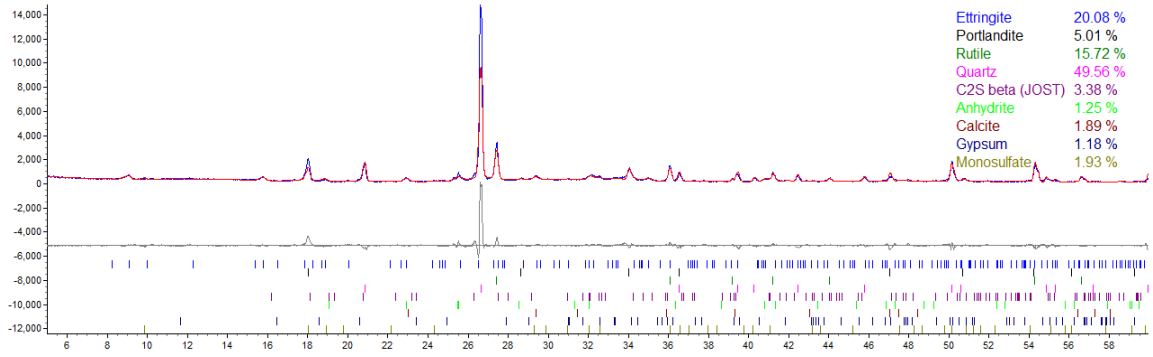

Figure A190 X-ray diffraction pattern and Rietveld refinement: C2-F3(20)-G(10) at 28 days.

28 Days C2-F3(20)-G(12A)

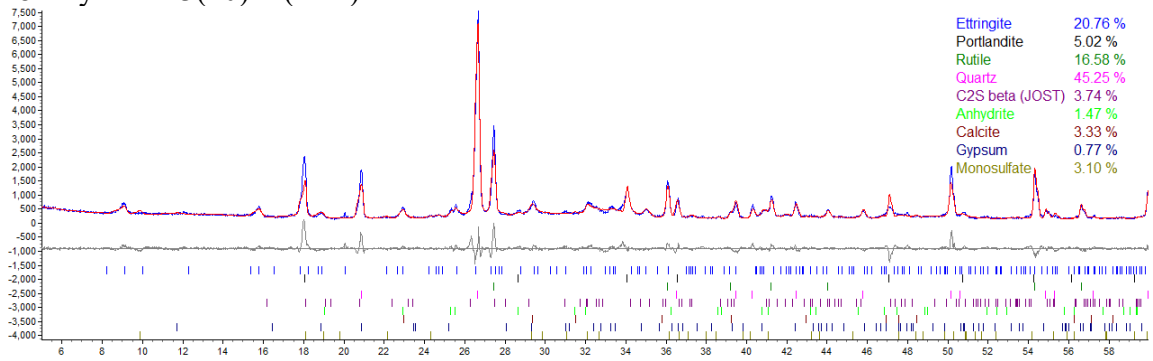

28 Days C2-F3(20)-G(12C)

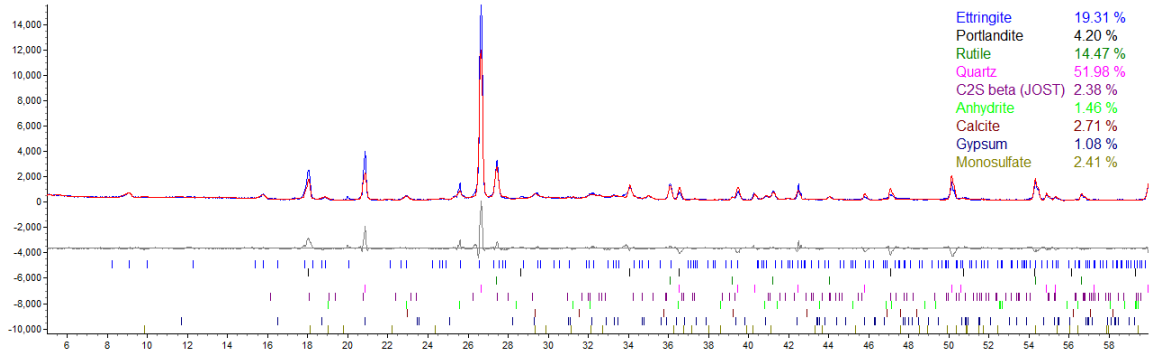

Figure A191 X-ray diffraction pattern and Rietveld refinement: C2-F3(20)-G(12) at 28 days.

28 Days C2-F3(20)-G(15A)

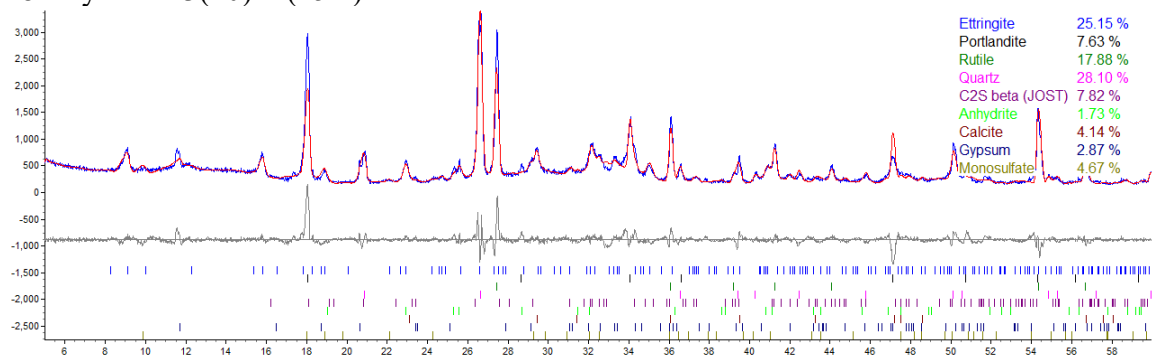

28 Days C2-F3(20)-G(15B)

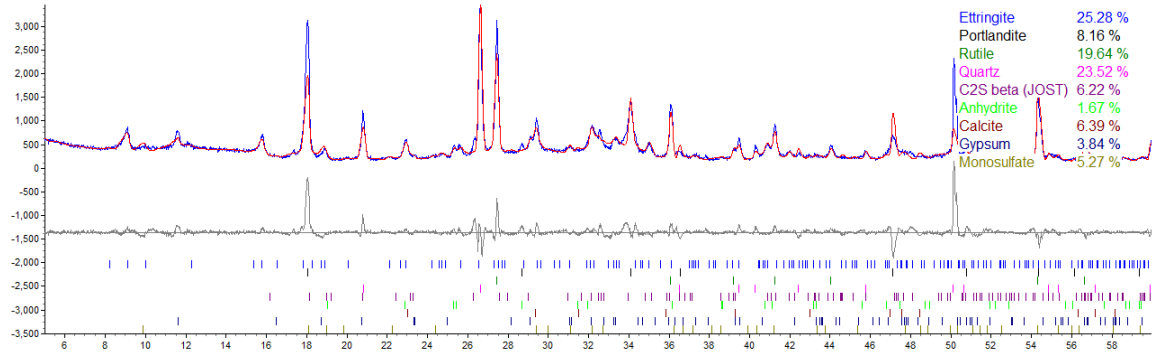

Figure A192 X-ray diffraction pattern and Rietveld refinement: C2-F3(20)-G(15) at 28 days.

C1-20 MPa (A)

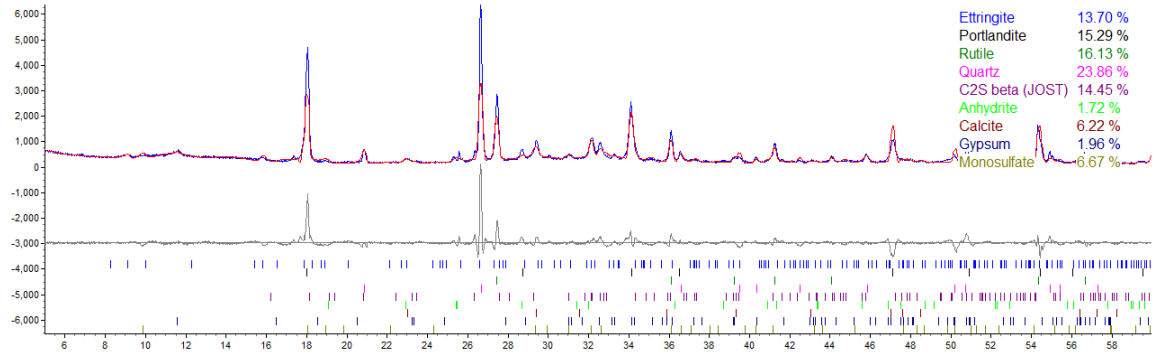

C1-20 MPa (B)

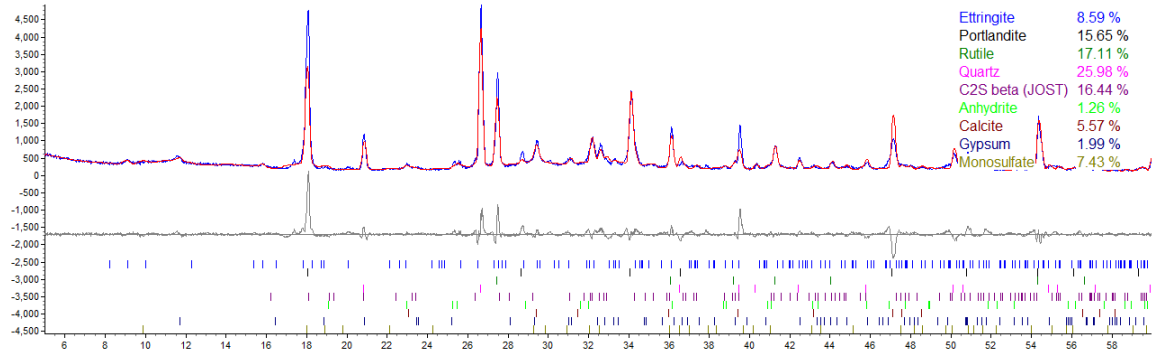

Figure A193 X-ray diffraction pattern and Rietveld refinement: C1.

C1-28 Days (A)

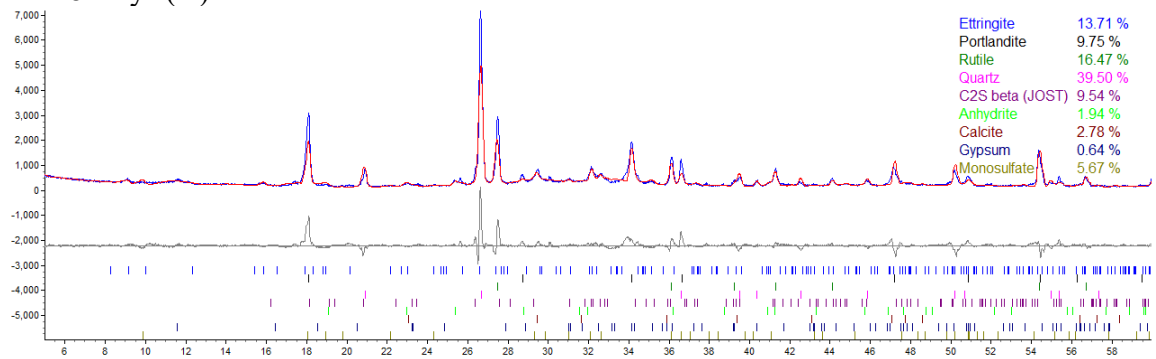

C1-28 Days (B)

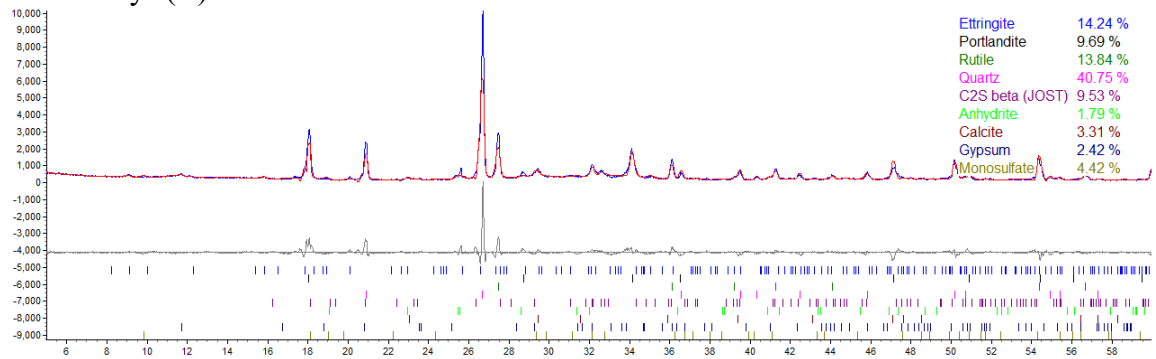

Figure A194 X-ray diffraction pattern and Rietveld refinement: C1 at 28 days.

C2-20 MPa (A)

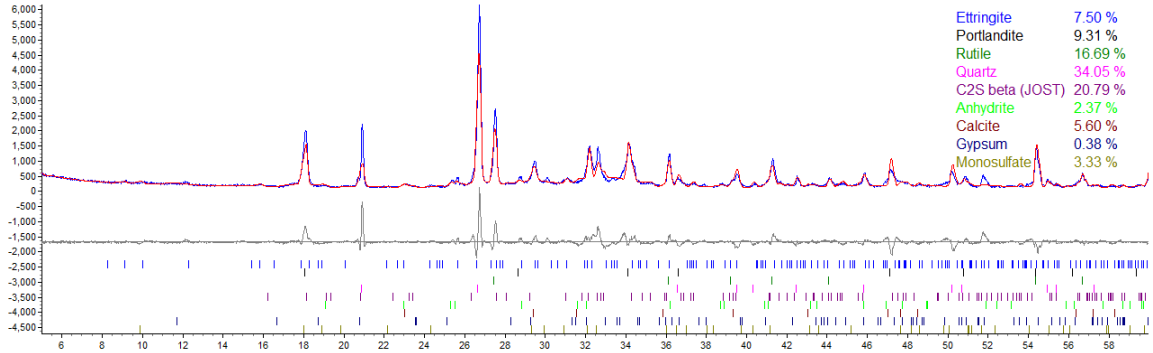

C2-20 MPa (B)

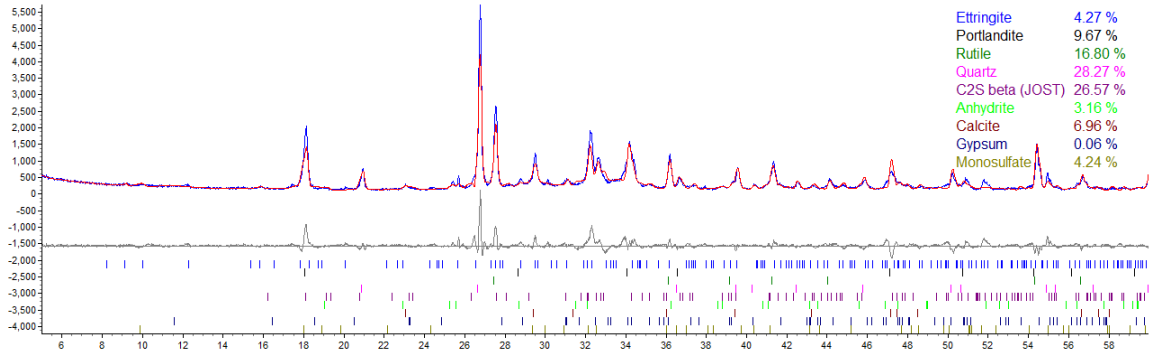

Figure A195 X-ray diffraction pattern and Rietveld refinement: C2.

C2-28 Days (A)

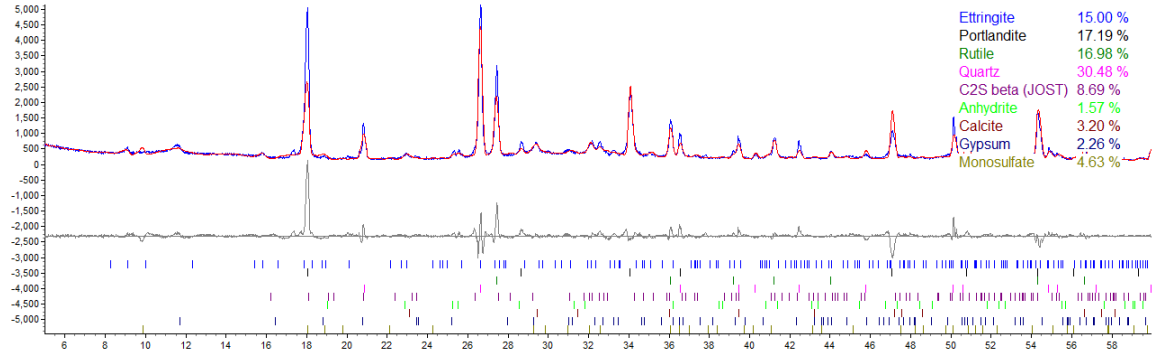

C2-28 Days (B)

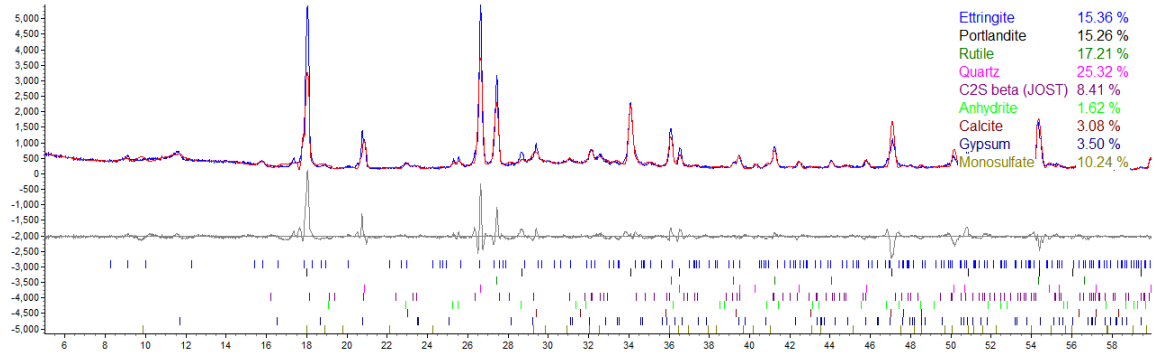

Figure A196 X-ray diffraction pattern and Rietveld refinement: C2 at 28 days.

F2-A

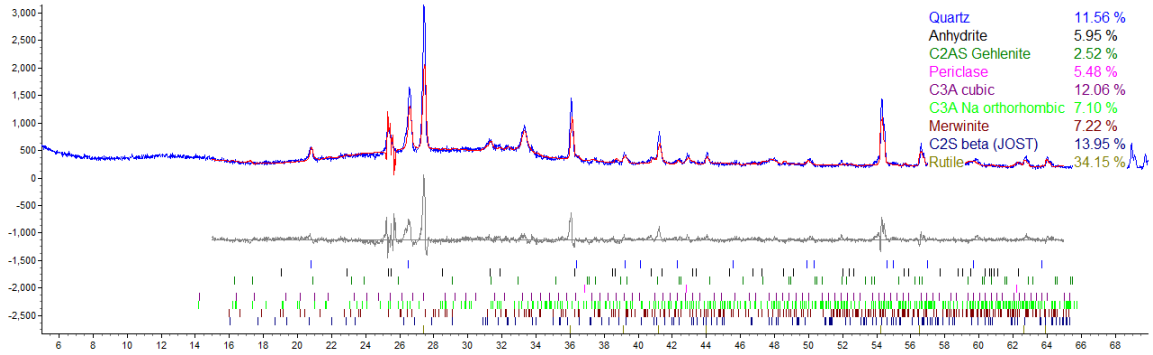

F2-B

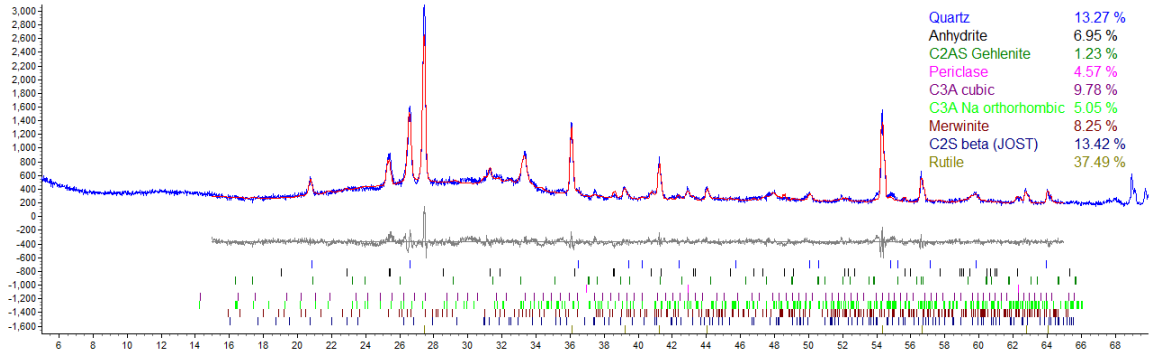

Figure A197 X-ray diffraction pattern and Rietveld refinement for fly ash F1.

F1-A

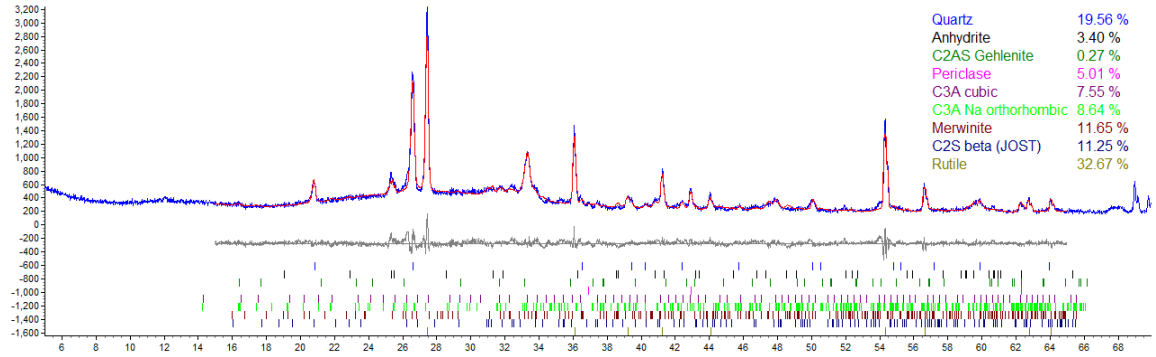

F1-B

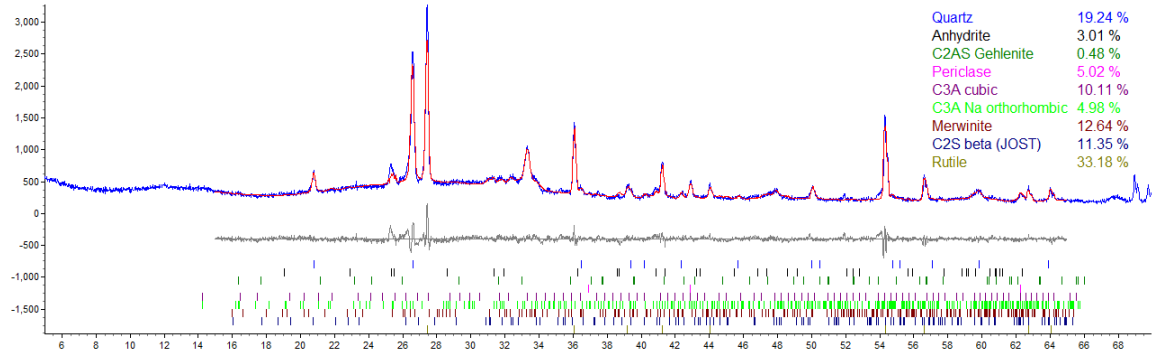

Figure A198 X-ray diffraction pattern and Rietveld refinement for fly ash F2.

F3-A

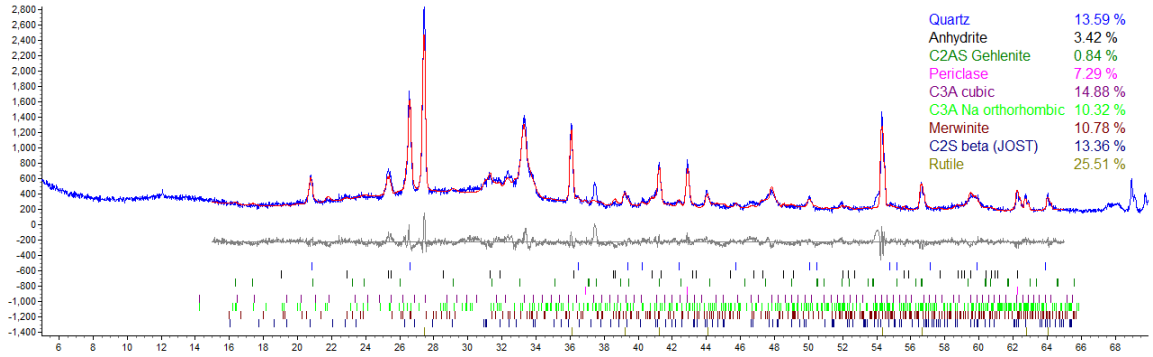

F3-B

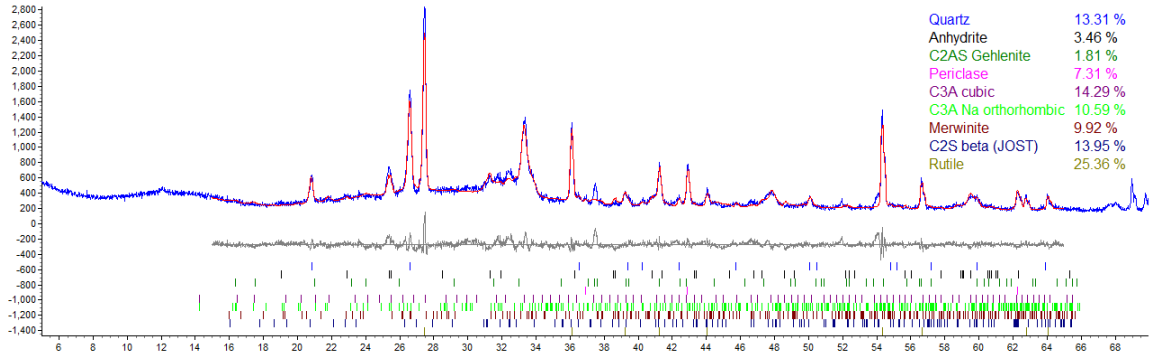

Figure A199 X-ray diffraction pattern and Rietveld refinement for fly ash F3.

8.0 References

[1] P. &. M. P. Mehta, Concrete - Microstructure, Properties, and Materials, Fourth ed., New York: McGraw Hill, 2014.

[2] S. H. Kosmatka,, B. Kerkhoff and W. C. Panarese, Design and Control of Concrete Mixtures, 14th ed., Skokie, Illinois: Portland Cement Association, 2002.

[3] American Society for Testing and Materials, *ASTM C150/C150M - 16, Standard Specification for Portland Cement,* West Conshohocken, PA: ASTM International, 2016.

[4] J. W. Bullard, H. M. Jennings, R. A. Livingston, A. Nonat, G. W. Scherer, J. S. Schweitzer, K. L. Scrivener and J. J. Thomas, "Mechanisms of cement hydration," *Cement and Concrete Research,* vol. 41, no. 1, pp. 1208-1223, 2011.

[5] E. R. Dunstan, "A Possible Method for Identifying Fly Ashes That Will Improve the Sulfate Resistance of Concretes," *Cement, Concrete, and Aggregates, CCAGDP,* vol. Vol. 2, no. No. 1, pp. 20-30, 1980.

[6] P. K. Mehta, "Effect of Fly Ash Composition on Sulfate Resistance of Cement," *ACI Journal, Technical Paper,* Vols. November-December, no. Title No. 83-39, pp. 83-89, 1986.

[7] P. J. Tikalsky and R. L. Carrasquillo, "The Effect of Fly Ash on the Sulfate Resistance of Concrete," Center for Transportation Research, The University of Texas at Austin, Austin, Texas, 1989.

[8] F. M. Aguayo, K. Folliard, M. D. Thomas, D. W. Fowler, J. C. Maria and H. Wheat, "External Sulfate Attack of Concrete: An Accelerated Test Method, Mechanisms, and Mitigation Techniques," The University of Texas at Austin, Austin, Texas, 2016.

[9] R. Dhole, "Sulfate Resistance of High Calcium Fly Ash Concrete," The University of New Brunswick, New Brunswick, 2008.

[10] K. Kruse, A. Jasso, K. J. Folliard, R. Ferron, M. Juenger and T. Drimalas, "Characterizing Fly Ash," The Center for Transportation Research at The University of Texas at Austin, Austin, 2012.

[11] S. G. Shashiprakash and M. D. A. Thomas, "Sulfate Resistance of Mortars Containing High-Calcium Fly Ashes and Combinations of Highly Reactive Pozzolans and Fly Ash," American Concrete Institute, SP199, Vol. 1, Farmington Hills, Michigan, 2001.

[12] M. D. A. Thomas, M. H. Shehata and S. G. Shashiprakash, "The Use of Fly Ash in Concrete: Classification by Composition," *Cement, Concrete, and Aggregates, CCAGDP,* vol. 21, no. No. 2, pp. 105-110, Dec. 1999.

[13] K. F. von Fay and J. S. Pierce, "Sulfate Resistance of Concretes with Various Fly Ashes," *ASTM Standardization News,* pp. 32-37, 1989.

[14] P. J. Tikalsky and R. L. Carrasquillo, "Influence of Fly Ash on the Sulfate Resistance of Concrete," Amercian Concrete Institution, Materials Journal, Farmington Hills, Michigan, 1992.

[15] R. Dhole, M. D. A. Thomas, K. J. Folliard and T. Drimalas, "Characterization of Fly Ahses for Sulfate Resistance," *ACI Materials Journal,* vol. 110, no. No. 2, pp. 159-168, 2013.

[16] G. J. McCarthy, J. K. Solem, O. Manz and D. J. Hassett, "Use of a Database of chemical, mineralogical and physical properties of north American fly ash to study the nature of fly ash and its utilization as a mineral admixture in concrete," *Materials Research Society,* vol. 178, pp. 3-33, 1990.

[17] T. Drimalas, J. C. Clement, K. J. Folliard, R. Dhole and M. D. A. Thomas, "Laboratory and Field Evaluations of External Sulfate Attack in Concrete," Center for Transportation Research at The University of Texas at Austin, Austin, Texas, 2010.

[18] Von Fay, Kurt F.; Bureau of Reclamation, "Effects of Various Fly Ashes on Compressive Strength, Resistance to Freezing and Thawing, Resistance to Sulfate Attack, and Adiabatic Temperature Rise of Concrete," U.S. Department of the Interior, Denver, Colorado, 1995.

[19] J. R. Prusinski and R. L. Carrasquillo, "Using Medium - to High-Volume Fly Ash Blended Cements to Improve the Sulfate Resistance of High-Lime Fly Ash Concrete," *ACI Materials Journal,* no. SP 153-3, pp. 43-65, 1995.

[20] R. L. Carrasquillo, "Methods of Producing Concretes Containing Class C Fly Ash That Are Stable in Sulphate Environments". United States of America Patent 5,578,122, 14 February 1994.

[21] American Society for Testing and Materials, *ASTM C618A -17a, Standard Specification for Coal Fly Ash and Raw or Calcined Natural Pozzolan for Use in Concrete,* Conshohocken, PA: ASTM International, 2017.

[22] American Society for Testing and Materials, *ASTM C452-15, Standard Test Method for Potential Expansion of Portland-Cement Mortars Exposed to Sulfate,* Conshohocken, PA: ASTM International, 2015.

[23] American Society for Testing and Materials, *ASTM C1012/C1012M -15, Standard Test Method for length Change of Hydraulic-Cement Mortars Exposed to a Sulfate Solution,* Conshohocken, PA: ASTM International, 2015.

[24] P. J. Sandberg and L. R. Roberts, "Cement-Admixture Interactions Related to Aluminate Control," *Journal of ASTM International,* vol. 2, no. 6, pp. 1-14, June 2005.

[25] W. Lerch, "The Influence of Gypsum on the Hydration and Properties of Portland Cement Pastes," American Society for Testing Materials, Philidelphia, PA, 1946.

[26] S. Bishnoi and P. Sandberg, "Sulfate Optimization of Hydraulic Cementitious Materials Using Isothermal Calorimetry," unknown, Delhi, India, unknown.

[27] C. Hesse, F. Goetz-Neunhoeffer and J. Neubauer, "A new approach in quantitative in-situ XRD of cement pastes: Correlation of heat flow curves with early hydration reactions," *Cement and Concrete Research,* vol. 41, no. 1, pp. 123-128, January 2011.

[28] D. Jansen, F. Goetz-Neunhoeffer, B. Lothenbach and J. Neubauer, "The early hydration of Ordinary Portland Cement (OPC): An approach comparing measured heat flow with calculated heat flow from QXRD," *Cement and Concrete Research,* vol. 42, pp. 134-138, 2012.

[29] L. G. Baquerizo, T. Matschei, K. L. Scrivener, M. Saeidpour and L. Wadso, "Hydration states of AFm cement phases," *Cement and Concrete Research,* vol. 73, pp. 143-157, 2015.

[30] Stark, David C.; Portland Cement Association, "Performance of Concrete in Sulfate Environments, RD 129," Portland Cement Association, Skokie, Illinois, 2002.

[31] Mehta, "MECHANISM OF SULFATE ATTACK ON PORTLAND CEMENT - Another Look," Department of Civil Engineering University of California Berkeley, Berkeley, 1982.

[32] American Society for Testing and Materials, *Standard Specification for Coal Fly Ash and Raw or Calcined Natrual Pozzolan for Use in Concrete,* West Conshohocken, PA: ASTM International, 2017.

[33] American Concrete Institute, ACI, Building Code Requirements for Structural Concrete (ACI 318-14), Farmington Hills, Michigan: American Concrete Institute, 2014.

[34] Hemmings, R. T.; Berry, E. E.; Ontario Research Foundation, "On The Glass in Coal Fly Ash: Recent Advances," *Materials Research Society,* vol. 113, pp. 3-38, 1988.

[35] American Society for Testing and Materials, *ASTM C1157/C1157M -17 Standard Performance Specification for Hydraulic Cement,* West Conshohocken, PA: ASTM International, 2017.

[36] American Society for Testing and Materials, *ASTM C595/C595M - 18 Standard Specification for Blended Hydraulic Cements,* West Conshohocken, PA: ASTM International, 2018.

9.0 Vita

Jeremy Wheeless is native Texan, and fifth generation Austinite. Prior to obtaining his Bachelor's and Master's degrees from the University of Texas at Austin, he spent seven years working as a journeyman steel worker in the local union 482. He is passionate about the civil infrastructure and finds joy in observing the built world. Additionally, he enjoys rollercoasters, and good food. But, not at the same time.

Email Address: jwheeless@utexas.edu

This thesis (every word of it) was typed by Jeremy Oran Wheeless